CAVITATION REACTION ENGINEERING

The Plenum *Chemical* Engineering Series

Series Editor:
Dan Luss, *University of Houston, Houston, Texas*

CAVITATION REACTION ENGINEERING
Y. T. Shah, A. B. Pandit, and V. S. Moholkar

COAL COMBUSTION AND GASIFICATION
L. Douglas Smoot and Philip J. Smith

ENGINEERING FLOW AND HEAT EXCHANGE, Revised Edition
Octave Levenspiel

INDUSTRIAL CRYSTALLIZATION: Process Simulation Analysis and Design
Narayan S. Tavare

REACTION ENGINEERING OF STEP GROWTH POLYMERIZATION
Santosh K. Gupta and Anil Kumar

THE STRUCTURE AND REACTION PROCESSES OF COAL
K. Lee Smith, L. Douglas Smoot, Thomas H. Fletcher, and Ronald J. Pugmire

TRANSPORT MECHANISMS IN MEMBRANE SEPARATION PROCESSES
J. G. A. Bitter

CAVITATION REACTION ENGINEERING

Y. T. Shah
Clemson University
Clemson, South Carolina

and

A. B. Pandit and V. S. Moholkar
University of Bombay
Bombay, India

Springer Science+Business Media, LLC

Library of Congress Cataloging–in–Publication Data

Shah, Yatish T.
Cavitation reaction engineering / Y.T. Shah, and A.B. Pandit, and V.S. Moholkar.
p. cm. -- (Plenum chemical engineering library)
Includes bibliographical references and index.

1. Cavitation. 2. Chemical processes. I. Pandit, A.B. II. Moholkar, V.S. III. Title. IV. Series
TP156.C38S48 1999
660'.284--dc21 99-37362
CIP

ISBN 978-1-4613-7168-7 ISBN 978-1-4615-4787-7 (eBook)
DOI 10.1007/978-1-4615-4787-7

Originally published by Kluwer Academic / Plenum Publishers in 1999
Softcover reprint of the hardcover 1st edition 1999

10 9 8 7 6 5 4 3 2 1

A C.I.P. record for this book is available from the Library of Congress.

To James, Keith, Jonathan, and Heather
Y.T.S.

PREFACE

The literature on cavitation chemistry is ripe with conjectures, possibilities, heuristic arguments, and intelligent guesses. The chemical effects of cavitation have been explained by means of many theories, consisting of empirical constants, adjustable parameters, and the like. The chemists working with cavitation chemistry agree that the phenomenon is very complex and system specific. Mathematicians and physicists have offered partial solutions to the observed phenomena on the basis of cavitation parameters, whereas chemists have attempted explanations based on the modes of reaction and the detection of intermediate chemical species. Nevertheless, no one has been able to formulate a unified theme, however crude, for its effects on the basis of the known parameters, such as cavitation and transient chemistry involving extremely high temperatures of nanosecond durations.

When one surveys the literature on cavitation-assisted reactions, it is clear that the approach so far has been "Edisonian" in nature. While a large number of reactions have showed either enhanced yields or reduced reaction times, many reactions have remained unaffected in the presence of cavitation. The success or failure of cavitation reactions ultimately depends on the collapse of the cavity.

Cavitation chemistry is based on the principles of the formation of small transient cavities, their growth and implosion, which produce chemical reactions caused by the generation of extreme pressures and temperatures and a high degree of microturbulence. Cavities can be generated either by expansion of pressure (caused hydrodynamically or acoustically) or by sharp penetration of energy by lasers or protons. This monograph deals with the reaction engineering associated with the cavitation phenomenon and its practical applications in the treatment of various types of aqueous waste or for organic synthesis.

Mathematical modeling of cavitation phenomena and the related chemical effects is rather complex; even for the simplest reactions, there appears no possibility of a generalized theory in the near future. The chemical effects observed and reported in the literature as either transient or time averaged most definitely have resulted from the cavitation phenomenon. All researchers and a few practitioners will not

have any difficulty in accepting newly coined terms of cavitation chemistry and cavitation reaction engineering, which encompasses all aspects of the chemical transformations caused by the cavitation phenomenon.

This monograph is an attempt to present the observed effects on a common basis, namely, the parameters affecting cavitation, those affecting chemistry, and those affecting both, which are important in an appropriate design of a cavitation reactor. The mathematical modeling of cavitation bubble dynamics, chemical reactions, and reactors is discussed, with an emphasis on the physical explanations of the phenomena on the basis of known parameters affecting cavitation or parameters affecting the chemical transformations and the performance of the reactors.

The cavitation process can be categorized according to the method used to produce cavities. Hydrodynamic cavitation is produced by the pressure variation in a flowing liquid that is caused by the variation of velocity in the system. At the points of highest velocity and lowest pressure, cavities can occur. These cavities can (1) move with the liquid and subsequently collapse (i.e., traveling cavitation); (2) remain fixed at a rigid surface under unsteady state condition (i.e., fixed cavitation); or (3) reside in the cores of vortices (i.e., vortex cavitation) that form in the regions of high shear and boundary layer separation. Traveling cavitation is most efficient for chemical conversion. Acoustic cavitation is produced by sound waves in a liquid that are caused by pressure variations. Optical cavitation is produced by a laser light rupturing the liquid. Finally, particle cavitation is produced by the deposition of energy using any other type of elementary particle, such as a proton.

Chapter 1 briefly discusses the underlying physics behind the sources of cavitation. Instruments are currently available to produce cavities from these different sources. Cavitation bubbles and their behavior under different environments form the basis for how the cavitation process affects chemical transformation.

A suitable mathematical description of bubble dynamics and their interaction with the surrounding liquid medium is given in Chapter 2. While a complete description of bubble behavior is rather complex, the mathematics outlined in this chapter form the basis upon which more complex models can be developed. The modifications of the equations and the incorporation of the parameters involving physical effects are presented for different modes of cavitation. Different types of cavitation are discussed on the basis of the mode of energy dissipation and the time scales involved for this energy dissipation. The similarities and differences arising are discussed as part of a unified theme of energy dissipation and conversion for cavitation.

Finally, the physical parameters that affect the nature of the process in each type of cavitation are described in Chapter 3. The relationship between the physical parameters and the nature of the cavitation behavior described in this chapter is qualitatively and in some instances quantitatively obtained from an evaluation of the basic equations for cavitation bubble dynamics.

The success or failure of cavitation-assisted reactions ultimately depends on the active or reactive species generated as a result of cavity collapse. The cavitation phenomenon consists of three stages: nucleation, growth, and collapse of a single cavity or a cluster of cavities. A scientific approach to cavitation chemistry requires the control of these three stages.

Although nucleation is a fairly random phenomenon, considerable control over the rate has been achieved in the crystallization process by controlling the degree of supersaturation (metastable region) or by the addition of external nuclei (seeding). It may be possible to do the same for the nucleation of cavities or a cluster of cavities. Growth and collapse behavior of the cavity or the cluster of cavities is controlled by the surrounding fluctuating pressure field, i.e., its frequency and amplitude. Since the generation of active and reactive species depends on this cavity behavior, the success or failure of the reaction is related to the frequency and amplitude of the surrounding pressure field.

It is expected that from Chapters 1–3, the reader will be made aware of the common underlying theme responsible for a variety of chemical effects reported in the literature. The reader will also become conversant with cavitation as a physical phenomenon and the factors affecting this physical phenomenon. Where there is no literature on an experimental proof of the physical phenomena predicted by the mathematical and physical equations, numerical predictions have been used liberally to explain cavitation-related physical effects. This involves the behavior of a single cavity or a cluster of cavities in a variety of surroundings; i.e. form, mode, and time scales of energy dissipation.

Cavitation can have beneficial effects on a reaction as a result of physical effects such as microstreaming or chemical effects such as generation of OH^- radicals (hydrolysis or oxidative reactions). Control of these effects requires a fundamental analysis of cavity dynamics and not a simple use of cavitation intensity, as is often done in the literature. In Chapters 4 and 5 on gas–liquid cavitation chemistry and gas–liquid–solid cavitation chemistry, an attempt has been made to relate or use the predicted and observed physical effects of cavitation to explain the chemical and physical transformations observed and reported in the literature. Wherever possible, the parameters responsible for the chemical transformations and the changes in these parameters as a result of the physical phenomena of cavitation are highlighted. Heterogeneous cavitation chemistry and homogeneous cavitation chemistry, which are incorrectly separated in the literature, are presented on a common footing here because cavitation chemistry is always heterogeneous (more than one phase) owing to the formation of vapor- or gas-filled cavities. The correct separation is indicated in the titles of these two chapters.

Various possible and suggested mechanisms of cavitation-aided practical chemical reactions are also briefly discussed in Chapters 4 and 5. The interesting behavior of a variety of chemical reactions in the presence of cavitation is illustrated with the support of the experimental facts. The emphasis is largely on chemical trans-

formations in the aqueous phase so that the results are useful in treating aqueous waste. The mode of generation of the cavitation, its physical effect, and its ultimate utilization in chemical conversion is discussed in detail, linking the physical effects of cavitation and the followup chemical transformations.

The next three chapters (Chapters 6, 7, and 8) deal with the engineering translation of the basic physical and chemical concepts discussed in Chapters 1 to 5 into their possible practical uses. Various designs reported in the literature using hydrodynamic, acoustic, or laser energy for the generation of cavitation are discussed in terms of operational and design difficulties and ease of the chemical transformation. New, probable, and/or novel reactor configurations have also been proposed. Specific examples have been selected to highlight the difficulty or the ease of operation of various types of cavitational reactors. Examples have been used with the results to discuss the efficacy of one type of cavitation compared with another. The effect of physicochemical properties and the optimum use of cavitation for the required chemical effects are also discussed.

In these chapters, the problems associated with energy efficiencies and scaleup are also discussed. It has been found that the industrial success of cavitation reactors and their design and optimization strategies differ from system to system or are system specific. The optimization of the cavitation reactor as required for any one system is not necessarily applicable to other systems. The specific parameters responsible for the success of this optimization are highlighted. Some new reactors for specific applications are proposed. These chapters are expected to generate curiosity and research interest in the people working in the field of cavitation chemistry and cavitation reactors.

Chapter 7 deals with mathematical models for cavitation reactors. This subject is very difficult because of the lack of appropriate experimental data, the complexity of the system, and the difficulty in predicting a reactor's behavior at different scales. Numerous models based on different sets of assumptions for the reaction zone are described. Probability density function is used to illustrate the behavior of the reaction zone in an acoustic cavitation reactor.

The cost effectiveness of a cavitation reactor depends very strongly upon the energy efficiency of the steps leading to the chemical transformation. The energy efficiency of the cavity implosion process as a function of frequency is discussed in Chapter 8. The range of frequency covers all types of processes and reactors, such as hydrodynamic (low frequency), acoustic (medium frequency), and laser (high frequency) cavitation. The performance of the acoustic reactor is also evaluated based on the concept of sonochemical yield, an empirical parameter that can help in comparing and evaluating the performance of various types of acoustic reactors.

Chapter 8 also uses concepts discussed in earlier chapters for the design and optimization of a cavitation reactor. It briefly presents some economic comparisons of a few standard effluent treatment and recovery techniques with new techniques

of cavitation-based chemical conversions. Both capital and the operating costs of conventional and nonconventional hydrodynamic, acoustic, and other types of cavitation reactors are briefly discussed. The need for further research is delineated. The chapter first deals with the efficiency of the energy conversion supplied for the global cavitational effect and then the optimized cavitational effect, i.e., the one required for a specific chemical or physical conversion. The results are illustrated with case studies.

Finally, Chapter 9 describes some pilot and large-scale applications of the cavitational chemical transformations. The examples clearly illustrate the commercial viability of the concept discussed in this monograph. While the examples are largely for a hydrodynamic cavitation process because of its favorable economics, a similar development for acoustic cavitation should appear in the near future. Commercial applications for laser and particle cavitations may require more development to make these technologies more economical.

Cavitation reaction engineering is rapidly changing, largely because of its ease of application to a variety of chemical reactions. It is hoped that this monograph summarizes the state of knowledge available on this subject and will fuel more momentum for research in this area. It is our hope that with increased knowledge of the subject, the present "Edisonian" approach will be replaced by a more scientific assessment of the possibilites and applications of cavitation processes.

A monograph such as this would not have been possible without the support of many people. We would like to thank Profs. Luss, Doraiswamy, Sharma, and Joshi for their constant encouragement on this project. One of the authors (ABP) would like to acknowledge the University Grants Commission and the Department of Science and Technology, Government of India for giving him the opportunity to work in this exciting field. We would also like to thank our students, in particular Parag Gogate, Nilesh Vichare and Prashant Tatake for their assistance and comments on the manuscript. Our sincere thanks to Mrs. Melody Land for all the hard and painstaking detail work she carried out for the completion of this project. Our thanks also to Mr. Ron Baker for his help with the drawings. Finally, and most importantly, projects such as this cannot be completed without the love and support of our wives, Mary and Anala, and our children.

CONTENTS

3. Factors Affecting Cavitation Behavior

4. Gas–Liquid Cavitation Chemistry

7. Models for Cavitation Reactors

8. Energy Efficiency and the Economics of the Cavitation Conversion Process

9. CAV-OX Process

CAVITATION REACTION ENGINEERING

1

SOURCES AND TYPES OF CAVITATION

1.1. INTRODUCTION

During the past few decades, a number of new technologies have been developed, each of which offers the hope of providing chemists with innovative routes and chemical engineers with sophisticated methods of introducing energy to bring about chemical change. In cavitation reaction engineering, the origin of the chemical effects lies in cavitation: the phenomenon of the formation, growth, and rapid collapse of bubbles. Cavitation by definition is the formation and activity of bubbles or cavities in a liquid. It may occur through the formation of bubbles or cavities in the liquid or it can be a result of the enlargement of cavities that are already present in the bulk liquid. These bubbles may be suspended in liquid or may be trapped in tiny cracks in the liquid–solid interface.

Although cavitation was first mentioned by Leonhard Euler in 1754, it was 150 years before it became important in ship propellers, turbines, pumps, and hydrofoils. This type of cavitation is called *hydraulic* or *hydrodynamic cavitation* (Knapp *et al.*, 1970). Acoustic cavitation showed up in connection with high-intensity underwater sound projectors in the late 1920s. More recently, it has been noted that when a liquid is irradiated with a light of high intensity (such as a laser), cavities are formed that can be used to study cavitation bubble dynamics. This new form of cavitation is called *optic cavitation* (Lauterborn and Bolle, 1975). While in this type of cavitation photons are used for the cavitation, there is no reason why other types of elementary particles such as protons or neutrinos cannot be used to break down the liquid. This effect has been used since the 1950s in bubble chambers and is often denoted as *particle cavitation.*

The method of production can be taken as the main criterion in distinguishing among different types of cavitation. The four principal types of cavitation and their causes can be summarized as follows:

- Hydrodynamic cavitation is produced by pressure variation in a flowing liquid caused by the velocity variation in the system.
- Acoustic cavitation is a result of pressure variation in a liquid when ultrasound waves pass through it.
- Optic cavitation is a result of the rupture of a liquid due to high-intensity light or a laser.
- Particle cavitation is produced by any type of elementary particle (e.g., a proton) rupturing a liquid, as in a bubble chamber.

According to Lauterborn (1980b), hydrodynamic and acoustic cavitations are the result of tensions prevailing in a liquid, while optic and particle cavitations are the consequence of local deposition of energy. He developed the classification scheme shown in Figure 1.1.

Once formed, the expansion of a minute bubble or a cavity may be achieved by reducing the ambient pressure using static or dynamic means. The bubble may contain gas or vapor or a mixture of gas and vapor. If the bubble contains gas, then the expansion may be by diffusion of gases from the liquid into the bubble, or by pressure reduction, or by temperature rise. If, however, the bubble contains mainly vapor, reducing the ambient pressure sufficiently at constant temperature causes an "explosive" vaporization into the cavities. On the other hand, raising the temperature will make a vapor bubble grow through the phenomenon of boiling. Both explosive vaporization and boiling do not occur until a threshold is reached. Thus bubble growth occurs:

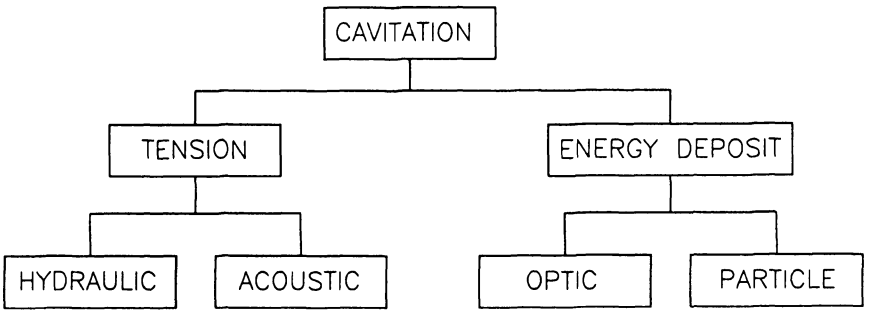

Figure 1.1. Classification scheme for the different kinds of cavitation. (From Lauterborn, 1980a, with permission.)

- by a pressure reduction or temperature increase in a gas-filled bubble: gaseous cavitation
- by pressure reduction in a vapor-filled bubble: vaporous cavitation
- by diffusion in a gas-filled bubble: degassing
- by sufficient temperature rise in a vapor-filled bubble: boiling

In cavitation reactors, two aspects of bubble (or cavity) dynamics are of prime importance: (1) the maximum size reached by the bubble before a violent collapse and (2) the life of the bubble. The maximum size reached by the bubble determines the magnitude of the pressure pulse and hence the cavitation intensity that can be obtained in the system. The life of the bubble determines the distance traveled by the bubble from the point where it is generated before collapse and hence it is a measure of the active volume of the reactor at which actual cavitation effects are observed. Hydrodynamic cavitation occurs at lower frequencies (i.e., lower than approximately 1–20 kHz), and the bubble collapse produces less intensity and therefore lower temperatures and pressures. Acoustic cavitation generally occurs in the frequency range of 20 kHz to 1 MHz; the bubble collapses with higher intensity and therefore produces higher temperatures and pressure than hydrodynamic cavitation. Optical and particle cavitation will require an intense energy source and generate intense temperatures and pressures. These methods of cavitation could be very useful in studying cavitation bubble dynamics and cavitation chemistry under controlled conditions. They may, however, be very expensive for large-scale operations.

1.2. HYDRODYNAMIC CAVITATION

There are various stages and types of hydrodynamic cavitation. The term "incipient stage" has long been used to describe cavitation that is just barely detectable. The conditions that mark the boundary or threshold between no cavitation and detectable cavitation are not always identical if they are observed as cavitation appears and again as cavitation disappears. The term "desinent cavitation" has been suggested for the latter. Hydrodynamic cavitation can be further subcategorized as (1) traveling cavitation, (2) fixed cavitation, (3) vortex cavitation, and (4) vibratory cavitation.

Traveling cavitation is composed of individual transient cavities or bubbles that form in the liquid and move with the liquid as they expand, shrink, and then collapse. Such traveling transient bubbles may appear at the low-pressure points along a solid boundary or in the liquid interior either at the cores of moving vortices or in the high-turbulence region in a turbulent shear field. The term "fixed cavitation" refers to the situation that sometimes develops after inception, in which liquid flow detaches from the rigid boundary of an immersed body or a flow passage to

form a pocket or cavity attached to the boundary. The attached or fixed cavity is stable in a quasi-steady sense. In vortex cavitation the cavities are found in the cores of vortices that form in zones of high shear. The cavities may appear as traveling cavities or as a fixed cavity. In all of these three types of cavitation, a particular liquid element passes through the cavitation zone only once. In vibratory cavitation, the velocity is so low that a given element of the liquid is exposed to many cycles of cavitation rather than only one.

While the above details on various types of hydrodynamic cavitation are worth noting, in cavitation reaction engineering the cavitation produced by flow through pipes and valves is most relevant and the following discussion is limited to these cases only. Hydrodynamic cavitation in a pipe is produced by pressure variation in a liquid flow due to the geometry of the system. Usually cavitation can also be obtained by throttling a valve downstream of a pump. When the pressure at the orifice or any other mechanical constriction falls below the vapor pressure of the liquid, cavities are generated which then collapse downstream with the recovery of pressure, giving rise to high pressure and temperature pulses. This effect pertains to a small area around these cavities.

Figure 1.2 shows the pressure variation profile. Cavity collapse during hydrodynamic cavitation is a result of pressure recovery from the lowest pressure encountered at the vena contracta of the orifice. This phenomenon can be explained as follows: If the liquid is flowing through an orifice, the reduction in the cross-section of the flowing stream increases the velocity head at the expense of the pressure head. During the reexpansion of flow, the fluid stream gets separated at the lower ends of the orifice and eddies are generated. Owing to this turbulence and the large friction loss generated by the motion of eddies, a permanent pressure loss is inevitable and full recovery of pressure does not take place. The static pressure at the vena contracta is less than the bulk pressure downstream of the flow. However, as velocity is increased, the pressure drop across the orifice increases and the pressure at the vena contracta decreases. At a particular velocity, the pressure may actually fall below the vapor pressure of the liquid being pumped, causing the generation of cavities.

1.2a. Cavitation Number

A dimensionless parameter generally used in the study of hydrodynamic cavitation is the cavitation number, which is defined as follows:

$$\sigma_c = (P_f - P_v)/\ 1/2\ \rho\ U^2 \tag{1.1}$$

where P_f and P_v are the downstream and vapor pressure, respectively; ρ is the density of the medium; and U is the average velocity near the orifice. The cavitation number, σ_c, measures the resistance of the flow to cavitation. The higher the

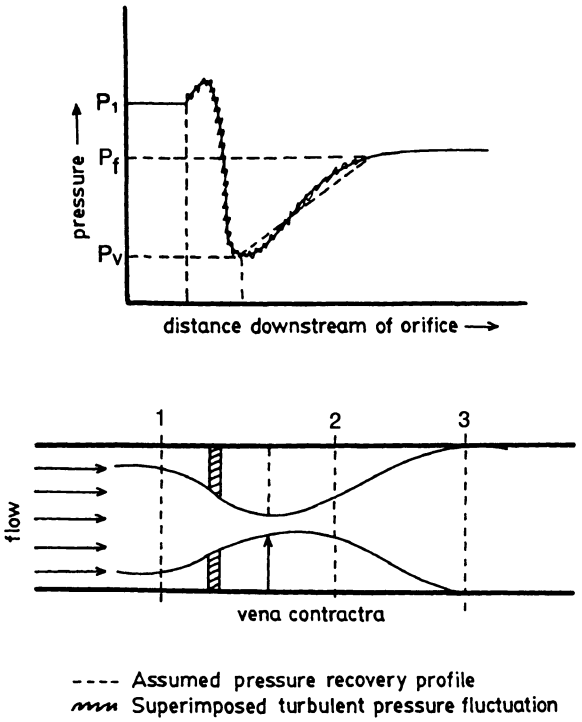

Figure 1.2. Typical pressure distribution across an orifice plate in pipe flow.

cavitation number, the less likely it is that cavitation will occur; conversely, the lower it is, the more likelihood there is for cavitation to occur. Similarly, if cavitation is occurring, lowering the cavitation number by decreasing the static pressure or by increasing the flow speed will increase the extent of cavitation; raising it may eliminate it entirely. A cavitation number equal to one indicates cavitation inception for gas-free liquids and ensures that the pressure in the close vicinity of the downstream side of the orifice has fallen to vapor pressure.

Yan and Thorpe (1990) reported the cavitation number for the inception of cavitation for different orifices. They observed that for a given orifice the cavitation inception number remains constant within a random experimental error for a specific liquid. The cavitation number does not change with the liquid velocity and is a constant for a given orifice size, shape, and medium. Yan *et al.* (1980) reported a variation in the cavitation number with the orifice-to-pipe diameter ratio, β. The results indicate that the cavitation inception number increases approximately linearly with the orifice-to-pipe diameter ratio. The results obtained by Yan *et al.* (1980),

also confirm the conclusion drawn by Numachi *et al.* (1960), and Tullis and Govindrajan (1973) that the cavitation inception number for an orifice cavitation is independent of the velocity of the fluid and of the downstream pressure. The typical ranges of cavitation numbers given by Yan *et al.* are 1.7–2.4 for $0.4 < \beta < 0.8$ and those given by Tullis and Govindrajan are 2–3 for $0.244 < \beta < 0.583$. The lower cavitation numbers observed by Yan *et al.* can be due to the fact that the diameters of the pipes downstream of the orifice in the study by Yan and Thorpe (1990) are almost half of those in the study conducted by Tullis and Govindarajan (1973). Thus it can be inferred that the cavitation inception number is strongly related to size of scale and is not a function of β alone. In addition, Yan *et al.* (1980), used sharp-edged orifices rather than the profiled orifices used by Tullis and Govindrajan (1973).

The minimum pressure at the vena contracta measured at inception is much higher than the vapor pressure and increases with the velocity of the liquid, which indicates that at inception the mechanism of bubble formation is the release of the dissolved gas or superimposed turbulent pressure fluctuations rather than just the vaporization of water. The minimum pressure is therefore not a unique value at the inception but is dependent on the turbulent flow structure. The severity of the cavitation increases with the decrease in the cavitation number.

The following relationship between the flow rate, Q, and the differential pressure $(P_1 - P_2)$ across an orifice or a valve is well known:

$$Q = C_d A \sqrt{\frac{2(P_1 - P_2)}{\rho\left(\frac{A^2}{a^2 - 1}\right)}} \tag{1.2}$$

where C_d is the discharge coefficient and A and a are the cross-sectional areas of the pipe and orifice, respectively. When the mean pressure at the vena contracta reaches the lowest possible value, there will be no further increase in the discharge rate regardless of the decrease in the downstream pressure. Here the downstream valve loses control over the flow. Obviously, in the present case, the lowest possible value for the minimum pressure is the vapor pressure of the cavitating medium.

In the case where the pressure downstream of the orifice actually falls to the vapor pressure, the cavitation is called *chocked cavitation*, i.e., the pressure loss is almost exclusively used for the vaporization. In case of chocked cavitation, the cavitation number was defined by Tullis and Govindrajan as follows:

$$\sigma_c = \frac{P_f - P_v}{P_1 - P_f} \tag{1.3}$$

The calculation of this chocked cavitation number is straightforward: First the discharge rate is plotted against the pressure drop $(P_1 - P_2)$. Before chocked cavitation, the relation between Q and the pressure differential is almost linear. As soon as vaporization is seen downstream of the orifice where Q remains constant while the pressure differential increases, this critical value of the pressure differential is then determined and the corresponding chocked cavitation number is calculated from Eq. (1.3). The relation between the cavitation number and the chocked cavitation number can be obtained as follows:

By applying Bernoulli's equation between points 1 and 2 in Figure 1.2 we get

$$P_1 - P_2 = 0.5\,\rho\left(\frac{U}{C_d}\right)^2\left(\frac{1}{\beta^4} - 1\right) \tag{1.4}$$

where U is the mean velocity in the pipe and β is the orifice-to-pipe diameter ratio. Application of the momentum equation between cross-sections 2 and 3 gives

$$P_2 - P_f = U^2\,\rho\left[1 - \frac{1}{C_c\beta^2}\right] \tag{1.5}$$

Thus the combination of Eqs. (1.4) and (1.5) gives

$$P_1 - P_f = \frac{1}{2}\rho\left(\frac{U}{C_d}\right)^2\left(\frac{1}{\beta^4} - 1\right) + \rho\,U^2\left(1 - \frac{1}{C_{C\beta^2}}\right) \tag{1.6}$$

Substituting $P_1 - P_f$ from this equation and $P_f - P_v$ from the cavitation number, we have,

$$\sigma_c' = \frac{\sigma_c}{\frac{1}{C_d^2}(1 - \beta^4) + 2\left(\beta^4 - \frac{\beta^2}{C_c}\right)} \tag{1.7}$$

Although most hydrodynamic cavitation reactors use the venturi nozzle or an orifice for pressure expansion, a simple valve can also be used to cause cavitation, depending on its construction and degree of openness. The more open the valve, the less likely is the cavitation. The throat cavitation number can be defined as (Luche, 1992a)

$$\sigma_T = (P_T - P_v)/1/2\,\rho\,U_T^2 \tag{1.8}$$

where P_T is pressure and U_T is the velocity in the throat. If σ_T is measured for the valve or orifice, this can be used to assess the degree of cavitation. For example,

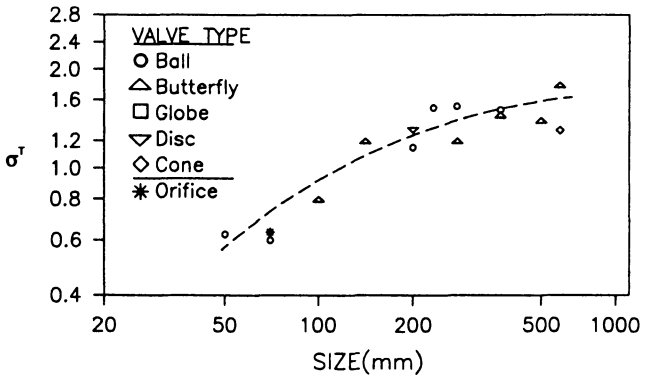

Figure 1.3. Critical σ_T for various valves. (From Young, 1989, with permission.)

$\sigma_T = 0$ corresponds to choking. For various sizes of orifice in a 7.5-cm diameter pipe, inception, corresponding to intermittent bursts of cavitation, occurs when σ_T is about 1. The onset of continuous cavitation occurs at a σ_T around 0.6. As shown in Figure 1.3, for various types of valves the critical values of σ_T corresponding to continuous cavitation increase with the size of the component.

1.3. Acoustic Cavitation

Though sound in the audible range has no effect on chemical reactions, ultrasound makes available a range of energies on time scales that are not available from any other source. The interest of chemists in power ultrasound has been established, whether it be to improve yields, speed up chemical or physical processes, use unpurified solvents or reagents, replace phase-transfer catalysts, permit the reaction to occur under milder conditions, or as seems in some cases, completely switch the reaction pathways. The reason for this has been the formation and implosion of cavities during pressure cycles of ultrasound in the frequency range of 22 kHz to 1 MHz.

The range of human hearing is from about 16 Hz to 16 kHz, with middle C at 261 Hz. The grasshopper operates at around 7 kHz. Ultrasound is the name given to sound waves having frequencies higher than those to which the human ear can respond, i.e. > 16 kHz. The upper limit of ultrasonic frequency is approximately 5 MHz for gases and 500 MHz for liquids and solids. While there are reports of chemistry being performed with audible and subaudible (i.e., infrasound) frequencies, by far the majority of sonochemistry work uses ultrasound. The uses of ultrasound within the large frequency range may be broadly divided into two areas: low power, high frequency (1–10 MHz), which is the ultrasound normally used for diagnostic purposes, medical scanning, and chemical analysis; and high-power, low

frequency (20–100 kHz), which is normally used for cleaning, plastic welding, and chemical reactions such as those considered in this monograph. The aim of high-power ultrasound is to effect a permanent chemical or physical change in a material. To achieve this, a relatively high power density (from less than 1 W to thousands of watts cm^{-2}) is required. The energy output produces cavitation and microstreaming in liquids. Various sound frequencies and their potential applications are shown graphically in Figure 1.4.

The chemical effects of ultrasound do not arise from any direct input of sonic energy to species at a molecular level. For example, the velocity of sound in water is 1500 ms^{-1} and the frequency range for ultrasound is between 20 kHz and 10 MHz. Hence the wavelength of the vibrations generated is in the region of 7.5 to 0.015 cm. That is, the direct energy output is not sufficient to produce chemical reactions. A direct comparison with the electromagnetic spectrum shows that it corresponds to the energy associated with long-wave radio broadcasts.

Sound of any frequency passes through an elastic medium as a longitudinal wave, i.e., a series of alternate compressions and rarefactions. This creates an acoustic pressure in the medium, P_A, which varies with time, t, as shown below:

$$P_A = P_{max} \sin 2\pi\nu t \tag{1.9}$$

where ν is the frequency and P_{max} is the maximum pressure amplitude. This equation defines an acoustic intensity, I, as the energy transmitted through 1 m^2 of fluid per unit time, as represented by

$$I = (P_{max})^2/2\,\rho c \tag{1.10}$$

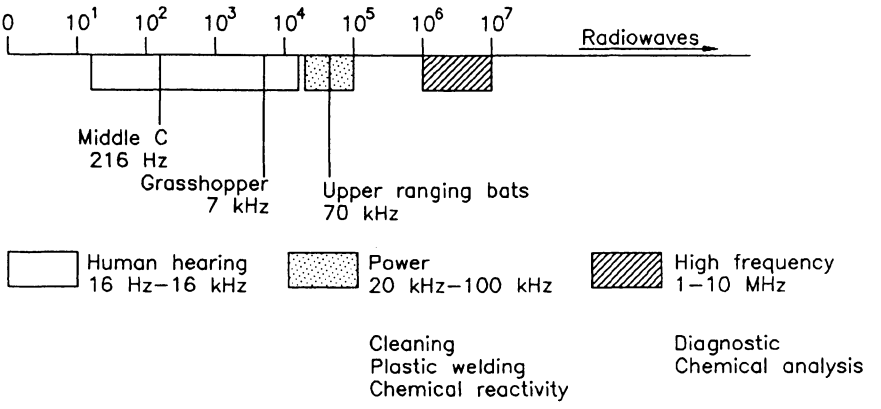

Figure 1.4. Range of acoustic frequencies (cps/Hz). (From Mason, 1990b, and Mason and Lorimer, 1988, with permission.)

where ρ is the density of the fluid in which the speed of sound is c.

For sonochemical applications, the usual unit of intensity is W cm^{-2} and the larger the intensity, the greater the value of P_A and the greater the displacement of molecules. Typical sonochemistry intensity–maximum acoustic amplitude values are given in Table 1.1.

Ultrasound intensity varies with distance, d, from its source due to attenuation promoted by viscous forces, which results in the heating of the liquid, as represented by

$$I = I_0 \exp(-2\alpha d) \tag{1.11}$$

where α is the absorption coefficient and is dependent on a range of factors, such as the thermal conductivity and viscosity of the medium. At constant temperatures, the ratio (α/v^2) must also remain constant so that attenuation is larger at higher frequencies.

Larger α values result in greater attenuation. Thus high frequencies are attenuated more rapidly than low frequencies. One can use Eq. (1.11) to calculate the source intensities, I_0, necessary to give an acoustic intensity, I, of 20 W cm^{-2} at a depth of 10 cm, i.e., a typical sonochemical reaction vessel. The results are summarized in Table 1.2. The results shown in this table indicate that higher the frequency of the ultrasound, the greater must be the initial intensity to provide an equivalent intensity at an equivalent depth. The results also show why sonochemistry is performed in the low-frequency (20–100 kHz) region, where there is minimal attenuation of sound intensity.

TABLE 1.1. Acoustic Intensity versus Pressure Amplitude[a]

Intensity (W cm^{-2})	P_A (atm)
0.1	0.54
0.2	0.76
0.5	1.21
1.0	1.71
2.0	2.42
5.0	3.82
10.0	5.41
20.0	7.65
50.0	12.10
100.0	17.15

[a]From Mason (1990b) with permission.

TABLE 1.2. Frequency–intensity Relationships[a]

Frequency	I_0 (W cm^{-2})
20 kHz	20.0
1 MHz	30.7
20 MHz	112.0

[a]From Mason (1990b) with permission.

Since the coupling of the sound field to the medium is imperfect, sonication causes increased molecular motion and, at the very least, this promotes very efficient mass transfer and mixing and thus can enhance the rates of chemical reactions. It can also lead to the disruption of liquid–liquid phase boundaries and efficient emulsification; however, the origin of most sonochemical effects is more complex.

Acoustic pressure varies over a range of several atmospheres at kilohertz frequencies. The characteristic effects of ultrasound actually arise from the manner in which sound is propagated through the media. Longitudinal molecular vibration in a liquid generates a series of compressions and rarefactions, which are simply areas of high and low local pressure. When solvent molecules are torn apart with sufficient force during a rarefaction, cavities are formed at the spots where the pressure in the liquid drops well below its vapor pressure. This can create a series of gas- and vapor-filled bubbles for which a variety of fates can be envisaged. In practice, this occurs at pressures much less than those required to overcome the tensile strength of a liquid since there are always minute dust particles or dissolved gases present that act as nucleating sites.

Cavitation is initiated at nucleation sites where the tensile strength is dramatically lowered. Possible sites of reaction induced by cavitation are illustrated in Figure 1.5. For both liquid and liquid–solid systems, as shown in Table 1.3, water is a more suitable liquid medium than an organic liquid for the cavitation. Thus sonochemistry is an attractive technology for the conversion of aqueous waste. An obvious site would be small gas bubbles present in the liquid. Free gas bubbles, however, present a double bind: small ones of the size needed for acoustic cavitation (a few microns in radius) redissolve in a few seconds, whereas larger ones rapidly rise to the surface. The nucleation mechanism generally accepted at this time involves gas entrapped in small-angle crevices of particulate contaminants. As the crevice-stabilized nucleus is subjected to large, negative acoustic pressures, the bubble column grows, releasing small free bubbles into solution or undergoing violent collapse itself. Those actions that remove such nucleation sites (e.g., ultrafiltration to remove particulates) thus increase the cavitation threshold. In liquids undergoing cavitation, it should be noted that after the initial cycle of cavitation, the implosive collapse of

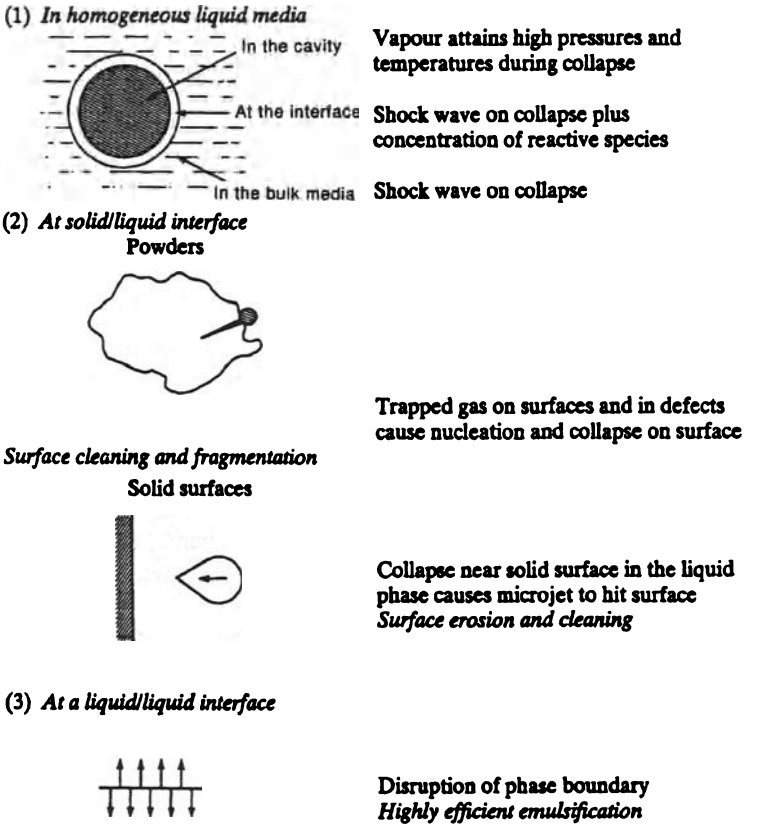

Figure 1.5. Possible sites of reaction induced by cavitation. (From Mason and Lorimer, 1988, with permission.)

bubbles generates microcavities, which can then serve as nucleation sites for the next cycle.

Flynn (1964) proposed the generally accepted division of cavitation phenomenon in liquids into (1) transient cavitation, in which a short-lived bubble undergoes large excursions of size in a few acoustic cycles and may terminate in a violent collapse; and (2) stable cavitation, in which a bubble oscillates many times with a limited change about its equilibrium radius. In practice, however, this distinction is of limited utility because both stable and transient cavitation may occur simultaneously in a solution, and a bubble undergoing stable cavitation may change to transient cavitation. The oscillatory behavior of cavities in an acoustic field has been well described by a variety of mathematical models. One can easily calculate from

TABLE 1.3. Comparison of Ultrasonic Cavitation Intensity in Various Liquids[a]

No.	Liquid	Bp/°C	Maximum cavitation intensity for a 1/2 liquid column (46 kHz) (%)	Temperature at which cavitation reaches maximum intensity/°C
1.	Water	100	100	35
2.	Styrene	146	74	37
3.	Toluene	111	71	29
4.	Tetralin	207	70	55
5.	Cyclohexane	155	70	36
6.	Morpholine	128	65	50
7.	Xylene	137	64	26
8.	Ethylene glycol	197	61	93
9.	Cyclopentanol	141	59	49
10.	Trichloroethylene	87	58	20
11.	Glycerine	290	57	85
12.	*n*-Amyl acetate	149	57	18
13.	Tetrachloroethylene	121	56	42
14.	*n*-Butyl acetate	126	56	21
15.	Pyrrole	130	55	40
16.	Methanol	65	52	19
17.	Chloroform	61	50	–3
18.	*n*-Amyl alcohol	137	47	23
19.	Ethanol	78	46	21
20.	Ethyl acetate	77	45	9
21.	Acetone	56	44	–36
22.	*n*-Butanol	118	43	32
23.	Benzene	80	43	19
24.	*n*-Propanol	97	42	27
25.	1,1,1-Trichloroethane	74	41	18
26.	Dichloromethane	40	38	–40
27.	Methyl acetate	57	38	–32
28.	Naphtha	242	38	35
29.	Isopropanol	82	38	16
30.	Formic acid (85%)	101	37	30

[a]From Mokry and Starchevesky (1993) with permission.

such models that at 20 kHz, a typical frequency of laboratory ultrasonic irradiations, the resonance size of cavities before implosive collapse will be ~170 μm, and at 1 MHz, ~ 3.3 μm. The dynamic process of bubble collapse has been observed by Lauterborn (1980b) and others by ultrahigh-speed photography of laser-generated cavitation, and the agreement between theory and experiment is remarkably good.

1.4. Optic and Particle Cavitation

As shown in Figure 1.6, optic and particle cavitation occurs when an intense energy is deposited on a liquid. Optic cavitation occurs when a liquid is irradiated with light of high intensity, such as large pulses of a Q-switched ruby laser. Under these conditions, breakdown of the liquid occurs and bubbles are formed that can be observed by a high-speed rotating mirror camera.

Optic cavitation can be achieved by many other laser systems which are capable of delivering the necessary intensity and energy in a short enough time, such as the neodymium glass or any laser used in nuclear fusion studies, provided the liquid under study is transparent enough for the wavelength of the laser. This type of cavitation can be observed easily through holography owing to its three-dimensional image storage capability. Holography can also be used to produce multiple breakdown sites in the liquid for bubble interaction studies.

In optic cavitation, photons are used to rupture the liquid. There is no reason why other types of elementary particles such as protons and neutrinos cannot accomplish a similar breakdown in the liquid. This type of cavitation is generally known as particle cavitation. In this type of cavitation, when the charged particle is sent through the liquid, it leaves an ionization trail for a fraction of a second. Some of the energy from these ions goes into a few fast electrons, which can give up about 1000 eV of energy in a small volume to produce rapid local heating. If the liquid has been superheated by expansion, boiling will occur along the track and this will result in the formation of a line of tiny bubbles. As in the other cases, a threshold condition is needed for this type of cavitation to occur. Both optic and particle cavitations are largely used to study bubble dynamics and the associated reactions for a single cavity and its implosion, as well as interactions among multiple cavities under a controlled environment.

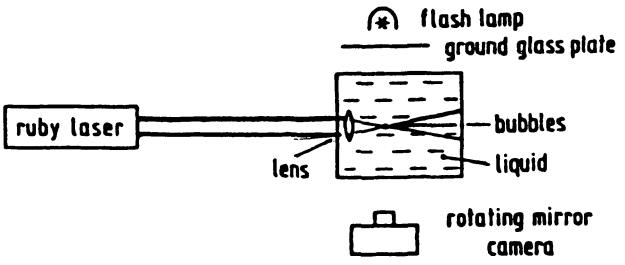

Figure 1.6. Schematic diagram of the set-up for optic cavitation. (From Lauterborn 1972 and 1980, with permission.)

2

CAVITATION BUBBLE DYNAMICS

2.1. INTRODUCTION

The basic problem in understanding bubble dynamics during the cavitation process is determining the pressure and velocity fields in the two-fluid medium along with the motion of the bubble wall under the influence of time-dependent (hydrodynamic, acoustic, or optical) pressure. In this chapter, differential equations describing the motion of a single cavity and a cluster of cavities are developed which indicate how the radius of a cavity (or cluster volume) varies with time. The basic physics of the problem is very complex. The complications arise from the following facts:

- The bubble interior is composed of both vapor and gas in an unknown ratio.
- Many energy losses are involved in damped oscillations of a cavity.
- A number of discontinuities, such as heat conduction, viscosity, compressibility, surface tension, mass transfer, diffusivity and temperature occur at the phase interface, and these have not been sufficiently quantified yet.

In cavitation bubble dynamics, the problem to be solved is a two-phase hydrodynamic one in which two phases are coupled through a moving bubble wall. This coupling is not strictly mechanical, but is also one involving mass and heat transfer across the bubble wall (i.e., rectified heat and mass diffusion). The mass transfer may consist of gas diffusion in and out of a liquid and evaporation–condensation of the liquid. Both heat and mass transfer effects are discussed in a separate section. Models considering these matters are briefly discussed in this chapter. Each of these models, with appropriate adjustments, can be applied to hydrodynamic, acoustic, and optical cavitations.

2.2. BUBBLE DYNAMICS

Consider a spherical bubble in an infinite liquid. For such a bubble, all the physical parameters are a strong function of r, i.e., the distance from the center of the bubble. So the physical picture can be imagined as a moving spherical bubble wall separating gas or vapor from a bulk liquid.

Application of the laws of conservation of mass, momentum, and energy will enable one to find the value of velocity and pressure at any point where the bubble oscillates under the influence of time-varying pressure. Conservation of mass gives an equation of continuity that does not have any constraint on its applicability, while conservation of momentum and energy are space dependent, i.e., conservation of momentum can be applied to any point in the system, while conservation of energy has to be applied to the complete system.

If the bubble velocity is small compared with the rate of variation in any other parameter (for example, pressure, temperature, and concentration of noncondensable gas) we can assume that these are constant throughout the bubble, i.e., a uniform bubble interior can be assumed. Neppiras (1980) has given the following equations for this general case as

Equation of continuity:

$$\frac{\partial \rho}{\partial t} + \frac{\partial(\rho u)}{\partial r} + \frac{2\rho u}{r} = 0 \tag{2.1}$$

Equation of momentum: (liquid)

$$\frac{\partial u}{\partial t} + u\frac{\partial u}{\partial r} = -\frac{\partial P}{\partial r} \tag{2.2}$$

Equation of energy:

$$\rho S_v\left(\frac{\partial T}{\partial r} + u\frac{\partial T}{\partial r}\right) = -P\left[\left(\frac{\partial u}{\partial r} + \frac{2u}{r}\right) + \frac{4\mu}{3}\left(\frac{\partial u}{\partial r} - \frac{u}{r}\right)^2 + k\left(\frac{\partial^2 T}{\partial r^2} + \frac{2}{r}\frac{\partial T}{\partial r}\right)\right] + \rho q \tag{2.3}$$

where S_v is specific heat capacity at a constant volume and q is the heat flux (energy flow per unit mass per unit volume).

Gas diffusion in liquid:

$$\frac{\partial C}{\partial t} + u\frac{\partial C}{\partial r} = D\left(\frac{\partial^2 C}{\partial r^2} + \frac{2}{r}\frac{\partial C}{\partial r}\right) \tag{2.4}$$

where C is the concentration of dissolved gas and D is the diffusivity of gas.

The boundary conditions at the bubble wall $r = R(t)$ are

$$D\frac{\partial C}{\partial r} = \frac{1}{4\pi R^2}\frac{\partial}{\partial r}\left(\frac{4}{3}\pi R^3 \rho_g\right) \tag{2.5}$$

$$P + \frac{2\sigma}{R} = P_T + \frac{4\mu}{3}\left(\frac{\partial u}{\partial r} - \frac{u}{r}\right) \tag{2.6}$$

The laws of mass and thermal diffusion in the liquid give

$$K\frac{\partial T}{\partial r} = \frac{1}{4\pi R^2}\frac{d}{dt}\left(\frac{4}{3}\pi R^3 \rho T\right)\left[L + \frac{4\mu}{3\rho}\left(\frac{\partial u}{\partial r} - \frac{u}{r}\right)\right] + \rho_T \frac{RC_v}{3}\frac{\partial T}{\partial t} + P_T u \tag{2.7}$$

where ρ_T is the density of the total gas content.

The boundary condition at $r = \infty$ for time-dependent pressure is as follows:

$$P = P_v + \frac{(P_f - P_v)}{(L/V)}t \tag{2.8}$$

for hydrodynamic cavitation (assuming linear pressure recovery).

$$P = P_0 - P_A \sin \omega t \qquad \text{for acoustic cavitation.} \tag{2.9}$$

The equation of state for liquid can be taken as

$$\rho = \text{constant} \tag{2.10}$$

i.e., an incompressible liquid. The equation for state of gas can be taken as the perfect gas equation:

$$PV = R_g T \tag{2.11}$$

This set of eleven equations, along with their boundary conditions, describes the pressure, temperature, velocity, and concentration behavior of bubbles.

2.2a. Bubble Nuclei: Blake Threshold

The theoretical tensile strength of water at room temperature is about 1000 atm. This implies that a sound wave used to induce cavitation should have a pressure amplitude of about 1000 atm. However, cavitation is observed with a pressure

amplitude of about 1 atm, implying that preexisting nuclei or sites for nucleation and growth of bubbles assist cavitation. The most obvious nucleus to consider is a small free spherical bubble in a liquid filled with a mixture of the liquid vapor and any gas dissolved in the liquid.

In spite of the physical fact that a bubble never achieves equilibrium, in the present analysis we proceed on an assumption of equilibrium. Neglecting vapor pressure, we have

$$P_g = P_0 + \frac{2\sigma}{R_0} \tag{2.12}$$

where P_g is pressure in the gas bubble, P_0 is ambient liquid pressure, R_0 is initial radius of the bubble, and σ is the surface tension.

Now rearranging

$$R_0 = \frac{2\sigma}{(P_g - P_0)} \tag{2.13}$$

let us call this value of R the critical radius R_c for stability. Therefore,

$$R_c = \frac{2\sigma}{(P_g - P_0)} \tag{2.14}$$

We can see that this is an unstable condition for if, $R < R_c$, the surface tension term $2\sigma/R$ predominates and the bubble contracts; and if $R > R_c$, the gas pressure P_g predominates and the bubble expands indefinitely.

A bubble may be destabilized by the following four events:

rise due to buoyancy
dissolution due to diffusion of gas outside the bubble
contraction due to surface tension
growth due to gas pressure

The minimum pressure amplitude, P_A, necessary for the growth of a bubble of radius R_B can be obtained with following assumptions: (1) the bubble is in a state of unstable equilibrium. (2) The bubble is rising slowly and dissolving.

Following Noltingk and Neppiras (1950), Neppiras (1980), Neppiras and Noltingk (1952) and Blake (1949), we note that if the bubble is in equilibrium, then the pressure inside must be $(P_0 + 2\sigma/R_B)$ at $t = 0$. At $t > 0$, the change in the size of the bubble can be assumed to be a result of the application of ultrasound and the new equilibrium condition is

$$\left(P_0 + \frac{2\sigma}{R_B}\right)\left(\frac{R_B}{R}\right)^3 = P_0 - P_A + \frac{2\sigma}{R} \tag{2.15}$$

The left-hand term represents the gas pressure in the bubble due to isothermal expansion. On the right, P_A is the peak negative acoustic pressure. The minimum value of the acoustic pressure required to achieve the steady growth of the bubble may be obtained by differentiating the pressure with respect to the bubble radius.

$$\frac{\partial(P_A - P_0)}{\partial R} = 0 \tag{2.16}$$

This gives

$$P_A - P_0 = \frac{4\sigma}{3R^*} \tag{2.17}$$

where

$$R^* = \sqrt{\left[\frac{3R_B^3(P_0 + 2\sigma/R_B)}{2\sigma}\right]} \tag{2.18}$$

and is called the *critical radius.*

Solving for P_A in terms of the initial bubble size, we find P_B, which is known as the Blake threshold pressure (Walton and Reynolds, 1984)

$$P_B = P_0 + \frac{8\sigma}{9}\left[\frac{3\sigma}{2(P_0 + 2\sigma/R_B)R_B^3}\right]^{1/2} \tag{2.19}$$

On approximation this gives

$$P_B = P_0 + 0.77\left(\frac{\sigma}{R_B}\right) \quad \text{when} \quad \left(\frac{2\sigma}{R_B}\right) >> P_0 \tag{2.20}$$

and

$$P_B = P_0 + \frac{8\sigma}{9}\left(\frac{3\sigma}{2P_0R_B^3}\right)^{0.5} \quad \text{when } P_0 >> \left(\frac{2\sigma}{R_B}\right) \tag{2.21}$$

R_B is the minimum bubble radius that will grow according to the Blake threshold. One major constraint on the application of this equation for P_B is that it can be

applied only to quasi-static processes since it has neglected inertial and viscous effects. However, it can be applied to systems where the frequency of the applied sound field is very much less than the natural oscillation frequency of the bubble. The above procedure is the basic one for estimating the pressure threshold required for steady growth of the bubble. More information about this can be found in Flynn (1962), Blake (1949), and Knapp *et al.* (1970).

2.2b. Dynamic Equations of a Spherical Bubble: Analysis of an Empty Bubble

An empty spherical bubble undergoing either an expansion or contraction can be considered as basis for the initial analysis (Figure 2.1). If R is the radius of the bubble wall at time t, then dR/dt is the radial velocity. Let dr/dt be the simultaneous radial velocity in the liquid space at any distance r. Thus with the assumption of the incompressibility of the liquid media:

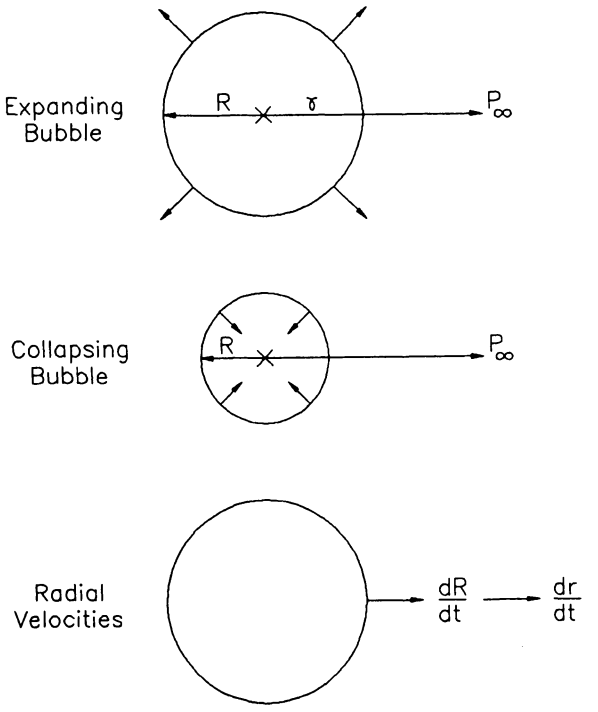

Figure 2.1. Expanding and collapsing bubbles. (From Young, 1989, with permission.)

$$\frac{dr}{dt} = \frac{R^2(dR/dt)}{r^2} \tag{2.22}$$

The radial motion of the bubble is assumed to be irrotational and therefore the velocity potential is given as

$$\Phi = -\int_r^\infty \frac{dr}{dt}\, dr = \frac{-R^2(dR/dt)}{r} \tag{2.23}$$

If P is the pressure in the liquid of a density ρ at a distance r, and P_∞ is the pressure in the liquid at infinity, then the equation of motion of the liquid is given by Bernoulli's theorem as

$$\frac{P_L - P_\infty}{\rho} = \frac{2R\left(\frac{dR}{dt}\right)^2 + R^2\left(\frac{d^2R}{dt^2}\right)}{r} - \frac{1}{2}\frac{R^4\left(\frac{dR}{dt}\right)^2}{r^4} \tag{2.24}$$

To consider the motion of a bubble wall, we put $r = R$ and get

$$\frac{P_L - P_\infty}{\rho} = R\left(\frac{d^2R}{dt^2}\right) + \frac{3}{2}\left(\frac{dR}{dt}\right)^2 \tag{2.25}$$

where $P_L = P(t)$ = pressure in the liquid at the bubble wall. This is the fundamental equation of bubble dynamics.

2.2c. Dynamics of a Gas Bubble

Next, we consider the dynamics of a bubble where the gas diffuses in and out during its oscillations (Figure 2.2). In this case, the gas that entered in the bubble during its expansion opposes the reverse motion (i.e., contraction) during the negative half-cycle of the operating acoustic pressure and prevents the bubble from collapsing.

We can apply the ideal gas law to this and write

$$P_g\left(\frac{4\pi}{3}R^3\right) = R_g T \tag{2.26}$$

where P_g is the gas pressure and R_g is the gas constant.

According to the gas law for adiabatic changes, that is, $P_g\,[(4\pi/3)R^3]^\gamma$ is constant where γ is the ratio of the specific heats of a gas, the initial pressure inside the gas

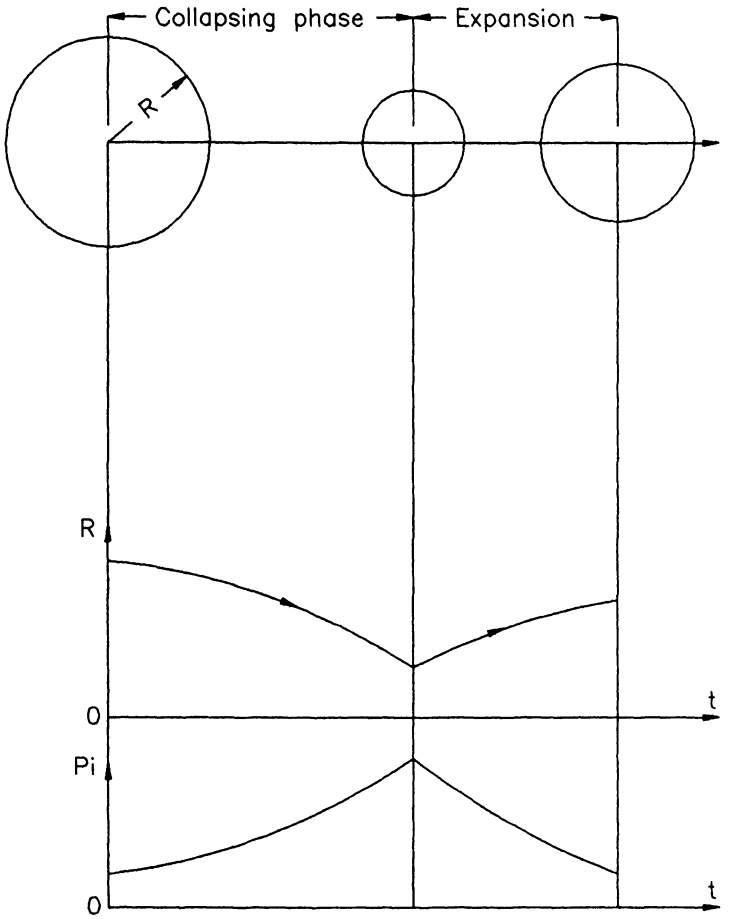

Figure 2.2. Schematic radius-time and pressure-time curves for a gas-filled spherical collapsing bubble. (From Young, 1989, with permission.)

bubble is given, according to Eq. (2.12) as $(P_0 + 2\sigma/R_0)$ where P_0 is the ambient pressure in the liquid and σ is the surface tension. If the radius changes from R_0 to R at constant temperature, the gas pressure is given as

$$P_i = \left(P_0 + \frac{2\sigma}{R_0}\right)\left(\frac{R_0}{R}\right)^{3\gamma} \tag{2.27}$$

Substituting this in Eq. (2.25) we get

$$R\frac{d^2R}{dt^2}+\frac{3}{2}\left(\frac{dR}{dt}\right)^2=\frac{1}{\rho}\left[\left(P_0+\frac{2\sigma}{R_0}\right)\left(\frac{R_0}{R}\right)^{3\gamma}-\frac{2\sigma}{R}-P_\infty\right] \tag{2.28}$$

This equation was derived by Noltingk and Neppiras (1950) and Neppiras and Noltingk (1952) in 1950. In this equation the viscous effects were neglected. Poritsky (1952) modified this equation to add the viscous effects. He showed that the viscous term arises in the boundary conditions only, rather than through the Navier–Stokes equation. If μ is the shear viscosity of the liquid, we now have

$$R\frac{d^2R}{dt^2}+\frac{3}{2}\left(\frac{dR}{dt}\right)^2=\frac{1}{\rho}\left[\left\{P_0+\frac{2\sigma}{R_0}\right)\left(\frac{R_0}{R}\right)^{3\gamma}-\frac{2\sigma}{R}-\frac{4\mu}{R}\left(\frac{dR}{dt}\right)-P_\infty\right] \tag{2.29}$$

This equation is the Rayleigh–Plesset equation. The assumptions involved in its derivation are:

1. The bubble has a spherical geometry during its entire lifetime.
2. There are no temperature and density gradients inside the bubble, i.e., there is a uniform bubble interior.
3. No body forces such as gravity are present.
4. The liquid is incompressible.
5. There is a constant volumetric fraction of gas and vapor in the bubble interior during its oscillations.
6. The partial pressure of the gas inside the bubble is predominant and the effect of vapor pressure is negligible.
7. Only one gas bubble or cavity is considered at a time.
8. There is no interference from dissolved gases.
9. Collapse is adiabatic and hence heat and mass transfer effects are neglected.
10. The effect of turbulence on bubble behavior is neglected.

This equation was also derived by Apfel (1981) in an interesting manner. The kinetic energy of a mass of liquid surrounding a pulsating sphere of radius R is given by $1/2\ [M_{\text{eff}}(dR/dt)^2]$, where M_{eff} is the effective mass felt by a sphere and is given by three times the mass of liquid that would fill the sphere, that is $M_{\text{eff}} = 3\rho\ [(4\pi/3)\ R^3]$, where ρ is the liquid density.

This kinetic energy minus the energy dissipation at the surface due to viscous effects is equal to the work done by σ and the internal and liquid pressures P_i and P_0, respectively. This can be expressed as

$$\frac{1}{2}M_{\text{eff}}\left(\frac{dR}{dt}\right)^2 - \int_{R_0}^{R}\left[-\frac{4\mu}{R}\left(\frac{dR}{dt}\right)\right]4\pi R^2\,dR = \int_{R_0}^{R}\left(P_i - P_0 - \frac{2\sigma}{R}\right)4\pi R^2\,dR \qquad (2.30)$$

where μ is the viscosity of the liquid and R_0 is the initial radius. Differentiating with respect to R and dividing by $4\pi R^2\rho$ yields

$$R\frac{d^2R}{dt^2} + \frac{3}{2}\left(\frac{dR}{dt}\right)^2 + \frac{4\mu}{\rho}\frac{(dR/dt)}{R} + \frac{2\sigma}{\rho R} + \frac{P_0 - P_i}{\rho} = 0 \qquad (2.31)$$

The first two terms in this equation represent the inertial effect; the next term is the effect of viscous stresses at the surface; the fourth term represents the surface tension effect; and the final term is the pressure effect.

2.2d. Equation Involving Compressibility of a Liquid

During collapse the bubble wall velocity exceeds the velocity of sound in the cavitating medium and in such cases the assumption of incompressibility is not valid. The simplest and most practical assumption in this regard will be that of constant stiffness and therefore the equation of state can be defined as $(\partial P/\partial\rho) = C^2$. However, this assumption restricts the applicability of the analysis to only those cases where the bubble wall velocity is smaller than the velocity of sound in water. Also, it introduces the effect of loss of energy by sound radiation. Flynn (1964) then showed that if we neglect surface tension and viscosity, Eq. (2.31) yields the acoustic approximation

$$R\frac{d^2R}{dt^2} + \frac{3}{2}\left(\frac{dR}{dt}\right)^2 = \frac{1}{\rho}\left[P_L + \frac{R}{C}\left(1 - \frac{(dR/dt)}{C}\right)\frac{dP_L}{dt} - P_\infty\right] \qquad (2.32)$$

In Herring's (1941) analysis, he took into consideration not only the sound radiation but also the storage of energy in the medium through the compression of liquid. He obtained a similar equation:

$$\left(1 + \frac{2(dR/dt)}{C}\right)R\frac{d^2R}{dt^2} + \frac{3}{2}\left(1 - \frac{4(dR/dt)}{3C}\right)\left(\frac{dR}{dt}\right)^2 = \frac{1}{\rho}\left[P_L + \frac{R}{C}\left(1 - \frac{(dR/dt)}{C}\right)\frac{dP_L}{dt} - P_\infty\right] \qquad (2.33)$$

Kirkwood and Bethe (1942) stated that during bubble collapse the shock waves produced travel in the fluid medium with a velocity that is equal to the sum of the

velocities of sound and fluid. Using this approximation, Gilmore (1952) obtained the equation

$$\left(1-\frac{(dR/dt)}{C}\right)R\frac{d^2R}{dt^2}+\frac{3}{2}\left(1-\frac{(dR/dt)}{3C}\right)\left(\frac{dR}{dt}\right)^2$$

$$=\left(1+\frac{(dR/dt)}{C}\right)H+\frac{R}{C}\left(1-\frac{(dR/dt)}{C}\right)\frac{dH}{dt} \qquad (2.34)$$

where H is the difference in the liquid enthalpy between the bubble wall and infinity and C is the velocity of sound at the bubble wall. Both H and C are functions of motion, thus giving a complex but very accurate equation. A comparison of the cavity-wall velocities developed on implosion for Rayleigh, Herring–Trilling, and Gilmore models of the empty cavity is shown in Figure 2.3 (Young, 1989).

The oscillations of a bubble in a compressible liquid have also been studied by Keller and Miksis (1980), Lastman and Wentzell (1981), and Prosperetti and Lezzi (1986, 1987) using a perturbation analysis method.

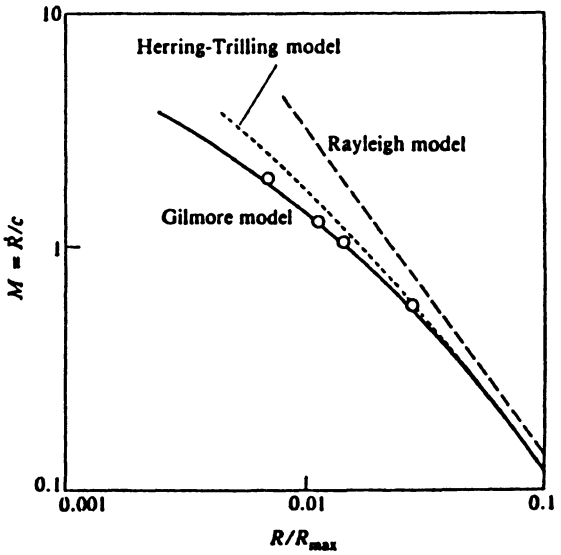

Figure 2.3. Comparison of the cavity-wall velocities developed on implosions for three models of the empty cavity: (1) Rayleigh model, (2) Herring-Trilling model, and (3) Gilmore model. (From Young, 1989, with permission.)

2.2e. Rayleigh Analysis of a Cavity and Its Extensions

According to Besant (1889), two main objectives of the formulation of bubble dynamics are (1) to determine the change in pressure at any point in the media, and (2) to calculate the time required for the cavity to grow fully, when a time-variant pressure is suddenly imposed on the fluid medium. Rayleigh (1917) worked along the same lines and in a paper published in *Philosophical Magazine* gave a complete treatment of bubble dynamics using energy considerations. This analysis, being most original and fundamental, is given below in detail.

If dR/dt is the velocity and R is the radius of a bubble boundary at a time t and dr/dt is the simultaneous velocity at any distance r (greater than R) from center, then

$$\frac{(dr/dt)}{(dR/dt)} = \frac{R^2}{r^2} \tag{2.35}$$

and if ρ is the density of the liquid, the whole kinetic energy of the liquid is

$$\frac{1}{2}\rho \int_R^\infty \left(\frac{dr}{dt}\right)^2 4\pi r^2\, dr = 2\pi\rho \left(\frac{dR}{dt}\right)^2 R^2 \tag{2.36}$$

(Note that R is constant in this integration.) Also, if we consider the hydrostatic pressure in the liquid to be constant, then

$$P_0 \text{ (the ambient liquid pressure)} = P_\infty \text{ (the liquid pressure at infinity)} \tag{2.37}$$

Therefore, if R_0 is the initial value of R, the work done by hydrostatic pressure is $(4\pi/3)\, P_0\, (R_0^3 - R^3)$, assuming isothermal compression. When these two expressions are equated, we get $2\pi\rho\, (dR/dt)^2\, R^3 = (4\pi/3)\, P_0\, (R_0^3 - R^3)$ and we get the expression for velocity as

$$\frac{dR}{dt} = \sqrt{\frac{2P_0}{3\rho}\left(\frac{R_0^3}{R^3} - 1\right)} \tag{2.38}$$

and integrating by separation of variables

$$dt = dR \sqrt{\frac{3\rho}{2P_0}\left(\frac{R_0^3}{R_0^3 - R^3}\right)} \tag{2.39}$$

and

$$t = \sqrt{\frac{3\rho}{2P_0}} \int_R^{R_0} \left[\frac{R^{3/2}}{\left(R_0^3 - R^3\right)^{1/2}} \right] dR \tag{2.40}$$

or

$$t = R_0 \sqrt{\frac{3\rho}{2P_0}} \int_\beta^1 \frac{\beta^{3/2} d\beta}{\left(1 - \beta^3\right)^{1/2}} \tag{2.41}$$

where $\beta = R/R_0$.

The time of collapse for a given fraction of the original radius is proportional to $R_0 \rho^{1/2} P_0^{-1/2}$. The time T for complete collapse is obtained by putting $\beta = 0$. Writing $\beta^3 = Z$, we have

$$\int_0^1 \frac{\beta^{3/2} d\beta}{\left(1 - \beta^3\right)^{1/2}} = \frac{1}{3} \int_0^1 z^{-1/6} (1 - z)^{-1/2} \, dZ \tag{2.42}$$

which may be expressed by means of Γ functions. Thus,

$$\tau = R_0 \sqrt{\frac{\rho}{6P_0}} \frac{\Gamma(5/6)\Gamma(1/2)}{\Gamma(4/3)} \tag{2.43}$$

therefore,

$$\tau = 0.91 \, R_0 \sqrt{\frac{\rho}{P_0}} \tag{2.44}$$

Rayleigh's analysis loses none of its simplicity if we assume that a cavity is filled with vapor at its constant equilibrium pressure P_v. The expression $(P_0 - P_v)$ then simply replaces P_0. Also, surface tension may be included with a little additional complication; the problem remains analytic.

Rayleigh's treatment can also be applied to the expansion of an empty cavity as well as to its collapse. The ambient pressure then has the form of a rectangular wave and we must assume that the cavity is drawn out from a nucleus in the form of an unwetted sphere.

It is easy to see that the radial velocity is approximately constant over most of the expansion phase, at the value $(dR/dt) = (2P_0^1/3\rho)^{1/2}$ where P_0^1 is the constant tension. It can also be shown that when $P_0 = P_0^1$, the collapse time is approximately three-quarters of the expansion time.

2.2f. Adiabatic Collapse of a Gas-Filled Cavity

The analysis described in the previous section loses its physical significance when the bubble wall radius reduces to zero. In this case, according to Eq. (2.35), the bubble wall velocity becomes infinity. This is physically absurd. To alleviate this problem, instead of an empty cavity, Rayleigh assumed a cavity that contained some gas in it initially. The compression of the gas was assumed to be isothermal rather than adiabatic, which presented a more authentic physical picture. In the isothermal case, the external work done on the system is equal to the sum of the kinetic energy of the liquid and the work done in compressing the gas; that is

$$\frac{4\pi P_0}{3}\left(R_{max}^3 - R^3\right) = 2\pi\rho\left(\frac{dR}{dt}\right)^2 R^3 + 4\pi\, QR_{max}^3 \ln\left(\frac{R_{max}}{R}\right) \tag{2.45}$$

where Q is the initial pressure of the gas, R_{max} is the maximum radius of the bubble, which is initial condition for a collapsing bubble, and $dR/dt = 0$ when

$$P(1 - Z) + Q \log Z = 0$$

where

$$Z = \left(\frac{R_{max}}{R}\right)^3 \tag{2.46}$$

Rayleigh (1917) assumed that whatever the (positive) value of Q, dR/dt returns to zero before complete collapse. The boundary oscillates between two points, one of which is initial. The equation gives, for the bubble wall velocity,

$$\left(\frac{dR}{dt}\right)^2 = \frac{2P_0}{3\rho}\left[\left(\frac{R_{max}}{R}\right)^3 - 1\right] - \frac{2Q}{\rho}\left(\frac{R_{max}}{R}\right)\ln\left(\frac{R_{max}}{R}\right) \tag{2.47}$$

In view of the short collapse time, an adiabatic rather than an isothermal collapse is more realistic. The bubble wall motion is now given by Eq. (2.47) which, if we neglect surface tension and replace the liquid pressure at infinity P by P_∞ (the liquid pressure at transient collapse), becomes

$$R\frac{d^2R}{dt^2} + \frac{3}{2}\left(\frac{dR}{dt}\right)^2 = \frac{1}{\rho}\left[Q\left(\frac{R_{max}}{R}\right)^{3\gamma} - P_\infty\right] \tag{2.48}$$

Neppiras (1980) showed that the first equation gives an energy equation for collapse

$$\frac{3}{2}\rho\left(\frac{dR}{dt}\right)^2 = P_m(Z-1) - Q\frac{(Z-Z^{\gamma})}{1-\gamma} \tag{2.49}$$

where Z is the ratio R/R_{max}. A numerical integration will give the R-t curve. This follows the Rayleigh solution for most of its trajectory. Differentiation of the above equation gives the acceleration of the bubble wall:

$$\frac{d^2R}{dt^2} = -\frac{P_m Z}{\rho R}\left[1 - \frac{Q\gamma}{P_m(\gamma-1)}Z^{\frac{1}{(\gamma-1)}}\right] \tag{2.50}$$

Setting $dR/dt = 0$ in Eq. (2.50), the minimum radius, R_{min}, is reached by the collapsing cavity and is given by

$$\frac{R_{min}}{R_{max}} = \left[\frac{Q}{P_m(\gamma-1)}\right]^{\frac{1}{3(\gamma-1)}} \tag{2.51}$$

Approximately, assuming $Q << P_m$ for a typical acoustically generated cavity, the maximum collapse speed given by $(d^2R/dt^2) = 0$ occurs at

$$\left(\frac{R}{R_{max}}\right)^{3(1-\gamma)} \approx \frac{P_m(\gamma-1)}{Q\gamma} \tag{2.52}$$

or alternately we can say $(R/R_{min})^{3(\gamma-1)} \approx \gamma$, and its value is

$$\left(\frac{dR_{max}}{dt}\right)^2 = \frac{2P_m(\gamma-1)}{3\rho\gamma}\left[\frac{P_m(\gamma-1)}{Q\gamma}\right]^{\left(\frac{1}{\gamma-1}\right)} \tag{2.53}$$

Under adiabatic compression we easily find the maximum pressure P_{max}, and maximum temperature T_{max} reached by the gas:

$$P_{max} \approx Q\left[\frac{P_m(\gamma-1)}{Q}\right]^{\left(\frac{\gamma}{\gamma-1}\right)} = QZ^{\gamma} \tag{2.54}$$

$$T_{max} \approx T_0\left[\frac{P_m(\gamma-1)}{Q}\right] = T_0 Z^{(\gamma-1)} \tag{2.55}$$

where Q is the initial pressure and T_0 is the initial temperature of the gas in the bubble.

Every bubble is associated with a resonance frequency. It is given, for a resonance size R_r, as

$$\rho\omega_r R_r^2 = 3\gamma\left[P_0 + \frac{2\omega}{R_r}\right] - \frac{2\sigma}{R_r} \tag{2.56}$$

Some interesting effects are predicted when the natural resonance frequency of the bubble matches the adiabatic collapse time. The maximum Mach number for the bubble wall velocity for a collapsing gas-filled bubble for various liquid pressures at transient collapse, P_m, is shown in Figure 2.4 (Young, 1989).

2.2g. Damping of Stable Bubbles

There are three ways in which bubble oscillations can be damped:

1. Viscosity acts on the surface as a retardant, i.e., it reduces the velocity of the bubble wall during both its contraction and its expansion. Mallock (1910) has treated this problem in detail. He considered a small shell of liquid at the bubble surface. This element has finite radial and lateral dimensions at the instant the bubble radius is at its mean position. When a bubble expands, the small liquid

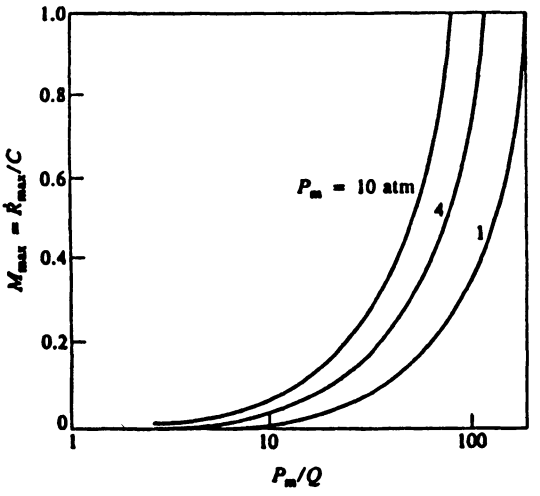

Figure 2.4. Maximum Mach number for the bubble wall velocity for a collapsing gas-filled bubble. (From Young, 1989, with permission.)

element is distorted and the radial thickness decreases while the lateral dimension increases. Since the liquid is incompressible, the distortion is not caused by a change in volume, but by viscous stresses. Consequently, more energy is required to compress the bubble than what is regained in the subsequent expansion.

The forced harmonic oscillator equation for an oscillating bubble is given as

$$m\frac{d^2\xi_b}{dt^2} + b\frac{d\xi_b}{dt} + k_s\xi_b = -4\pi R_0^2 P_A \cos \omega t \tag{2.57}$$

The damping constant due to viscous dissipation is given by

$$\delta = \frac{b}{\omega_r m} \tag{2.58}$$

To obtain an expression for b, the velocity u of the liquid at radius r is $[R_0^2(d\xi_b/dt)]/r^2$ where $d\xi_b/dt$ is the velocity at the bubble surface of radius R_0. Lamb (1975) has given the expression for the dissipation function, that is, $3\mu(du/dr)^2$ per unit volume of liquid, where μ is the coefficient of shear viscosity of the liquid. In the liquid, this volume rate of dissipation becomes $12\mu R_0^4\,[(d\xi_b/dt)^2/r^6]$. To obtain the total rate of energy loss, the latter expression is integrated over all space outside the bubble, although there are no effective contributions to the integral beyond a few bubble radii from the center. The result can be expressed in the form $b(d\xi_b/dt)^2$, where $b = b_v$ (damping constant) and is equal to $16\pi\,\mu R_0$. Letting δ_v be the contribution to damping from viscous dissipation, we obtain, by using the expression for $m = 4\pi R_0^3\rho$,

$$\delta_v = \frac{b_v}{\omega_r m} = \frac{16\pi\,\mu R_0}{\omega_r m} = \frac{4\mu}{\rho\omega_r R_0^2} \tag{2.59}$$

Here $\omega_r = 2\pi f_r$, where f_r is the resonance frequency of the bubble. For an air bubble in water, $\delta_v = 0.06$.

2. Sound radiation damping occurs because an oscillating bubble radiates surface waves, thereby expending some of its energy. This energy loss can be seen from the fact that a spherical wave at the bubble surface has a component in phase with the particle velocity. If the velocity of the bubble surface is $d\xi_b/dt$, the interface pressure component is given by $\rho\, C(\omega R_0/C)^2\,(d\xi_b/dt)$, where C is the velocity of sound in liquid. The rate at which work is done by the bubble on the media per unit area of its surface is then $\rho\, C(\omega R_0/C)^2\,(d\xi_b/dt)^2$. For the entire bubble this should be multiplied by $4\pi R_0^2$, yielding $4\pi R_0^4\rho(\omega^2/C)\,(d\xi_b/dt)^2 = b_r(d\xi_b/dt)^2$. The time average of this expression is not zero and the bubble continually loses energy to the

surrounding liquid in generating a spherical wave. The damping constant δ_r arising from radiation losses is

$$\delta_r = \frac{b_r}{m\omega_r} = \frac{4\pi R_0^4 \rho}{4\pi R_0^3 \rho} \frac{\omega_r^2}{C\omega_r}$$

This gives

$$\delta_r = \frac{\omega_r R_0}{C} = \frac{2\pi f_r R_0}{C} \tag{2.61}$$

For an air bubble in water, δ_r is about 0.014.

3. Thermal damping is the result of thermal conduction from gas in the bubble to the liquid, which will tend to lower any increase in the temperature and pressure in the cavity. This thermal coupling turns out to be the most important source of damping in most cases. Devin (1954) provided a detailed survey comparing the three processes for an air bubble in water. Flynn (1964) has discussed the three forms of damping for both stable and transient conditions. The most recent account of the three forms is given by Prosperetti (1977).

Devin (1954) derived an expression for damping due to thermal conduction. The damping constant δ_t is evaluated in terms of R_0, P_0, γ, and α, where α is the ratio of R_0 to L_g, the thermal diffusion length in the gas, given by $L_g = (2D_g/\omega)^{1/2}$ where D_g is the thermal diffusivity in the gas, $D_g = k\rho/C_p$, where k is the thermal conductivity and C_p is the specific heat at constant pressure. After a complicated analysis, Devin (1954) deduced the following expression for the damping constant:

$$\delta_t = \frac{\alpha - 1}{\alpha + 2\alpha^2/3(\gamma - 1)} \approx \frac{3(\gamma - 1)}{2\alpha} \tag{2.62}$$

which is valid for large bubbles where $\alpha \geq 2.5$. For small bubbles, where $\alpha \leq 1$, the result is

$$\delta_t = \frac{2\alpha^2(\gamma - 1)}{15\gamma} \tag{2.63}$$

Very small and very large values of α correspond to isothermal and adiabatic behavior, respectively. For a bubble in water, δ_t is about 0.07. The total damping constant is calculated by adding the three contributions:

$$\delta = \delta_v + \delta_r + \delta_t \tag{2.64}$$

Few reported experimental measurements (Schneider, 1949; Hickling and Plesset, 1964) agree reasonably well with the numerical predictions obtained from the above sets of equations.

2.2h. Modifications for Hydrodynamic Cavitation

In earlier sections a general equation was presented that takes into account the effects of viscosity and surface tension on the gas content of a cavity. The bubble behavior is a function of applied pressure, which in turn is time dependent. In the case of acoustic cavitation, it is represented as $P_0 - P_A \sin \omega t$ where P_A is the peak amplitude pressure and ω is the angular frequency. In hydrodynamic cavitation, the cavity collapse is a result of pressure recovery from the lowest pressure encountered at the vena contracta of the orifice. The distance of the recovery of pressure has been converted into a time scale by dividing it by the velocity of the fluid in the pipeline. Thus, P_∞ in the Rayleigh–Plesset equation for the case of hydrodynamic cavitation is replaced by

$$P_\infty = P_v + (P_2 - P_v)\frac{t}{(L/V)} \tag{2.65}$$

where P_v is the vapor pressure of the medium that is equivalent to absolute pressure at the vena contracta for the initiation of the cavity and P_2 is the final recovered pressure. The value of P_2 and L/V (equivalent to $1/f$) can be varied independently; this is similar to the independent variations of acoustic pressure amplitude and frequency of irradiation in the case of acoustic cavitation.

Role of Turbulence. The reexpansion of flow downstream of the orifice results in the formation of eddies that are responsible for turbulence (Kolmogoroff, 1941a, b, c). The generation of turbulence causes fluctuations in the velocity of the flow downstream of the orifice. In turbulent flow, the instantaneous velocity in the x direction is given as

$$v_x = \bar{v}_x + \bar{v}'_x \tag{2.66}$$

where $\bar{v}_x$ is the time-averaged velocity at any point in the flowing fluid and $\bar{v}'_x$ is the instantaneous fluctuation velocity. It is convenient to express the amplitude of the fluctuating velocities in the x direction as $(\bar{v}_x)^2$, which is the mean of the squares of the fluctuation velocities, this being necessarily positive. One can also take the square root of the mean of squares to get a root-mean-square fluctuating velocity $\bar{v}'_x$. A similar treatment can be used for fluctuations in other directions. The turbulent kinetic energy per unit mass is

$$K.E. = -1/2\ [(\overline{v}_x')^2 + (\overline{v}_y')^2 + (\overline{v}_z')^2] \tag{2.67}$$

Hence the rate of loss of kinetic energy due to turbulence is given as

$$P_M = -1/2\ d/dt\ [(\overline{v}_x')^2 + (\overline{v}_y')^2 + (\overline{v}_z')^2] \tag{2.68}$$

Here we make an assumption of isotropic turbulence (where $\overline{v}_x' = \overline{v}_y' = \overline{v}_z'$). Then the above expression becomes

$$P_M = -3/2\ d/dt\ (\overline{v}')^2 \tag{2.69}$$

For isotropic turbulence, the fluctuation velocity v' and the length scale of the eddy (l) can be defined in terms of the power input per unit mass of the system, P_M. It is equal to the rate of dissipation of energy by a unit mass of turbulent fluid, and the relations are (Kolmogoroff, 1941a, b, c)

$$P_M = (v')^3/l \tag{2.70}$$

The frequency of the velocity perturbations within the eddies is given as

$$f_T = \overline{v}'/l \tag{2.71}$$

In the present analysis we estimated P_M by considering the permanent pressure head loss a function of the ratio of orifice-to-pipe diameter. The product of the head loss and the volumetric flow rate will give the energy dissipated due to eddy and turbulence losses. This energy divided by the mass of the water in the region of pressure recovery (typically eight pipe diameters downstream of the orifice) gives P_M. Also, the pressure drop in skin friction, which is given as (for turbulent flow)

$$\Delta P = \frac{2f' L v_p^2 \rho}{d_p} \tag{2.72}$$

is added to P_M. Here f' is the friction factor, L is the length of the pressure recovery zone, and d_p is the diameter of the pipe.

The Prandtl eddy model has been used to estimate the length scale. According to this model, the length scale is given as

$$l = 0.08\ d \tag{2.73}$$

where d is the diameter of the conduit through which fluid and associated material flow. In the region near the orifice where the fluid stream narrows down and the flow area becomes equal to the area of the orifice, the eddy size is 0.08 d_o (d_o =

diameter of the orifice). Thereafter as the stream expands and the flow area equals the area of the pipe after full pressure recovery, the scale is 0.08 d_p (d_p = pipe diameter). To find the frequency of turbulence, we have taken the average length scales at two extremes.

Now, for hydrodynamic cavitation, the pressure recovery profile is assumed to be a linear one over which turbulent pressure fluctuations can be superimposed. The pressure P_∞ (i.e., the pressure at a large distance from bubble) decides the bubble behavior. Here the local pressure without turbulence can be estimated as

$$P = P_v + (P_2 - P_v)\, t/\tau \tag{2.74}$$

where τ is the pressure recovery time.

The time for pressure recovery can be found through Newton's equations. For an assumed recovery pressure (P_2) downstream of the orifice, the velocity near the orifice can be estimated from Eq. (1.1) for $\sigma_c = 1.0$. This velocity decreases with the distance downstream of the orifice and reaches the mean pipe velocity when full pressure recovery takes place. The pipe velocity can be calculated by equating volumetric flow rate,

$$(d_o)^2 v_o = (d_p)^2 v_p \tag{2.75}$$

Given the knowledge of v_o and v_p, the time of pressure recovery can be calculated using the following two equations:

$$v_p = v_o + at \tag{2.76}$$

$$L = v_p t + 1/2\, at^2 \tag{2.77}$$

where L is the distance for the total pressure recovery, which is typically eight pipe diameters downstream of the orifice and a is the acceleration or deceleration of the fluid stream.

For simulation purposes, the downstream pressure on the orifice at a particular point was obtained by assuming a linear recovery profile in Eq. (2.74). Using this pressure and Bernoulli's equation (between that particular point and a point where full pressure recovery takes place), the velocity at that particular point was calculated (v_t). The turbulent pressure fluctuations were then superimposed over it by assuming a sinusoidal velocity variation in the instantaneous velocity. Thus the new velocity is given as

$$v_{tn} = v_t + v' \sin (2\pi f_T t) \tag{2.78}$$

where v_{tn} is also a function of time and t is the numerical integration step. Using this new turbulent velocity, the static pressure was back calculated. It is given as

$$P_t = P_v + 1/2\rho\, V_0^2 - 1/2\rho\, V_{tn}^2 - \Delta P \tag{2.79}$$

This pressure profile (shown diagramatically in Figure 1.2) can be substituted as P_∞ in Eq. (2.74). This equation can then be solved using the Runge–Kutta fourth-order method to get the radius-time and pressure-time history of bubble oscillations. The effects of various system variables on the cavity behavior obtained from this model are described in Chapter 3.

2.3. CLUSTER DYNAMICS

Research in the field of cavitation chemistry has largely concentrated on the analysis of the dynamics and collapse of a single cavity or bubble. In reality, nucleation of a number of cavities can occur in a narrow region, resulting in the formation of clusters of cavities or bubbles. Within the clusters of cavities, different cavities and bubbles are in different modes of oscillation at the same time. Here the dynamics of a single cavity are affected not only by the bulk pressure variation but also by the pressure fluctuations resulting from oscillations of adjacent bubbles. The cavities collapse successively from the outer boundary of the cluster so that those collapsing first strengthen the collapse of their successors. The experimental measurements of the pressure pulses show a mismatch with the pressure pulses obtained from the simulations of a single cavity and this observation further supports the observation that bubbles and cavities exist in the form of clusters and not individually. The formation of a cluster of cavities is graphically illustrated in Figure 2.5.

A study of the dynamics and collapse of a bubble cluster will help a designer to model and scale up a cavitation reactor in a better and more reliable way. In this section, therefore, a model illustrating the dynamics of a bubble cluster under both hydrodynamic and acoustic cavitations is described. Some important conclusions on the effects of various system parameters on cluster behavior are discussed in Chapter 3. A mathematical model illustrating cluster behavior is described below. For hydrodynamic cavitation, this model should be combined with the role of turbulence as described in Section 2.2h. For acoustic cavitation, P_∞ should be substituted from the equations in Sections 2.2a to 2.2g. The model predicts the radius and pressure pulse history of the clusters.

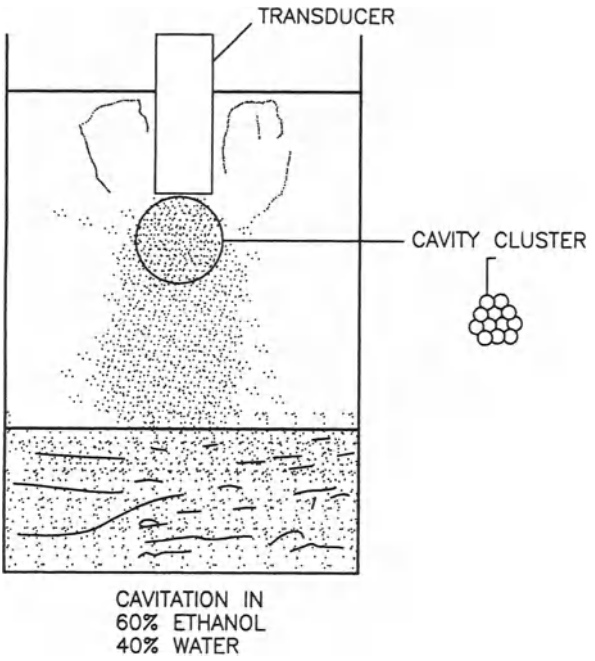

Figure 2.5. Schematics of typical cavity clusters in an alcohol–water mixture.

2.3a. Model Equations for Cluster Dynamics

In a hydrodynamic cavitation reactor, just like single cavity formation, a cluster of cavities is produced by throttling a valve downstream of a pump. When the discharge of a pump is passed through an orifice, the liquid loses its pressure head at the expense of the velocity head downstream of the orifice, and pressure falls. As a result, the dissolved gas may be liberated and if the pressure falls below the vapor pressure of the liquid, some local evaporation may occur, giving rise to vapor bubbles. When the nuclei of these bubbles are very close to each other, they form clusters that oscillate and later collapse with the recovery of pressure downstream of the orifice.

We consider a cluster of cavities that is bounded by an incompressible fluid and possibly by solid surfaces. Initially the system is supposed to be in equilibrium, the pressure inside the cluster being equal to the pressure of the surrounding liquid. An increase in the far-field pressure in the liquid with the corresponding decrease in the velocity initiates the collapse of the cluster from its free boundary, which moves toward the center as the cavities collapse. Just after the pressure increase, the energy of the system is purely potential, but as the cluster volume shrinks this energy

gradually first gets converted into kinetic energy of the liquid in the region Ω_1 outside Ω_c. As the individual cavities collapse, a part of the wave energy is radiated into the remaining cluster where it is absorbed and contributes to the further collapse of cavities. The remaining portion of the wave energy is radiated to the bulk liquid and is usually lost. Thus, the change in the sum of the potential and the kinetic energies of the system due to a small change in volume of the cluster $d\Omega_c$ (at the local pressure in the liquid surrounding the individual cavity) which is lost by radiation and dissipation can be expressed as

$$d\left[\int_{\Omega_c} P_\infty \beta' d\Omega_c + \int_{\Omega_1} 1/2\rho \times v^2 \times d\Omega_1\right] = (1-\gamma)P/2\beta'\, d\Omega_c \tag{2.80}$$

[The first term on the left-hand side (l.h.s.) in the bracket represents the potential energy of the cluster, while the second term represents the kinetic energy of the liquid. The term on the right-hand side (r.h.s.) represents the mean potential energy of the collapse of cavities.] Here ρ and v are the density and velocity in the liquid, respectively, while P is the pressure at the liquid boundary. The sound velocity in the two-phase medium and the pressure ratio across the cluster boundary give

$$P = V_{sh}^2\, P\beta' (1-\beta') \tag{2.81}$$

where V_{sh} is the velocity of the cluster boundary, and β' is measured just inside the boundary. If the cluster configuration is specified, Eqs. (2.80) and (2.81) determine the collapse equation of the cluster. For a spherically symmetrical cavity cluster of initial radius R_0 and instantaneous radius R in an infinite liquid, we have $V_{sh} = dR/dt$ and $v = (\beta'\dot{R})\, R^2/r^2$, which gives the collapse equation

$$R\left(\frac{d^2R}{dt^2}\right) + \left[\frac{3}{2} - \frac{1}{2}(1-\gamma)(1-\beta') + \frac{R}{\beta}\frac{d\beta'}{dR}\right]\left(\frac{dR}{dt}\right)^2 = -\frac{P_\infty}{\rho\beta'} \tag{2.82}$$

It should be noted that for $d\beta'/dR = 0$, $\gamma' = 1$, the equation is analogous to the spherical collapse equation of a single cavity. In spherical collapse of individual cavities, about half the collapse energy is radiated into the cluster, while in nonspherical collapse, a larger fraction is preserved. The collapse time as well as the pressure P are significantly affected by the $\beta'(R)$ function while γ' primarily affects P and thus the violence with which individual cavities collapse. Theoretically the collapse velocity becomes infinity as $R \to 0$ and P grows unrestrictedly, but the model ceases to be valid when R becomes of the order of the cavity distance. For small R, the pressure P is independent of β', but for large ones P decreases with β'.

The above sets of equations can be solved with appropriate substitutions for P for both hydrodynamic and acoustic cavitations as described in Section 2.2. The effects of various system variables on cluster behavior based on this simulation are described in Chapter 3.

2.4. HEAT AND MASS TRANSFER EFFECTS IN CAVITATION

In order to understand the cavitation phenomenon in a better way, it is necessary to understand the heat and mass transfer effects associated with bubble oscillations. Here we briefly review the literature concerning heat and mass transfer effects. The subject is covered in three parts:

rectified diffusion, i.e., mass transfer of gas through a bubble surface where heat transfer effects are neglected
rectified heat transfer in bubble oscillations (mainly oscillations of vapor bubbles)
effect of simultaneous diffusion and heat transfer on bubble dynamics (simultaneous heat and mass transfer)

2.4a. Rectified Diffusion

A concept of general interest in the area of acoustic cavitation is that of rectified diffusion. This process involves the slow growth of a pulsating gas bubble due to an average flow of mass into the bubble as a function of time. This rectification of mass is a direct consequence of the pressure field applied and can be important wherever a sufficiently intense sound field of acoustic pressure amplitude greater than 0.01 MPa or so exists in a liquid containing dissolved gas; i.e., the liquid may be undersaturated, saturated, or oversaturated with gas. In the presence of an applied sound field, however, the bubble radius is forced to oscillate about an equilibrium value, and these oscillations can prevent eventual dissolution of the bubble and even cause it to grow because of the following effects:

Area effect. When a bubble contracts, the concentration of the gas in the interior of the bubble increases, and the gas diffuses from the bubble. Similarly, when a bubble expands, the concentration of the gas decreases and gas diffuses into the bubble. Since diffusion rate is proportional to area, more gas will enter during expansion than will leave during contraction of the bubble. Therefore, over a complete cycle there will be a net increase in the amount of the gas in the bubble.

Shell effect. The diffusion rate of gas in a liquid is proportional to the gradient of the concentration of the dissolved gas.

Consider a spherical shell surrounding a bubble. When a bubble contracts, this shell expands, and the concentration of the gas near the bubble wall is reduced. Thus the rate of diffusion of gas away from the bubble is greater than when the bubble is at its equilibrium radius. Conversely, when a bubble expands, the concentration of the gas near the bubble is increased, and the rate of diffusion toward the bubble is greater than the average. The net effect of this convection is to enhance the rectified diffusion.

Both area and shell effects are necessary for an adequate description of the phenomenon. Historically, the concept of rectified diffusion was apparently first recognized by Harvey *et al.* (1944), who considered the importance of this concept in the formation of bubbles in animals. They were able to recognize the area effect that would lead to growth, and they called rectified diffusion the *principle of incremental enlargement*, recognizing that the growth during one cycle may be quite small.

Blake (1949) was the first to attempt a theoretical analysis of rectified diffusion, but considered only the area effect and thus his crude approach was in considerable disagreement with the first reported measurement by Strasberg (1976). The equation obtained by Blake for rectified diffusion was

$$\frac{dm}{dt} = \frac{2}{3}\pi D C_0 R_0 \left(\frac{P_A}{P_0}\right)(1 + 2\Phi) \tag{2.83}$$

where D is the diffusivity of gas through the liquid, C_0 is the concentration of the dissolved gas in the liquid when it is saturated at the static pressure, R_0 is the initial bubble radius, and P_A is peak pressure amplitude. $\Phi = R_0 (\pi f/D)^{1/2}$ is a parameter expressing the ratio of a bubble radius to the diffusion thickness and f is the sound frequency. The derivation of this equation assumes that a bubble pulsates isothermally and linearly and that $\Phi >> 1$. In the absence of sound, if the liquid is undersaturated, a steady diffusion occurs out of the bubble, causing it to dissolve. The steady outward diffusion in the absence of sound is given approximately by

$$\frac{dm'}{dt} = -4\pi D R_0 \left\{C_0\left[1 + \left(\frac{2\sigma}{R_0}\right)\right] - C_\infty\right\} \tag{2.84}$$

where σ is the surface tension and C_∞ is the actual concentration of the dissolved gas in the liquid far from the bubble. The threshold sound pressure can be calculated by adding Eqs. (2.83) and (2.84) and solving for P_A, setting $d(m + m')/dt = 0$. The threshold obtained by Blake was

$$P_A(t) = (6)^{1/2} P_0 \left[\frac{1 + (2\sigma/R_0 P_0) - (C_\infty/C_0)}{1 + R_0 \Phi} \right]^{1/2} \tag{2.85}$$

Pode (1953) and Rosenberg (1953) attempted to refine Blake's theory. Pode's analysis differed from Blake's in two aspects:

1. A convection term is included in the differential equation that represents the diffusion of gas through the liquid, to account for transport of gas molecules brought about by the alternating radial motion of the liquid surrounding the pulsating bubble.
2. The effect of the motion of the bubble wall on diffusion is included. Although Pode's analysis began with these factors being taken into account, apparently because of approximations made to solve the equation, the influence of the convection term disappeared and his results were not much different from those of Blake.

The importance of the convection term was demonstrated when Hsieh and Plesset (1961) included this effect in a correct way. This paper was a landmark in the development of the theory of rectified diffusion. Since the primary concern of the paper was the effect of diffusion rather than the dynamic aspects, in the analysis the oscillating pressure inside the gas bubble was given preference over the pressure in the liquid at infinity. The procedure was not very arbitrary since in the linearized approximation at steady state the pressure inside the bubble behaves in essentially the same manner as the externally applied pressure except for a phase difference and a small modification of amplitude. A paper highlighting this result was published by the same authors (1961).

The pressure within a gas bubble was assumed to be uniform and can be denoted as $P(t)$, which can be expressed as

$$P(t) = P_0 (1 - \varepsilon \sin \omega t) \tag{2.86}$$

where P_0 is the initial pressure and ω is the angular frequency of ultrasound. It is assumed that $\varepsilon << 1$ so that the linearization procedure may be carried out. It is also assumed that the gas inside a bubble behaves isothermally during expansion and compression. It follows that

$$R(t) = R_0 (1 + \delta \sin \omega t) + O(\delta^2) \tag{2.87}$$

where $-3\delta = \varepsilon$, R is the radius of the bubble at time t, and R_0 is the initial or equilibrium radius corresponding to P_0. A more general assumption regarding the thermodynamic behavior of the bubble leads to a phase difference between $(P - P_0)$ and $(R - R_0)$. This possibility is not considered since no essential new feature is introduced by this complication. Thus,

$$\int_{t_0}^{t_0+\Delta t} \Delta t = \int_s D\nabla C \, ds \tag{2.88}$$

where C is the concentration of gas dissolved in the liquid, D is the coefficient of diffusion, and the integration is over the surface S of the bubble wall. Since the bubble is assumed to be spherical, this expression simplifies to

$$\int_{t_0}^{t_0+\Delta t} 4\pi DR^2 \left[\frac{\partial C}{\partial r}\right] dt \tag{2.89}$$

The concentration C is a solution of the diffusion equation

$$\left[\frac{\partial C}{\partial t}\right] + q\nabla C = D\nabla^2 C \tag{2.90}$$

Here q is the flow velocity of the liquid. For an irrotational flow field in the liquid, it is known that $q = [(R^2/r^2)(dR/dt)]$.

The boundary conditions are specified in the following way: The amount of gas dissolved in the liquid does not change with time at a large distance from the bubble; that is, $C \rightarrow C_\infty$, a constant, as $r \rightarrow \infty$. The dissolved gas concentration in the liquid near the bubble wall is determined in accordance with Henry's law, which says that the concentration of dissolved gas at a constant temperature is proportional to the pressure. It follows that at $r = R$, $C = aP(R)$ where a is a constant characteristic of the liquid–gas combination. Also, since $C \rightarrow C_\infty$ everywhere when there is no disturbance in the equilibrium, one has $aP_0 = C_\infty$. The formulation of the boundary condition for the solution of the equation is thus

$$C = C_\infty \text{ as } r \rightarrow \infty \tag{2.91}$$

$$C = C_\infty (1 + \varepsilon \sin\omega t) \text{ at } r = R \tag{2.92}$$

The initial condition is specified as follows:

$$C(r, t) = C_\infty \quad \text{for } t \leq 0 \text{ for all } r \tag{2.93}$$

Because of the steady-state assumption, only an asymptotic solution for a large t was found. After a rigorous procedure to solve the equations, Hsieh and Plesset obtained the rate of gas flow into the bubble as

$$J = 24\pi DC_\infty R_0\delta^2\left[1 + O\left(\frac{1}{R_0\sqrt{\omega/2D}}\right) + O\left(\frac{1}{t^{3/2}}\right)\right] + S + O(\delta^2) \tag{2.94}$$

Thus, the leading term for the average rate of flow of gas into the bubble is

$$<J> = 24\pi DC_\infty R_0\delta^2 \tag{2.95}$$

Since

$$\delta = -\varepsilon/3 = -\frac{1}{3}[(P_s - P_0)/P_0] = -\frac{1}{3}(\Delta P/P_0) \tag{2.96}$$

One may also write

$$<J> = (8/3)\pi\, DR_0C_\infty(\Delta P/P_0)^2 \tag{2.97}$$

Thus, when the ratio of the pressure amplitude P_A to the mean pressure P_0 is sufficiently small, bubble growth by rectification is determined by this leading term. The mass of gas inside the bubble is

$$m = \frac{4}{3}\pi\rho_g R_0^3 \tag{2.98}$$

The mean density of the gas, ρ_g, remains unchanged during the slow growth so that

$$\frac{dm}{dt} = 4\pi\rho_g R_0^2\,(dR_0/dt) \tag{2.99}$$

Therefore the rate of increase of mass in the bubble by rectification is

$$\frac{dm}{dt} = <J> = (8\pi/3)\, DC_\infty\varepsilon^2 R_0 \tag{2.100}$$

Strasberg (1976) showed that Eq. (2.100) correctly justified the results of his measurements.

Eller and Flynn (1965) extended the analysis to include nonlinear or large-amplitude effects by treating the boundary condition of the moving wall in a slightly different way. Their approach was to separate the general problem into an equation for the motion of the bubble wall and a diffusion equation (Fick's law of mass transfer) for the concentration of gas in the liquid alone. The equation for the gas bubble motion is given as

$$R\frac{d^2R}{dt^2}+\frac{3}{2}\left(\frac{dR}{dt}\right)^2+\frac{1}{\rho}\left\{P_0\left[1-(R_0/R)^{3\eta}\right]-P_A\cos\omega t+\rho R_0\omega_r\sigma\frac{dR}{dt}\right\}=0 \quad (2.101)$$

Eller and Flynn (1965) showed that the time rate of change in the number of moles n of a gas in a bubble is given by

$$\frac{dn}{dt}=4\pi DR_0C_0\left[\left\langle\frac{R}{R_0}\right\rangle+R_0\left(\frac{\langle R/R_0\rangle^4}{\pi Dt}\right)^{1/2}\right]H \quad (2.102)$$

where C_0 is the equilibrium or saturation concentration of the gas in the liquid in moles per unit volume; the pointed brackets imply time average; t is time and H is defined by

$$H=\frac{C_\infty}{C_0}-\left\{\frac{\left\langle\left(\frac{R}{R_0}\right)^4\left(\frac{P_i}{P_0}\right)\right\rangle}{\left(\frac{R}{R_0}\right)}\right\} \quad (2.103)$$

Here C_i is the concentration of dissolved gas in the liquid far from the bubble. P_i, the pressure of the gas in the bubble at radius R, is given by

$$P_i=P_g(R_0/R)^{3\eta} \quad (2.104)$$

where η is the polytropic index. The values of R/R_0 to be used in the above equations are obtained by an expansion solution in the form

$$\frac{R}{R_0}=1+\alpha(P_A/P_0)\cos(\omega t+\delta)+\alpha^2K(P_A/P_0)^2+\ldots \quad (2.105)$$

where

$$\frac{1}{\alpha}=\left(\frac{\rho R_0^2}{P_0}\right)\left[\left(\omega^2-\omega_t^2\right)^2+(\omega\omega_t b)^2\right]^{1/2} \quad (2.106)$$

$$K=\frac{(3\eta+1-\beta^2)/4+(\sigma/4R_0P_0)(6\eta+2-4/3\eta)}{1+(2\sigma/4R_0P_0)(1-1/3\eta)} \quad (2.107)$$

$$\delta = \tan^{-1}\left(\frac{\omega\omega_r b}{\omega^2 - \omega_r^2}\right) \tag{2.108}$$

and

$$\beta = \frac{\rho\omega^2 R_0^2}{3\eta P_0} \tag{2.109}$$

ω_r is the resonance frequency of the oscillations of a bubble and is given as

$$\omega_r^2 = \frac{1}{\rho R_0}\left(3\eta P_0 - \frac{2\sigma}{R_0}\right) \tag{2.110}$$

Here b is the damping constant of bubbles and is made up of contributions from the thermal, viscous, and radiation effects.

The results of Hsieh and Plesset (1960, 1961) were essentially equivalent to those of Eller and Flynn where inertial effects were added to the Hsieh and Plesset approach. The measurements by Strasberg were extended by Eller (1972, 1975) to include both threshold and growth rate. He obtained the threshold for rectified diffusion as

$$P_A(t) = \frac{P_0}{\alpha}\left(\frac{1 + 2\sigma/R_0P_0 - C_i/C_0}{(3 + 4k)(C_i/C_0) - (1 + 2\sigma/R_0P_0)(4 - 3\eta)k}\right)^{1/2} \tag{2.111}$$

The polytropic index η is given as

$$\eta = \gamma\left(1 + d_t^2\right)^{-1}\left[1 + \frac{3(\gamma - 1)}{\chi}\left(\frac{\sin h\chi - \sin\chi}{\cos h\chi - \cos\chi}\right)\right]^{-1} \tag{2.112}$$

where

$$d_t = 3(\gamma - 1)\left[\frac{\chi(\sin h\chi + \sin\chi) - 2(\cos h\chi - \cos\chi)}{\chi^2(\cos h\chi - \cos\chi) + 3(\gamma - 1)\chi(\sin h\chi - \sin\chi)}\right] \tag{2.113}$$

and $\chi = R_0(2\omega/\alpha)^{1/2}$. Here γ is the ratio of specific heats and $\alpha = k/\rho C_p$ where k is the thermal conductivity of the gas in the bubble, ρ is the density of gas, and C_p is the specific heat at constant pressure for the gas.

Eller (1972, 1975) found that the theory was adequate in predicting the thresholds for growth by rectified diffusion but was unable to account for some large growth rates he observed. He suggested that acoustic streaming may be the cause of rates

of growth that were larger than predicted. Gould (1974) was able to directly observe gas bubble growth by rectified diffusion through a microscope and discovered that growth rates could be greatly enhanced by the onset of surface oscillations of the bubble, which in turn seemed to induce significant acoustic microstreaming. However, his attempts to apply the acoustic streaming theories of Davidson (1971) and of Kapustina and Statnikov (1970) to explain his results were not successful. Additional theoretical treatment was presented by Skinner (1970, 1972) and Eller (1972, 1975) to account for growth through resonance.

Later, the growth of gas bubbles by rectified diffusion was measured by Crum (1980), who obtained both threshold and growth rates for a variety of conditions. He extended the theory to include effects associated with the thermodynamic behavior of the bubble interior and found excellent agreement between theory and experiment for both the rectified diffusion threshold and the growth rate for air bubbles in pure water. Anomalous results were obtained, however, when a small amount of surfactant was added to water. The rate of growth of bubbles by rectified diffusion increased by a factor of about 5 when the surface tension was lowered by a factor of 2, with no discernible surface wave activity. Although some increase was predicted, the observed growth rates were much higher than expected. A slight reduction in the threshold with reduced surface tension was also observed. Some explanations offered by Crum for this anomalous behavior were that there was some rectification of mass due to surfactant on the surface of the bubble and/or microstreaming was occurring even in the absence of surface oscillations.

Crum and Hansen (1982) examined the theoretical expressions in the literature that predict the threshold and growth rate for rectified diffusion and found that the various equations have limited ranges of applicability. They obtained a set of generalized equations that have a broader range of applicability and are not limited to a specific bubble size or acoustic frequency. Also, Prosperetti (1982) in his paper generalized the Rayleigh–Plesset equation of bubble dynamics to include the effects of mass transfer and extended its applicability to non-Newtonian liquids. The equation is

$$RU_1 + \frac{3}{2}U_1^2 - \frac{J}{\rho}\left[2U_1 + J\left(\frac{1}{\rho_T} - \frac{1}{\rho}\right)\right]$$

$$= \frac{1}{\rho}\left(P_i - P_\infty \frac{2\sigma}{R} + 3\int_R^\infty \gamma^{-1}\tau_\pi dr\right) \tag{2.114}$$

where U_1 is radial liquid velocity, τ is the stress tensor, J is mass flux on the inner side of interface, ρ_T is density on the inner side of interface, and ρ is bulk liquid density.

2.4b. Rectified Heat Transfer in Bubble Oscillations

The dynamics of vapor-filled bubbles under an oscillating pressure field were considered by Finch and Neppiras (1973) and the case of a bubble containing both vapor and a foreign gas was treated by Wang (1974a, b). The important feature of these theories is the supposition that vapor bubbles can be stabilized against collapse under surface tension by an elevation of the vapor pressure inside the bubble—a process termed "rectified heat transfer." An early attempt to estimate the acoustic pressure amplitude necessary to maintain such a stabilization process for bubbles in helium was reported briefly by Finch and Neppiras. However, the first complete treatment was given by Wang. Patel *et al.* (1985) extended Wang's approach and presented the correct analysis of rectified heat transfer. A summary of their analysis is given below.

In the paper by Finch and Neppiras, the dynamics of a vapor bubble were assumed to be governed by the laws of conservation of mass, momentum, and energy. The liquid was assumed to be inviscid and incompressible and the vapor to obey the ideal gas law. Heat conduction was assumed to follow Fourier's law and the temperature and pressure of the vapor to be related by the Clausius–Clapeyron equation. The bubble wavelength was assumed to be small compared with the sound wavelength and thermal diffusion length in the vapor.

The following set of equations was found to govern the bubble behavior:

Equation of motion:

$$R\frac{d^2R}{dt^2}+\frac{3}{2}\left(\frac{dR}{dt}\right)^2=\frac{1}{\rho}\left(P_i-\frac{2\sigma}{R}-P_0+P_Ae^{j\omega t}\right) \tag{2.115}$$

Energy equation:

$$3\gamma P_v\frac{dR}{dt}+R\frac{dP_v}{dt}$$

$$=3(\gamma-1)\,\xi k(T_L)_R-\left[L-C_vT-(P_v\,4\pi R^3)/3M\right]\frac{dM_v/dt}{(4\pi R)^2} \tag{2.116}$$

Equation of state:

$$P_i\frac{4}{3}\pi R^3=M_vR_gT \tag{2.117}$$

Heat conduction equation:

$$\frac{DT_L}{Dt} = \alpha_L \nabla^2 T_L \tag{2.118}$$

Temperature-vapor pressure relation:

$$T_v - T_{L\infty} = \Phi(P_v - P_{v\infty}) \tag{2.119}$$

The unknown quantities in these five equations are R, P_v, T_v, T_L, and M_v. An approximate solution may be obtained by assuming the following linearization.

$$R = R_0(1 + a' e^{j\omega t}) \tag{2.120}$$

$$P_v = P_{v0}(1 + \psi e^{j\omega t}) \tag{2.121}$$

$$T_v = T_0(1 + \theta' e^{j\omega t}) \tag{2.122}$$

$$M_v = M_0(1 + \mu' e^{j\omega t}) \tag{2.123}$$

Here a', ψ, θ', and μ' are assumed to be much less than unity.

Area and convective heat transfer can briefly be explained as total heat transfer into the bubble.

$$\langle Q_T \rangle = \int_0^T \int_s k_L \nabla T_L \, d\bar{S} \, dt \tag{2.124}$$

For a spherical bubble

$$\langle Q_T \rangle = k_L \langle 4\pi R^2 \left(\frac{\partial T_L}{\partial r} \right)_{r=R} \rangle \tag{2.125}$$

There is no first-order heat transfer over a period, but there is a second-order net heat transfer. Rectified heat transfer resulting from $\delta'_{(1)}$ is termed the "area effect," $Q_{(1)}$. The additional heat transfer resulting from $\delta'_{(2)}$ is called the "convection effect," $Q_{(2)}$. Total heat transfer $\langle Q_T \rangle$ is

$$\langle Q_T \rangle = \langle Q_1 \rangle + \langle Q_2 \rangle \tag{2.126}$$

where

$$<Q_{(1)}> = -k_L(4\pi R_0)T_\infty|a'|\,|\theta'|\left\{0.5\left[1 + R_0(\omega/2\alpha_L)^{1/2}\right]\cos(\Delta)\right.$$
$$\left. - 0.5\left[R_0(\omega/2\alpha_L)^{1/2} - 2R_0^2(\omega/2\alpha_L)^{1/2}\right]\sin(\Delta)\right\} \tag{2.127}$$

and

$$<Q_{(2)}> = k_L(4\pi R_0)T_\infty\,|a'|\,|\theta'|\,R_0^2(\omega/2\alpha_L)$$
$$\times\left[0.5R_0(\omega/2\alpha_L)^{1/2}(\cos\Delta + \sin\Delta) - 0.5\sin\Delta - R_0^2(\omega/2\alpha_L)\exp\left[R_0(\omega/2\alpha_L)^{1/2}\right]\right.$$
$$\times \ln\{\exp[j(\pi/2 - \Delta) - R_0(\omega/2\alpha_L)^{1/2}\}E_1[R_0(\omega/Z\alpha_L)^{1/2}(1-j)]\}$$
$$+ k_L(4\pi R_0)T_\infty|a'||\theta'|R_0^2(\omega/2\alpha_L)(1/R_0)\sin\Delta \tag{2.128}$$

Owing to area effect as given in Eq. (2.127), $<Q_1>$ is proportional to the products of the amplitude of oscillation. Therefore a larger heat transfer is seen near resonance. To examine the direction of heat flow, the phase difference must be determined. The magnitude of Δ diminishes from $\pi/2$ for small bubbles and low frequencies as R_0 and ω increase, approaching 0 when $R_0(\omega/2\alpha_L)^{1/2} >> 1$. This is a case of a thin diffusion layer. Since $Q_{(2)}$ involves the exponential integral function in the complex domain, it is difficult to determine its sign analytically. For a thin diffusion layer $Q_{(2)}$ is given as

$$<Q_{(2)}> = k_L 4\pi R_0 T_\infty a'\theta' R_0^2(\omega/2\alpha_L)\left[\sin\Delta - \frac{1}{2}\frac{(\cos\Delta - \sin\Delta)}{R_0(\omega/2\alpha_L)^{0.5}}\right.$$
$$\left. - \frac{3}{2}\frac{\cos\Delta}{R_0^2(\omega/2\alpha_L)} \pm \ldots\right] \tag{2.129}$$

For larger diffusion lengths, i.e., $R_0(\omega/2\alpha_L)^{1/2} << 1$, $Q_{(2)}$ can be expressed as

$$<Q_{(2)}> = k_L 4\pi R_0 T_\infty a'\theta' R_0^2(\omega/2\alpha_L)\left\{\frac{1}{2}\sin\Delta + \frac{1}{2}R_0(\omega/2\alpha_L)^{1/2}\right.$$
$$\left.(\cos\Delta + \sin\Delta) + O\left[R_0(\omega/2\alpha_L)^{1/2}\right]\right\} \tag{2.130}$$

In this limit, the convection heat transfer is small compared with the heat transfer due to the area effect; hence $<Q_T> \sim <Q_{(1)}>$. In addition to the heat transfer due to

area and convective effect, heat transfer due to evaporation is also important. Patel *et al.* (1985) indicated that $<Q_{(3)}>$ is given as

$$<Q_{(3)}> = (P_0 G R_0 \omega)^2 b/2 \tag{2.131}$$

where b is the mechanical resistance of the bubble.

$$G = a'/P_0 \tag{2.132}$$

They also extended their analysis and using thermal equilibrium criteria obtained the minimum acoustic pressure amplitude required for the growth of a bubble. It is given as

$$P^2_{\min} = 8\pi\sigma\Phi/(2\Gamma T_\infty/P_{v0})(S + 8\pi\sigma)\, G^2 \cos\Delta \tag{2.133}$$

The most important point that this theory could explain is that the thermal equilibrium by which the temperature elevation is maintained can be supported by heat transfer.

2.4c. Effect of Simultaneous Diffusion and Evaporation on Bubble Dynamics

A bubble usually contains both foreign gas and vapor of the liquid. However, in most cases only one of the components is dominant. The terms "gas bubble" and "vapor bubble" are therefore used for bubbles consisting essentially of undissolved foreign gas or liquid vapor, respectively. It is of interest to see how diffusion and the evaporation process affect the motion of an oscillating bubble. Wang (1974b) analyzed this problem and a brief summary of his analysis follows.

Wang assumed that the interior of a bubble is in a uniform state, i.e., the temperature, pressure, and density are uniform throughout the bubble. This is true if the bubbles are small compared with the diffusion length and the wavelength of sound in the bubble, and the velocity of the bubble wall is small compared with the sound. The gas components in the bubble are also assumed to behave as perfect gases so that

$$P' = \rho' B T' \tag{2.134}$$

$$P'_g = \rho'_g B_g T' \tag{2.135}$$

and the vapor pressure inside the bubble is taken to be at the equilibrium vapor pressure at the temperature on the bubble wall.

$$P'_v = P'_v(T') \tag{2.136}$$

The internal energy of the mixture is also taken to be a function of T' only, so that

$$U' = C_v' T' \tag{2.137}$$

In the above equations, the primed variables are used to denote the corresponding variables inside the bubble. Also, $\rho' = \rho_v' + \rho_g'$ and $P' = P_v' + P_g'$. B and B_g are the gas constants of the mixture and gas component, respectively. Using these assumptions, Wang has given the equations and boundary conditions as follows:

$$R\frac{d^2R}{dt^2} + \frac{3}{2}\left(\frac{dR}{dt}\right)^2 + \frac{4\mu}{\rho R}\left(\frac{dR}{dt}\right) + \frac{2\sigma}{\rho R} =$$

$$\frac{1}{4\pi R\rho}\frac{d^2}{dt^2}\left(\frac{4}{3}\pi R^3\rho'\right)$$

$$-\left(R - \frac{4\mu}{\rho R}\right)\frac{1}{4\pi R^2\rho}\frac{d}{dt}\left(\frac{4}{3}\pi R^3\rho'\right) + \frac{P' - P_\infty}{\rho} \tag{2.138}$$

where P_∞ is the ambient pressure field. The energy equation is given as

$$\frac{\partial(rT)}{\partial t} - \frac{R^2}{r}\left[\frac{dR}{dt} - \frac{1}{4\pi R^2\rho}\frac{d}{dt}\left(\frac{4}{3}\pi R^3\rho'\right)\right]\frac{\partial T}{\partial r}$$

$$= \alpha_L \frac{\partial^2}{\partial r^2}(rT) + \alpha_L \frac{4\mu}{k}\frac{3R^4}{r^6}\left\{\frac{dR}{dt} - \frac{1}{4\pi R^2\rho}\frac{d}{dt}\left(\frac{4}{3}\pi R^3\rho'\right)\right\}^2 \tag{2.139}$$

where $\alpha_L = \dfrac{k}{\rho C_v}$ and finally the diffusion equation is given as

$$\frac{\partial}{\partial t}(r\rho_g) - \frac{R^2}{r}\left[\frac{dR}{dt} - \frac{1}{4\pi R^2\rho}\frac{d}{dt}\left(\frac{4}{3}\pi R^3\rho'\right)\right]\frac{\partial \rho_g}{\partial r} = D\frac{\partial^2}{\partial r^2}(r\rho_g) \tag{2.140}$$

In order to complete the formulation, the boundary conditions on the bubble wall, $r = R(t)$ are needed. These are

$$\rho\left(v - \frac{dR}{dt}\right) = \frac{-1}{4\pi R^2}\frac{d}{dt}\left(\frac{4}{3}\pi R^3\rho'\right) \tag{2.141}$$

$$\rho_g\left(v_g - \frac{dR}{dt}\right) - D\frac{\partial \rho_g}{\partial r} = \frac{-1}{4\pi R^2}\frac{d}{dt}\left(\frac{4}{3}\pi R^3\rho_g\right) \tag{2.142}$$

$$\rho_v\left(v_v - \frac{dR}{dt}\right) - \frac{1}{4\pi R^2}\frac{d}{dt}\left(\frac{4}{3}\pi R^3 \rho_v'\right) \tag{2.143}$$

$$P + \frac{2\sigma}{R} = P' + \frac{4\mu}{3}\left(\frac{\partial v}{\partial r} - \frac{v}{r}\right) \tag{2.144}$$

$$k\frac{\partial T}{\partial r} = \frac{1}{4\pi R^2}\frac{d}{dt}\left(\frac{4}{3}\pi R^3 \rho'\right)L + \frac{\rho' R}{3}\frac{dv'}{dt} - \frac{\rho' R}{3\rho'}\frac{d\rho'}{dt} \tag{2.145}$$

$$\rho_g = \alpha_g P_g' \tag{2.146}$$

$$T = T' \tag{2.147}$$

Wang has given analytical solutions of these equations to find expressions for R, ρ_g, and T. Since these solutions [Equations (41)–(43) of Wang, 1974b] are extremely lengthy and complex, they are not given here, but their relevant features are briefly discussed.

1. It was found that diffusion is important only when

$$\left|R_0^2 \frac{i\omega}{D}\right| \leq O\left(3\frac{\rho_0'}{\rho_0}\right) \tag{2.148}$$

   where $\rho_0' = \alpha_g \overline{\rho_0}$ and $\rho_0 = \rho_{v0} + \rho_{g0}$. This criterion leads to the fact that for large bubbles at higher frequencies, diffusion is insignificant.
2. ρ_0, the equilibrium density of dissolved gas, decreases with an increase in ambient temperature; therefore, the diffusion effect is even less important at higher temperatures.
3. The amplitude of radius oscillation is less affected by the evaporation process; however, a sharp rise and dip are observed near resonance. The evaporation effect cannot be ignored if we are mainly concerned with thermal behavior or dynamic behavior at resonant radii.

For rectified diffusion, the available experimental data tend to confirm the validity of existing equations provided (1) the acoustic pressure amplitude is not large, (2) the liquid does not contain surface-active additives, and (3) the concentration ratio of dissolved gas is near saturation. The areas that need further study are as follows:

1. The addition of surface-active agents to water resulted in measured values of the threshold and growth rate considerably different from those indicated by theory. An adequate explanation of this is not yet available.
2. The analytical expressions for the rectified diffusion threshold are not in good agreement with the few data that exist at dissolved gas concentration ratios significantly different from saturation. Numerical studies give much better agreement. An extension of the analytical results that accounts for the discrepancy with the dissolved gas concentration ratio is needed.
3. Gas bubbles driven at the pressure amplitudes experienced in rectified diffusion studies will experience considerable fluctuations in their pulsation amplitude as they are driven through their harmonic resonances. At some radial positions, the bubble may experience rapid growth, which is not taken into account in the published analytical expressions.
4. Gould found that increased growth by rectified diffusion occurred in the presence of acoustic streaming in the vicinity of the bubble. An adequate theory for evaluating the effect of acoustic streaming on rectified diffusion has not been developed. Compared with rectified diffusion, little literature is available for rectified heat transfer, which plays a major role in the dynamics of vapor bubbles. Most theories of rectified gas diffusion ignore heat transfer effects. A major contribution in this area is by Patel *et al.* (1985), who extended Wang's theory (1974a).

The reported experimental data do not precisely fit the theory because:

1. At the frequencies that have been used, the acoustic pressure fields are not uniform.
2. Owing to buoyancy, radiation pressure, and Bjerkness forces, bubbles exposed to the sound field may not remain in any one location long enough to reach stable equilibrium.
3. Bubbles pulsating in the neighborhood of solid surfaces do not conform to the theoretical conditions.

Also, the reported theory does not explain the nucleation of bubbles. It ignores the heat transfer associated with the formation of bubbles. The mechanism of bubble nucleation remains unclear, but once bubbles in the micron size range appear in the liquid, this theory can explain how they are able to grow to millimeters in diameter. Also, the theory assumes a liquid to be incompressible and inviscid and hence in practical cases where these assumptions are unrealistic, it introduces error. The linearized solutions used cannot be accurate when displacement amplitudes become large compared with the bubble radius. Nonlinear solutions of the governing equations are necessary to explain such effects as the generation of harmonics and subharmonics. Additional work needs to be done in this area.

2.5. CONCLUDING REMARKS

In the preceding sections, a brief survey of cavitation bubble dynamics was presented. A detailed review of this subject is also given by Young (1989) and Mason and Lorimer (1988). In order to implement hydrodynamic, acoustic, or optical cavitation technology effectively in industry, it is necessary to know more about the cavitation bubble dynamics that are the source for all cavitational effects. The equations given in this chapter form the basis for determining the effects of various physical parameters on cavitation behavior. These effects are described in detail in Chapter 3. Further development of the theories outlined in this chapter is strongly recommended.

3

FACTORS AFFECTING CAVITATION BEHAVIOR

3.1. INTRODUCTION

In Chapter 2 we evaluated the equations that govern the dynamics of both single cavities and clusters of cavities. These equations can be solved to evaluate the effects of various physical parameters on cavitation behavior. This knowledge is very important from the point of view of controlling the parameters that affect cavitation chemistry as well as performance of the cavitation reactor. In this chapter, we discuss the effects of various system parameters on the dynamics of a single cavity as well as on clusters of cavities. The results are presented for hydrodynamic, acoustic, and optical cavitations.

3.2. FACTORS AFFECTING CAVITY BEHAVIOR IN HYDRODYNAMIC CAVITATION

As seen in Chapter 2, the first analysis of the problem of cavitation and bubble dynamics was made by Rayleigh (1917), who solved the problem of the collapse of an empty cavity in a large mass of liquid. Rayleigh also considered the problem of a gas-filled cavity under the assumption that gas undergoes isothermal compression. The equation derived by Rayleigh for the bubble boundary is given as

$$R\frac{d^2R}{dt^2}+\frac{3}{2}\left(\frac{dR}{dt}\right)^2=\frac{P(R)-P_\infty}{\rho} \tag{3.1}$$

where ρ is the liquid density and P_∞ is the pressure in the liquid at a large distance (infinity) from the bubble, and $P(R)$ is the pressure in the liquid at the bubble boundary. Although Rayleigh's equation suffers from shortcomings, such as the assumption of constant viscosity and surface tension and ρ being kept constant, this

equation can easily be extended to include variable physical properties. For a spherical bubble, viscosity and surface tension affect only boundary conditions, so that the pressure at the bubble wall surface is given as

$$P(R) = P_i - \frac{2\sigma}{R} - \frac{4\mu}{R}\left(\frac{dR}{dt}\right) \tag{3.2}$$

Here P is the pressure inside the bubble; σ and μ represent the surface tension and viscosity, respectively. The final equation for bubble wall motion can be written as

$$R\frac{d^2R}{dt^2} + \frac{3}{2}\left(\frac{dR}{dt}\right)^2 = \frac{1}{\rho}\left[P_i - P_\infty - \frac{2\sigma}{R} - \frac{4\mu}{R}\left(\frac{dR}{dt}\right)\right] \tag{3.3}$$

where P_i, the pressure in the liquid at the bubble, is a function of time, and the pressure in the liquid at infinity is also a function of time. By allowing P_i to vary with time (either linearly or sinusoidally), one can use the above equation to predict the growth and collapse of a cavitation bubble in a liquid flow.

For nonturbulent conditions, Eq. (3.3) is substituted in Eq. (3.2) to get the radius-time history and pressure pulses of bubble oscillations. Typical plots of pressure and bubble radius versus time profiles under nonturbulent conditions are shown in Figure 3.1. These plots not only demonstrate the erratic behavior of bubble radius and pressure profiles but also show the effect of final recovery pressure on pressure and bubble radius. It can be inferred from this figure that the magnitude of pressure pulses changes significantly with the value of the final recovery pressure. The higher the final discharge pressure, the higher is the amplitude of the bubble oscillations and therefore the magnitude of pressure pulses. The nature of the pressure and bubble radius versus time profiles under other operating conditions was similar to that shown in Figure 3.1. Since the nonturbulence scenario is an unrealistic one for most practical situations, the results for other parametric effects are not given here.

For simulations under turbulent conditions, it is necessary to estimate the intensity of the turbulence in terms of its magnitude and frequency. The magnitude of the turbulent pressure fluctuations is dependent on the turbulent fluctuating velocity and its estimation is necessary. Isotropic turbulence can be used to estimate the turbulent fluctuating velocity. Kolmogoroff (1941a, b, c) defined the fluctuating velocity and length scale of the eddies when their distribution reaches an equilibrium in terms of power input per unit mass to the system, P_M. (This can be expressed as watts per kilogram). For an orifice, the total recovery of pressure takes place approximately eight pipe diameters downstream of the orifice. For a given value of the volumetric flow rate, the permanent pressure head loss can be estimated from the literature correlations. The product of the volumetric flow rate and the perma-

nent pressure head loss will give the total energy dissipation rate. This loss divided by the mass of liquid in the region of pressure recovery gives the total energy input per unit mass. Thus now the fluctuation velocity of turbulence is given as

$$V^1 = (P_M \times l)^{1/3} \tag{3.4}$$

where P_M is power input to the system per unit mass and l *is* the length scale of the eddy.

To determine the length scale of the eddy, a Prandtl model was used (1 = 0.08d) where d is the diameter of the conduit through which a bubble flows and the average of the sizes of the eddies in the orifice and in the pipe is taken. The frequency of the velocity and thus the turbulent pressure fluctuations within the eddies are determined by dividing the turbulence fluctuation velocity by the length scale of the eddy.

The effects of various geometric design parameters of hydrodynamic cavitation reactors on bubble behavior can be studied by numerically solving Eq. (3.3). The P_M for this case can be defined in terms of the pressure recovery rate with superimposed turbulent pressure fluctuations. It was found that bubble behavior in hydrodynamic cavitation reactors under the effect of turbulence resembles that found in acoustic cavitation. A summary of the important operating parameter effects on the radius-time and pressure-time profiles under turbulent conditions is given in the next section. It should be noted that the turbulent pressure fluctuations cause a significant change in the pressure pulse spectrum of bubble oscillations.

3.2a. Recovered Discharge Pressure and Time of Pressure Recovery

For hydrodynamic cavitation, faster recovery rates not only increase the life of the bubbles but also the number and magnitude of the pressure pulses obtained from them. This can be explained on lines similar to the effect of increasing frequency under acoustic cavitation. A more detailed illustration of the effect of pressure recovery rate or equivalent frequency on the number and size of pressure pulses is shown in Figure 3.2. It is seen from this figure that with the faster recovery rates, the pattern of pressure pulses shifts from a zone of low magnitude and more pressure pulses to one of high magnitude and fewer pressure pulses. A special case of this variation is seen when the reciprocal time of pressure recovery matches the natural oscillation frequency of the bubble. The expression for the natural oscillation frequency of the bubble is given in Chapter 2. The magnitudes of the pressure pulses are significantly higher under nonresonant conditions. These data indicate that in general, with faster recovery rates, reactions requiring higher temperatures and pressures can be carried out more efficiently.

The effect of pressure recovery rate on the pressure and bubble radius was examined by Moholkar (1996). This study indicated that the maximum value of the

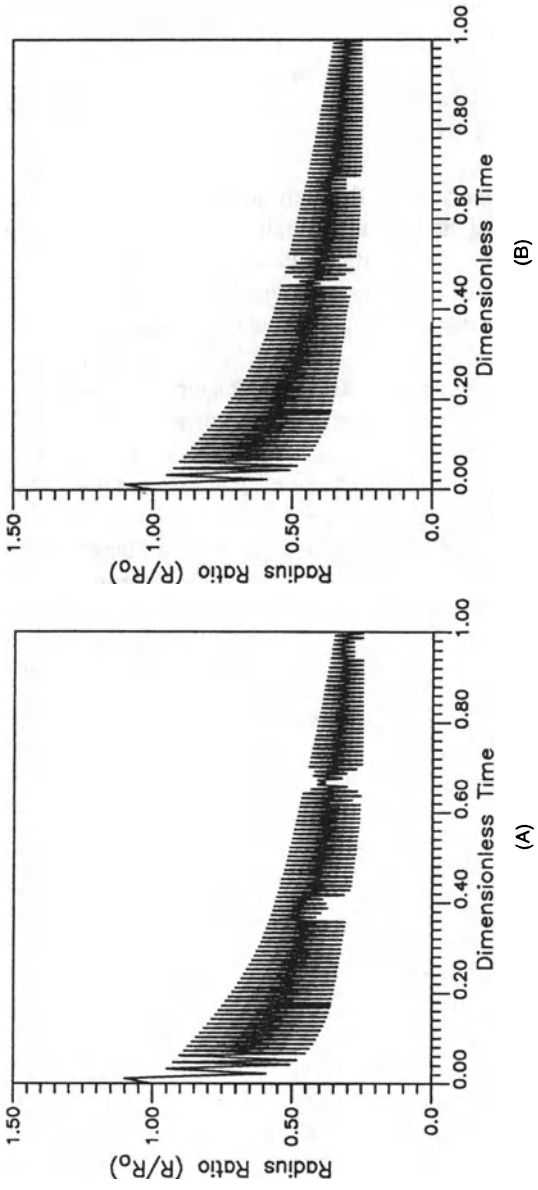
Radius Ratio (R/R$_o$)
1.50
1.00
0.50
0.0
0.00
0.20
0.40
0.60
0.80
1.00
Dimensionless Time
(A)
(B)

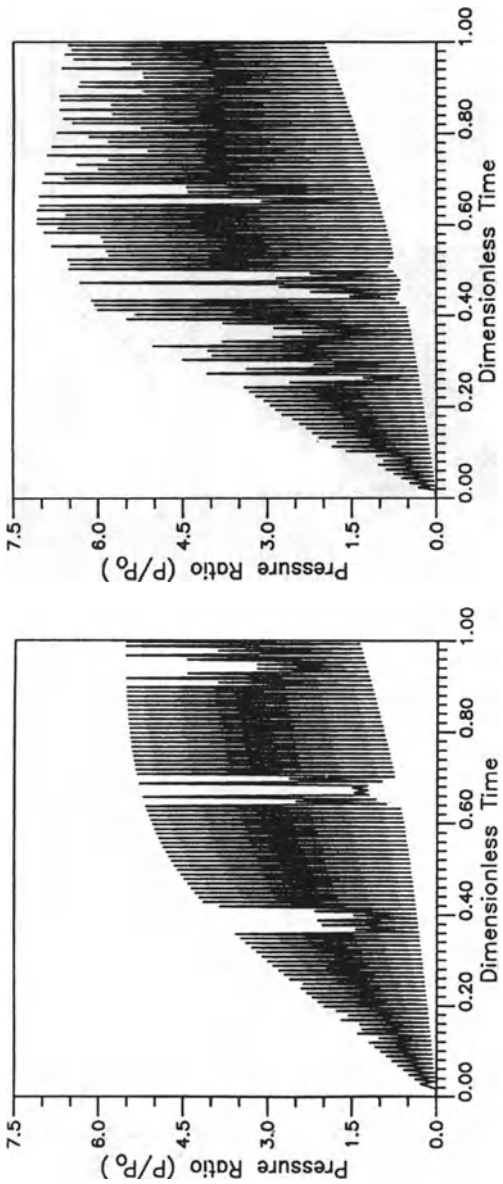

Figure 3.1. Effect of final recovery pressure on hydrodynamic cavitation. Parameters for simulation: initial bubble radius, 0.3 mm; recovery time, 0.01 s; (A) recovery pressure, 5 atm; (B) recovery pressure, 7 atm.

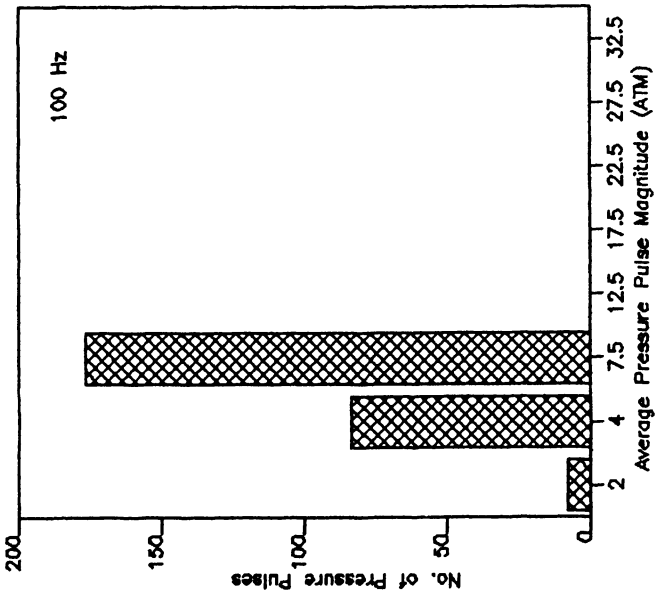
100 Hz
No. of Pressure Pulses
0
50
100
150
200
2
4
7.5
12.5
17.5
22.5
27.5
32.5
Average Pressure Pulse Magnitude (ATM)

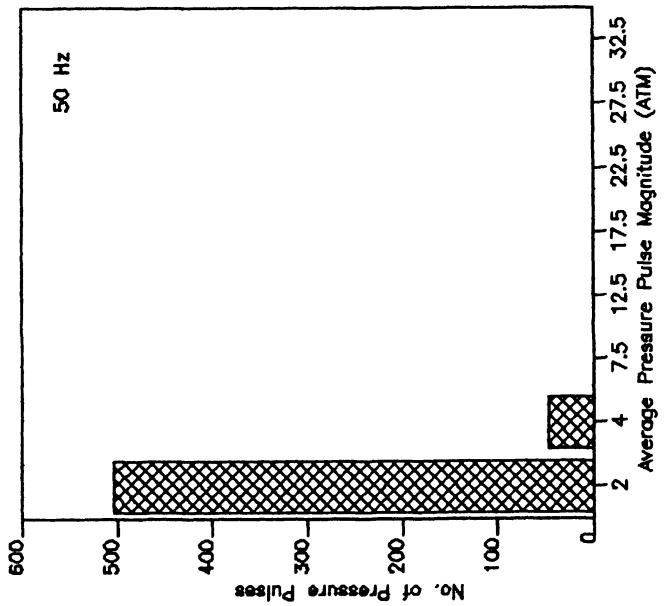
50 Hz
No. of Pressure Pulses
0
100
200
300
400
500
600
2
4
7.5
12.5
17.5
22.5
27.5
32.5
Average Pressure Pulse Magnitude (ATM)

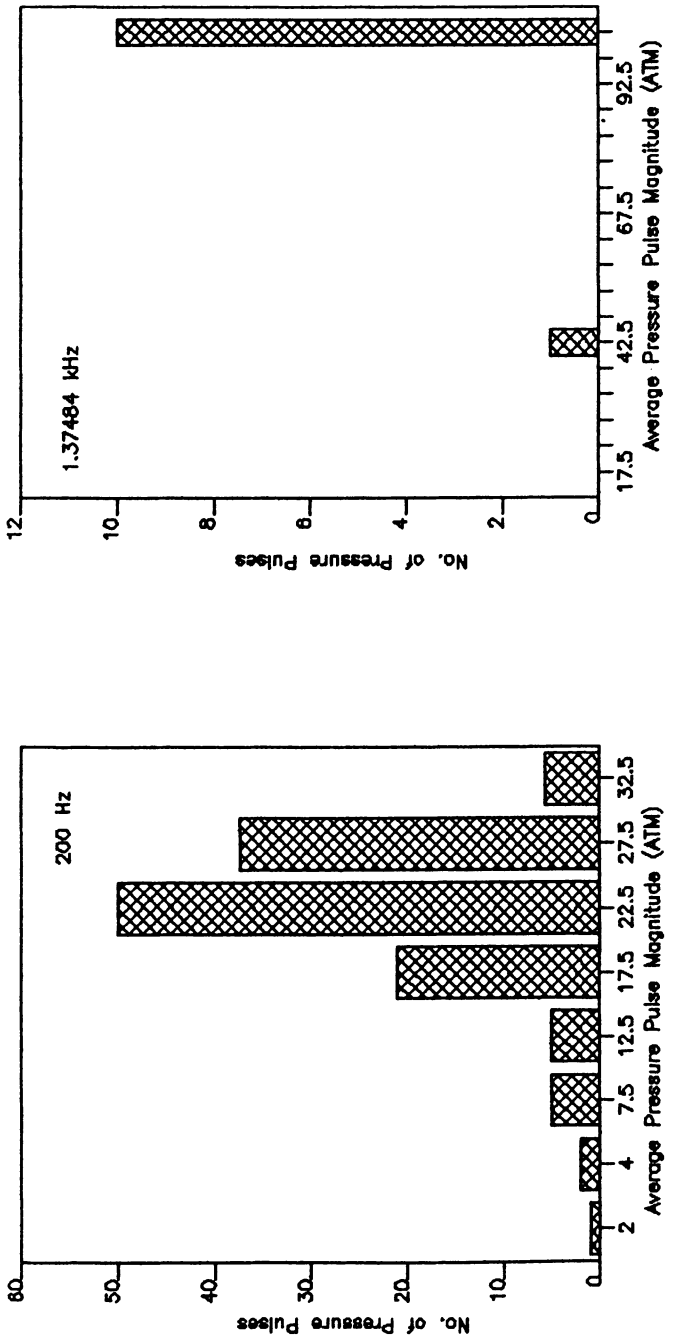

Figure 3.2. Bar chart showing comparison of pressure pulses with varying recovery rates.

bubble radius before an implosion increases with an increase in recovery pressure. An increase in pressure drop increases the cavitational effect, i.e., the magnitude of the pressure and temperature pulses produced varies proportionately with the pressure drop across the orifice. Also, the life of the bubble and the downstream active volume (i.e., the volume in which cavitational effects are realized) changes with the recovery pressure. When considering the discharge pressure as a tool to vary the magnitude of temperature and pressure pulses, the increase in the cost of operation during the change in the discharged pressure must also be kept in mind. An optimization in terms of the discharge pressure is necessary. For an efficient reactor design, an optimum value of the discharged pressure should be ascertained in order to produce pressure pulses of the magnitude desired for a specific chemical reaction or physical effect.

3.2b. Downstream Pipe Size

The effects of the downstream pipe size on bubble behavior were examined by Moholkar (1996). His study indicated that a variation in pipe size downstream of the orifice does not affect the life of the bubble. However, with a larger pipe size, the maximum bubble size reached during growth increases and this in turn results in higher temperature and pressure pulses during subsequent adiabatic collapse of the bubbles. Thus, in order to produce a maximum pressure impulse, a pipe as large in diameter as possible should be utilized. In practice, however, there is a physical limitation to this concept. This limitation can be overcome by mounting the orifice on the pipe wall itself, which will allow maximum expansion of the stream after it passes through the orifice, resulting in the maximum effect during implosion.

3.2c. Orifice-to-Pipe Diameter Ratio

The effect of the orifice-to-pipe diameter ratio β on bubble dynamics was examined by Moholkar (1996) for a set of system conditions listed in Table 3.1. The results shown in Figure 3.3 indicate that the variation in the orifice-to-pipe diameter ratio mildly changes the maximum radius value reached during the oscillations of a single bubble. The life of the bubble, however, increases proportionately with the orifice-to-pipe diameter ratio. Therefore it is possible to manipulate the residence time of the reaction mixture in the cavitating zone (i.e., active volume for cavitating bubbles) by altering the ratio of the orifice-to-pipe diameter.

3.2d. Initial Bubble Radius and the Noncondensable Gas Fraction in Cavitating Liquids

The study by Moholkar (1996) indicates that it is necessary to assess the dynamics of bubbles of all sizes in a similar environment. Both pressure pulses and bubble

TABLE 3.1. Parameters for the Effect of Orifice-to-Pipe Diameter Ratio

β	P_2 (atm)	d_p (inch)	d_0 (inch)	R_0 mm	f_T (kHz)	1/τ (kHz)
0.6	3	2	1.2	10	1.056	0.0439
0.75	3	2	1.5	10	0.961	0.0569

After Moholkar (1996).

size significantly depend upon the initial bubble radius. The ratio of maximum radius reached during oscillations to the initial bubble radius is higher for smaller bubbles. Therefore the intensity of the cavity collapse will be larger for a smaller initial bubble radius since the magnitudes of the pressure pulse produced by these bubbles during an implosive collapse are proportional to the ratio of the maximum radius value before collapse and the initial bubble radius. The reactor zone where these pressure pulses are felt is also very important. This zone is larger for the larger initial bubbles. Thus one needs to evaluate the contribution of both small and large initial bubble radii during the cavitation process.

The noncondensable gas content of a bubble tries to cushion the collapse of the bubble during its oscillations. Therefore the life of a bubble and hence the volume downstream of the orifice increases with the increased noncondensable gas content of a bubble. Also, a larger noncondensable gas fraction gives a larger magnitude of pressure pulse because of the larger amplitude of the bubble oscillation.

Since the magnitudes of the pressure impulse as well as the residence time of the reaction mixture in the cavitating zone can be altered, an optimization of the physical and geometrical parameters required to conduct a specific chemical reaction should be carried out. This is equivalent to altering the frequency and intensity of irradiation in acoustic cavitation, which has some limitation in terms of the available hardware. Since smaller bubbles give larger pulses of pressure and temperature, for reactions requiring extreme conditions, it may be desirable to introduce external gas bubbles of the required size so as to produce pressure and temperature pulses of the required magnitude.

In the case of hydrodynamic cavitation, the amplitude of the pressure pulses is low. On the other hand, in acoustic cavitation, the number of pressure pulses is very small (just one or two), but they are generally high in amplitude. Figure 3.4 compares the pressure pulse spectrum for hydrodynamic and acoustic cavitation for similar representative conditions.

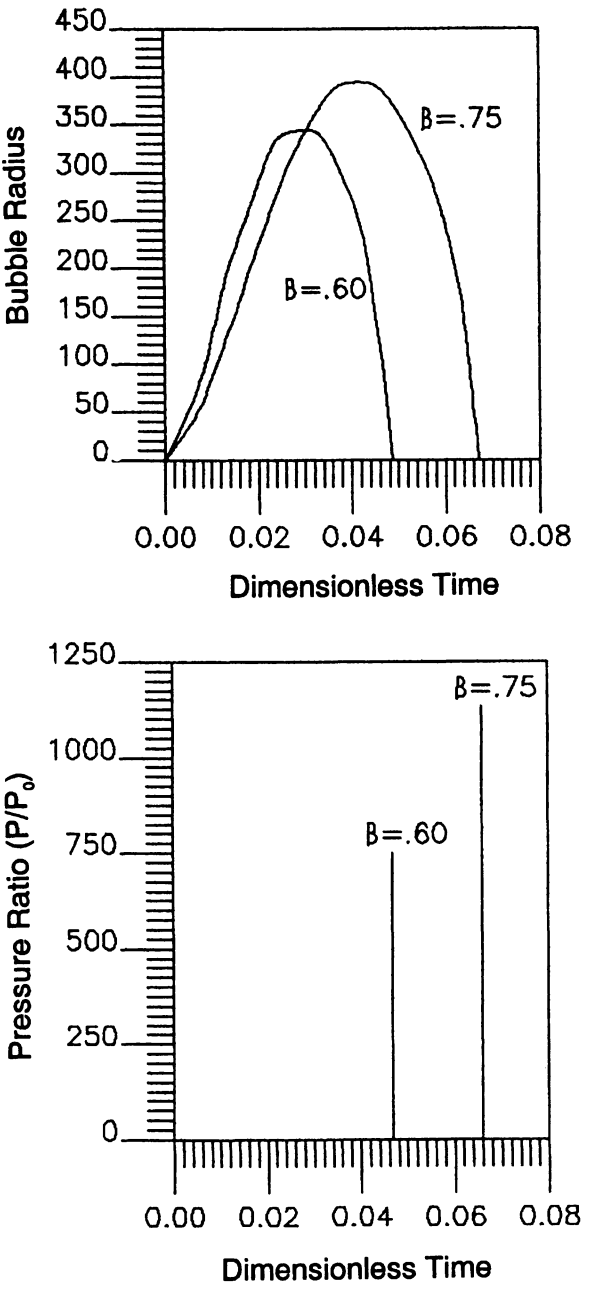

Figure 3.3. Effects of orifice-to-pipe diameter ratio on pressure and bubble diameter ratios: parameters for simulation are described in Table 3.1.

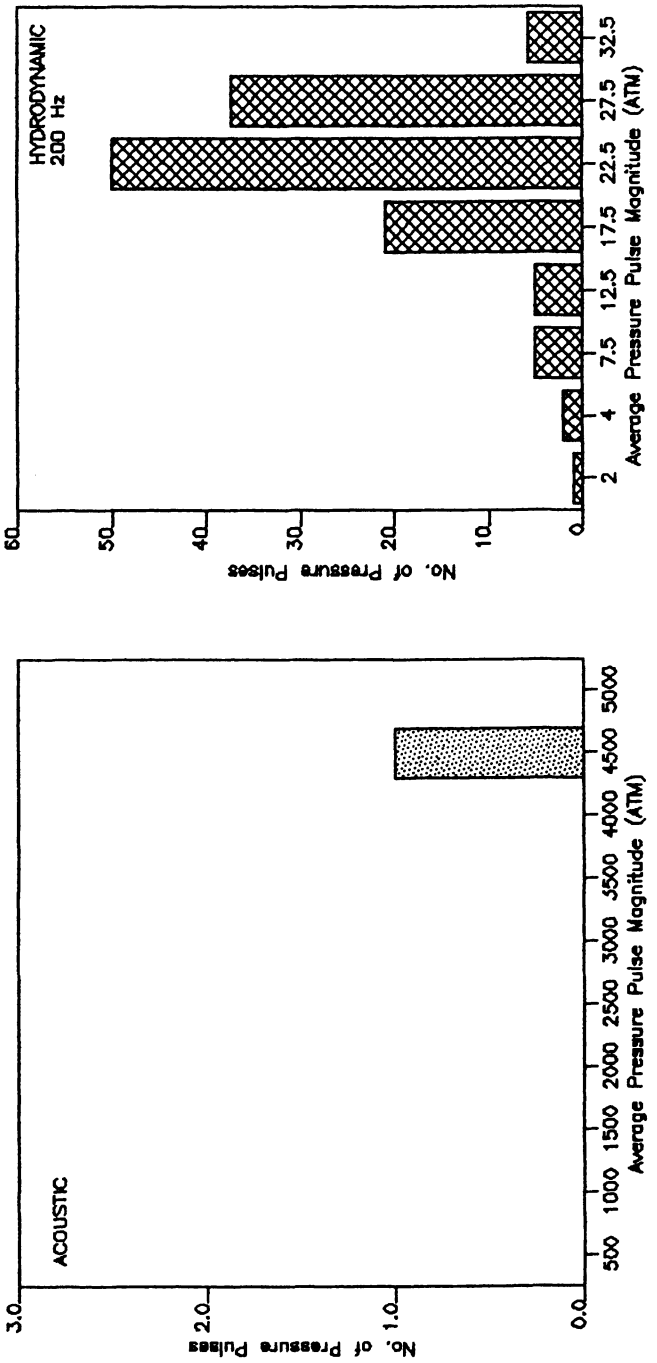

Figure 3.4. Comparison of pressure pulse in hydrodynamic and acoustic cavitation.

3.3. FACTORS AFFECTING CAVITY BEHAVIOR IN ACOUSTIC CAVITATION

When the net negative pressure developed in the rarefaction cycle of a sound wave is applied to a liquid so that the distance between the molecules exceeds the critical molecular distance necessary to hold the liquid intact, the liquid will break down and voids will be created, i.e., cavitation bubbles will form. If we assume that the critical distance for water is 10^{-5} cm, then the tensile stress or pressure required can be calculated to be on the order of 10,000 atm.

This calculation assumes that the water is completely pure. In practice, the pressure required for liquid to cavitate occurs at considerably lower acoustic pressures than such calculations would suggest. This is caused by the presence of weak spots in the liquid that lower its tensile strength. If we consider the factors that influence acoustic cavitation, then we will be some way toward identifying the conditions that govern the effectiveness of cavitation in a chemical reacting system.

Cavitation is a three-step process consisting of nucleation, growth, and collapse of gas or vapor-filled bubbles in a body of liquid. The cavitation threshold for ultrapure (with no nucleic impurities) homogeneous liquids is on the order of hundreds of atmospheres (e.g., for CCl_4 it is 265 atm^{-1}). The presence of microparticles, dissolved gas, or other cavitation nuclei considerably reduces the liquid strength by acting as weak spots. For example, in the presence of microparticles, CCl_4 can be cavitated at an acoustic pressure amplitude of only 1.75 atm^{-1}. For a given size distribution of nuclei, the fraction of cavitation bubbles that will behave as oscillating bubbles or transient cavities depends on acoustic parameters. The macroscopic effect will depend on both the size and the number of bubbles and the intensity of the collapse. Table 3.2 describes the effects of various physical parameters on acoustic cavitation behavior.

3.3a. Acoustic Frequency

The cavitation threshold is strongly frequency dependent because for a given acoustic field, only those bubbles with a resonant frequency greater than the acoustic frequency will cavitate. Consequently, as acoustic frequency is increased, the size of a cavitating bubble decreases, resulting in the cavitation threshold. Typical variations in threshold intensity with ultrasonic frequency are illustrated in Figure 3.5. The examples given are for both degassed and aerated water at room temperature. It should be noted that the intensity required to produce vaporous cavitation above a frequency of ~100 kHz rises rapidly. These results indicate that acoustic cavitation can be economically achieved only within a certain frequency range. Commercial reactors cannot afford to have excessive power requirements. An increase in frequency means shorter acoustic periods, lower maximum bubble size, and thus less cavitation intensity. It has also been shown that ten times more

TABLE 3.2. Effect of Physical Parameters on Cavitation[a]

No.	Independent variable	Dependent variable	Effects	Remarks
A	Nature of liquid	Compressibility of liquid	Gas bubble dynamics	• The higher the vapor pressure, the less violent the collapse (increased penetration of vapor into the bubbles)
		Vapor pressure	Intensity of collapse	• Induction of cavitation is more difficult in solvents with low vapor pressure
		Surface tension	Size of smallest nuclei	• Cavitation is easier in solvents with low viscosity and surface tension
		Gas solubility	Number of cavitation events, gas content	
		Viscosity	Transient cavitation threshold	
		Type of active intermediates or radicals formed	Nature of chemical reaction	
B	Pretreatment of liquid	Size distribution of cavitation nuclei	Cavitation threshold	
C	Nature of gas	Gas solubility	Number of cavitation events, gas content	• $\gamma = C_p/C_v$ should be high because the collapse temperature is proportional to $(\gamma - 1)$ • The smaller the thermal conductivity of the gas, the greater the local heating during the collapse

(*continued*)

TABLE 3.2. Continued

No.	Independent variable	Dependent variable	Effects	Remarks
		Chemical reactivity	Primary and secondary sonochemistry	• The greater the amount of dissolved gas, the smaller the intensity of the shock wave
		Specific heat, thermal diffusivity	Intensity of cavitation events	• Dissolved gas acts as cavitation nuclei and leads to more facile cavitation
D	Static pressure	Size distribution of cavitation nuclei, gas solubility impedance of liquid	Number and intensity of cavitation events, cavitation threshold, velocity of bubble collapse, efficiency of energy transfer, bubble content	• Pressure rise decrease vapor pressure and collapse is more violent; a higher intensity is necessary to induce cavitation • Optimum depends on frequency
E	Ambient liquid temperature	Gas solubility, liquid vapor pressure	Gas content of bubbles, cavitation intensity	• Temperature rise increases vapor pressure and collapse is less violent; less intensity necessary to induce cavitation
		Thermal activation	Enhanced secondary reaction rates	• Temperature near the boiling point of the solvent dramatically increases the number of bubbles, which can act as sound barriers
		Sound wavelength	Resonance conditions	

F	Acoustic intensity	Size of cavitation zone	Probability of cavitation events per unit volume	• Considerably higher intensity at high frequency is necessary to maintain the same cavitation as at low frequency • Indefinite increase limited by the material stability of transducer, decoupling with the medium, and a large number of bubbles (transmission barrier)
G	Acoustic frequency	Half-period of collapse	Resonant bubble radius, probability of cavitation events per unit time	• Low: long cycle, large bubbles, low amplitude required to induce cavitation • High: short cycle, high amplitude necessary, increased attenuation, weak or no cavitation in the megahertz range (rarefaction cycle is too short to create bubbles)
H	Time of irradiation	Total energy input	Extent of reaction, heat dissipation	

[a]From Peters (1996) with permission.

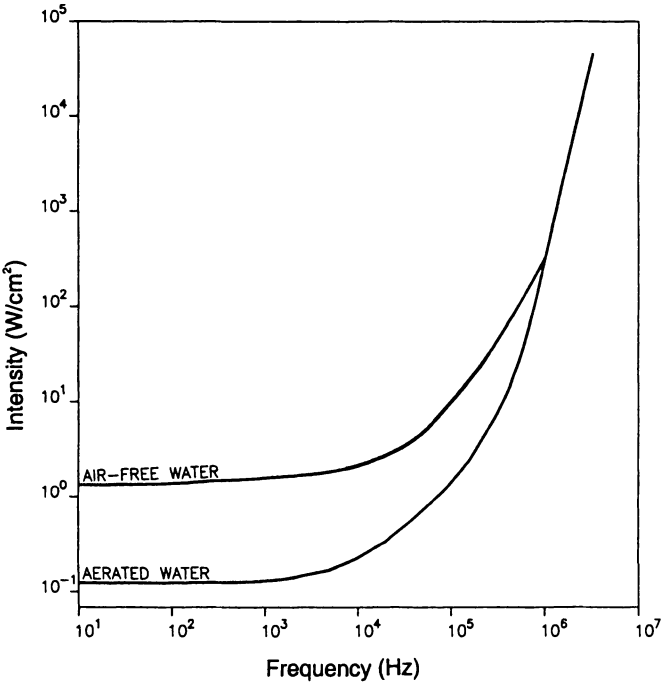

Figure 3.5. Variation in threshold intensity with ultrasonic frequency. (From Edmonds, 1990c, with permission.)

power is required to make water cavitate at 400 kHz than at 10 kHz. This effect is due to the increased power losses that occur as the rate of molecular motion within the liquid increases. Generally, the changes in chemical reactivity are observed in the frequency range of 20 to 50 kHz.

It is worthwhile briefly examining the physical reasons behind the behavior illustrated in Figure 3.5. There will be a natural delay between the application of a rarefaction wave to a fluid and the response of the molecules of that fluid. At frequencies in the megahertz range, one must compensate for this delay by applying a wave of greater intensity—a greater power to pull apart the molecules in rarefaction. But because of the constraints on the stability of the transducer and the ultrasonic probe, a very high frequency probe cannot be run with a very high intensity. Bubble behavior for two different ultrasonic frequencies under conditions that are otherwise the same are shown in Figure 3.6. The bubble oscillations reach their highest amplitude and have the shortest life when the frequency of irradiation matches the natural oscillation frequency of the bubble. One such case is shown in Figure 3.6.

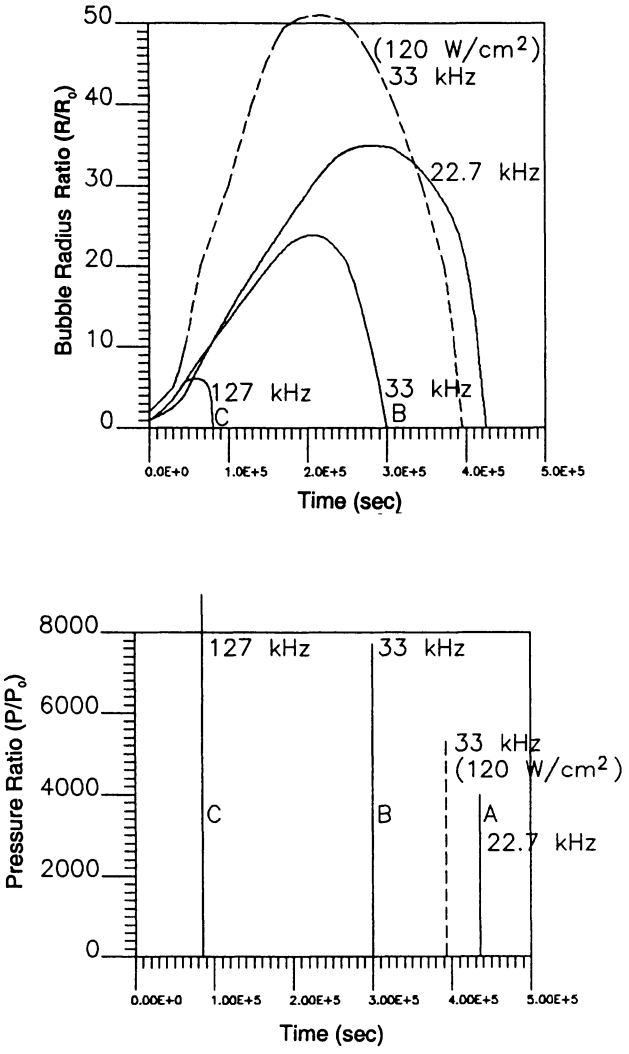

Figure 3.6. Effects of irradiation frequency and intensity on bubble behavior in acoustic cavitation. Parameters for simulation: Top: intensity, 10 W/cm^2; initial cavity size, 10 mμ; (A) frequency, 22.7 kHz; (B) frequency, 33 kHz; (C) resonant frequency, 127 kHz. Bottom: intensity, 120 W/cm^2; frequency, 33 kHz.

3.3b. Acoustic Intensity

Obviously the larger the intensity, the larger will be the acoustic amplitude and collapse pressure and hence the faster and more violent the collapse. Corresponding to a given distribution of nuclei sizes, there is a minimum acoustic pressure amplitude, called the *threshold pressure amplitude*, which is necessary to produce cavitation. As the acoustic pressure amplitude is further increased, smaller bubbles become unstable and start contributing to cavitation activity. The maximum bubble radius also increases with acoustic pressure amplitude and is independent of the initial bubble size. Hence, as the acoustic intensity is increased, both the number of bubbles and their maximum size increase, resulting in increased cavitation activity. The increase is not indefinite, however, because as the maximum radius of a bubble increases, so does the Rayleigh collapse time. If the collapse time becomes greater than the half-period of the wave, the cavitation bubble will not have time to collapse before the sound field reverses itself and the rarefaction phase of the wave begins acting on the collapsing bubble. This will result in a lower number of collapsing bubbles, and therefore lower cavitation intensity. A maximum acoustic intensity is feasible provided the Rayleigh collapse time is equal to or less than one half the period of the acoustic wave.

Generally an increase in intensity increases the bubble growth. Figure 3.6 shows typical bubble behavior under two different irradiation intensities. As shown, an increase in intensity increases the bubble growth and decreases the pressure ratio. It must be realized that the intensity cannot be increased indefinitely. Under higher intensities, the bubble will grow so large that it may not collapse in the following rarefaction cycle due to insufficient time available for the collapse. Also, a large bubble formed near the probe tip of an ultrasonic horn will reduce the coupling of sound energy to the system. An indefinite increase in the intensity is also detrimental to the horn because as the amplitude of oscillation increases, it can cause mechanical damage to the tip of the horn. This indicates that generally there is an optimum power for the acoustic cavitation conversion whose value may be system specific.

3.3c. External Pressure

The greater the external pressure, the larger the collapse pressure and the shorter and more violent the bubble collapse. This postulation has, however, been questioned and is further complicated by consideration of the events that lead to nucleation of the bubbles.

At present, the generally accepted mechanism for nucleation of bubbles suggests that gas trapped in small-angle crevices of particulate contaminants expands and contracts with the acoustic cycle. Free air bubbles would not be expected to act as nucleation sites because they are inherently unstable under these conditions and would be expected to dissolve as a result of surface tension. As the bubble volume

grows, two possibilities arise: On the one hand, small gas bubbles may be released into the surrounding liquid and on the other hand, implosive collapse of the bubble will release a stream of microcavities at which nucleation can occur. This theory was proposed in the light of observations that the cavitation threshold is increased with both pressurization and evacuation of the system. Hence, nucleation is suppressed by the flooding of the crevices.

An increase in static pressure over a liquid can lead to an increase in the mechanical impedance of a cavitating liquid due to a resonance effect. This improved mechanical impedance results in increased acoustic power being transferred to the liquid without any increase in electrical consumption by the transducer. The optimum static-to-acoustic power ratio for maximum acoustic power has been shown to be 0.4.

3.3d. Nature of the Dissolved Gas

A cavitation bubble initiated in the rarefaction cycle will not enclose a vacuum, but will almost certainly contain some vapor of the liquid within which it is formed. The extent to which a gas is discharged in a bubble is a function of pressure. A sudden reduction in the pressure will release the gas and it is natural that any dissolved gas will be forced inside the bubble during its formation.

The removal of gas from a liquid will reduce the available nuclei and it will become increasingly more difficult to cavitate that liquid. It has already been demonstrated that the passage of ultrasound degasses a system and therefore most workers in a field either (1) bubble gas continually during the course of the experimental investigation or (2) apply ultrasound to the system for at least 10 min prior to introducing the reactants to ensure sufficient degassing. Although this is purely a matter of choice on the experimenter's part, most workers favor the former procedure.

The specific heat ratio of the gas in the bubble plays an important role in the collapse temperature and pressure. For monoatomic gases, this ratio is the highest and therefore it is advisable to bubble any monoatomic gas through the solution being irradiated. The pressure of gas in the bubble will cushion the collapse and lead to a stable cavitation.

During the rarefaction phase of an acoustic wave, a cavitation nuclei grows to some maximum size and then starts to collapse (nearly adiabatically) during the compression phase. The final temperature and pressure for an adiabatic collapse depend on the ratio of specific heats, $\gamma = C_p/C_v$ of the gas within the cavities. In fact, a polytropic index η dictates the final temperature and pressure rise, where $1 < \eta < \gamma$, in most real situations. This topic was discussed in Chapter 2.

3.3e. Physical Properties of the Cavitating Medium

Each solvent has its own particular set of properties so that the choice of the solvent medium becomes very important when considering the appropriate reaction conditions. Typical relevant physical properties are (1) solvent viscosity, (2) vapor pressure, and (3) surface tension. Higher surface tension, lower viscosity, and lower vapor pressure favor cavitation. Therefore when choosing a cavitating medium, a judicious choice of these properties must be made to assist cavitation. As mentioned earlier, water is a very good medium for cavity formation.

3.3f. Pretreatment of the Liquid

It is believed that the size of a typical cavitation nucleus depends on the previous history of the liquid. For example, Flynn (1964) states that in fresh tapwater that has been allowed to stand open to the atmosphere for a few seconds, a typical nucleus radius is 5×10^{-3} cm. In water that has been standing for several hours, the average nucleus has a radius of 5×10^{-4} cm, while water subjected to elevated hydrostatic pressure has an average nucleation radius of 10^{-5} cm. Even for a liquid free of cavitation nuclei, bombardment by high-energy particles creates minute nuclei 10^{-6} to 10^{-7} cm in radius.

If prior to cavitation a liquid is subjected to elevated hydrostatic pressure, the average nucleus size is reduced (the cavitation threshold is thus increased) because the increased gas solubility in the liquid leads to dissolution of some of the gas present in the nucleus. Harvey (1939) reported that after increasing static pressure over water to 1000 atm, he could not produce cavitation even after the pressure was released. Any increase in the viscosity or the surface tension will require an increase in the amount of energy needed to separate the liquid.

3.3g. Bulk Liquid Temperature

For the best cavitation chemistry, it is necessary to use lower temperatures. This is a direct result of the decrease in vapor pressure that accompanies the lowering of solvent temperature, thus increasing the cavitation intensity. If the cavitational chemical reaction is carried out at higher bulk liquid temperatures, the yields will be lower since any cavitation bubble formed would fill almost instantly with solvent vapor. The collapse of these vapor-filled bubbles during the compression cycle would be "cushioned," thereby reducing the magnitudes of the temperatures and pressures generated.

3.3h. Initial Bubble Radius

The effects of initial bubble radius on bubble growth and pressure amplitude are similar to those described earlier for hydrodynamic cavitation. Both the extent of

growth and pressure amplitude are larger for a smaller initial bubble radius. These results are in agreement with the theory reported in Chapter 2, which showed that both P_{max} and T_{max} are proportional to $(R/R_0)^x$, where x is positive and a function of γ.

3.4. FACTORS AFFECTING OPTICAL CAVITATION

Laser-induced cavitation is generally examined in the laboratory to study the behavior of single cavities or multiple cavities (distributed in a prescribed manner) under controlled conditions. This type of cavitation can create perfectly spherical bubbles because of the sharpness of the laser intensity. The size and shape of the cavity, in general, depend on the intensity and sharpness of the laser beam.

Teslenko (1980) examined the collapse of laser-induced cavities in water, glycerine, and Vaseline. For the case of nonsurfacing bubbles, the ratio of bubble energy of the subsequent pulsation to the foregoing one is a function of the relative consumption of energy stored by a bubble. Some typical results obtained by Teslenko (1980) are described in Table 3.3. The energy difference between two subsequent pulsations corresponds to the shock acoustic radiation energy of the collapsing bubble as well as to nonsymmetric bubble collapse. It is clear that for the first pulse, laser-induced bubbles in water behave very differently than those created in glycerine and Vaseline.

An analysis of the typical pressure pulse oscillograms obtained in his study indicate that in the case of nonsymmetric bubble collapse, the pressure transducer records the "precursors," i.e., the pressure pulses preceding the basic pulse radiated at the bubble collapse. When precursors are observed, the steepness of the pressure growth of the basic pulse is decreased, and the maximum pressure amplitude is also decreased by more than 50% as well. The maximum pressure amplitudes of

TABLE 3.3. Energy Conservation during Subsequent Pulsation of Cavity[a]

Type of pulsation	$E_r^{(2)}/E_r^{(1)}$ [b]	$E_r^{(3)}/E_r^{(2)}$ [c]
Explosion of chemical charges in water	0.34	0.54
Electrical discharge in water	0.05	—
Laser breakdown in water	0.07	0.5
Laser breakdown in glycerine	0.26	0.5
Laser breakdown in Vaseline	0.35	0.51

[a]From V.S. Teslenko, "Experimental investigation of bubble collapse at laser induced breakdown in liquids," in W. Lauterborn, ed., *Cavitation and Inhomogeneities in Underwater Acoustics*, p. 30, with permission from Springer-Verlag, New York, 1980).

[b]Bubble energy of the second pulsation relative to the energy of the first pulsation.

[c]Bubble energy of the third pulsation relative to the energy of the second pulsation.

different collapsing bubbles recorded at a distance of 1.5 cm are given in Figure 3.7. These results indicate that cavitation in water generates a much higher pressure pulse during the collapse than that in glycerine. When glycerine is heated, its viscosity decreases by three orders, but it does not lead to an appreciable increase in the pulse amplitude. Similar results are expected for Vaseline. The scatter in the water data in Figure 3.7 is caused by the kinetics of bubble collapse, its sphericity, and the stability of the spherical shape at the moment of collapse. The collapse of a perfectly spherical cavity can generate maximum velocity of 530 m/s and temperatures as high as 6000 K due to the high degree of adiabatic gas compression. Teslenko (1980) observed sonoluminescence of bubbles produced by a laser in water, carbon tetrachloride, acetone, and benzene, but not in glycerine and Vaseline. A symmetric bubble collapse in liquid can radiate up to 90% of the energy contained in the bubble as sound. Asymmetry influences the stability of the succeeding bubble pulsations and decreases acoustic and light radiation pulses.

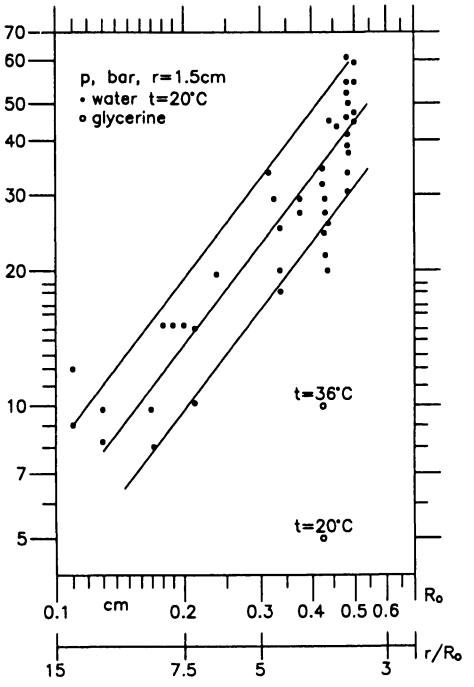

Figure 3.7. Experimental values of pressures at bubble collapse 1.5 cm from the breakdown center (From V.S. Teslenko, "Experimental investigation of bubble collapse at laser induced breakdown in liquids," in W. Lauterborn, ed., *Cavitation and Inhomogeneities in Underwater Acoustics*, p. 30, Springer-Verlag, New York, 1980, with permission.)

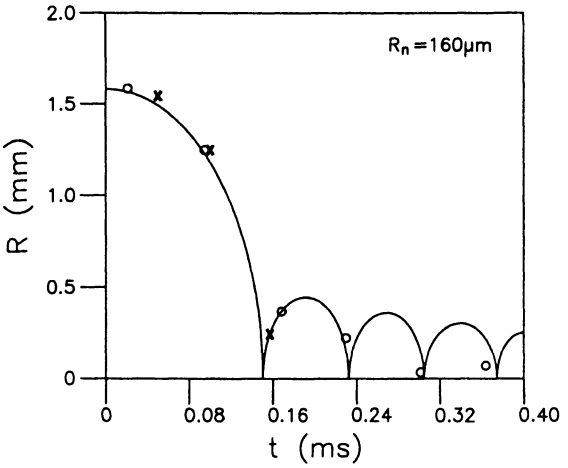

Figure 3.8. Bubble wall motion as a function of time computed according to Gilmore's model. Crosses and squares are experimental data. (From K.J. Ebeling, "Application of high speed holocinematographical methods in cavitation research," in W. Lauterborn, ed., *Cavitation and Inhomogeneities in Underwater Acoustics*, p. 35, Springer-Verlag, New York, 1980, with permission.)

The spherical bubbles produced by a laser in water carry strong damping. This cannot be explained by Rayleigh's theory of bubble wall motion, even when gas content, surface tension, and viscosity are taken into account. It, however, can be explained when the liquid is assumed to be compressible (Ebeling, 1978). This is demonstrated by Figure 3.8, where the radius-time curve of bubble wall motion is computed according to Gilmore's model (see Chapter 2). The crosses and open circles are the experimental data of Ebeling (1980). The strong damping of the oscillation after the first collapse is caused by sound radiation. In laser-induced cavitation, multiple bubbles can be produced by a holographic technique. These multiple bubbles will follow the same behavior as that of a single bubble described earlier.

3.5. FACTORS AFFECTING CAVITY CLUSTER BEHAVIOR IN HYDRODYNAMIC CAVITATION

Moholkar (1996) and Moholkar and Pandit (1997) and Moholkar *et al.* (1999) examined various cases of air bubble clusters and their behavior under hydrodynamic cavitation. The assumptions made in their analysis were:

1. Bubble clusters are spherical.

2. Both bubble cluster and individual bubbles collapse spherically, so that half of the energy released after the collapse is preserved.
3. A cluster collapses when the cluster size becomes equal to or less than 5 μm (the typical size of an individual bubble in a cluster).

The main variables that affect the dynamics and collapse of a bubble cluster in hydrodynamic cavitation are (1) recovered discharge pressure, (2) time of pressure recovery, (3) initial cluster radius, and (4) bubble fraction in the cluster. The effects of these variables on cluster behavior have been studied by Moholkar and co-workers. The results of their simulations are briefly presented in the following sections.

3.5a. Effect of Recovery Pressure

The studies by Moholkar and co-workers mentioned earlier showed that cluster life is not altered with increasing recovery pressures. This is simply because of the cushioning provided to the inner cavities by the outer ones. The collapse of a cluster itself depends on the individual collapse of the bubbles in the inner core. This latter is influenced more by the pressure pulses during the collapse of the bubbles at the boundary than by the recovery pressure, which has a limited exposure. As a result, bubble cluster life does not vary with variation in the recovered pressure.

3.5b. Effect of Time of Pressure Recovery

The studies by Moholkar and co-workers also indicated that with decreasing time of pressure recoveries (i.e., faster pressure recovery), the life of the cluster increases. This may be explained on the basis that with increasing rates of pressure recovery, the life of a single cavity increases. Thus the collapse of the bubbles in the inner core of the cluster is not triggered because of the higher life of the bubbles that are on the boundary. This, therefore, results in an overall growth in cluster life of the bubbles.

3.5c. Effect of Initial Cluster Radius

The effect of the initial cluster radius on the cluster dynamics for three cluster sizes of 2, 4, and 8 mm were examined by Moholkar and co-workers for a typical set of operating conditions outlined in Table 3.4. In these simulations, the bubble volume fraction inside the clusters was assumed to be the same. The typical results are illustrated in Figure 3.9. It is evident from these results that a larger cluster lives longer even though the bubble fraction in it remains the same. This is because of a rise in the absolute number of bubbles in the cluster (although the fraction remains the same) and because the total life of a cluster increases with increasing cluster radius. A larger cluster also results in a larger pressure amplitude upon its collapse.

TABLE 3.4. Effect of Initial Cluster Radius on Cluster Dynamics[a]

γ	α	d_p (inch)	d_0 (inch)	v_0 (ms^{-1})	V (ms^{-1})	f_T (kHz)	P_2 (atm)	R_0 (mm)	β	$1/\tau$ (kHz)
0.5	0.6	2	1.2	14.92	1.979	0.609	1	2	10^{-8}	0.025
0.5	0.6	2	1.2	14.92	1.979	0.609	1	4	10^{-8}	0.025
0.5	0.6	2	1.2	14.92	1.979	0.609	1	8	10^{-8}	0.025

[a]After Moholkar (1996).

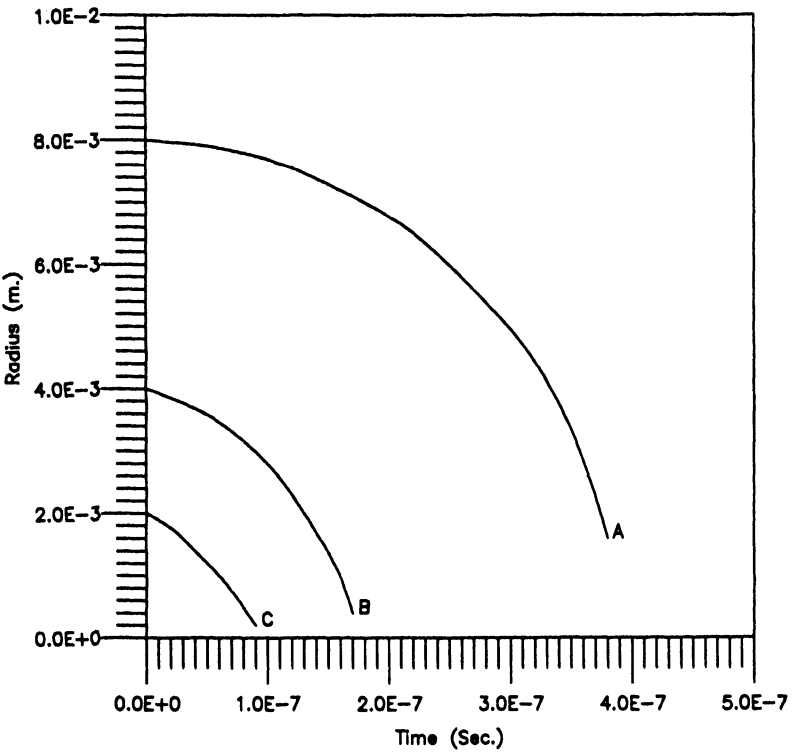

Figure 3.9. Effects of initial cluster radius on cluster dynamics; parameters for simulations are described in Table 3.4. A, 8 mm; B, 4 mm; C, 2 mm.

3.5d. Effect of Bubble Volume Fraction

The results obtained by Moholkar and co-workers indicate that the life of the cluster decreases as the bubble fraction decreases. This can be explained on the basis that the life of the bubble cluster depends on the life of the individual bubbles. Thus the lower the bubble volume fraction, the lower the cluster life. In addition, since the number of the bubbles in the inner core is lower at a lower bubble volume fraction, the energy released by the collapse of the bubbles on the outer boundary of the cluster is shared by the smaller number of bubbles. Since each remaining bubble receives a larger fraction of energy, its collapse is hastened, thereby reducing the life of the cluster.

Based on this analysis, the following recommendations about the design and scaleup of hydrodynamic cavitation reactors can be made:

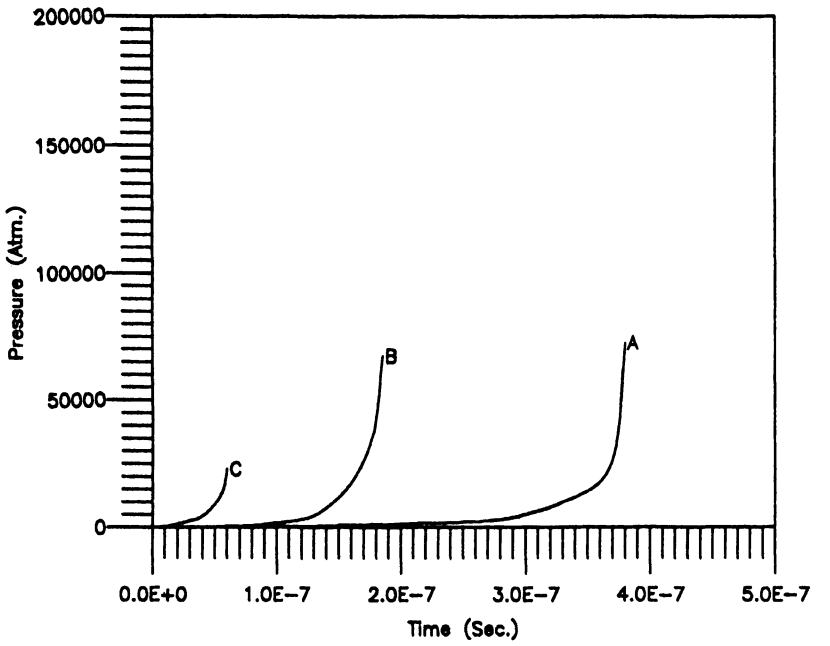

Figure 3.9. (Continued)

1. An increase in discharge pressure will not change the distribution of cavitation energy and hence should not be used as a variable to alter the performance of the reactor.
2. The time of pressure recovery can be used to alter the residence time of the reaction mixture since it alters the cluster life. With a larger rate of pressure recovery, both cluster life and the distance traveled by the cluster downstream of the orifice before its collapse increase. Thus, by changing the rate of pressure recovery (by changing either orifice to the pipe diameter ratio or size of the pipe downstream of the orifice), one can change the volume downstream of the orifice that actually experiences the cavitational effects.

3.6. FACTORS AFFECTING CAVITY CLUSTER BEHAVIOR IN ACOUSTIC CAVITATION

A number of parameters such as acoustic intensity and frequency, initial cluster radius, and bubble volume fraction affect the cluster dynamics in acoustic cavitation. Typical effects of acoustic intensity and frequency, initial cluster radius, and bubble volume fraction within the cluster on the cluster radius and life were examined by Moholkar and co-workers. Their results were obtained from the

simulation of the model equations described in Chapter 2. Important conclusions are briefly summarized below.

Simulations were carried out in initial cluster diameters of 4 mm to 8 mm, an acoustic intensity between 5 and 20 W/cm^2, an acoustic frequency between 20 and 50 kHz, and bubble volume fractions between 10^{-8} and 10^{-6}. Their results indicate that the life of the cluster decreases with an increase in the intensity of the acoustic field and a decrease in acoustic frequency. The pressure ratio decreases with an increase in acoustic intensity and frequency. Finally, a larger initial cluster diameter and an increase in bubble volume fraction increase the cluster life, with a minor effect on the pressure ratio.

3.7. CONCLUDING REMARKS

Based on the simulation of the cavitation bubble dynamics and other assessments outlined in this chapter, the following conclusions can be made:

1. The magnitude of the pressure impulse obtained as a result of cavity collapse increases with an increase in cavity size for both acoustic and hydrodynamic cavitations.
2. With increasing irradiation frequency in acoustic cavitation and faster recovery rates in hydrodynamic cavitation, the life of an individual cavity increases. As a result, the number of pressure pulses corresponding to each oscillation of the cavity before collapse increases. In hydrodynamic cavitation, however, this rise is also accompanied by an increase in the magnitude of the pressure pulse.
3. A study of the effect of increasing intensity of irradiation in acoustic cavitation and the resulting recovered pressure in hydrodynamic cavitation reveals that in both cases the magnitude of the pressure pulse increases with an increasing ultrasonic intensity for acoustic cavitation and with recovery pressure in the case of hydrodynamic cavitation.
4. An increase in the noncondensable gas content increases the life of the bubble; hence, the number of pressure pulses is simultaneously increased, but they are of a lesser magnitude.
5. A laser-induced cavity can be perfectly spherical, which can generate large pressure and temperature pulses as well as acoustic velocity upon its collapse. There is significant damping during the collapse of a spherical cavity. Just as for hydrodynamic and acoustic cavitations, laser cavitation produces the most favorable results in water (compared with organic liquids).
6. Cluster life increases with a decrease in acoustic intensity and an increase in frequency. A larger initial cluster radius and a larger bubble volume fraction

also increase cluster life. A smaller initial cluster size and smaller frequency produce larger pressure impulses upon the collapse of the cluster.

The pressure pulses obtained from bubble oscillations in hydrodynamic cavitation are lower in magnitude but very large in number. Therefore the reactions that require relatively milder conditions of temperature and pressure can be carried out efficiently in hydrodynamic cavitation reactors. The simulations reported by Moholkar (1996) and Moholkar and Pandit (1997), and their methodology can be used to decide on the operating conditions of the cavitating equipment, the likely conditions of temperature and pressure generated during the collapse of the cavity, and whether they are adequate for carrying out a specific chemical reaction. The pressure pulse obtained from acoustic cavitation, on the other hand, is larger in magnitude and creates much higher temperatures and pressures upon the implosion of the cavity. The reactions that require high temperatures and pressures are thus more suitable for acoustic cavitation. Optical cavitation would be most suitable for laboratory study of cavitation chemistry under extreme temperature and pressure conditions.

4

GAS–LIQUID CAVITATION CHEMISTRY

4.1. INTRODUCTION

As described in Chapter 3, the source of cavitation chemistry is the phenomenon of cavitation, which is largely caused by the reduction of pressure within a liquid. In an ultrapure system, a large pressure reduction will be required to form the cavities. However, cavities can be formed with a small pressure reduction if there are small amounts of dissolved or undissolved impurities present in the bulk liquid. The cavities can also be formed at liquid–solid interfaces, as is the case in many gas–liquid–solid cavitation-induced transformations. Possible sites of the reaction induced by cavitation were graphically illustrated in Figure 1.5. We examine here the chemical transformations induced by the cavities that are generated by either acoustic or hydrodynamic forces.

When liquid is exposed to ultrasound, chemical transformation occurs through a process defined by the behavior of the small bubbles. Their lifetime is generally a few acoustic cycles, during which they expand by vapor pumped into the bubble as its surface expands and contracts with the changing pressure in the liquid. The degree of expansion (which can be of the order of 3 to 400 times) depends on the size of the initial nuclei. These bubbles then move toward the pressure antinodes and collapse violently during the next compression half-cycle. The local temperatures and pressures generated by this collapse are very large. Schematic representations of the lifetime of a small bubble (i.e., transient cavitation), during an acoustic cycle, the nature of its growth and collapse, and the regimes where cavitation is unlikely are given in Figure 4.1. It should be pointed out that no liquid cavitation reaction occurs without cavitation and several published examples contain parallel experiments showing that vigorous stirring or mechanical agitation will not produce a marked increase in the reaction rate. The interaction of sound with matter through the process of cavitation offers a range of energies for chemical conversion that are not available from other sources. Hydrodynamically caused

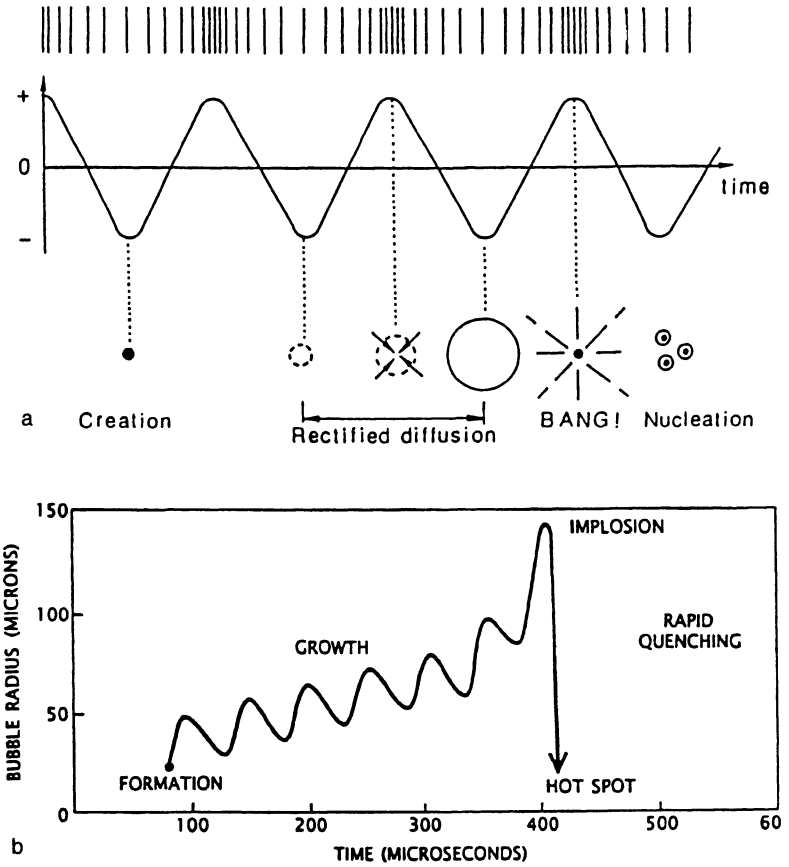

Figure 4.1. (a) Schematic representation of the lifetime of a transient cavitation bubble. (From Suslick, 1986b, with permission.) (b) Schematic representation of bubble growth and implosion in a liquid irradiated with ultrasound. (From K. Suslick, "Sonochemistry" in *Kirk Othmer Encyclopedia of Chemical Technology*, 4 ed., vol. 26, pp. 516–541. Copyright © 1998, John Wiley & Sons, Inc. Reprinted by permission of John Wiley & Sons, Inc.) (c) Region where cavitation is unlikely. (From K.S. Suslick, "The chemical effects of ultrasound," *Scientific American*, Feb. 1989, pp. 82,83, reproduced with permission of Slim Films.)

cavitation has similar behavior, although the frequency, time, and recovery pressure are of different magnitudes.

The implosion of cavities formed by ultrasound or other hydrodynamic forces establishes an unusual environment for chemical reactions. The gases and vapors inside the cavity are adiabatically compressed, generating intense heat that raises the temperature of the liquid immediately surrounding the cavity and creates a local hot spot. Even though the temperature of this region is extraordinarily high, the

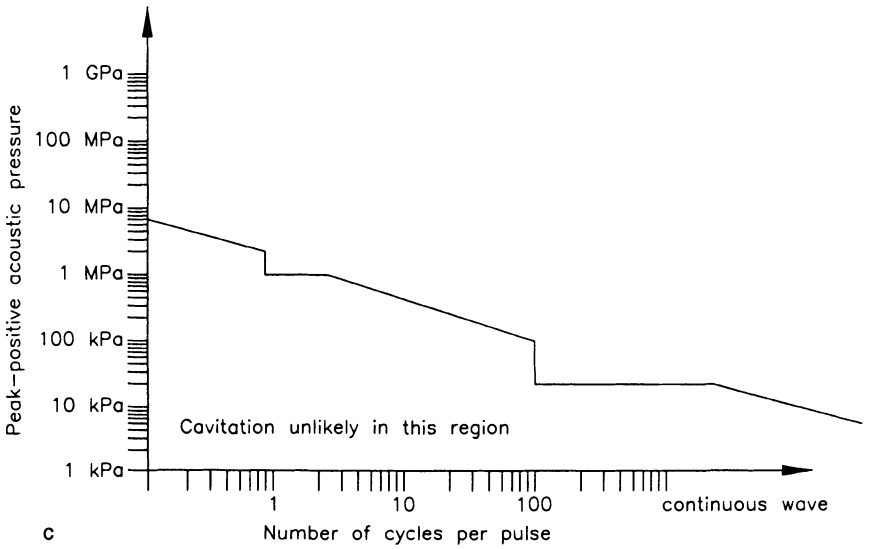

Figure 4.1. (continued)

region itself is so small that the heat dissipates quickly. The heating and cooling rates during cavitation are estimated to be more than a billion degree Celsius per second. This is similar to the cooling that occurs if molten metal is splattered onto a surface cooled near absolute zero. At any given time, therefore, the bulk of the liquid remains at the ambient temperature.

The exact temperatures and pressures generated during cavity implosion are difficult to calculate theoretically and to determine experimentally. Yet these quantities are fundamental to describe the potential of cavitation chemistry. Theoretical models have been proposed that approximate the dynamics of cavity implosion at various levels of accuracy. All these models have difficulty in accurately describing cavity dynamics during the last stages of implosion. The most sophisticated models give temperatures of thousands of degree Celsius, pressures of hundreds to thousands of atmospheres, and heating times of less than a microsecond.

Although the pressures attained during cavity implosion are harder to determine experimentally than temperature, the two quantities are correlated. One can therefore estimate the peak pressure to be 500 atm, which is half the pressure at the deepest region of the ocean, the Mariana Trench. Even though the local temperature and pressure conditions created by cavity implosion are extreme, the system parameters that affect cavitation chemical reactions are reasonably well defined. The intensity of cavity implosion, and hence the nature of the reaction, can easily be altered by such factors as acoustic frequency, acoustic intensity, ambient tem-

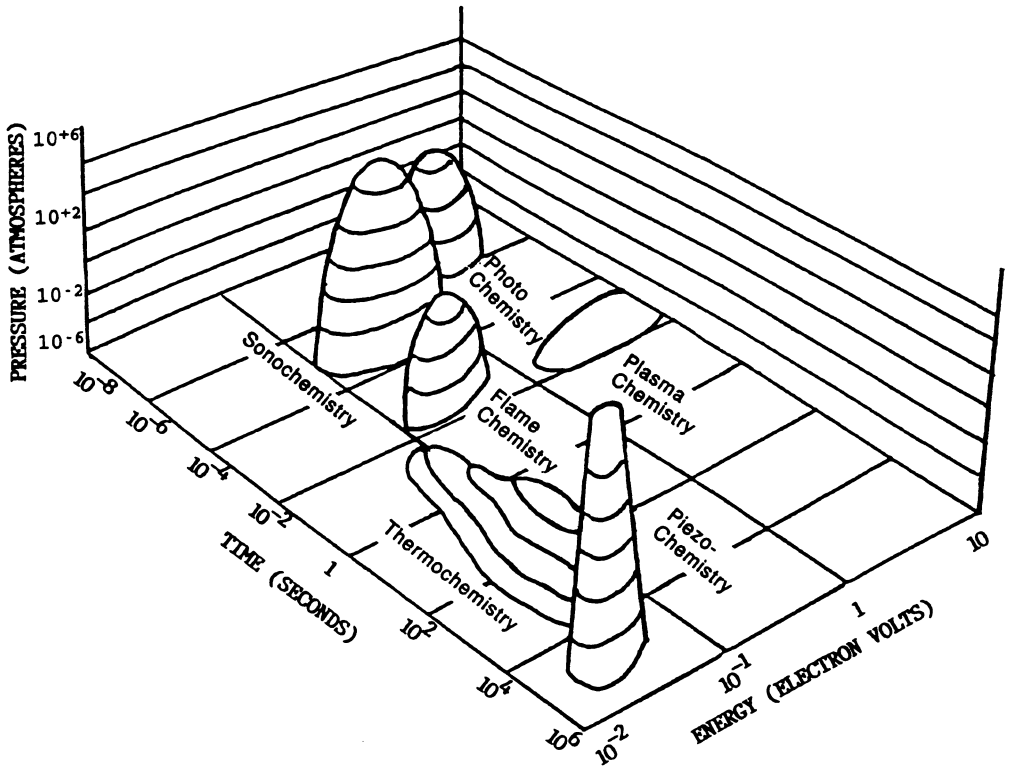

Figure 4.2. Chemistry: the interaction of energy and matter. To convert atmospheres to pascals, multiply by 1.013×10^5. (From K. Suslick, "Sonochemistry," in *Kirk Othmer Encyclopedia of Chemical Technology*, 4 ed., vol. 26, pp. 516–541. Copyright © 1998, John Wiley & Sons, Inc. Reprinted by permission of John Wiley & Sons, Inc.)

perature, static pressure, choice of liquid, pretreatment of liquid, initial size of bubbles, or choice of the ambient gas. The way in which these factors alter cavitation chemistry often defies basic intuitions about chemistry.

Sonochemistry makes available a range of energies as well as a combination of pressures and duration not available from any other source. The relations among energy, pressure, and time for sonochemistry and other chemistry are illustrated in Figure 4.2. The effects of ultrasound on liquids have also been used to enhance the chemistry of compounds in solution. Compounds that contain metal–carbon bonds, called *organometallics*, are particularly illustrative. This diverse class of chemicals is important in the formation of plastics, in the production of microelectronics, and in the synthesis of pharmaceuticals, herbicides, and pesticides. The conversion of $Fe(CO)_5$ (see Table 4.1), when compared with the effects of light and heat, underscores the distinctive chemistry that ultrasound can induce. When $Fe(CO)_5$ is exposed to heat, it decomposes into carbon monoxide (CO) and a fine iron powder, which ignites spontaneously in air. When $Fe(CO)_5$ is exposed to ultraviolet light, it first breaks down into $Fe(CO)_4$ and free CO fragments. $Fe(CO)_4$ can then recombine to form $Fe_2(CO)_9$. Cavity implosion creates different results. It delivers enough heat to dissociate several CO molecules but cools quickly enough to quench the reaction before decomposition is complete. Thus when $Fe(CO)_5$ is exposed to ultrasound, it yields the unusual cluster compound $Fe_3(CO)_{12}$. The literature has shown that the rate of decomposition of $Fe(CO)_5$ is exponentially dependent upon the solvent vapor pressure at 25°C under argon for a series of hydrocarbon solvents. Cavitation chemistry induced by hydrodynamic forces carries milder temperatures and pressures and thereby has slower rates and perhaps somewhat different sets of reactions.

The sonochemistry of two immiscible liquids (such as oil and water) stems from the ability of ultrasound to emulsify liquids so that microscopic droplets of one liquid are suspended in the other. Pressure fluctuations (caused by either acoustic

TABLE 4.1. Reaction Schemes for Sonolytic, Thermolytic, and Photolytic Decomposition of $Fe(CO)_5$[a]

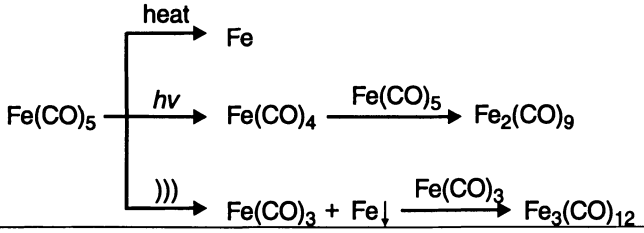

[a]From Peters (1966) with permission.

or hydrodynamic forces) stress liquid surfaces, overcoming the cohesive forces that hold a large droplet together. The droplet bursts into smaller ones and eventually the liquids are emulsified. Emulsification can accelerate chemical reactions between immiscible liquids by greatly increasing their surface contact. A large contact area enhances crossover of molecules from one liquid to the other, an effect that can make some reactions proceed quickly. The emulsification of mercury with various liquids has a particularly interesting chemistry.

4.2. MECHANISMS FOR CAVITATION REACTION

The chemical and biological effects of ultrasound were first reported by Richards and Loomis (1927) more than 70 years ago. Within 15 years of that work, widespread applications of ultrasound were found. Given the detailed understanding of the dynamics of cavitation outlined earlier, the relevant question for the chemist lies in the actual mechanisms responsible for the liquid cavitation reactions. A number of mechanisms discussed in the literature are briefly outlined here.

While the "hot-spot" pyrolysis theory of the collapse of cavitation bubbles, first proposed in 1950 (Neppiras, 1980; Neppiras and Noltingk, 1950,1952), is now the generally accepted model, many other theories have also been proposed to explain sonochemical behavior. The first of these arose from observations that water emits light when it is exposed to ultrasound. This process, "sonoluminescence," was proposed to occur via some mechanism similar to that which generates lightning. Charge separation in the atmosphere tears apart water droplets, with a buildup in potential. The rapid discharge of this built-up energy results in a flash of lightning. It was suggested that cavitation bubbles are created as lenticular rather than spherical cavities in the first instance and thus enormous electric stresses are invoked within the bubble. These stresses were thought to generate moving charges in the surface layer of the bubble. In the limiting case where charge separation is complete (i.e., the positive charges are distributed diametrically opposite to the negative charges), the electric field strength across the bubble was calculated to be 600 V cm^{-1} (Apfel, 1981; Arakeri and Chakraborty, 1990; Barbier, 1899). These gradients are large enough to result in bond breakage and chemical activity. Thus the reactions were mainly electrochemical in nature.

This theory dominated sonochemistry until the 1970s, gaining legitimacy from observations that sonolysis of water creates species similar to those of electrical discharge or radiolysis. Some sonochemical effects are similar to those produced in plasma. Careful investigation has shown that the reaction rate of sonolysis is inversely proportional to the vapor pressure from the surrounding solvent. A similar relationship was obtained by Suslick (1986a,1986b), who monitored the loss of color (blue 525 nm) of the free radical scavenger DPPH (1,1-Diphenyl-2-pieryl hydroxyl) in various solvents under argon at a temperature of 4°C and an intensity

of 50 W cm^{-2}. These results are summarized in Table 4.2. These findings are justified in terms of the "hot spot" model: the adiabatic heating effects of rapid compression decrease as the vapor recondenses. Furthermore, heat conduction to the surroundings further reduces the local heating effect. The overall effect is that increasing the vapor pressure reduces the intensity of cavitational collapse, the maximum temperature attainable, and subsequently the ongoing reaction rate.

Thus ultrasonic reactions have an interesting characteristic: reaction rates decrease as the ambient temperature increases. The electrical discharge theory, which was supported until the mid-1970s, has at last been rejected as being inconsistent with experimental results (Harvey 1939, 1960; Harvey *et al.*, 1944). Another theory that attempts to account for the degradation of large polymers in ultrasonic fields suggests that direct mechanical cleavage of bonds may occur as a result of the intense shock generated by either transient cavitation or the direct effect of the accelerations produced by the sound or hydrodynamic field; these have been estimated to be as high as 105 *g* at 500 kHz. However, polymer interactions with reactive species produced as a result of solvent breakdown could also account for this effect.

The most recent theory was proposed as a result of studies using binary water–ethanol mixtures. In considering the solvolysis of *tert*-butyl chloride, Mason (1986, 1987, 1990a,b) and Mason and co-workers (1983, 1988) theorized that the reaction rate must be dependent on the degree of solvation in the transition state prior to ionization. This reaction was monitored by conductometric measurement of HCl. The authors suggest that ultrasonic irradiation alters the structure of the liquid, which facilitates the chemical reaction. However, the system is too complex to make such generalizations at this time.

On the assumption that the bubble collapse is adiabatic, Noltingk and Neppiras (1950) and others have shown that the maximum temperatures and pressures generated in the bubbles are given by

TABLE 4.2. Rate of DPPH Trapping in Nonaqueous Solvents[a]

Solvent	-d[DPPH]/*dt* (μmol min^{-1})	Viscosity (cp)	Surface tension (dyn cm^{-1})	Vapor pressure (torr)
Decane	7.75	0.9	—	0.25
1-Butanol	6.2	2.9	26.2	1.1
1-Propanol	5.43	2.3	23.8	4.6
Toluene	2.17	0.6	28.5	8.7
Propyl ether	1.61	0.5	—	22.8
Acetone	0.88	0.3	23.7	33.1

[a]From Perkins (1990) with permission.

$$T_{max} = T_0[P_m(\gamma - 1)/P] \tag{4.1}$$

and

$$P_{max} = P[P_m(\gamma - 1)/P]^{\gamma/(\gamma-1)} \tag{4.2}$$

where T_0 is the temperature of the bulk liquid; P is the bubble pressure after collapse; P_m is the pressure before collapse, which generally corresponds to the vapor pressure of the liquid; and γ is the ratio of specific heats of the dissolved gas or vapor. Depending on the conditions used, a solution of Eqs. (4.1) and (4.2) leads to maximum pressures of 1000–2000 bar and maximum temperatures of 4000–6000 K. For heptane–decane mixtures, a schematic diagram showing the calculated values of effective temperature immediately prior to collapse of the cavitation bubble under an argon atmosphere is shown in Figure 4.3.

There is significant experimental evidence to support the "hot spot" theory. Sehgal *et al.* (1977a,b), Seghal and Verrall (1982), and Verrall and Nomura (1977), and more recently, Suslick (1986a,b, 1987) and Suslick and co-workers (1981, 1983, 1987) have shown that the sonoluminescence induced in alkane solvents is the same as that arising from their combustion at several thousand kelvin. Also, they showed that chemical reactions, such as the decomposition of metal carbonyls, occurred under cavitation in the same manner as thermal processes at these temperatures. Regardless of the exact origin of these chemical effects, one can

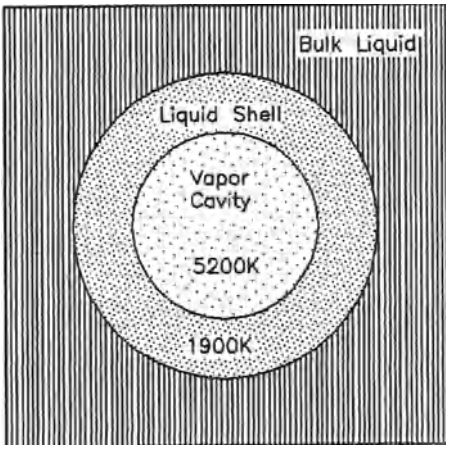

Figure 4.3. Schematic diagram showing the calculated values for the effective temperatures immediately prior to collapse of the cavitation bubble in heptane–decane under an argon atmosphere. (From Henglein, 1993, with permission.)

identify three zones (see Figure 4.3) in a cavitation system: (1) the bulk liquid, in which there is no primary cavitational chemical activity, although subsequent reaction with either acoustically or hydrodynamically generated intermediates may occur; (2) the bubble's center, where the harsh conditions lead to reactions in vapors and gases; and (3) the interfacial region, where there are large gradients of pressure and temperature, as well as extremely high shear gradients due to shock waves and the motion of solvent molecules around the collapsing bubbles.

Few experimental determinations of the nature of the sonochemical reaction site or of cavitational conditions have been made. Sonoluminescence spectra have been used by Sehgal *et al.* (1977a,b), Sehgal and Verrall (1982), and Verrall and Nomura (1977) to estimate the local conditions at the site of sonoluminescence. It is not yet established, however, whether sonoluminescence arises in the same location as most cavitation chemistry. The important questions regarding the nature of the cavitation chemical reaction site have been examined by Suslick (1986a,b, 1987) and Suslick and co-workers (1981, 1983, 1987) by evaluating the sonochemistry of volatile metal carbonyls. In order to determine whether the sonochemical reactions were occurring in the gas phase or the liquid phase of the cavitation event, the first-order rate coefficients of sonochemical ligand substitutions were measured as a function of metal carbonyl vapor pressure. If the sonochemical reaction site is gas phase only, then a plot of reaction rate coefficient versus dosimeter vapor pressure will be linear with a zero intercept; if the site is liquid phase only, then the plot will have a nonzero intercept with a zero slope (i.e., the rate coefficient will be independent of dosimeter vapor pressure).

The rate constants for sonochemical substitutions at various ambient temperatures carried out in solutions of two *n*-alkanes that had been mixed in the proper proportions to keep the total system's vapor pressure constant at 5.0 torr (6.7 mbar) were obtained by Suslick (1986a,b, 1987) and Suslick and co-workers (1981, 1983, 1987). The results indicated that the sonochemical rate coefficient increased linearly with increasing dosimeter vapor pressure and had a nonzero intercept. The linear dependence of the observed rate coefficients on metal carbonyl vapor pressure is expected for reactions occurring in the gas phase; as the dosimeter vapor pressure increases, its concentration within the gas-phase cavity increases linearly, thus increasing the sonochemical rate coefficients. In addition, the nonzero intercept indicates that there is a vapor pressure-independent component of the overall rate. There must be, therefore, an additional reaction site within the liquid phase, presumably in the thin liquid shell surrounding the collapsing cavity.

With these data, one may also estimate the effective temperatures reached in each site by the use of comparative rate thermometry, a technique developed for similar use in shock tube chemistry. If the chemical reaction rate coefficients follow Arrhenius behavior [$k = A \exp(E_a/R_gT)$, where A is the frequency factor, E_a is the activation energy, and R_g is the gas constant], then a plot of $\ln(k_i/A_i)$ against E_{ai} for a series of reactions i gives a line with the slope $1/R_gT_{\text{eff}}$ Using the sonochemical

kinetic data for ligand substitution of metal carbonyls, in combination with the activation parameters (A and E) determined by high-temperature gas-phase laser pyrolysis, the effective temperatures of both sonochemical reaction sites have been experimentally estimated by Suslick (1986a,b, 1987) and Suslick and co-workers (1981, 1983, 1987): the gas-phase reaction zone effective temperature is 5200 ± 650 K, and the liquid-phase effective temperature is ~1900 K. Using a simple thermal conduction model, the liquid reaction zone is estimated to be ~200 nm thick and to have a lifetime of less than 2 μs.

The sonochemical estimates of cavitational temperature in the liquid shell are comparable to those determined by sonoluminescence, which may mean that the site of sonoluminescence (at least for the alkali metal ions) is in the heated liquid shell surrounding the collapsing bubble. Regardless of the details, it is clear that cavitational collapse generates hot spots with effective temperatures of several thousand degrees. The cavitation efficiency is determined by the possibility of the components reacting by a mechanism in which a reactive intermediate is directly generated by the cavitational events. Such intermediates should be radicals or radical ions, and the cavitation-sensitive step should follow a single electron transfer (SET) mechanism. For volatile species in water, the reactions will predominantly occur in gas cavities. For nonvolatile species, the reactions would predominantly occur in the liquid film surrounding the gas cavities.

It is important to compare the relative strength of free radical reactions (mainly occurring in the liquid shell surrounding the bubble) during ultrasonic radiation with radiolysis and photolysis. From the "collapse" of one cavitation bubble in sonication, approximately 10^4–10^6 radical pairs can be formed; this is between three and five orders of magnitude higher than the corresponding number of ions and radicals produced in tracks of ionizing radiation and the number of radicals generated in a "cell" during the photolysis process. Taking into consideration the sizes of the gas microbubbles (10^{-6}–10^{-7} m in diameter), their steady-state concentration within a cavitation liquid (10^{13}–10^{14} bubbles/m^3), as well as the ultrasonic energy density (10^3–10^6 W/cm^3 at an intensity of 10^5 W/cm^2), it is easy to understand the success of this ultrasonic cavitation technique as a "new" initiation method. Table 4.3 gives values of the radical recombination coefficients (B_R) for several organic free radicals produced in an ultrasonic field, as well as the corresponding values obtained using the photolysis method. Table 4.4 shows the comparative yields of various products of the free radicals generated by sonolysis, radiolysis, and photolysis techniques.

Riesz *et al.* (1990) demonstrated with the help of electron paramagnetic resonance and spin-trapping studies of the free radical intermediates generated by the sonolysis of aqueous solutions of volatile solutes (methanol and ethanol) and nonvolatile solutes (acetate, amino acids, sugars, pyramidines, nucleotides, and surfactants) that these reaction zones exist in aqueous sonochemistry. The very high temperatures and pressures induced by acoustic cavitation in collapsing gas bubbles

TABLE 4.3. Values of the Radical Recombination Coefficients, B_R for a Number of Organic Free Radicals Produced by either Ultrasonification (U) or Photolysis (P) Treatment[a]

Organic compound	Atmosphere	Radicals produced	B_R (U)	B_R (P)
CH_3CHO	Ar	$CH_3^\bullet$	30–35	0.5
		$CHO^\bullet$	16–22	0.5
C_6H_{12}	Ar	$^\bullet C_6H_{11}$	16–19	0.2
		$H^\bullet$	5–8	—
CH_3CHO	O_2	$CH_3COOO^\bullet$	46–50	—
C_6H_{12}	O_2	$C_6H_{11}OO^\bullet$	33–38	—

[a]From Mokry and Starchevsky (1993) with permission.

TABLE 4.4. Comparative Yields of the Products from Sonolysis [$F(y)$], Radiolysis [$G(y)$], and Photolysis [$\pi(y)$] of Acetaldehyde and Cyclohexane, carried out in the Presence of Different Gases[a]

Organic precursor	Products	$F(y)$	$G(y)$	$\pi(y)$[b]
CH_3CHO	CH_4	2.06	7	+
	CO	3.04	1.8	1
	HCOH	1.1×10^{-5}	—	—
	H_2	1.2×10^{-5}	1.2	+
	C_2H_6	1×10^{-3}	1.1	+
C_6H_{12}[c]	H_2	2.0	5.2	+
	C_6H_{11}–C_6H_{11}	0.81	1.7	+
	C_6H_{10}	0.21	2.4	+
CH_3CHO[d]	CH_3COOH	17,150	—	20,000
	CH_3COOOH	5410	—	+
	CO_2	202	—	—
	CO	28	—	—
	CH_4	72	—	—
C_6H_{12}[d]	$C_6H_{11}OOC_6H_{11}$	2.75	0.5	—
	$C_6H_{11}OOH$	0.1	1.0	—
	$C_6H_{11}OH$	0.38	—	—
	$C_6H_{10}O$	0.29	0.7	—

[a]From Mokry and Starchevsky (1993) with permission.

[b]+ indicates that the product is known to be present but a quantitative determination of the yield has not been reported.

[c]Experiments carried out in an argon atmosphere.

[d]Experiments carried out in an oxygen atmosphere.

in aqueous solutions lead to the thermal dissociation of water vapor into hydrogen atoms and hydroxyl radicals. Reactions take place in the gas phase (pyrolysis reactions), in the region of the gas–liquid interface, and in the bulk of the solution at ambient temperature (similar to radiation chemistry reactions). By using rare gases with different thermal conductivities, the contributions of individual reaction steps with widely different energies of activation can be evaluated. In this case the cavitation efficiency is determined by the possibility of the components reacting by a mechanism in which a reactive intermediate is directly generated by the cavitational events. Such intermediates should be radicals or radical ions, and the cavitation-sensitive step should follow a single electron transfer mechanism. For volatile species in water, the reactions will predominantly occur in gas cavities. For nonvolatile species, the reactions will predominantly occur in the liquid film surrounding the gas cavities.

4.3. FACTORS AFFECTING CAVITATION CHEMISTRY

Just like cavitation physics, cavitation chemistry is strongly affected by a variety of external parameters, including acoustic frequency, acoustic intensity, bulk temperature, static pressure, choice of ambient gas, choice of solvent, etc. These are important considerations in the effective use of ultrasound or hydrodynamic forces to influence chemical reactivity and are also easily understandable in terms of the cavitational hot-spot mechanisms. These effects are summarized in Table 4.5.

4.3a. Acoustic Frequency

Historically there have been two underlying misconceptions in cavitation chemistry. The first suggests that there is no frequency effect. This misconception arises from the idea that once the cavitation threshold is crossed, the ensuing cavitational collapse will provide the same effects whatever the frequency. The second concerns the frequencies employed in cavitation chemistry, which are generally in the power ultrasound range defined as 20 to 100 kHz. The latter is the case despite the fact that there is a considerable amount of information on sonochemistry, which uses frequencies higher in the ultrasonic range (around 1 MHz) but still involves cavitation. Even if we restrict our considerations to ultrasound in the kilohertz range, there are still some interesting frequency effects. Petrier and co-workers (1982, 1984, 1985, 1992a,b) and Petrier and Luche (1987) compared the effectiveness of 20- and 514-kHz irradiation in the oxidation of aqueous KI to iodine and the generation of hydrogen peroxide in water at the same input power. The rate of production of iodine in oxygen-saturated KI (10^{-2} M) was some six times faster, and peroxide formation in water 12 times faster at the higher frequency. This result is ascribed to the fate of the $OH^{\cdot}$ radical formed by the breakdown of water on

TABLE 4.5. Effects of Extrinsic Variables on Cavitation Chemistry[a]

Extrinsic variable	Physical property	Effect
Acoustic frequency	Period collapse	Resonant bubble size
Acoustic intensity	Reaction zone size	Cavitation events per volume
Bulk temperature	Liquid vapor pressure	Bubble content, intensity of collapse
	Thermal activation	Enhanced secondary reaction rates
Static pressure	Total applied pressure	Intensity of collapse
	Gas solubility	Bubble content
Ambient gas	Polytropic ratio	Intensity of collapse
	Thermal conductivity	Intensity of collapse
	Chemical reactivity	Primary or secondary sonochemistry
	Gas solubility	Bubble content
Choice of liquid	Vapor pressure	Intensity of collapse
	Surface tension	Transient cavitation threshold
	Viscosity	Transient cavitation threshold
	Chemical reactivity	Primary or secondary sonochemistry

[a]From Suslick (1986a) with permission.

collapse of the cavitation bubble. The OH^- can be destroyed by reactions in the bubble or can migrate into the bulk and produce peroxide. At the higher frequency, a shorter bubble lifetime allows more of the OH^- to escape from the bubble. The efficiency of OH^- production thus increases as the irradiation frequency is increased (see Table 4.6). There is also some evidence for this frequency effect in work involving OH^- detection by fluorescence. When aqueous sodium terephthalate reacts with OH^-, it forms fluorescent hydroxyterephthalate, and its concentration can be estimated spectroscopically.

In a recent study, Seymour and Gupta (1996, 1997, 1998) and Seymour *et al.* (1997) showed that the oxidation of KI is significantly enhanced with higher ultrasound frequency. They showed that in a novel reactor, an ultrasound frequency of 640 kHz gave a 100% enhancement over the best reported rate for the oxidation of potassium iodide, on a per watt basis. In this study, increasing the KI concentration by over eightfold merely increased the iodine production rate by twofold. This

TABLE 4.6. Effect of Frequency on OH^- Production[a]

Frequency (kHz)	20	40	60
Fluorescence	30	40.2	29.3
Power (W)	50	26	11
Efficiency	0.6	1.6	2.7

[a]From Mokry and Starchevsky (1993) with permission.

suggested that in the oxidation region surrounding the bubble, the KI concentration was much different than in the bulk. It was proposed that the hydrophobic bubble region had a lower and near saturation KI concentration. In subsequent work, Seymour and Gupta (1997, personal communication) showed that the addition of NaCl salt further enhanced the sonochemical degradation of aqueous pollutants at 640 kHz frequency. The magnitudes of enhancement are quite large: threefold for *para*-ethylphenol and ninefold for phenol. These reaction rate enhancements were due to better partitioning of the pollutant molecules near the cavitation bubble.

Cavitation induced by very low-frequency sound (< 100 Hz) has an observational advantage because of its large spatial (~1 cm) and temporal (~0.1 s) scale, which permits more easily detailed insights into bubble dynamics. At very high frequencies (above a few megahertz) cavitation ceases, and sonochemistry is generally not observed. The observed thresholds for liquid cavitational chemical transformation are strongly frequency dependent. The existence of an optimum pressure amplitude for a given frequency has been demonstrated for some cavitation-related phenomena, e.g., sonoluminescence cavitation erosion.

4.3b. Acoustic Intensity

Acoustic intensity has a dramatic influence on the observed rates of sonochemical reactions. Below a threshold value, the amplitude of the sound field is too small to induce nucleation or bubble growth. Above the cavitation threshold, increased intensity of irradiation (from an immersion horn, for example) increases the effective size of the zone of liquid undergoing cavitation and thereby increases the sonochemical rate. Furthermore, as the acoustic pressure increases, the range of bubble sizes that undergo transient cavitation increases; this too increases the sonochemical rate. It is often observed experimentally, however, that as one continues to increase acoustic amplitude, eventually rates begin to diminish again. Possible explanations for this behavior include bubble shrouding of the sonic horn and overgrowth of bubbles.

The effect of pressure amplitude on sonochemical reactions has not exhibited a maximum. Thus, yields increase with increasing amplitude. This may, however, be because high-intensity ultrasonic horns have not been used so far in studying sonochemical reactions. Luche (1987, 1991, 1992a,b, 1993, 1998) and Luche and co-workers (1983, 1984, 1989) have reported that the Barbier reaction rate between an alkyl lithium and an aldehyde increases continuously as the voltage input to the transducer is increased from 60 to 160 V (Figure 4.4). While the temperature in these experiments was not stable, the experimental observations show that there is an upper limit to power input beyond which no additional rate increase is seen. Explanations put forward suggest that penetration of sound into the body of the liquid is hindered if cavitation is so intense that, as indicated earlier, the radiating surface becomes shrouded in a layer of bubbles. Conversely, it may simply be that bubble growth becomes so rapid that the boundary for transient cavitation is exceeded before the next

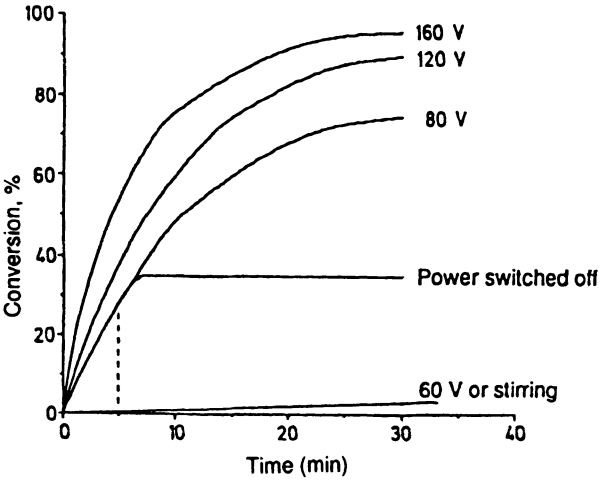

Figure 4.4. The effects of increasing power input on the rate of the reaction between an alkyl lithium and benzaldehyde. (From Luche, 1991, with permission.)

compression half-cycle. In any case, very high intensity generally does not produce high rates of reaction and is therefore not very desirable. Similar arguments will also hold for hydrodynamic cavitation. A sharp pressure drop could cause clouds of bubbles, not all of them effective in creating useful cavitation chemistry.

4.3c. External Pressure

The greater the external pressure, the larger the collapse pressure and the shorter and more violent the bubble collapse. This postulation has, however, been questioned and is further complicated by consideration of the events that lead to nucleation of the bubbles.

An increase in the static pressure: (1) decreases the gas content of a bubble; (2) increases the maximum pressure during the final stages of collapse; (3) increases the temperature reached during the final stages of collapse; (4) increases erosion, which depends on shock wave intensity; (5) may increase the threshold for cavitation; and (6) may or may not increase chemical reaction yields. The chemical reaction rate will increase with the increased final temperatures and pressures associated with higher static pressures (lower gas content). However, a lower gas content also means a lower concentration of gas molecules in a bubble, thus lowering the reaction rate and reaction product yield. Depending on which of these two effects is greater, elevated static pressure may or may not enhance sonochemical reaction yields. The effects of static pressure on the yields of some reactions are listed in Table 4.7.

TABLE 4.7. Effect of Elevated Static Pressure on Cavitation Processes[a]

Author	System studied	Nature of effect
Weissler (1950, 1951a,b, 1953, 1959, 1960, 1962)	Yield of H_2O_2	Shows a maximum yield at 2 atm
Weissler *et al.* (1950)	Sonoluminescence	Shows a maximum intensity at 2 atm
Finch (1965)	Sonoluminescence of H_2O_2	Luminescence increases with pressure in the range of 0–10 psi, then decreases with further pressure increase
Siryotuk (1966, 1971)	Cavitation, erosion	Erosion increases with pressure by a factor of 10^2 to 10^3 until a pressure of 45 atm, then starts decreasing with a further increase in pressure
El'Piner (1964)	Oxidation of KI in aqueous solution in presence of O_2	Yield decreases monotonically from X to 40 atm pressure
Bronskaya *et al.* (1968)	Formation of HCOOH from a ketoglutaric acid	Yield decreases with increasing pressure from 1 to 4, then starts to increase
	Irradiation of biological cells	Mortality of cells rises abruptly when pressure is increased above 4 atm
Chendke and Fogler (1974, 1983a,b) Fogler (1971)	Decomposition of CCl_4 in the presence of argon	Yield of Cl_2 increases up to a pressure of 1.8 atm (higher pressures not investigated owing to equipment limitations)
Bogachev and Korobeinikov (1972)	Cavitation erosion in liquid oxygen	The cavitation erosion vs. static pressure curve shows a maximum at a pressure that depends on the acoustic frequency applied

[a]Reprinted from *Chem. Eng. J.*, **8**, P.K. Chendke and H.S. Fogler, "Second-order sonochemical phenomena-extensions of previous work and applications in industrial processing," pp. 165–178, copyright 1974, with permission from Elsevier Science.

Sonochemical yields as a function of increasing static pressure have been reported by different researchers to increase, to decrease, and to increase to some point and then decrease. One would expect cavitational collapse to increase in intensity with increasing external pressure because the total imposed pressure at the initiation of collapse would be increased. Given a fixed acoustic intensity, however, nucleation of cavities can no longer occur above some limiting applied pressure, since the acoustic field must overcome the combined tensile strength of the liquid and the ambient pressure. In contrast, as one reduces the ambient pressure, eventually one deactivates the gas-filled crevices that serve as nucleation sites and therefore also diminishes the sonochemistry. Further experimental difficulties occur when one attempts to maintain a pressure vessel at constant temperature while under

ultrasonic irradiation. In reactions that involve the ambient gas directly, enhanced solubility also plays a role in the overall rates observed. While very little is known about the effect of pressure on hydrodynamic cavitation, in principle, arguments similar to those for acoustic cavitation would hold.

4.3d. Gas Solubility

Bebchuk and Rozenburg (1951) found that cavitation erosion decreased monotonically with increased gas solubility. Fitzgerald and co-workers (1956) Prudhomme (1950, 1957), Prudhomme and Grabar (1949a,b, 1958), and Prudhomme and Guilmart (1957) studied the effects of various dissolved gases on the formation of H_2O_2 from water. Fitzgerald varied the composition of an argon–helium mixture over the range of 0 to 100% argon and found that H_2O_2 yield decreased linearly with the square root of the thermal conductivity of the gas mixture and increased linearly with the solubility of the Ar–He mixture in the water. These results demonstrate a statistical relationship between cavitation and the amount of dissolved gas. Ceschia and Iernetti (1973) observed a decrease in cavitation threshold for incipient sonoluminescence with increasing gas solubility. They also found that the concentration of cavitation nuclei is directly proportional to the gas solubility.

4.3e. Nature of the Gas

Srinivasan (1955) and Srinivasan and Holroyd (1955, 1961) studied the spectral distribution of the sonoluminescence of water saturated with different gases and found that the spectrum was continuous and that the spectral distribution closely resembled that of a blackbody radiation of 10,000 K for water saturated with monoatomic gases and 8800 K for water saturated with diatomic gases. Triatomic gases like CO_2 suppress both sonoluminescence and sonochemical reactions. However, different gases with the same specific heat will luminesce with different intensities and also enhance chemical reactions to different extents. This difference may be attributed to a departure from adiabatic conditions and to differences in the solubilities of the gases.

The choice of ambient gas also has a major impact on sonochemical reactivity. The maximum temperature reached during cavitation is strongly dependent on the polytropic ratio ($C_p/C_v = \gamma$) of the ambient gas, which defines the amount of heat released during the adiabatic compression of that gas. This can have a dramatic impact: all other factors being equal, the difference between cavitation in the presence of xenon ($C_p/C_v = 1.67$) and a Freon ($C_p/C_v \sim 1.1$), for example, would increase the ratio of maximum temperatures by sevenfold. As mentioned earlier, sonochemical rates are also significantly influenced by the ambient gas's thermal conductivity of the ambient gas. The role of thermal transport during cavitational

collapse has long been recognized as evidence in favor of the hot-spot mechanism of sonochemistry. Sonochemical reactions often involve the gases present in the cavitation event. For example, H_2, N_2, O_2, and CO_2 are not inert during cavitation and undergo a variety of redox and radical reactions.

Heat Dissipation by Conduction. Departures from adiabatic bubble collapse may be due to heat conduction from the hot bubble contents to the liquid, which acts as a heat sink. If this mechanism is valid, then the thermal diffusivity of the bubble contents should have a pronounced effect on cavitation intensity. Generally, heat and mass transfer effects have been proven insufficient.

Effect of Heat Dissipation on Chemical Reaction. Table 4.8 shows the properties of various gases and their effectiveness in enhancing cavitation phenomena. One observes that the sonochemical yields and the sonoluminescent intensity increases with a decrease in thermal conductivity. Fitzgerald *et al.* (1956) indicated that the yield of H_2O_2 is linearly related to the square root of the thermal conductivity of the gas mixture. This linear dependence of the H_2O_2 yield on the square root of the thermal conductivity is sometimes cited as evidence in support of the hot spot theory of bubble collapse.

Prudhomme and Guilmart (1957) also examined the effects of the nature of the dissolved gas on the yield of H_2O_2 from water. Their data on the rare gases indicate an increasing yield of H_2O_2 with decreasing thermal conductivity of the gas up to a point, beyond which the yield remains essentially the same on further reduction of the thermal conductivity of the gas. This suggests that there is a region in which the bubble collapse is adiabatic and one in which it is heat transfer controlled. A third region is, of course, one in which the collapse is isothermal.

If H_2O in the bubble is dissociating into (H) and (OH) radicals, a portion of the heat of compression is absorbed by this dissociation, thus lowering the final temperature in the bubble. Similarly, a possible explanation of inhibitive action of dissolved CO_2 on sonoluminescence and chemical reactions may be the thermal dissociation of CO_2 to CO and O_2 in the cavitation bubble, resulting in a lower bubble temperature.

4.3f. Liquid Properties

Water is a good solvent for gases and other solutes since water vapor molecules in a cavitation bubble are dissociated into atomic H and OH radicals. These radicals serve as initiators of various chemical reactions, such as the formation of H_2O_2, the liberation of CO_2 from a saturated water–CO solution, and the oxidation of KI to give iodine.

There are other examples of ultrasonically induced chemical reactions between two dissolved gases in an aqueous medium. For example, molecules of N_2 and O_2

TABLE 4.8. Effect of Physical Properties of the Dissolved Gas on the Cavitation-Induced Phenomena of Sonoluminescence and Chemical Reaction[a]

Gas	Mol weight	Ionization potential (eV)	Specific heat ratio	Solubility in water (ml/100 ml H_2O) at 0 °C	Thermal conductivity (cal/sec · cm · °C) × 10^6 at 300 K	Specific heat (cal/g mol °C at 300 K)	Amount of H_2O_2 formed (10^{-6} g/ml)	Relative intensity of UV spectra	Luminous intensity photos × 10^{-10} (1650 Å–6500 Å)
Hydrogen	2	15.6	1.41	2.14	440.0	6.86	—	0	—
Nitrogen	28	15.51	1.40	2.33	61.7	6.80	2.5	45	1.22
Oxygen	32	12.5	1.40	4.89	63.2	6.26	13.5	35	2.44
CO_2	44	14.4	1.33	171.3	39.2	8.89	0	—	—
Helium	4	24.46	1.65	0.94	357.5	4.97	1	1	1.16
Neon	20.18	21.47	1.64	2.6	114.2	4.97	7	18	3.20
Argon	39.95	15.60	1.65	5.6	42.4	4.97	21.5	54	30
Krypton	83.8	13.93	1.67	11.0	22.6	4.97	24.0	226	50

[a]Reprinted from *Chem. Eng. J.*, **8**, P.K. Chendke and H.S. Fogler, "Second-order sonochemical phenomena-extensions of previous work and applications in industrial processing," pp. 165–178, copyright 1974, with permission from Elsevier Science.

dissolved in water combine to form oxides of nitrogen. If the water is saturated with N_2 and H_2, ammonia is formed. A mixture of N_2, H_2, and CO can lead to formation of HCN and HCOOH. These and many other examples are discussed later.

The presence of dissolved impurities in a liquid affects cavitation phenomena. Negishi (1961) found that the relative sonoluminescent intensity of aqueous solutions of some electrolytes (Na_2CO_3, NaCl, $Na_2S_2O_3$, and $NaNO_3$) was a factor of 1.5 to 4 greater than that of tapwater. The presence of $NaHCO_3$, on the other hand, decreased sonoluminescence appreciably; organic liquids have similar effects on sonoluminescence in water. Liquids such as CS_2, B_7, and CH_3I enhance the sonoluminescent intensity of water by an order of magnitude. Most liquids that enhance the sonoluminescence of water do not sonoluminesce to any appreciable degree in their pure state, whereas ethylene glycol and glycerine, which luminesce brightly by themselves, do not enhance the sonoluminescent intensity of water.

Sonoluminescent intensity has been related to the product of the dipole moment of the liquid molecules and the viscosity and shown to be directly proportional to the square of the surface tension and inversely proportional to the vapor pressure. Table 4.8 also shows how the various physical properties of the dissolved gas affect the cavitation-induced phenomena of sonoluminescence and chemical reaction.

The solvent vapor pressure has a profound influence on cavitation chemistry. It is the principal determinant of the conditions formed during cavitation. Other liquid properties, such as surface tension and viscosity, alter the threshold of cavitation, but this is generally a minor concern. Aqueous sonochemistry is dominated by secondary reactions of OH^- and H^- formed from the sonolysis of water vapor in the cavitation zone. No solvent is inert under the high-temperature conditions of cavitation: even linear alkanes undergo pyrolysis, such as cracking during high-intensity sonication. Similarly, one must anticipate secondary solvent reactivity in the trapping of the high-energy species produced during cavitation. While intensities of pressure and temperature are lower during hydrodynamic cavitation, most organic chemicals will undergo transformation in these conditions as well. Many examples of this are given later in this chapter.

4.3g. Bulk Temperature

In general, raising the temperature lowers the threshold intensity required to produce cavitation. This could be due to a lowering of viscosity and/or surface tension, but is more likely to be due to a raising of the liquid vapor pressure. Based on an earlier discussion of the effects of solvent vapor pressure on the implosion of cavitation bubbles, one may expect that lowering the ambient temperature of the medium would lead to increased rates of reaction. However, several workers have shown that an optimal temperature exists. This can be explained if one assumes that the number of cavitation nuclei present will increase with increasing temperature

to a point at which the increase in vapor pressure dominates the reactivity of the system.

Most authors have, however, reported a monotonic decrease in sonochemical yields with increasing temperature of the liquid (Ibishi and Brown, 1967; Sokol'skaya and El'Piner, 1957, 1958a,b, 1960, 1973). In Sokol'skaya and El'Piner's 1973 work on the synthesis of NH_3 from N_2 and H_2 dissolved in water, the yield of NH_3 increased by a factor of 3 when the temperature of the liquid was decreased from 60 to 10°C. This may be due to an increase in the effective (useful) cavitation with a decrease in temperature. Gunther *et al.* (1959) and Siryotuk (1966, 1971) have shown that sonoluminescence, which follows some of the same trends as sonochemical reactions, decreases monotonically with increasing liquid temperatures. There is some disagreement in the literature as to the effect of ambient liquid temperature on cavitation erosion. Ibishi and Brown (1967) and Bebchuck (1957) report a maximum in cavitation erosion at a temperature of approximately 50°C. Siryotuk (1966, 1971), on the other hand, reports a monotonic decrease in cavitation erosion when the temperature of the liquid is increased.

This apparent discrepancy can be resolved by noting that as the liquid temperature is increased, the vapor pressure in the bubble nuclei increases and some dissolved gas comes out of the solution into the bubble. These factors increase the average radius of the cavitation nuclei and increase the number of active bubbles (i.e., the global intensity of the cavitation zone). However, the increased air content at higher liquid temperatures should produce lower cavitation intensity. If the test specimen is smaller than the cavitation zone, the increase in the size of the zone with temperature is of no consequence. For such a specimen, the erosion rate will decrease due to the lower intensity of cavitation. However, for a test specimen larger than the cavitation zone, the enlargement of the zone means that a large area of the specimen is exposed to attack, but at a decreased intensity. These competing phenomena may explain the maximum in the temperature-cavitation erosion curve obtained by Ibishi and Brown (1967) and Bebchuck (1957), but not that of Siryotuk (1966, 1971).

The effect of the bulk solution temperature lies primarily in its influence on the bubble content before collapse. As the ambient temperature is increased, in general, sonochemical reaction rates are slowed. From a different perspective, sonochemical reactions usually have apparent negative activation energies. This reflects the dramatic influence that solvent vapor pressure has on the cavitation event: the greater the solvent pressure found within a bubble prior to collapse, the less effective the collapse. In fact, one can quantitate this relationship rather well. Three different derivations from three different approaches all predict that the effective peak temperature generated during cavitational collapse will be inversely proportional to P_v, the vapor pressure of the system. Assuming Arrhenius behavior $[k = A_{exp}(-E_a/RgT)]$, one expects that the sonochemical rate coefficient (k_{obs}) should follow:

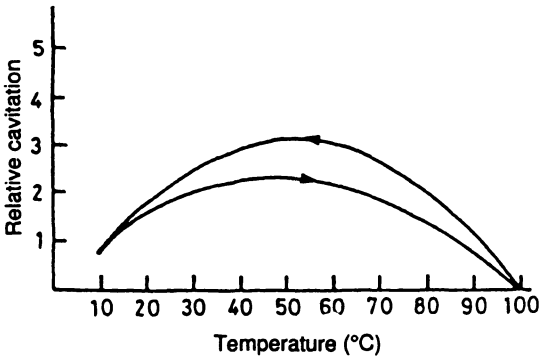

Figure 4.5. Effect of temperature on cavitation in tapwater and its associated hysteresis effect. (From Perkins, 1990, with permission. Redrawn from G. Kurtze, *Nachr. Akad. Wiss. Goettingen*, 1958, IIA.)

$$k_{obs} = \overline{C}_0 \ln A - (E_a/\overline{C}_1)P_v/T_0 \tag{4.3}$$

where T_0 is the ambient temperature of the bulk liquid; $\overline{C}_0$ and $\overline{C}_1$ contain various constants, including the number of cavitation events per volume per time, and parameters that determine the efficiency of the cavitational collapse (e.g., the polytropic ratio). These derivations are only rough approximations of very complex events. Nonetheless, the linear correlation of ln k_{obs} and P_v is the experimentally observed behavior in a wide range of sonochemical systems in a variety of solvents. When secondary reactions are important, then temperature can play its usual role in thermally activated chemical reactions.

Finally, Figure 4.5 illustrates the effect of temperature on cavitation and its associated hysteresis effect. This example is for tapwater, and the increase in intensity as the temperature is increased can be observed before it falls at the boiling point. When the temperature is allowed to fall, an increase is found in the region of 5–60°C. This is a quite significant effect and appears to occur in all liquids. Since the objective of a sonochemical reactor is to enhance cavitation at the lowest energy consumption, the results shown in Figure 4.5 indicate that most sonochemical reactors would be operated at low temperatures (below 60°C). The hysteresis effect implies that control of the bulk temperature is essential in the control of sonochemical reactor performance.

4.4. INORGANIC AND ORGANIC CAVITATION REACTIONS

Before we present more recent literature on inorganic and organic cavitation reactions, it is appropriate to first briefly review earlier oxidation studies that used ultrasound. The first description of oxidations promoted by ultrasound appeared in 1929. Oxidation of halide ions in neutral solutions by atmospheric oxygen in the

dark is known to be an extremely slow reaction. However, when a clear aqueous solution of CCl_4 is irradiated with ultrasound in the presence of starch and potassium iodide, the blue color develops immediately and is much deeper than the color that is obtained by reaction of KI and starch alone. Air and water must both be present for any reaction to occur. Hydrogen sulfide is also oxidized to colloidal sulfur.

Flosdorf and Chambers (1933) and Chambers and Flosdorf (1936) noted that in the frequency range for audible sound, solutions of egg albumin were instantly coagulated at 30°C, and sucrose was hydrolyzed to glucose about twice as fast at 50°C, as it ordinarily is at the boiling point. These authors were the first to report that the hydrolysis of esters is accelerated and the *n*-tetradecane and vegetable oils containing olein are cracked. Furthermore, inorganic halides in solutions are oxidized to free halogen, and hydrogen sulfide is rapidly oxidized to sulfur. Flosdorf and Chambers (1933) and Chambers and Flosdorf (1936) also examined the mechanism of denaturation by sound waves by using high-intensity sonic waves that caused vigorous cavitation in the solution; however, no denaturation was observed in the absence of air, CO_2, or O_2, or in the presence of N_2 or H_2.

Szalay (1933a,b,c) described how ultrasonic waves of 722 kHz can be used to depolymerize starch, gum arabic, and gelatin. The depolymerization was measured by a change in viscosity. He also found that there was slight decomposition of cane sugar to monosaccharides and of paraformaldehyde to its monomer, but other organic compounds showed no change on sonication. Moriguchi (1933a,b, 1934) studied the effect of ultrasonic waves on metal–acid reactions such as zinc with hydrochloric acid. He also described how a colloid of copper resulted from dipping a zinc plate in a copper sulfate solution that was being subjected to ultrasound.

Schultes and Gohr (1936) observed the possible fixation of atmospheric nitrogen when they showed that 540-kHz ultrasound produced hydrogen peroxide in water saturated with oxygen, while in the presence of air, nitrous oxide was also formed. If sufficient oxygen is present, further oxidation occurs and nitric acid is produced.

A major advance in sonochemistry was made in 1938 when Porter and Young (1938) described a molecular rearrangement induced by ultrasonic waves. When Porter and Young determined the rates of decomposition of benzoyl azide in benzene and aniline at 25°C with and without the effect of sound waves, they found that the rate of decomposition was increased severalfold with ultrasound. In the first patent based on sonochemistry, which appeared in 1938, it was claimed that depolymerization of solid, liquid, or gaseous hydrocarbons could be carried out at lower temperatures if they were subjected at the same time to ultrasonic waves.

4.4a. Water

In a bubble produced in a cavitating water system (see Figure 4.6), the vaporized molecules undergo homolytic cleavage to give hydrogen atoms and hydroxyl

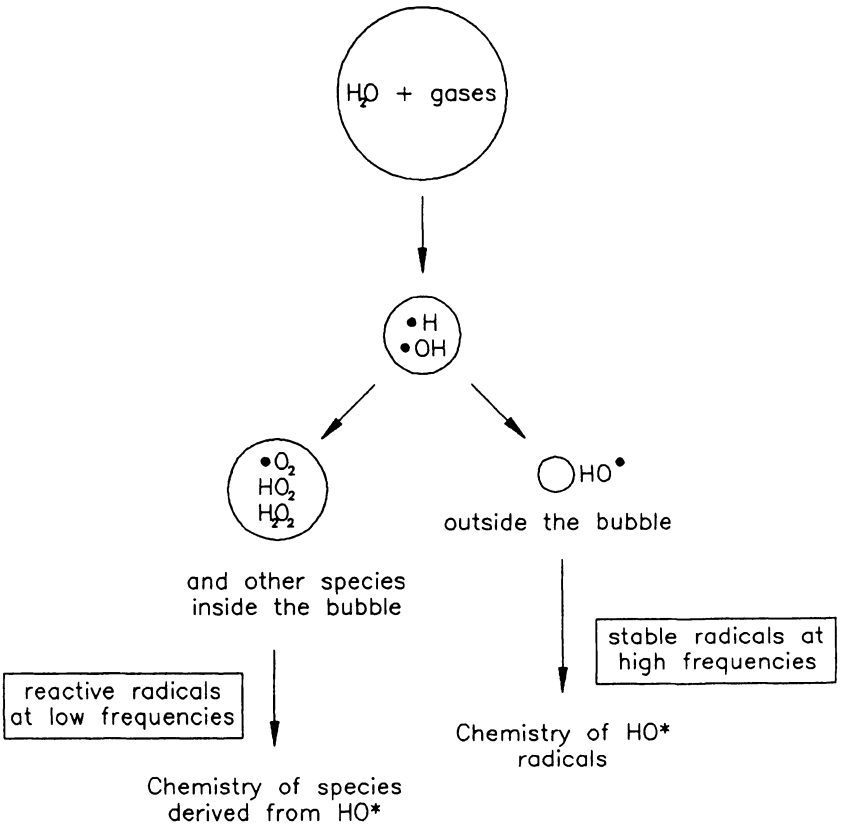

Figure 4.6. The sonolysis of water, showing how different radicals can be formed according to the frequency of the ultrasound irradiation. (From Henglein, 1993, with permission.)

radicals. According to Margulis (1969, 1974, 1975a,b, 1976a–d, 1980, 1981, 1984, 1985a,b,c, 1986, 1990), Margulis and Mal'tsev (1968a,b), and Mal'tsev and Margulis (1968), the lifetime of an HO^* radical is approximately 10^{-6} s, with the time taken for the collapse of a bubble being generally estimated as 1/5 of a cycle. At this stage, the frequency obviously becomes a very important parameter. With a high frequency (e.g., 500 kHz), the collapse occurs in 4×10^{-7} s, a period of time shorter than the lifetime of the radicals. This means that these species will be able, after the complete collapse of the bubble, to "perform" their own chemistry by migration into the liquid phase. Some aspects of the sonochemical oxidation of iodide and bromide ions can be understood by using this approach. On the other hand, at a frequency of 20 kHz, the bubble collapses in 10^{-5} s. During this relatively long time period, the initially formed HO^* radicals should be able to undergo

various reactions, such as mutual combination to give hydrogen peroxide, recombination to water, or other complex processes induced by the presence of gases. One consequence is that the chemical transformations caused by the first radical that is generated are less important at low frequencies than at high frequencies. This prediction has been tested by investigating the sonochemical oxidation of 2,2,5,5-tetramethylpiperidin-4-one, which yields the easily quantified nitroxide. It is significant that at 520 kHz the oxidation of amino groups takes place under oxygen, but is absent when argon is used. In contrast to this, at 20 kHz the more efficient cavitation effects generated under argon led to an oxidation rate that was higher than that measured under oxygen because the latter probably traps the residual radicals that have escaped recombination.

In another interpretation of this important aspect of the time factor, the results are slightly different. The lifetime of a bubble is given as 5×10^{-7} s (at a frequency of 1 MHz), and that of the radicals as between 10^{-3} and 10^{-4} s. Even with these figures, the low-frequency transformation of the initial radicals is most likely to occur because of the influential effect of vaporous cavitation under such conditions.

When pure water is exposed to ionizing particles such as fast electrons and γ-rays, practically no decomposition occurs, although many water molecules are ionized and become dissociated into radicals. The radicals H^+ and OH^- form H_2 and H_2O_2 by a mutual combination process in concentrations as low as 10^{-5} M. Water is re-formed by chain reactions:

$$H^+ + H_2O_2 \rightarrow H_2O + OH^- \tag{4.4}$$

$$OH^- + H_2 \rightarrow H_2O + H^+ \tag{4.5}$$

Densely ionizing particles such as α-rays decompose water. High local concentrations of H^+ and OH^- allow very rapid radical combinations and do not allow the above recombination process to occur successfully. When water is sonicated under argon, the following free radical reactions occur:

$$H_2O \rightarrow H^- + OH^-$$

$$2H^- \rightarrow H_2$$

$$2OH^- \rightarrow H_2O_2$$

$$2OH^- \rightarrow H_2O + O^-$$

$$H^- + O_2 \rightarrow HO_2$$

$$2HO_2 \rightarrow H_2O_2 + O_2$$

$$2O^- \rightarrow O_2$$

$$H^- + OH^- \rightarrow H_2O$$

$$\frac{1}{2}O_2 + 2H^- \rightarrow H_2O \tag{4.6}$$

Parke and Taylor (1956) and Taylor and Jarman (1970) confirmed the presence of OH^- radicals by forming *ortho*, *meta*, and *para*-hydroxybenzoic acids on sonication of aqueous solutions on benzoic acid saturated with air, oxygen, and nitrogen.

The literature data indicate that the yield of hydrogen peroxide passes through a maximum at a concentration of 25% oxygen in an Ar–O_2 gas mixture. With an increasing O_2 concentration, more H^+ atoms are scavenged and in this way are prevented from recombining as follows:

$$H^+ + OH^- \rightarrow H_2O \tag{4.7}$$

On the other hand, the decomposition of water molecules is less effective at higher oxygen concentrations. This can be understood in terms of the different γ values (ratio of the specific heats) of the two gases; the higher the argon content of the cavitation bubble, the higher is the temperature reached in the adiabatic compression phase. A study by Parke and Taylor (1956) on the dependence of H_2O_2 yield on the concentration of hydrogen in an Ar–H_2 atmosphere indicated that the yield decreases rapidly as the content of hydrogen increases. In these solutions, the reducing effects of ultrasound, such as the reduction of iodine to iodide, were also observed. The study also shows a rather unusual result obtained during the sonication of water under a mixture of two gases: the yield of hydrogen peroxide in water, which is sonicated under various H_2–O_2 gas mixtures, has two maxima; this indicates a change in the mechanism as the gas ratio varies.

Generally, the effect of frequency on the sonolysis of water has not been examined. Petrier and co-workers (1982, 1984, 1985, 1992a,b) and Petrier and Luche (1987) showed that in the presence of Ar or O_2, oxidative processes in water result in enhanced yields when a high frequency, 514 kHz, is used, in comparison with the more commonly used 20-kHz low frequency.

4.4b. Effect of Other Dissolved Gases

If the radiated water is saturated with hydrogen or carbon monoxide instead of oxygen, then no oxides are formed. Under these conditions, reduction of nitrogen

occurs to produce ammonia. If carbon monoxide is introduced along with nitrogen and hydrogen, then HCN and formaldehyde are the major products. It is interesting that HCN is also observed when carbon monoxide is replaced by methane.

Ultrasound can produce ammonia, HCN, and formaldehyde from aqueous solutions saturated with N_2, CO, and H_2. Since these gases are thought to have been present in the atmosphere of the earth at the beginning of time, it is conceivable that amino acids may have been synthesized ultrasonically. El'Piner (1964, 1968) and El'Piner and Kolesnikova (1950), El' Piner and Sokol'skaya (1957, 1958, 1971a,b), El'Piner and Stekol'nikov (1961), El'Piner and Surovova (1953), and El'Piner *et al.* (1951, 1965, 1968) have identified a number of amino acids on sonication of organic aliphatic acids in the presence of nitrogen in aqueous solutions.

CO and O_2 are the main products of the sonolysis of CO_2, and the yields of these products pass through a maximum value when water is sonicated under Ar–CO_2 mixtures of various compositions. This maximum can be explained on the same basis as that for H_2O_2 in the sonication of water under argon–oxygen mixtures. Two opposing effects are operative: with an increasing CO_2 content, the rate of decomposition is increased (since CO_2 is a reactant), but the temperature reached in the hot cavitation bubbles actually decreases because of the low value of γ (ratio of specific heats) of this gas. The yield of H_2 decreases gradually, while a maximum is also observed in the H_2O_2 yield. A small amount of formic acid is also produced.

The main reactions of the proposed mechanism include the dissociation of water molecules and carbon dioxide as

$$CO_2 \rightarrow CO + O \tag{4.8}$$

$$CO_2 + H \rightarrow HCO_2 \tag{4.9}$$

and the disproportionation of HCO_2 radicals to form HCOOH. The increased H_2O_2 yield observed at low CO_2 concentration can be explained on the basis of fewer recombination events as the H^+ atoms are partly removed and therefore more OH^- radicals are available to form H_2O_2.

The studies reported thus far show that the concepts developed in radiation chemistry concerning the formation of the primary radicals H^+ and OH^- with different spatial distributions can help us to understand certain sonochemical phenomena. However, the radical scavengers that are often used in the reported studies (i.e., iodide and formate) are very hydrophilic, and it can therefore be expected that they will only react with radicals that have reached the liquid phase. New ideas, however, have to be developed to understand the sonolysis of solutes that have a high enough vapor pressure to be present in the gas phase of the cavitation spot, or are hydrophobic and therefore accumulate at the interface. These

phenomena, which can cause sonochemical reactions, are quite different from radiation chemistry processes.

Irradiation of water under mixtures of H_2 and CO yields formaldehyde; irradiation of N_2 with CO, CH_4, or HCHO gives a variety of amino acids in low yields. It has, in fact, been suggested that cavitation induced by turbulent flow in ocean waves may have been a significant source of prebiotic organic compounds in the "primordial soup." A summary of the aqueous sonochemistry of gases is given in Table 4.9.

4.4c. Inorganic Reactions

Hydrogen Sulfide, Sulfur Dioxide, and Nitrogen Oxides. Kotronarou *et al.* (1991, 1992a,b) examined the oxidation of hydrogen sulfide in aqueous solutions. They showed that some of the initial elementary reactions involved in the high-temperature pyrolysis of H_2S within the collapsing bubble or within the interfacial region of the bubble are as follows

$$H_2S \rightarrow H^\bullet + HS^\bullet \tag{4.10}$$

$$HS^\bullet + HS^\bullet \rightarrow H_2 + S_2 \tag{4.11}$$

$$HS^\bullet + S_2 \rightarrow H^\bullet + S_3 \tag{4.12}$$

Additional reactions involving the addition of O_2 to $HS^\bullet$ radical and elemental sulfur with sulfite will lead to an array of intermediates and products. S(-II) is destroyed via two different pathways during sonication, i.e., oxidation by $^\bullet OH$ (rate constant k_0) and thermal decomposition (rate constant k_1). The calculated rate

TABLE 4.9. Aqueous Sonochemistry of Gases[a]

Substrate present	Principal products
HD	H_2, D_2
$H_2 + N_2$	NH_3
$H_2 + CO$	HCHO
$^{14}N_2 + {}^{15}N_2$	$^{14,15}N_2$
N_2	HNO_2, HNO_3, NH_2OH, N_2O, NH_3
N_2 + (CO, CH_4, or HCHO)	Amino acids
$^{18}O_2 + {}^{16}OH_2$	$^{16,18}O_2$, $^{16}O_2$
O_3	O_2
N_2O	N_2, O_2

[a]From Suslick (1989) with permission.

constants over the pH range of 7.4–12.0 indicate that, as expected, k_1 is near zero between pH 10 and 12 and increases with decreasing pH. k_0 values increase with pH up to pH 10 and then decrease and level off for pH > 11. This may be partly due to the decrease in the concentration of total sulfide available for free-radical solution reactions and lower concentrations of the $^{\bullet}OH$ radical. As H_2S fills the gas phase within the bubbles, it will cushion the implosion, resulting in lower temperatures upon bubble collapse and lower [$OH^{\bullet}$]. Thus, the reaction of $HS^{\bullet}$ with $^{\bullet}OH$ is the main pathway for the oxidation of S(-II) at a pH ≥ 10. When O_2 is present, the rate of S(-II) oxidation increases linearly with initial sulfide concentration. At a pH ≤ 8.5, thermal decomposition of H_2S within or near the collapsing cavitation bubbles becomes the important pathway.

Both sulfur dioxide and nitrogen oxides are major pollutants in flue gas. One method for the treatment of these pollutants is to absorb them in water and convert the dissolved species by the use of ultrasound. Shojaie *et al.* (1992) investigated both batch and continuous-flow treatment (in which gases containing SO_2 and NO_x were bubbled simultaneously with the sonication of the water) of gas mixtures of 1960 ppm SO_2 in argon or 514 ppm NO in argon using power ultrasound of 45 W intensity and 20 kHz frequency. The results were obtained for water as well as NaOH solutions. The important conclusions of this study were as follows:

- The sonication of aqueous SO_2 and NO species yields H_2SO_4, HNO_2, and HNO_3, respectively, as a result of their interaction with H_2O_2 generated from the decomposition of water during the adiabatic collapse of the microbubbles in solution. The formation rate of H_2O_2 limits the yields of oxidation products. The free radical reactants for SO_2 in water and NaOH solutions are given in Table 4.10.
- Although H_2O_2 is the limiting reagent, sonication experiments of aqueous SO_2, in both the presence and absence of NaOH, show dependence of SO_4^{2-} yield on the total sulfur species concentrations. At higher total sulfur concentration, larger yields of SO_4^{2-} are observed. Some typical results illustrating the effects of sonication in both water and NaOH solutions for batch and continuous flow are shown in Figure 4.7.

When ultrasound is applied to aqueous solutions, NO is absorbed at conditions where negligible NO removal is normally observed. When N_2O is sonicated in argon, cavitation bubbles contain N_2, O_2, NO_3^- and NO_2^- (S_2). The results indicate that the yields pass through a maximum at 20 to 30 vol.% of N_2O. The O_2 yield never reaches 50% of the N_2 yield, which would be the case if the overall reaction is

$$N_2O \rightarrow N_2 + 1/2\ O_2 \qquad (4.13)$$

TABLE 4.10. Mechanisms for Sonication of SO_2 in Water and NaOH[a]

Water
$SO_2\,(g) \rightarrow SO_2\,(aq)$
$SO_2\,(aq) + H_2O \rightarrow H^+ + HSO_3^-$
$HSO_3^- + H_2O_2 \rightarrow HSO_4^- + H_2O$
$HSO_4^- + H^+ \rightarrow H_2SO_4$
NaOH solution
$SO_2 + 2NaOH \rightarrow Na_2SO_3 + H_2O$
$Na_2SO_3 + H_2O_2 \rightarrow Na_2SO_4 + H_2O$

[a]From Shojaie *et al.* (1992).

The oxygen deficit is present in the atomic products, i.e., a second reaction:

$$3N_2O + H_2O \rightarrow 2HNO_2 + 2N_2 \tag{4.14}$$

with some HNO_2 being oxidized to HNO_3. Reactions 4.13 and 4.14 occur in the ratio of 4:1. N_2O strongly decreases the H_2 yield from the sonication of water, which

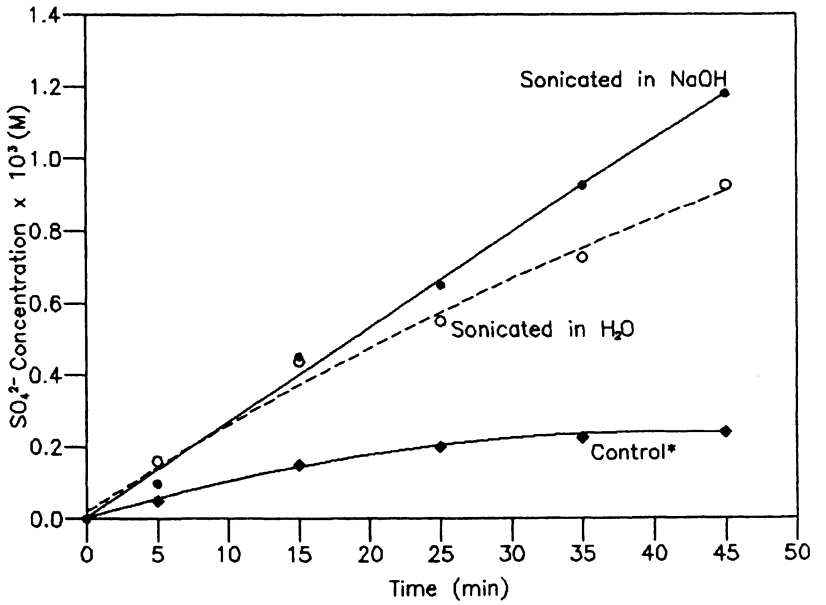

Figure 4.7. Continuous-flow sonication of SO_4^{2-}, SO_2 yield in NaOH solution (●) and in water (○) (Control* = no sonication.) (From Shojaie *et al.*, 1992.)

can be explained by the scavenging of H^- atoms. Some O_2^+ may react with nitrous oxide to form nitrogen monoxide as

$$O_2^+ + N_2O \rightarrow 2NO \tag{4.15}$$

HNO_2 and HNO_3 are produced by the oxidation of NO by O atoms or OH^- radicals and hydrolysis of intermediate NO_2. It is important to note that N_2O can still be decomposed when water is sonicated under a pure N_2O atmosphere.

Other Examples of Inorganic Species. Richards and Loomis (1927) reported that the iodine clock reaction is accelerated by ultrasound. The effect was due to a decrease in sulfite concentration as a result of sonolytic oxidation as

$$2IO_3 + 5SO_3^{2-} + 2H^+ \rightarrow I_2 + 5SO_4^{2-} + H_2O \tag{4.16}$$

The oxidation and reduction of iodine was later investigated by El'Piner (1964, 1968), El'Piner and Kolesnikova (1950), El'Piner and Sokol'skaya (1957, 1958, 1971a,b), El'Piner and Stekol'nikov (1961), El'Piner and Sunovova (1953), and El'Piner *et al.* (1951, 1965, 1968), who found that from an aqueous KI solution the amount of I_2 produced by ultrasound increases with the concentration of KI to a limiting value at 3.5 M. Not surprisingly, oxidation was completely suppressed if the solution was previously saturated with hydrogen gas. Weissler (1950, 1951a,b, 1953, 1959, 1960, 1962) and Weissler *et al.* (1950) discovered that the addition of carbon tetrachloride greatly enhances (by a factor of 30) the rate at which KI is oxidized.

A number of purely inorganic aqueous sonochemical reactions have been reported (Table 4.11). The outcome of any particular reaction largely depends on the nature of the gas dissolved in the solution.

Sonochemical redox reactions occur for both simple inorganic ions and for transition-metal complexes as well. For example, in the studies by El'Piner and co-workers, the sonochemical degradation of $[Co(NH_3)_5N_3]^{2+}$ was examined. In these studies, using electron spin resonance (ESR) trapping, the transient formation of $N_3\cdot$ was demonstrated. Given the high liability of Co(II) complexes, the following mechanism was proposed:

$$H_2O \rightarrow H^- + OH^- \tag{4.17}$$

$$H^- + [Co(NH_3)_5N_3]^{2+} \rightarrow Co^{2+} + [NH_4] + 4NH_3 + N_3^- \tag{4.18}$$

$$OH^- + N_3^- \rightarrow OH^- + N_3^- \tag{4.19}$$

Shirgaonkar and Pandit (personal communication) examined the effects of sonication (at 22 kHz) on the conversion of KI and NaCN in aqueous solutions. For KI, they suggested a relation for the kinetic constant k as $k = 5.17 \times 10^{-19}(P/V)^{1.87}$ ($r^2 = 0.87$) (where k is in s^{-1}). Here P/V is the power per unit volume. The rate constant was dependent on the presence and the amount of CCl_4 concentration. The degra-

TABLE 4.11. Inorganic Aqueous Sonochemical Reactions[a]

Starting material	Major products
Oxidations	
As^{3+}	As^{5+}
Br^-	Br_2
Cl^-	Cl_2
Fe^{2+}	Fe^{3+}
H_2S	$S_8 + H_2$
I^-	I_2
$[PO_3]^{2-}$	$[PO_4]^{2-}$
Sn^{2+}	Sn^{4+}
Tl^+	Tl^{3+}
$[Co(NH_3)N_3]^{2+}$	$Co^{2+} + N_3^{\bullet}$
Reductions	
Br_2	Br^-
Ce^{4+}	Ce^{3+}
$[Fe(III)(C_2O_4)_3]^{3-}$	Fe^{2+}
$[MnO_4]^-$	MnO_2
$[NO_3]^-$	$[NO_2]^-$
OsO_4	OsO_2

[a]From Peters (1966) and Suslick (1988) with permission.

dation of sodium cyanide marginally decreased with an increase in sonic intensity (or amplitude). The presence of carbon tetrachloride and its amount increased the rate of NaCN degradation. An increase in bulk temperature decreased the rate constant for KI conversion.

Boerner and Orloff (1996) evaluated the effect of ultrasound on dry HCl gas scrubbing with CaO. The results indicate significant enhancement in the reaction rate between lime and HCl in the presence of ultrasound. Peters and Wu (1996a,b) showed enhancement in the dissolution of $BaSO_4$ scale by ultrasound.

4.4d. Organic Reactions

Hydrocarbon Gases. The rate of the consumption of CH_4 in sonicated water depends on the methane concentration in Ar–CH_4 mixtures. Essentially every possible hydrocarbon in the C_2–C_4 range is found, with the most prominent products being acetylene, ethylene, and ethane. The products observed are very similar to

the ones produced in cold methane flames with a deficit of oxygen. The rates of formation of all products exhibit maxima around 15 to 30 vol.%.

As seen in the preceding cases, the yield versus concentration curves all pass through a maximum, with the composition of the sonolysis products also depending on the CH_4 concentration. The methyl radical was postulated to be the most important intermediate of methane sonolysis:

$$CH_4 \rightarrow CH_3 + H^{\cdot} \tag{4.20}$$

and acts as a precursor for the formation of ethane, ethylene, and acetylene, as follows:

$$2CH_3 \rightarrow C_2H_6 \tag{4.21}$$

$$2CH_3 \rightarrow C_2H_4 + H_2 \tag{4.22}$$

$$C_2H_4 \rightarrow C_2H_2 + H_2 \tag{4.23}$$

One could thus calculate the temperature in the hot argon–methane bubbles from the ratio, r, of the yields, y, of the three hydrocarbons:

$$r = y(C_2H_4) + y(C_2H_2)/y(C_2H_6) \tag{4.24}$$

The results of such calculations are depicted in Figure 4.8, where it can be seen that the temperature in argon bubbles containing little methane is 2720 K, and even for pure methane bubbles the temperature is as high as 1930 K.

For the sonolysis of ethane in argon bubbles, the yield ratio $y(C_2H_2)/y(C_2H_4)$ decreases as the temperature is reduced. Since C_2H_2 is formed through the thermal decay of ethylene, its relative abundance is lower at the lower temperatures reached in the cavitation bubbles. Experiments have also been carried out with other gaseous hydrocarbons of the C_2 to C_4 series, and from these results some "rules" concerning the formation of the various products have been derived: (1) The yield of H_2 for the higher saturated hydrocarbons does not change substantially with increasing chain length, and the yield of H_2 for unsaturated compounds is lower than that obtained for the saturated species. (2) At equal concentrations in argon bubbles, the rate of consumption of the unsaturated hydrocarbons is significantly higher than that of the saturated ones, with the former materials mainly undergoing polymerization reactions.

A very detailed investigation of the sonolysis of acetylene in argon cavitation bubbles has been recently published (Reisz, 1991). This study indicated the following: (1) Acetylene is efficiently consumed in argon bubbles, with the maximum rate

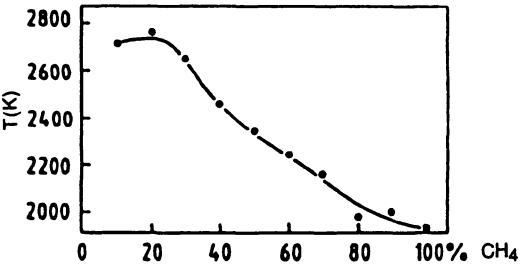

Figure 4.8. Temperatures reached in argon–methane cavitation bubbles formed in the sonication of water under various argon–methane mixtures, as a function of the methane concentration. (From Henglein, 1993, with permission.)

appearing at a concentration of 5 vol.% in the gas mixture under which the water is sonicated. (2) A great number of products were identified; in addition to H_2CO and CO_2, a number of soluble, oxygen-containing products such as formaldehyde and acetaldehyde, and formic acid and acetic acid, were observed, which shows that the decomposition of water molecules accompanies that of acetylene. Various volatile hydrocarbons, such as methane, ethane, ethylene, allene, propene, propylene, and butadiene, were also found, all of which are known to be formed in acetylene flames. (3) The relative abundance of the products produced from acetylene depends on the C_2H_2 concentration, which is in part attributable to the varying temperature in the hot cavitation bubbles. At low acetylene concentrations (i.e., at high temperatures), the product molecules having larger mass are less abundant than at lower temperatures. The experiments have shown (Reisz, 1991) that the large molecules are formed in one cavitation event. A succession of many elementary processes can occur in a hot cavitation bubble, despite the short lifetime of the collapsing bubble. The high pressures (i.e., up to 100 atm) that exist in such collapsing bubbles may facilitate this succession of reactions as a result of the high local concentration of acetylene.

Sweet and Casdonte (personal communication) examined first-order degradation of various hydrocarbons in water at 35°C. The results are briefly summarized in Tables 4.12 and 4.13. It is interesting to note that for both benzene and decane, higher concentrations gave lower kinetic constant. Petrier and co-workers (1982, 1984, 1985, 1992a,b) and Petrier and Luche (1987) indicated that benzene is generally converted into CO, CH_4, CO_2, and C_2H_2. As shown in Figure 4.9 (Reisz, 1991) also indicated that a hydrocarbon mixed with O_2 degraded faster than the one mixed with Ar.

Quiros and Williford (1995) examined ultrasonically enhanced destruction of benzene and toluene. They found that ultrasonic intensity and duration played a strong role in the destruction of toluene. The addition of H_2O_2 did not affect the

TABLE 4.12. First-Order Aromatic Degradation Kinetics[a]

[Aromatic] (100 ppm)	k_{obs} (s^{-1})	$t_{1/2}$ (s)
Benzene	2×10^{-4}	3465
Toluene	7×10^{-4}	990
m-Xylene	7×10^{-4}	990
Hexane	1×10^{-4}	6930
Octane	4×10^{-4}	1730
Nonane	3×10^{-4}	2310
Decane	1×10^{-3}	690
Undecane	5×10^{-5}	13,900
Tetradecane	8×10^{-5}	8660

[a]After Sweet and Casadonte (personal communication).

destruction of toluene. The initial pH, sound intensity, and H_2O_2 addition interacted in the destruction of benzene. They also found an optimum temperature for maximum benzene conversion. In a subsequent study, Quiros and Williford (1995) also showed that 1, 2-dichloroethane was destroyed by ultrasound-effected conversion of organic chloride in a wastewater stream from a wood treatment plant in southern Arkansas.

Chlorinated Hydrocarbons. The effects of power ultrasound on a series of chlorinated hydrocarbons have been investigated by Bhatnagar and Cheung (1994) and Wu *et al.* (1992). Together, in these studies aqueous solutions of methylene chloride, chloroform, carbon tetrachloride, 1,2-dichloroethane, 1,1,1-trichloroethane, trichloroethylene, perchloroethylene, CFC-11 (fluorotrichloromethane) and CFC-13 (trifluorotrochloroethane) in concentrations ranging from 50 to 350

TABLE 4.13. Concentration Effect on First-Order Benzene and Decane Degradation Kinetics[a]

[Benzene] (mM)	k_{obs} (s^{-1})	$t_{1/2}$ (s)
1.28	2×10^{-4}	3465
6.40	2×10^{-4}	3465
12.8	7×10^{-5}	9900
[Decane] (mM)		
0.378	1×10^{-3}	690
0.757	1×10^{-3}	690
1.89	4×10^{-4}	1730

[a]After Sweet and Casadonte (personal communication).

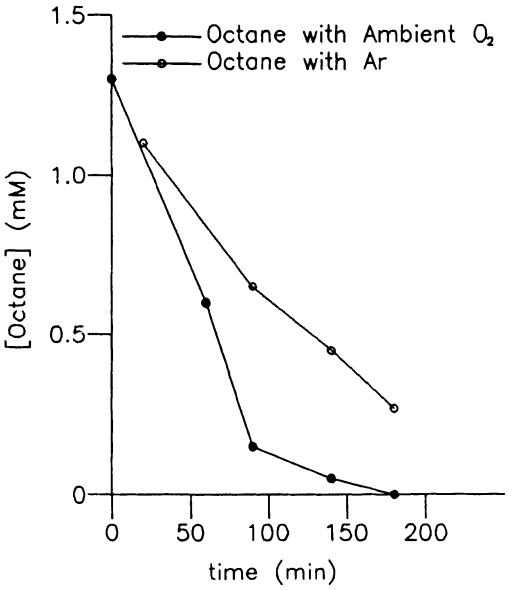

Figure 4.9. Sonication of octane in the presence of Ar or dissolved O_2. (From Riesz, 1991, with permission.)

ppmv were irradiated with 20-kHz ultrasound in a batch operation. Some results for CFCs were obtained in a circulating system. Solutions were prepared before they were exposed to ultrasound at ambient conditions.

In all cases the concentrations of volatile organic compounds (VOCs) in water declined rapidly with the sonication time (Bhatnagar and Cheung, 1994; Wu *et al.*, 1992). In the case of C_1 and C_2 hydrocarbons, the results were dependent upon the pH of the solution. For CFCs, the solution pH decreased upon sonication, indicating acidic species as a final halogen acceptor for at least a portion of the C_1 and F. A general free-radical mechanism for the sonolytic decomposition of the organic compounds described by Bhatnagar and Cheung (1994) is given in Table 4.14. The reaction rates were adequately described by a pseudo-first-order reaction and the rate constants for each species are given in Table 4.15. The rate constant decreased somewhat with an increase in temperature, a phenomenon not unusual for sonochemical reactions. For CFC solutions, liquid vaporized only slightly due to sonication.

Petrier and co-workers (1982, 1984, 1985, 1992a,b) and Petrier and Luche (1987) studied the conversion of chlorobenzene to CO, CH_4, CO_2, and C_2H_2. They examined sonochemical degradation at 530 kHz of pentachlorophenate (PCP) in aqueous solutions saturated with different gases: air, oxygen, and argon. The

TABLE 4.14. Sonolytic Decomposition of the Organic Compounds[a]

$C^b \rightarrow$ products
$C + H^- \rightarrow$ products
$C + OH^- \rightarrow$ products
$C + HO_2 \rightarrow$ products
$C + O \rightarrow$ products

[a]After Bhatnagar and Cheung (1994).

[b]C = Volatile organic compound of the type $C_xH_yCl_z$.

reaction steps include the following: Fast cleavage of the carbon–chlorine bond, releasing Cl^-, mineralization of PCP to CO_2 when the solution is saturated with air or oxygen; CO production when Ar is the saturating gas; and nitrile and nitrate production when the reaction is conducted with aerated solutions. The study (Petrier and Luche, 1987) shows that the disappearance of PCP is followed by a decrease in the toxicity of the medium for the green algae *Scenedesmus subspicatus*.

TABLE 4.15. Rate Constant for the Destruction of VOCs in a Sonochemical Reactor[a]

Compound[b]	k (min^{-1})	Vapor pressure (mm) at 20°C
C1		
CH_2Cl_2	$0.0315 \pm 8 \times 10^{-3}$	348.9
$CHCL_3$	$0.04067 \pm 2 \times 10^{-3}$	160
CCl_4	0.04259	90
C2		
1,2-DCA	0.02564	64
TCE	0.02065	57.8
PCE	$0.02184 \pm 4 \times 10^{-3}$	20
1,1,1-TCA		
at 15°C	0.03413	100
at 23°C	$0.04019 \pm 6 \times 10^{-3}$	
at 32°C	0.03703	
CFC-11		
Batch	0.236 ± 0.031	ml/watt min at 5°C
Circulating	0.229 ± 0.036	ml/watt min at 5°C
	0.187 ± 0.024	ml/watt min at 10°C
CFC-13		
	0.23 ± 0.034	ml/watt min at 5°C
	0.204 ± 0.026	ml/watt min at 10°C

[a]From Bhatnagar and Cheung (1994).

[b]DCA = dichloroethane; TCE = trichloroethene; PCE = perchloroethene; TCA = trichloroethane.

Degradation of CCl_4 in aqueous $AgNO_3$ was studied by Shirgaonkar and Pandit (1996, 1997, 1998). The rate was correlated by a relation rate = 3.85×10^{-20} $(P/V)^{2.16}$. This relationship indicates that the rate of degradation is independent of the system studied and solely dependent on the type of ultrasonic equipment. Thoma *et al.* (1995, 1996; personal communication) showed significant enhancement in the degradation of chlorobenzene in aqueous solution in the presence of ultrasound.

Sodium Acetate in Aqueous Solutions. In general, during sonication a solute experiences attack by both the free radicals and atoms from the decomposition of water vapor (i.e., H^+, OH^-, and O^{+2}), and pyrolysis in the hot cavitation bubble or a layer surrounding it. The two types of reactions produce different products, with the relative abundance of these depending on the nature of the solute and its concentration. g-radiolysis of sodium acetate in aqueous solutions in the absence of air produces one product (i.e., succinic acid) as

$$OH^- + CH_3CO_2^- \rightarrow CH_2CO_2^- + H_2O \tag{4.25}$$

$$2CH_2CO_2^- \rightarrow (CH_2CO_2^-)_2 \tag{4.26}$$

Succinic acid is also a product of sonolysis under argon, as can be seen from Figure 4.10, where the yields of the various products are plotted as a function of the acetate concentration. With increasing acetate concentration, the yield of succinic acid increases and reaches a limiting value. The H_2O_2 yield decreases as more and more OH^- radicals are scavenged. However, a number of other products are also observed. Three of these, (i.e., glycolic acid, carbon dioxide, and formaldehyde) are known to be formed in g-radiolysis treatment under air. Their appearance in sonolysis under argon is explained by the fact that a small amount of oxygen is generated in the sonolysis of water, as mentioned earlier. The oxygen formed reacts with the $CH_2CO_2^-$ radicals produced in reaction (4.25) to yield peroxy radicals, which mutually interact, thus leading to these three products. The contribution to the decomposition of acetate by pyrolysis is even greater at high solute concentrations than the contribution by free-radical attack.

Aldehydes and Acids in Aqueous Solution. Sonolysis of mixtures of formic acid and water, both liquids having approximately the same boiling point, has also been examined in the literature (Reisz, 1991). It is known from conventional experiments on the pyrolysis of formic acid that carbon dioxide, carbon monoxide, and hydrogen are the products. This is explained by the following two routes of thermal decomposition:

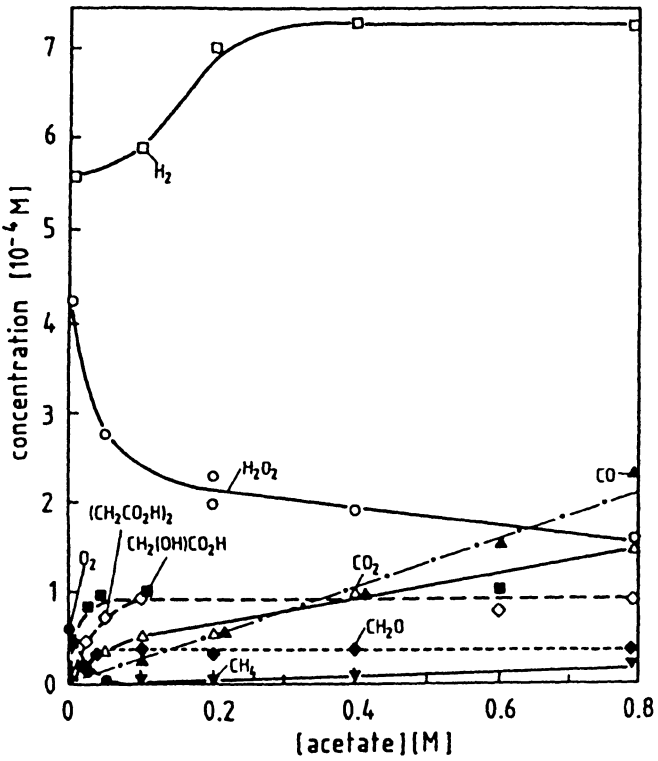

Figure 4.10. Yield of the various sonolysis products from sodium acetate, as a function of the acetate concentration. (From Henglein, 1993, with permission.)

$$HCOOH \rightarrow CO_2 + H_2 \tag{4.27}$$

$$HCOOH \rightarrow CO + H_2O \tag{4.28}$$

These products also appear in a sonolysis treatment. Figure 4.11 shows the yields (as rates) as a function of the formic acid concentration. H_2 and CO_2 are formed at equal rates while CO is produced at a substantially higher rate. All yields pass through a maximum at a concentration of 15 M HCOOH. In addition to these products, small quantities (micromoles per liter) of oxalic acid are found; the yields of this product, however, do not pass through a maximum but decrease gradually with increasing formate concentration.

From these observations, it can be concluded that pyrolysis is by far the major route for the acoustic decomposition of formic acid. The formation of oxalic acid

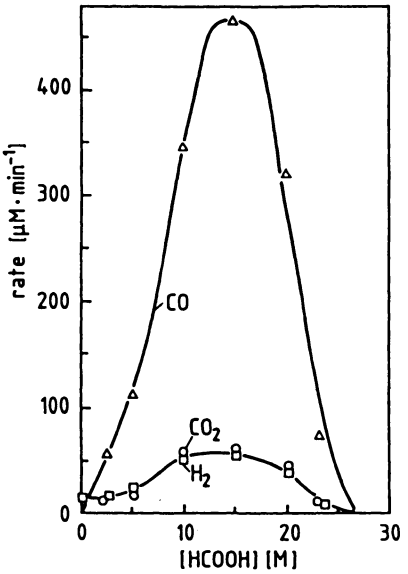

Figure 4.11. Rate of formation of CO, CO_2, and H_2 from the pyrolysis of water–formic acid mixtures, as a function of the formic acid concentration (sonication under argon). (From Henglein, 1993, with permission.)

by the free radical reations play only a minor role. However, at low formic acid concentrations (<1 M), the radical mechanism is the predominant route. The maximum in Figure 4.11 can be explained in terms of HCOOH having a greater heat capacity than H_2O; lower temperatures in the cavitation bubbles containing the vapor of the liquid are therefore brought about with increasing formic acid content.

The sonochemical stereoisomerization of maleic acid to fumaric acid in the presence of Br_2 or some bromocarbons is an interesting example. This is a general reaction independent of the frequency of sound used over a very wide range. This reaction is an unusual example of sonocatalysis, since the Br^- formed from sonolysis is a competent catalyst for the isomerization. No isomerization is observed in the absence of Br_2 or in the absence of ultrasound.

The use of ultrasound during acetylaldehyde and crotonaldehyde oxidations leads to increases in the rates of initiation. The relationship between the constants of chain propagation and chain breaking remains unchanged. Aliphatic aldehydes and carboxylic acids were also sonicated by 800 kHz ultrasound to give a variety of products. From an analysis of the solution, it was seen that two reaction pathways exist for aldehydes: oxidation to the corresponding carboxylic acid, or fragmentation to smaller acids with the formation of one or two carbon gases. For carboxylic

acids only the latter, less favored, process is available. The effect of ultrasound frequency (20 kHz versus 500 kHz) on the oxidation of fulvic acids by ozone was demonstrated by Barbier (1898) and Olson and Barbier (1994). The effect of peroxide addition on the sonochemical destruction of citric acid in an aqueous solution was examined by Cheung *et al.* (1993).

Alcohol–Water Solutions. In the sonolysis of water–methanol mixtures, either under argon or oxygen, the typical pyrolysis and combustion products of methanol are detected (H_2, CH_2O, CO, CH_4, and traces of C_2H_4 and C_2H_6 under argon; CO_2, CO, HCOOH, CH_2O, H_2O_2, and traces of H_2 under oxygen). The relative yields of these products change with the composition of the water–methanol mixture, as can be seen from Figure 4.12. It should be noted that the yields pass through maxima and are practically zero at methanol concentrations above 70%. This effect can be explained on the basis that methanol vapor has a greater heat capacity than water vapor, and thus lower temperatures are produced with increasing methanol concentrations. At the lower methanol concentrations, CO_2 is the main product, but the combustion of methanol in the cavitation bubbles is incomplete, and other products are also present in appreciable amounts. At higher methanol concentrations, CO_2 is no longer the main product, which indicates a stronger reducing atmosphere in the cavitation bubbles.

When 0.1–1.9% aqueous solutions of methanol are sonicated at 40°C, the concentration of formaldehyde gradually increases along with HNO_2 and HNO_3 (formed from the fixation of atmospheric N_2 and subsequent oxidation). Aqueous ethanol produces acetaldehyde, diethyl oxalate, acetic acid, and ethyl acetate under similar conditions. Aromatic alcohols, such as hydroquinone, are also oxidized though in this case the product is *para*-benzoquinone.

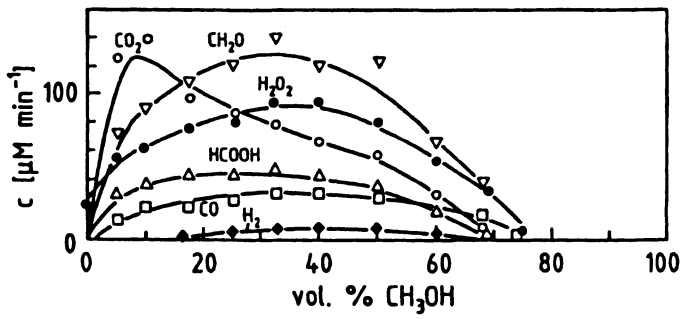

Figure 4.12. Rates of formation of the products of the sonolysis of water–methanol mixtures under an oxygen atmosphere, as a function of the composition of the mixture. (From Henglein, 1993, with permission.)

In the solvolysis of 2-chloro-2-methylpropane in aqueous alcoholic media, the rate enhancements have generally been quite small (<50%) at room temperature, but increase sharply with decreasing temperature. Apparent activation parameters have been measured as a function of alcohol concentration, but the effects of solvent vapor pressure have not been included in this analysis, which precludes unambiguous interpretation of the origin of these rate enhancements. The ultrasonic cleavage of cyclohexanol in aqueous suspension produces acetylene. The rate of reaction is independent of cyclohexanol concentration and is unaffected by the addition of the solid radical scavengers acrylamide and allylthiourea, but is reduced in the presence of oxygen and nitric acid.

The sonolytic oxidation of isopropanol in aqueous conditions under argon was investigated by following the evolution of H_2 and the formation of acetone. The reaction takes place in the cavitating bubbles, which induce a monomolecular dehydrogenation of the alcohol. Petrier and co-workers (1982, 1984, 1985, 1992a,b) and Petrier and Luche (1987) examined the effects of ultrasound frequency (20 kHz versus 487 kHz) on the degradation of phenol in dilute aqueous solutions. Petrier *et al.* (1992a) showed that for the same acoustic powers (30 W) the conversion was more efficient at higher frequency. The initial rates were found to be dependent on the initial phenol concentration, reaching limiting values of $k_{20\ kHz} = 1.84 \times 10^{-6}$ M min^{-1} and $k_{487\ kHz} = 11.6 \times 10^{-6}$ M min^{-1} where k's are the appropriate reaction rate constants. Identification of first intermediates of the reactions (hydroquinone, catechol, benzoquinone) indicates OH^* involvement in the degradation pathways. The rate of H_2O_2 formation was higher at higher frequencies. The rate of sonochemical degradation was directly linked to the OH^* availability in the solution. Petrier and co-workers (1992b) also examined conversion of 4-chlorophenol in the presence of ultrasound at 20 and 500 kHz. Both phenol and chlorophenol produce CO and CO_2.

Nitrogen Compounds—Water. Oxidation of aniline also occurs readily in water. The reaction mechanism proposed for the formation of azobenzene is shown below:

$$C_6H_5NH_2 \rightarrow C_6H_5NH^-$$

$$C_6H_5NH_2 \rightarrow C_6H_5N^{-2}$$

$$2C_6H_5NH^- \rightarrow C_6H_5NH\text{–}NHC_6H_5$$

$$2C_6H_5N^{-2} \rightarrow C_6H_5N{=}NC_6H_5$$

$$C_6H_5NH\text{–}NHC_6H_5 + OH^- \rightarrow C_6H_5N{=}NC_6H_5 \qquad (4.29)$$

Anbar and Pecht (1964a,b,c, 1967) examined the formation of OH^- under sonolysis by following the oxidative deamination of ethylene diamine. The behavior of the diamine on sonolysis was compared with that under radiolysis.

Irradiation of alkyl amines in aqueous solution or in suspension results in the formation of aldehydes, an alcohol, amines, an N-oxide, and several gaseous products. The products and their ratios are dependent on the structure of the amine, and the order of reactivity is primary > secondary > tertiary. The hydrated electrons and 1-hydroxy alkyl radicals, which are formed in the g-radiolysis of aqueous alcohol solutions, react with tetranitromethane in the presence of ultrasound as follows:

$$e^-_{aq}(\text{or ROH}) + C(NO_2)_4 \rightarrow C(NO_2)_3^- + NO_2 + (R{=}O + H^+) \qquad (4.30)$$

The tetranitromethane is often used as a scavenger for reducing radicals. The stable anion of aci-nitroform, $C(NO_2)_3^-$, is colored and allows a spectrophotometric determination of the number of radicals that are formed.

Cost *et al.* (1993) examined sonochemical degradation of *p*-nitrophenol at 20 kHz in the presence of the chemical components of natural waters such as particulate matter, phosphate, bicarbonate, and humic acid. The degradation of 4-nitrocatechol (a product of *p*-nitrophenol sonolysis) was also examined. The decay of *p*-nitrophenol followed first-order kinetics with $k_{obs} = 4.6–4.2 \times 10^{-4}\ s^{-1}$. The rate of *p*-nitrophenol degradation in pure water and natural environments was very similar. The observed first-order rate constants for both *p*-nitrophenol and 4-nitrocatechol decay were independent of the humic acid concentration (in the range of 0–20 mg/liter). The kinetic results indicate that high-temperature denitration reactions of *p*-nitrophenol at the interface of cavitating bubbles are not affected by the presence of chemical components of natural waters. Kotronarou *et al.* (1991, 1992a,b) showed that at 20 kHz, 84 W, *p*-nitrophenol was primarily degraded by denitration to yield NO_2^-, NO_3^-, benzoquinone, hydroquinone, 4-nitrocatechol, formate, and oxalate. The main reaction pathway is carbon–nitrogen bond cleavage. The average effective temperature of the interfacial region surrounding cavitation bubbles is estimated to be 800 K.

The sonochemical degradation of *p*-nitrophenol in a near-field acoustic processor (NAP) was also investigated by Hua *et al.* (1995). Once again, the decay followed first-order kinetics, with the kinetic constant k varying from 1.0×10^{-4} to $7.94 \times 10^{-4}\ s^{-1}$ with an increasing power-to-volume ratio (i.e., power density) over the range of 0.98–7.27 W/cm^3. An increase in the power-to-area ratio (i.e., sound intensity) resulted in an increase in k up to a maximum value of $8.60 \times 10^{-4}\ s^{-1}$ at a sound intensity of 1.2 W/cm^2. The nature of the cavitating gas (Ar, O_2) was found to influence the overall degradation rate and the resulting distribution of product. The rate constant for *p*-nitrophenol degradation in the presence of pure O_2, k_{O_2} =

5.19×10^{-4} s^{-1}, was lower than in the presence of pure Ar, $k_{Ar} = 7.94 \times 10^{-4}$ s^{-1}. A 4:1 (v/v) Ar/O_2 mixture yields the highest degradation rate, $k_{Ar/O_2} = 1.2 \times 10^{-3} s^{-1}$. The results of this study demonstrate the potential application of large-scale, high-power ultrasound to the remediation of hazardous compounds present at low concentrations. The reactor used in this study was a parallel-plate reactor that allowed for a lower sound intensity but a higher acoustical power per unit volume than a conventional probe-type reactor.

Pesticide–Water Solutions. Ultrasound has also been used to degrade pesticide impurities in water. Kotronarou *et al.* (1991, 1992a,b) examined the decomposition of parathion in aqueous solutions. Parathion (*O,O*-diethyl *O*-*p*-nitrophenyl thiophosphate)-saturated deionized water solution was sonicated at 30°C and with ultrasound operating at 20 kHz and 75 W cm^{-2} intensity. Over a broad pH range, *p*-nitrophenol was found to be the major hydrolysis product of parathion. The reactions are shown in Figure 4.13. During sonication, temperatures near 2000 K have been determined for the interfacial region near the collapsing bubble.

Igar *et al.* (1995) evaluated the sonochemical degradation of a hydrophobic organochlorine compound, lindane [the g isomer of hexachlorocyclohexane (g-HCH)], in water. Lindane decomposition rates were first order with respect to the concentration of lindane, and its half-life was 57 min when the power input to the solution was 108 W. Based on the inhibition of the reaction in the presence of a surfactant, sodium dodecyl sulfate, the reaction site appears to be the cavitation bubble interface. The rate of reaction was not affected by changes in the initial pH over a pH range of 4 to 10.

Other Examples of Organic Compounds. In many studies the degradation of organic compounds is lumped and expressed in terms of chemical oxygen demand (COD). Chen *et al.* (1973) examined the effect of ultrasound on oxidation of wastewater with ozone–catalyst and air–catalyst systems. As shown in their study, the chemical oxygen demand content of the liquid decreased dramatically in the presence of ultrasound for both MnO_2 and nickel catalysts. In the case of an MnO_2 catalyst, ultrasound decreased COD concentration by about 100% whereas for the nickel catalyst it reduced COD content by about fourfold.

Sierka and Skaggs (1979) evaluated the ability of ozone and ultrasound to treat hospital wastewaters through reverse osmosis and ultrafiltration. The results obtained in this study indicate that ultrasound enhances the organic oxidation rate as measured by COD and destruction of total organic carbon (TOC) in the wastewater. Sierka and Amy (1985) evaluated the singular and composite effects of two catalysts—ultraviolet (UV) light and ultrasound—on the ozone oxidation of a purified solution of a commercially available humic acid with the objective of maximizing the potential for trihalomethane formation. Their results indicate the enhanced destruction of nonvolatile organic carbon in the presence of ultrasound.

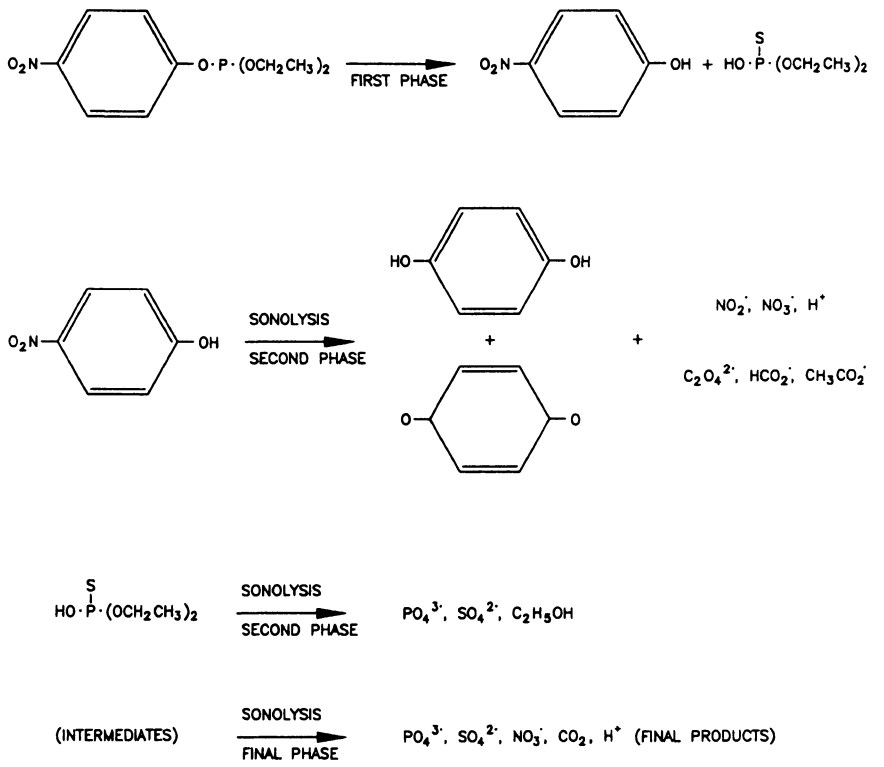

Figure 4.13. Schematic presentation of the effect of ultrasonic irradiation on parathion. (Reprinted with permission from A. Kotronarou, G. Mills, and M.R. Hoffmann, "Decomposition of parathion in aqueous solution by ultrasonic irradiation," *Env. Sci. Technol.* **26**(7), 1460–1462, 1992. Copyright © 1992 American Chemical Society.)

Thoma *et al.* (1995, 1996; personal communication) showed that the magnetostrictive transducers are considerably more durable than piezoelectric transducers and thus well suited for the degradation of organochlorine contaminants found in wood treatment wastewater. They used both simulated wastewater and an actual wastewater stream from a wood treatment plant. Peters and Wu (1996a,b) examined the enhancement in the rates of organic destruction and thereby scale control on the reactor walls using ultrasound. Seymour and Gupta (1996, 1997, personal communication) and Seymour *et al.* (1997) studied the effects of ultrasound on the oxidation of aqueous pollutants. They examined the effects of a variety of bulk conditions on the reaction rates and these data are presented in terms of empirical correlations.

Various organics have been sonicated either as aqueous solutions or suspensions, and are compiled in Table 4.16. Aqueous sonochemistry of organic compounds

TABLE 4.16. Aqueous Sonochemistry of Organic Compounds[a]

Substrate present	Principal products
CCl_4	Cl_2, CO_2, HCl, C_2Cl_6, HOCl
CH_3I	CH_4, I_2, CH_3OH, HI, C_2H_6
R_2CHCl	R_2CHOH, HCl
$Cl_3CCH(OH)_2$	HCl
C_6H_5Br	Br^-, C_2H_2
Maleic acid + Br_2	Fumaric acid
CS_2	S, H_2S
$(C_4H_9)_2S$	$(C_4H_9)_2SO$, polymer
$[R_2NC(=O)S]^-$ + R'Cl	$R_2NC(=O)SR'$
RCHO	CO, CH_4, C_2H_4, $C_2H_4O_2$, RCO_2H
HCO_2^-	CO_2
C_5H_5N	HCN, C_2H_2, C_4H_2
C_6H_5OH	$C_6H_4(OH)_2$
$C_6H_5CO_2H$	$C_6H_4(OH)(CO_2H)$
$C_6H_{11}OH$	C_2H_2
RCO_2H	CO, CH_4
ClH_2COO_2H	H_2, CO, CH_4^-, Cl^-
RCO_2R'	RCO_2H, R'OH, CH_4,CO
Amines	H_2, CH_4, NH_3, RCHO, RCH_2OH, ROH
$(CH_2NH_2)_2$	NH_3
Thymine	Hydroxylated products
Uracil	Hydroxylated products
Various amino acids	H_2, CO, NH_3, RNH_2, HCHO
Cysteine	Cystine
$C_6H_5CHCH_2$	Polymerization
$H_2CC(CH_3)(CO_2H)$	Polymerization
$H_2CCH(CONH_2)$	Polymerization
Many polymers	Depolymerization
RCl	Cl_2, HCl, HOCl, CO, RH, ROH
Chlorofluorocarbons	CO, CO_2, HCl, HF
Bu_2S	Bu_2SO, polymeric species
ROH	RH
Amino acids	H_2, CO, HCHO, NH_3, RNH_3

[a]From Peters (1966) and Suslick (1988) with permission.

usually results in the generation of a large number of highly oxidized or degraded products. Since extremely reactive intermediates are formed at respectable rates from the sonolysis of water itself, it is not surprising to see a general lack of specificity for sonochemistry in aqueous media. If we consider the nature of the cavitation event, the high vapor pressure of water relative to inorganic species or to

dilute organic compounds, it is no surprise that aqueous sonochemistry is dominated by secondary chemical reactions unrelated to the direct processes that such dissolved substrates might undergo had they been the major species found in the collapsing bubble.

The effects of temperature, acoustic intensity, and frequency on a number of organic reactions in an aqueous phase have also been investigated in the literature. Figure 4.14 shows the effects of intensity and frequency on conversion of acid-catalyzed hydrolysis of methyl ethanoate at 303 K. As the figure shows, lower rate enhancements were obtained at the higher frequency. The optimum power for 540 kHz was found to vary quite substantially with reaction volume. Similar results were obtained at other temperatures. It was concluded that there is an optimum

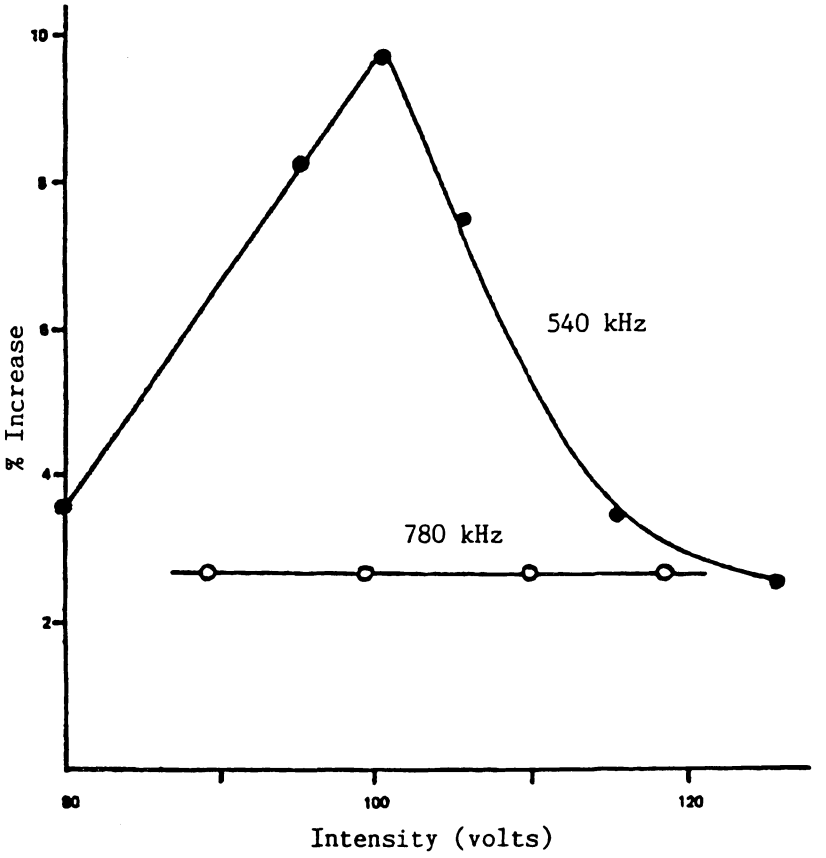

Figure 4.14. Effect of intensity and frequency on conversion of methyl ethanoate. $T = 303$ K, volume = 105 cm^3. (From Henglein, 1993, with permission.)

power for each volume and temperature at which the reaction rate is maximum. Jozefowicz and Witekowa (1995) studied the effects of frequency, acoustic intensity, temperature, and nature of gas on a wide variety of aqueous redox reactions. Eight out of twelve reactions studied showed zero-order kinetics. While not evaluated, these kinetic expressions may have been influenced by the type of equipment used in this study. Although redox reaction rates were found to be independent of the frequency, maxima were observed with respect to temperature and intensity. For various gases, the order of kinetic constants for the reaction was $k_{air} > k_{oxygen} > k_{argon} > k_{nitrogen}$. The large rate constants with air and oxygen are due to the HO_2^* radical. The optimum in rate enhancement with respect to intensity was also observed for solvolysis of 2-chloro-2 methyl propane in 50% EtOH–H_2O at various temperatures. For solvolysis in both ethanol–water and butanol–water mixtures, the rate of enhancement decreased with an increase in bulk temperature. The typical effects of power and frequency on Weissler reactions are illustrated in Figure 4.15. As shown, the effect of power on the reaction rate is much more

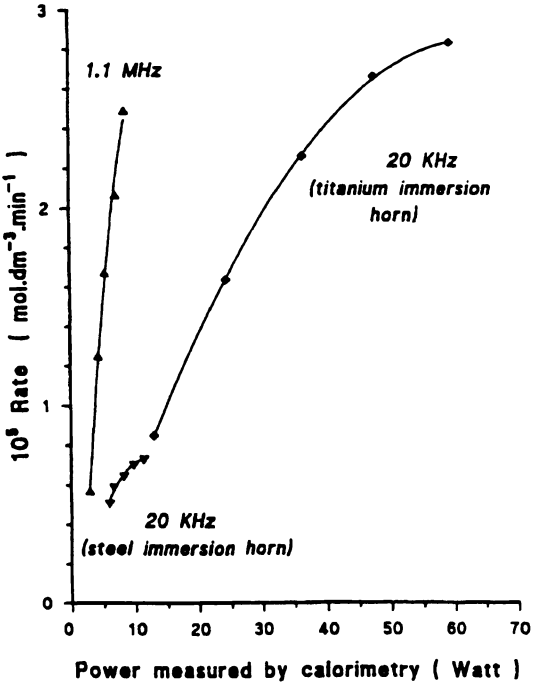

Figure 4.15. Effect of frequency and ultrasound intensity on the Weissler reaction. (The Weissler reaction is the oxidation of I^- by an oxidant generated by the sonication of water saturated with CCl_4). (From Luche, 1992b, with permission.)

pronounced at higher frequencies. In general, the rate of reaction is proportional to $(P/V)^c$, where P/V is the power per unit volume. The constant c may be dependent upon the nature of the equipment and the reaction medium, among other intrinsic reaction parameters.

Cyclohexane oxidation in the presence of an ultrasonic field is also accelerated compared with oxidation without this influence. Ultrasonic initiation produces the same oxidation products as those formed in an auto-oxidation system, but their relative proportions differ. For example, during the oxidation of cyclohexane, the concentration of hydroperoxide increases, and the concentration of the acids is reduced, while the quantity of alcohol and ketone remains unchanged compared with the analogous auto-oxidation process. The oxidation of cumene in the liquid phase in the temperature range of 365–367 K gives the hydroperoxide as the most stable product. Ultrasonic initiation of this oxidation reaction reduces the induction period to 3–4 h, but the oxidation rate does not change significantly. However, as soon as the concentration of cumene hydroperoxide reaches about 15–17%, the oxidation rate suddenly decreases. The concentration of the accumulated hydroperoxide, which at first remains unchanged, soon begins to decrease.

Thus, the effect of the ultrasonic cavitation process on both the initiation and the intensification of organic auto-oxidation reactions can produce different results, namely: (1) an intensive acceleration of the aldehyde oxidation reaction, (2) an inhibiting effect on the cumene oxidation reaction, and (3) a "small" acceleration of the cyclohexane oxidation reaction. The reasons for this are not completely clear.

The effect of ultrasound on the hydration of acetylene to produce acetaldehyde is achieved more efficiently with ultrasound:

$$HC^{-}{=}CH + H_2O \rightarrow [CH_2{=}CHOH] \rightarrow CH_3CHO \qquad (4.31)$$

Ethylene and methane are also oxidized in an ultrasonic field. With saturated aqueous solutions of CH_4, a 24% conversion to formaldehyde is obtained. Ethylene gives acetaldehyde, presumably via the oxidation of ethanol, which is initially formed.

Spurlock and Reifsneider (1970) and Reifsneider and Spurlock (1973) examined the oxidation of di-*n*-butyl sulfoxide in pure water and in saturated aqueous solutions of carbon tetrachloride. The main product under both conditions was di-*n*-butyl sulfoxide, along with several minor products that included *n*-butylsulfonic acid.

Olson and Barbier (1994) evaluated an advanced oxidation process that combines ultrasound and ozone for the oxidation of natural organic matter to determine whether the approach could extend the application of sonolysis to refractory electrolytes.

Evidence from radical scavenging and dosimetry experiments confirmed that ozone decomposition does not significantly occur in bulk solution during sonica-

tion. Under conditions of constant ultrasonic irradiation and continuous ozone gas application, total organic carbon removal rates were enhanced by ultrasound. Direct combustion of volatile intermediates in the cavitation bubble may partially explain the improved mineralization efficiency that was obtained with sonolysis. Hydroxyl radical scavengers such as carbonate were found to inhibit TOC removal rates. When the process was applied to a high color groundwater sample containing bicarbonate, TOC removal was completely inhibited. After pretreatment of the groundwater sample to remove carbonate species, however, 90% of the TOC was removed in 40 min. Some results are briefly summarized in Table 4.17. The decomposition rate of ozone was significantly catalyzed by ultrasonic irradiation. This rate increases with power input, with a maximum achieved at about 60–70 W.

Ingale and Mahajani (1995) examined a novel way to treat refractory waste: sonication followed by wet oxidation (SONIWO). They showed that sonication followed by wet oxidation is a better hybrid system. Sonication in the presence of a catalyst is more effective than without a catalyst. The catalyst used in the wet oxidation system may be used with sonication to yield better results. Oxidation efficiencies in the presence of $CuSO_4$ and $NiSO_4$ were very effective in this hybrid system; the oxidation rate was, however, higher in the presence of $CuSO_4$ than $NiSO_4$.

A very interesting comparative study between hydrodynamic and acoustic cavitation chemistry was reported by Pandit and Joshi (1993). They examined hydrolysis of castor oil and kerdi oil using an ultrasonic generator and a cavitating valve. The conversion in both cases was indicated by the acid value. Some typical results are shown in Figures 4.16(a) and 4.16(b). As indicated in these figures, the induction period with the ultrasonic generator was considerably shorter than with the cavitating valve. The rate of energy consumption for the ultrasonic generator was 1384 J/ml of emulsion versus that for the cavitating valve of 1080 J/ml. The nature of the reactions for both species was similar for both cavitating media. Slower reactions in the latter case are in line with the lower rate of energy consumption. The study indicates that organic reactions that otherwise require extreme temperatures and pressures can be carried out at room conditions through the process of hydrodynamic or acoustic cavitation.

TABLE 4.17. TOC Mineralization Efficiencies for 10 mg TOC Per Liter Fulvic Acid Solutions[a]

Process[b]	% TOC removed	%TOC mineralized
O_3 only	40	28
O_3 + ultrasound	91	87

[a]From Olson and Bambier (1994) with permission.

[b]Reaction period was 60 min; ozone flow rate was 3.2 mg min^{-1}. Ultrasonic power input was 55 W.

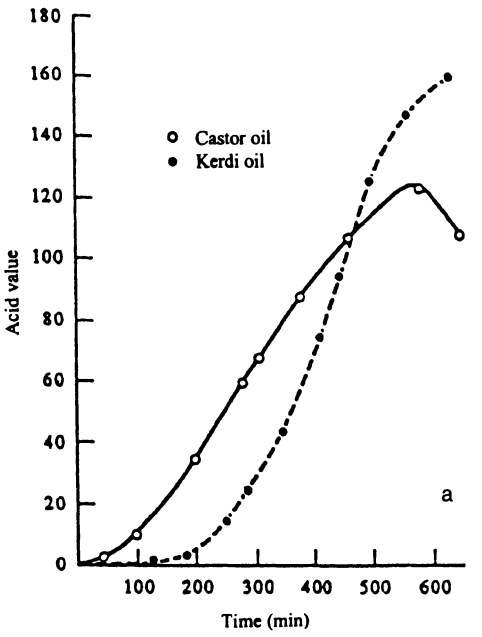

Figure 4.16. (a) Hydrolysis of castor oil and kerdi oil with ultrasonic generator: (--o--) castor oil, (--•--) kerdi oil. (b) Hydrolysis of castor oil and kerdi oil with cavitating valve: (--•--) castor oil, $P_d = 21$ psi; (--o--) castor oil, $P_d = 45$ psi; (--•--) kerdi oil, $P_d = 40$ psi. (Reprinted from *Chem. Eng. Sci.*, **48**(19), A.B. Pandit and J.B. Voshi, "Hydrolysis of fatty oils: Effect of cavitation," pp. 3440–3442, copyright 1993, with permission from Elsevier Science.)

Shirgaonkar and Pandit (1996) showed that the rate of hydrolysis of 2,4-dichlorophenyl benzoate in the presence of base alone was enhanced by 400% by ultrasound. While the rate in the presence of ultrasound was still lower than the one obtained with a surfactant, the results offer an alternative for enhancing the hydrolysis reaction without the use of a surfactant. The application of ultrasound to the isomerization of maleic acid to fumaric acid enhanced the yield substantially. The effects of solvent vapor pressure on the yield of fumaric acid in both the presence and absence of ultrasound are illustrated in Figure 4.17. Higher vapor pressure decreases the yield. The study by these authors also indicated that there is an optimum temperature for the production of fumaric acid. The process worked the best at optimized conditions of higher catalyst loading, lower solvent vapor pressure, and ambient temperature.

Finally, acoustic cavitation has also been used for numerous organic synthesis reactions. Some of these reactions are summarized in Tables 4.18 and 4.19 (Pandit and Moholkar, 1996). A more detailed list can be found in an article by Luche and co-workers (1989).

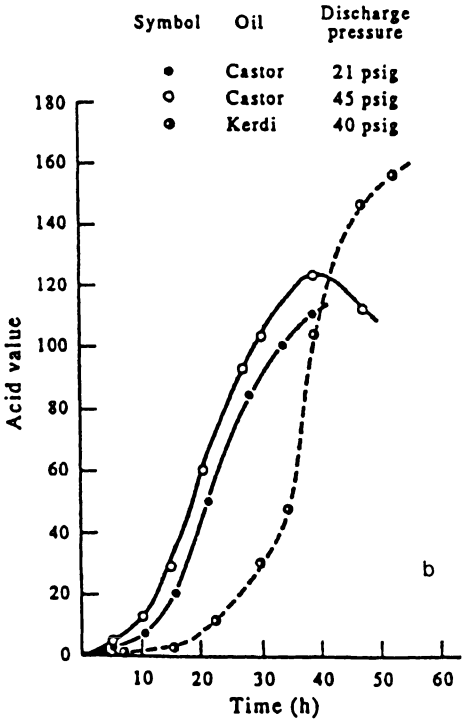

Figure 4.16. (continued)

4.4e. Solute Hydrophobicity and Reactivity

H_2O_2 is produced during the sonication of water under an argon atmosphere and is formed by the combination of OH^- radicals, which are present in the interfacial region at a high local concentration. The yield of H_2O_2 decreases in the presence of an OH^- radical scavenger. Figure 4.18 shows typical examples of this behavior. It can be seen that *tert*-butanol decreases the yield more efficiently than either dioxin or methanol, although it is known from radiation chemistry that the specific rate of reaction with OH^- radicals is the lowest with *tert*-butanol. An explanation of the results shown in Figure 4.18 thus requires a different approach.

In Figure 4.19 the half-concentration, $c_{1/2}$ (i.e., the concentration at which the H_2O_2 yield is decreased by 50%), is shown for a large number of organic compounds. It can be seen that $c_{1/2}$ ranges over five orders of magnitude, although the various compounds are known to react with OH^- radicals with rate constants over the narrower range of 10^7–10^9 Ms^{-1}. In this figure $c_{1/2}$ is plotted as a function of the hydrophobicity ratio, $\overline{R}$, of the solutes, with the latter being defined as the ratio

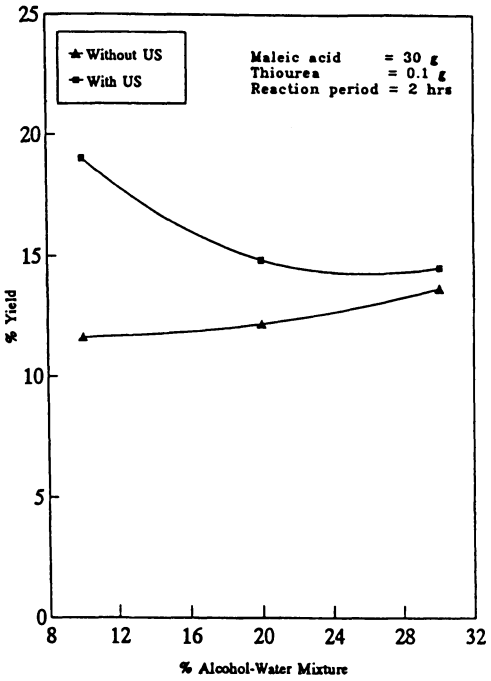

Figure 4.17. Effect of solvent vapor pressure on the yield of fumaric acid. (From Shirgaonkar and Pandit, 1996.)

of the number of hydrophobic groups to the number of hydrophilic groups in a solute molecule. For example, in ethanol there are two hydrophobic groups (i.e., CH_3 and CH_2) and one hydrophilic group (i.e., OH): $\overline{R}$, in this case, therefore, is 2. This hydrophobicity effect is explained by the accumulation of solute molecules at the interface of the gas bubbles where H_2O_2 is formed from the OH^- radicals. Therefore, the higher the concentration of solute molecules at the interface, the lower the value of $c_{1/2}$ will be. Molecules with a high $\overline{R}$ value have a strong tendency to accumulate at the interface.

Hydrophobicity effects were also encountered in studies of the reaction of hydrogen atoms with solutes. H^+ atoms escape less efficiently from the cavitation bubbles and practically no reaction could be observed with strongly hydrophilic solutes such as iodide and formate. However, other solutes can be reduced, as shown in Figure 4.20, where the rate of reduction is plotted as a function of the concentration of the various solutes. The sonication occurred under an 80 to 20% volume mixture of argon and hydrogen, in which the OH^- radicals are efficiently scavenged by H_2 to form additional H^+ atoms in the gas bubbles. The solutes shown in Figure 4.20 are known to react with H^+ atoms in homogeneous solution with diffusion-

TABLE 4.18. Homogeneous Reactions Affected by Ultrasonication[a]

Reaction	Time (h)	Yield (%)	Scale of operation
1. Curtis rearrangement			
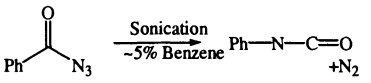			Laboratory
2. Sulfur extrusion from 1,3,4-thiadiazines			
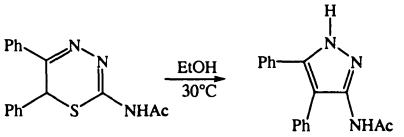	20	87	Laboratory
3. Sonochemical isomerization of maleic acid to fumaric acid			
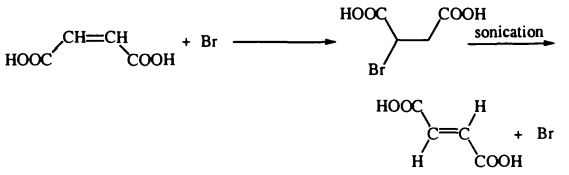	2	75	Laboratory
4. Conversion of iron pentacarbonyl to iron dodecacarbonyl (with heptane as solvent)			
$Fe(CO)_5 \xrightarrow{\text{Sonication}} Fe_3(CO)_{12}$			
5. Preparation of nitroxyl radicals from hindered piperazines			
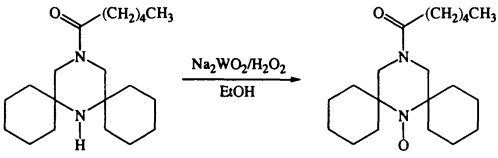	20	63	Laboratory
6. Nitrones addition to olefins			
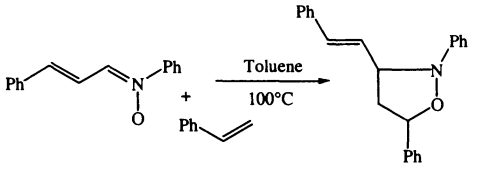	1	81	Laboratory

[a]From A.B. Pandit and V.S. Moholkar, "Harness cavitation to improve processing," *Chem. Eng. Prog.* July 1996, 57–69. Reproduced with permission of the American Institute of Chemical Engineers. Copyright © 1996 AIChE. All rights reserved.

TABLE 4.19. Gas Liquid–Liquid Reactions Affected by Cavitation[a]

Reaction	Time (h)	Yield (%)	Scale of operation
1. Ester hydrolysis 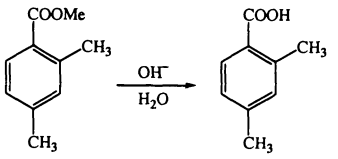	1	94	Laboratory
2. Addition of sodium azide to alkynoate ester 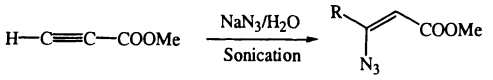		86	Laboratory
3. Hydroformylation reaction 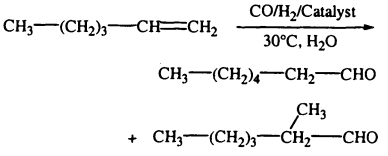	15	100	Laboratory

[a]From A.B. Pandit and V.S. Moholkar, "Harness cavitation to improve processing," *Chem. Eng. Prog.* July 1996, 57–69. Reproduced with permission of the American Institute of Chemical Engineers. Copyright © 1996 AIChE. All rights reserved.

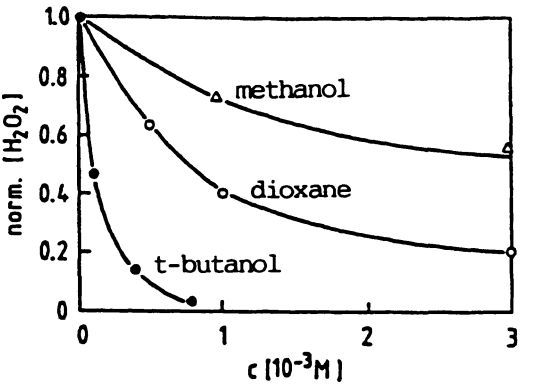

Figure 4.18. Relative yields of H_2O_2 as a function of the concentration of some organic solutes. (From Henglein, 1993, with permission.)

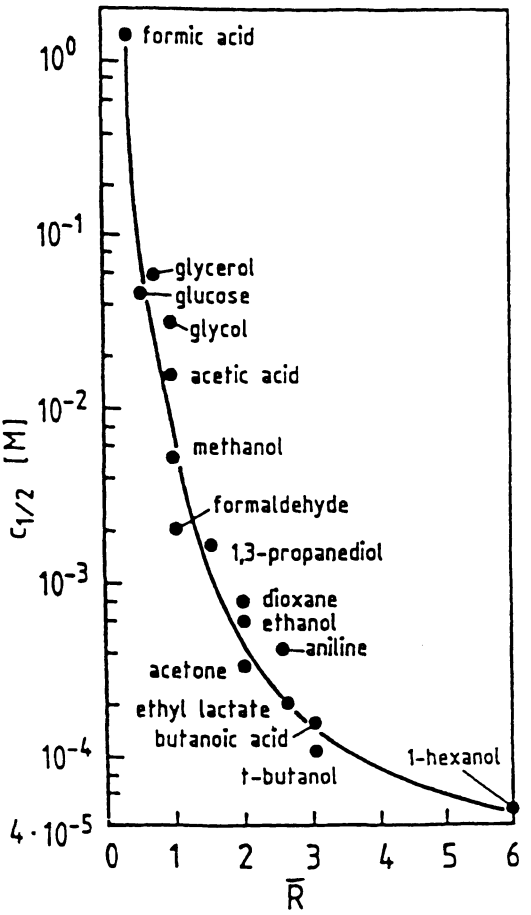

Figure 4.19. Half concentration $c_{1/2}$, of various organic OH^- radical scavengers, as a function of hydrophobicity ratio, $\bar{R}$. (From Henglein, 1993, with permission.)

controlled rates, and rate constants close to 10 Ms^{-1}. However, in the case of sonolysis, their reactivities toward the H^+ atom are quite different. Among the solutes used, Br_2 and I_2 are the least hydrophilic in nature. Among the ionic solutes, the anions MnO_4^- and $AuCl_4^-$ are certainly less solvated than the small cation Ag^+. One thus encounters a relationship between hydrophobicity and reactivity toward the H^+ atom similar to that found for the reaction of various organic compounds with the OH^- radical.

Hydrophobicity can also play an important role in free radical-initiated redox reactions and the pyrolysis of low vapor pressure molecules. The theory described above can also be applied to polymer solutions. Polymers that accumulate to only

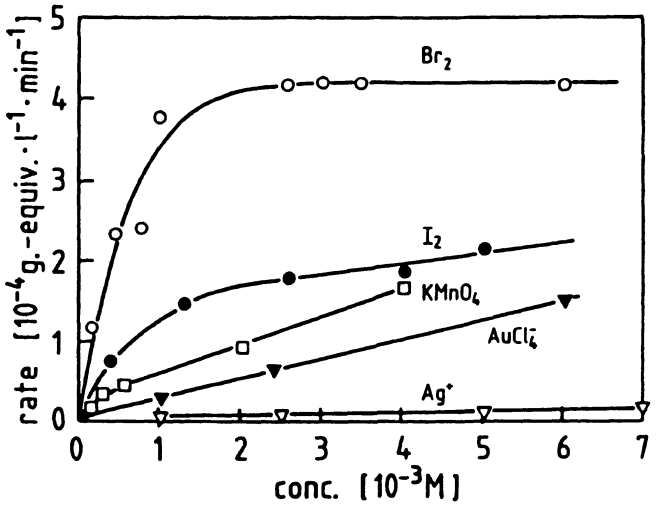

Figure 4.20. Rate of reduction of various H^+ atom scavengers, as a function of their concentration. The reduction rate is expressed as g-eq. × liter^{-1} min^{-1} to produce comparable measurements because the various solutes require different numbers of equivalents for reduction. (From Henglein, 1993, with permission.)

a small extent at the interface are expected to have a high $c_{1/2}$ in order to be able to compete with the combination reaction of the OH^- radicals. In fact, DNA has one of the highest values of $c_{1/2}$, while poly(ethylene glycol) has one of the lowest. The magnitude of the change in surface tension when a polymer is dissolved in water is an indicator of the location of the polymer accumulation. The more negative this value, the more strongly a polymer is accumulated at the surface or interface: DNA is the least surface-active polymer, while poly(ethylene glycol) is the most active. All of these results combined indicate that a strong hydrophobicity effect is present in the polymer systems as well.

Finally, in a recent study Seymour and Gupta (1997) demonstrated the enhancement of reaction rates by the addition of sodium chloride salt. They showed that for a 20-kHz frequency ultrasound, large salt-induced enhancements are observed: sixfold for chlorobenzene, sevenfold for *p*-ethylphenol, and threefold for phenol oxidation. The reaction rate enhancements were proportional to the diethyl ether–water partitioning coefficient of the pollutants. They showed that the majority of the oxidation reactions occurred in the bubble–bulk interface region. The addition of salt increased the ionic strength of the aqueous phase, which drove the organic pollutants toward the bubble–bulk interface. This study clearly shows the importance of hydrophobicity in the cavitation reaction rate.

4.5. DEPOLYMERIZATION AND REPOLYMERIZATION REACTIONS

As early as 1933, Szalay (1933a,b,c) described how ultrasonic waves depolymerize starch, gum arabic, and gelatin, as measured by a change in viscosity. Schmid and Rommel (1939b) carried out a similar study for polyacrylic acid, polyvinyl acetate, and nitrocellulose. Surprisingly, in their study a reduction in viscosity was observed even in conditions that excluded oxidation and cavitation effects. Schmid and Rommel (1939b) also found that initially depolymerization was rapid but soon slowed and eventually ceased when a minimum molecular weight was reached. Similar findings have been reported by others.

In general, ultrasonic depolymerization is closely linked to the cavitation phenomenon, as has been clearly demonstrated by Weissler (1950, 1951a,b, 1953, 1959, 1960) and Weissler *et al.* (1950). They examined the degradation of polystyrene in toluene and of hydroxyethyl cellulose in water in the presence and absence of cavitation. A carefully degassed sample showed no cavitation bubbles during irradiation and no degradation was observed. Further evidence of the need for cavitation to facilitate depolymerization comes from the effect of increasing ultrasonic intensity. At low ultrasonic intensities, when cavitation is absent, no depolymerization is observed. At higher intensities, depolymerization begins. Prudhomme and Grabar (1949a,b, 1958) also found similar effects when the irradiated liquid was saturated with gases that promote cavitation but observed that no depolymerization occurred in a degassed liquid. Melville (1955) and Melville and Murray (1950) proposed that cavitation, only accelerates degradation through mechanical hydrodynamic effects occurring in a sonicated liquid. They observed a reduction in the molecular weight of polystyrene in benzene from 7,000,000 to 260,000 when the solution was degassed. In the presence of air, the molecular weight of the polymer was reduced to 47,000.

Several mechanisms have been proposed to explain the depolymerizing action of ultrasound. Since little difference exists between the mechanism of degradation of synthetic polymers in organic solvents and natural polymers in water, it would appear that chemical effects play little or no role. Depolymerization is caused by mechanical forces mainly associated with cavitation. As cavitation bubbles collapse, strong velocity gradients are generated that can produce cleavage of the polymer chains. Polymer molecules become distorted and stretched as they enter the area of the high-velocity gradients generated by collapsing cavitation bubbles. At the final stage of collapse, the shock wave (10^5 *g* at 500 kHz) radiated from the cavity generates sufficient stresses with the polymer to be finally responsible for bond cleavage. Secondary reactions with high-energy species produced from solvent sonolysis may also contribute to polymer degradation. There is now a large volume of experimental evidence to support the mechanochemical cleavage of polymers.

Probably the most interesting facet of depolymerization studies is the homogenization of molecular weights. Schmid (1939, 1940a,b, 1960), Schmid and Rommel (1939a,b), and Schmid *et al.* (1951) were the first to observe this phenomenon in polymethyl methacrylate. Sata and Harisaka (1951) and Sata *et al.* (1951) found that sonication of aqueous solutions of polyvinyl alcohol produces a more homogeneous molecular weight, but they failed to observe such effects with heat or oxidation with $KMnO_4$. Melville (1955) and Melville and Murray (1950) showed that depolymerization does not take place at particularly weak points in the polymer chain. They degraded two different poly(methyl methacrylate)–polyacrylonitrile copolymers and found that they gave similar molecular weight fractions after ultrasound treatment. This indicated that rupture did not occur preferentially at the copolymer linkage points in the polymer chain.

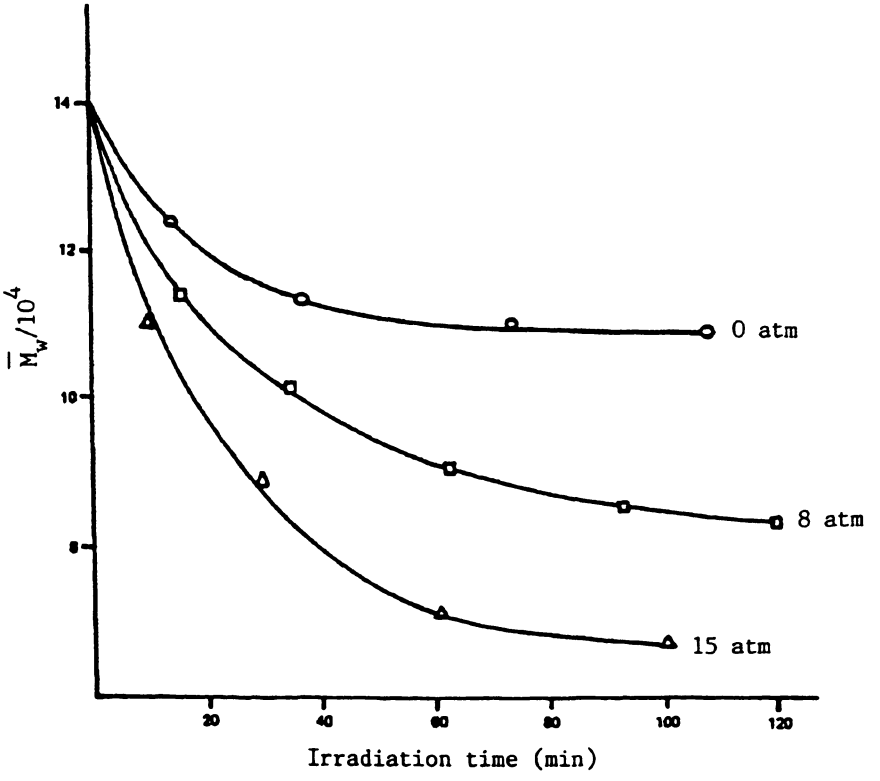

Figure 4.21. Degradation of polystyrene in toluene at various applied pressures. $T = 20°C, f = 300$ kHz, intensity = 10 W cm^{-2}. (From Perkins, 1990, with permission.)

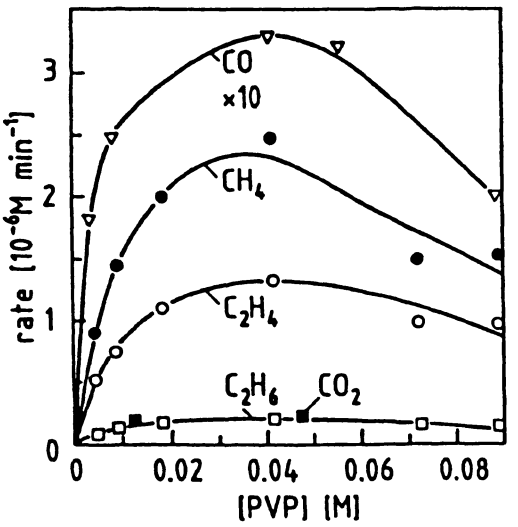

Figure 4.22. Yield of CO from the pyrolysis of various polymer solutions (sonication for 20 min). (From Henglein, 1993, with permission.)

According to Schmid (1939, 1940a,b, 1960), Schmid and Rommel (1939a,b), and Schmid *et al.* (1951), the breakage of bonds at different positions in the polymer chain will occur in long macromolecules. This results in molecular fragments of various lengths and an increase in polydispersion. As irradiation continues, homogenization of the polymer molecular weights is observed. Mostafa (1958a,b) and Lamb (1975) have shown that ultrasonic degradation is a nonrandom process. From a study of many ultrasonic depolymerizations, it has been concluded that in dilute solutions, degradations follow first-order kinetics, with the rate constants of degradation being proportional to the molecular weight of the polymer. Molecules appear to break preferentially at points close to their midpoints, although they do not appear to break at the exact center.

The rate of ultrasonic depolymerization decreases with decreasing molecular weight of the polymer; there is a limiting molecular weight below which no further cleavage occurs. The rate of degradation also depends on the duration of irradiation, concentration in solution, nature of polymer and solvent, and the intensity of the ultrasound. Limited data indicate that excess external pressure slows down the degradation rate. For low molecular weight polymers, the opposite results have also been obtained. One notable exception, however, is the fact that polymer degradation is independent of the ambient (inert) gas, which indicates that the cleavage is not occurring inside the collapsing bubble by thermal processes, since polyatomic gases greatly reduce the cavitational temperature. Ultrasonic degradation of polymers in

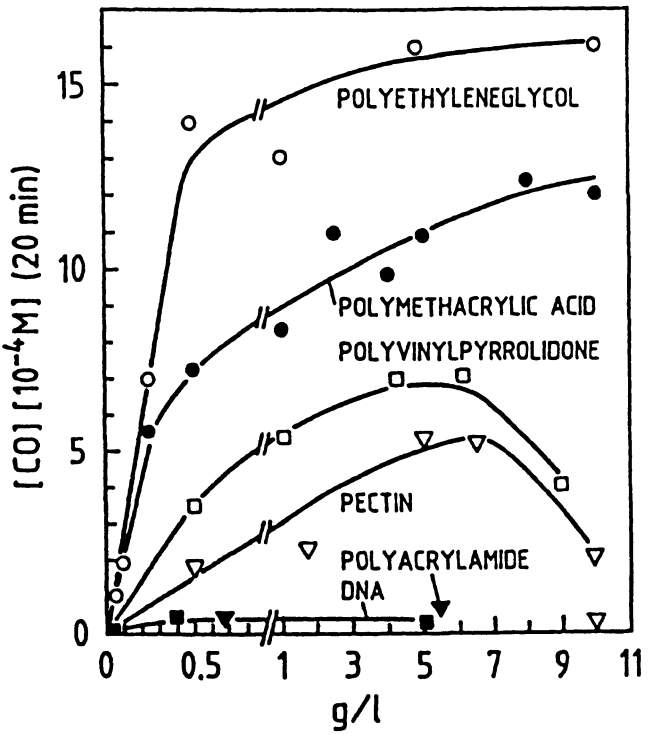

Figure 4.23. Sonication of poly(vinylpyrrolidone) in aqueous solutions under argon showing the rate of formation of the various pyrolysis products as a function of the polymer concentration. (From Henglein, 1993, with permission.)

solution creates a nonrandom scission, with a well-defined preference for rupture near the middle of the chain. The degradation rate of aqueous polyethylene oxide increases with a decrease in polymer concentration. Similar results have been obtained with hydroxyethyl cellulose in an aqueous solution. The effect of applied pressure on the degradation of polystyrene in toluene is illustrated in Figure 4.21. As shown, an increase in pressure increases the degradation rate.

The pyrolysis of several polymers, including DNA, has been examined. Figure 4.22 shows the production of CO (the dominant product) as a function of polymer concentration for various polymers. At low concentrations where viscosity of the solution does not change significantly and cavitation quality remains unchanged, the different yields for different polymers indicate different sensitivities to pyrolysis in an ultrasonic field; e.g., DNA is the most stable and poly(ethylene glycol) is the most strongly affected. These results can be explained on the basis of the accumulation of various polymers at the interfacial region.

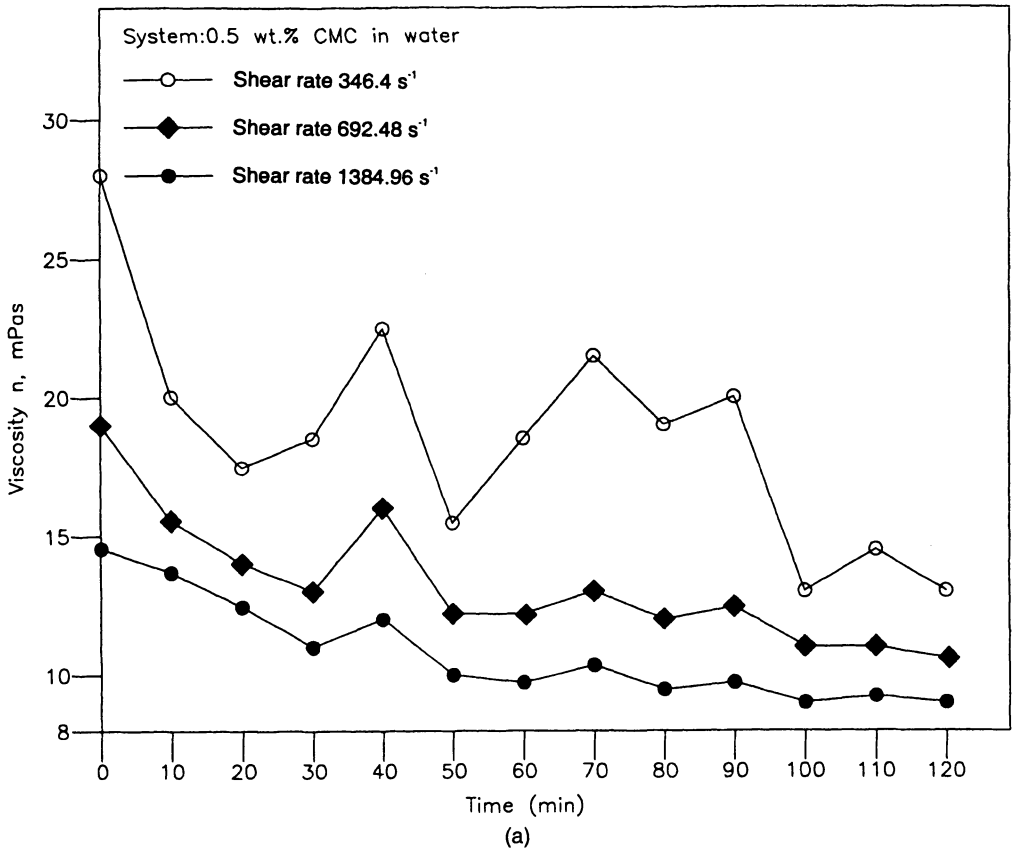

Figure 4.24. (a) Effect of ultrasonic irradiation on viscosity. (b) Effect of hydrodynamic cavitation on viscosity. (From Chivate and Pandit, 1993, with permission.)

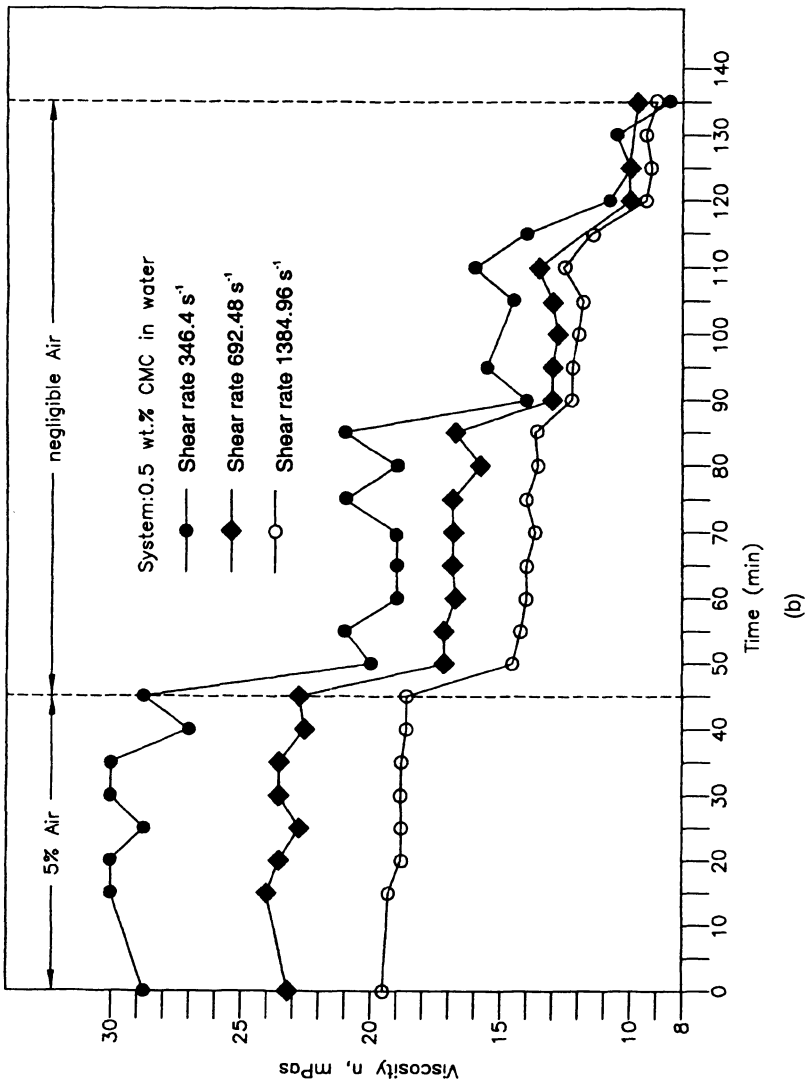

Figure 4.24. (a) Effect of ultrasonic irradiation on viscosity. (b) Effect of hydrodynamic cavitation on viscosity. (From Chivate and Pandit, 1993, with permission.)

Polymers have zero vapor pressure and they cannot penetrate the gas phase. However, thermal decomposition in the hot interfacial layer has been observed. Figure 4.23 shows the yields of typical pyrolysis products from solutions of poly(vinylpyrrolidone) (PvP): all products show maxima with respect to PvP concentrations. The decrease in rate is attributed to a decrease in cavitation efficiency caused by the high viscosity of the more concentrated solutions. To date, the mechanical degradation of polymers in an ultrasonic field was thought to be the main reaction occurring in polymer solutions. However, in certain cases for aqueous solutions, the yield of the pyrolysis products may exceed the yield of the main chain-scission products in a polymer.

Chivate and Pandit (1993) examined the degradation of aqueous polymeric solutions by acoustic and hydrodynamic cavitation. Aqueous solutions of polyethylene oxide (PEO) and carboxymethyl cellulose (CMC) were used for the study. They showed that the cavitation generated in a flow loop system and with ultrasonic radiation gave similar results. In both cases the cavitation changed the chemical

TABLE 4.20. Parameters Influencing Polymer Degradation[a]

Parameter	Effects of degradation
Frequency	Increasing the frequency reduces the extent of degradation.
Intensity	Increasing the intensity increases the rate and the extent of degradation.
	There is an upper intensity limit due to the material stability of the transducer, decoupling with the medium, and a large number of bubbles (transmission barrier).
Solvent	The higher the vapor pressure, the less violent the cavitation collapse and the less the extent of degradation.
	Cavitation occurs more readily in solvents with low viscosity and surface tension.
Bubbled gas	The solution should be saturated with a noble gas that has a low thermal conductivity, resulting in higher local heating, more violent cavitation collapse, and increasing polymer degradation.
	The greater the amount of dissolved gas, the smaller the intensity of the shock wave; i.e., the lower the gas solubility, the higher the degradation.
External temperature	Increasing temperature increases vapor pressure and collapse is less violent, resulting in decreasing degradation.
	Increasing temperature towards the boiling point of the solvent increases dramatically the number of bubbles that can act as sound barriers.
Concentration	Decreasing the concentration of the polymer in solution increases the degradation process.
Molecular mass	A larger initial molecular mass of the polymer increases the degree of degradation.
	There is a molecular mass limit below which there is no degradation.

[a]From Peters (1996) with permission.

properties. They also suggested that the generation of hydrodynamic cavitation is much simpler, cheaper, and more energy efficient than the acoustic method. Admittance of air is a good means to control the extent of damage due to cavitation. A typical comparison of viscosity versus time for CMC in water for both acoustic and hydrodynamic cavitation is shown in Figures 4.24(a) and 4.24(b), respectively. A brief summary of the effects of system parameters on polymer degradation is given in Table 4.20.

4.6. ULTRASOUND AND HOMOGENEOUS OXIDATION

While water-soluble homogeneous catalysts that can be used to convert organic compounds in an aqueous phase have not yet been extensively investigated, in principle, ultrasound can have a significant effect on homogeneously catalyzed reactions. Mokry and Starchevsky (1987, 1993) and Mokry *et al.* (1987) examined the effects of an ultrasonic field on the homogeneous oxidation of a variety of organic compounds.

Ultrasound accelerates the initiation process in homogeneously catalyzed oxidation reactions. For oxidation of cyclohexane, these authors show that in the presence of $CoNf_2$ (cobalt dinapthalide), the application of ultrasonic radiation enables one to (1) decrease the nucleation period, (2) increase the oxidation rate, and (3) improve the total process selectivity with regard to final products (see Figure 4.25). The same features were observed when the oxidation was carried out in the presence of numerous other metal catalysts. In all of these systems, the synergism phenomenon was observed, i.e., the rate of catalytic cyclohexane oxidation in an ultrasonic field was higher than the sum of the respective rates of the acoustic chemical and "pure" catalytic oxidation.

While similar results were obtained for acetaldehyde oxidation, the synergistic effect in this case was not as pronounced. Since the rate of catalytic reaction is an order of magnitude higher than the rates of possible acoustic-chemical reaction (through free radicals generated by the cavitation), Mal'tsev (1976), Mal'tsev and Solv'eva (1970), and Chervinskii and Mal'tsev (1966) believe that in these systems the application of ultrasound influences the decomposition of the catalysis–substrate complexes formed in the system, leading to increased rates.

Mokry and Starchevsky (1987, 1993) and Mokry *et al.* (1987) also found that without the catalyst under the given conditions, ultrasound does not influence the decomposition of cyclohexyl hydroperoxide (see Table 4.21). Also, pretreatment of the catalyst solution in cyclohexane hinders the formation of the catalyst–hydroperoxide complex and as result of this, slows down the hydroperoxide decomposition process. These studies have thus shown that although the use of ultrasound in a homogeneously catalyzed process should have positive effects, the time at which the ultrasound is applied (before or during the reaction) can have a

significant impact on the final outcome of the results. Some experimental values of the various kinetic constants of the homogeneous catalytic decomposition of cyclohexyl hydroperoxide for both sonicated and nonsonicated samples are given in Table 4.21 (Boudjouk, 1986, 1987; Boudjouk and Han, 1983).

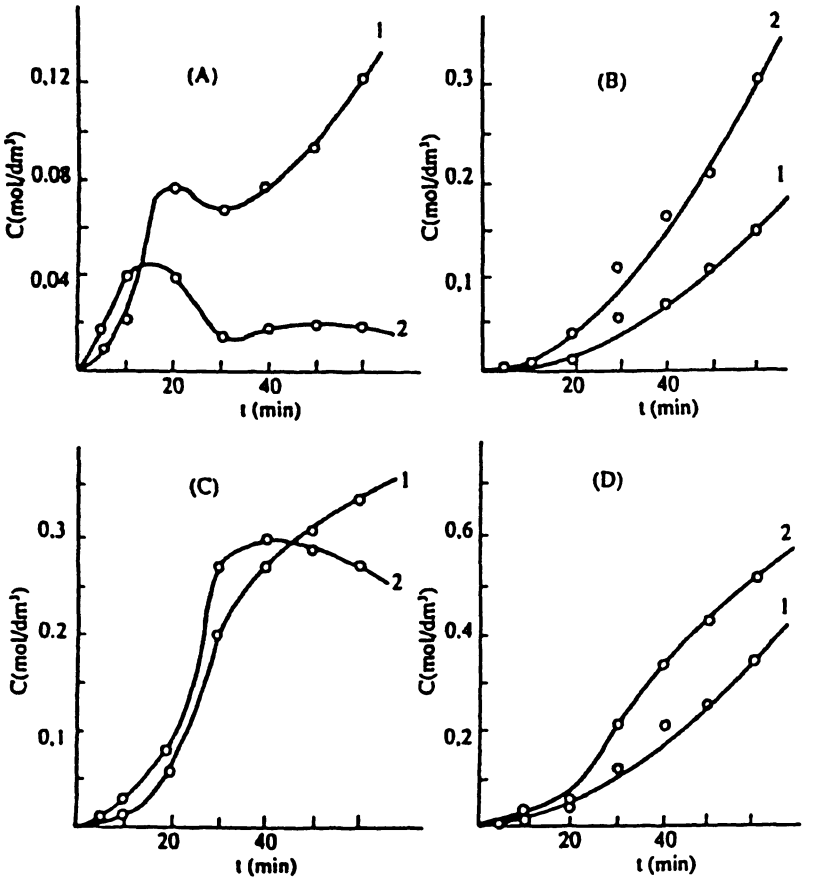

Figure 4.25. Increase in the concentration of the various products of the cyclohexane oxidation process as a function of time, with cobalt dinaphthalide ($CoNf_2$) present as a catalyst, for both nonsonicated (curves 1) and sonicated (curves 2) sytems. Kinetic curves obtained for: A, hydroperoxide; B, acids; C, cyclohexanol; and D, cyclothhexane. (From Mokry and Starchevsky, 1993, with permission.)

TABLE 4.21. Experimental Values of the Various Kinetic Constants of the Homogeneous Catalytic Decomposition Process of Cyclohexyl Hydroperoxide, for both Sonicated and Nonsonicated Samples[a]

T(k)	k(s^{-1})	K(dm^3/mol)	$k_p(=kK)^b$ (dm^3/mol s)	Experimental conditions
348	0.27	13	3.51	In an ultrasonic field of 22 kHz frequency
333	0.18	21	3.78	
348	0.21	16	3.36	Catalyst, in cyclohexane, initially subjected to an ultrasonic field of 22 kHz
333	0.15	26	3.90	
348	—	—	1.26	In an ultrasonic field of 44 kHz
333	—	—	0.70	
348	0.22	26	5.72	In the absence of an ultrasonic field
333	0.17	34	5.78	

[a]From Mokry and Starchevsky (1993) with permission.

[b]k_p includes the concentration of catalyst.

4.7. ULTRASOUND AND LIQUID–LIQUID PHASE-TRANSFER REACTIONS

Phase-transfer reactions have been increasingly used in various organic transformations. While phase-transfer catalysis has not been applied directly to the conversion of pollutants in an aqueous stream, it has potential for some selective pollutants. Ultrasound can aid phase-transfer catalysis in a number of ways. Cavitation during sonication can induce some free radical reactions. Ultrasound can also cause emulsification between two liquids and enhance liquid–liquid interfacial area and transport rates, thereby increasing the reaction rates.

The use of ultrasound to produce either extremely fine emulsions (from immiscible liquids) or efficient mass transfer has led to the use of ultrasound to enhance or even replace phase-transfer catalysts (PTC). The normal function of a PTC is to enable the transfer of a water-soluble reagent into an organic phase, where it can more readily react with an organic substrate. As an example of phase-transfer catalysis, consider the quaternary ammonium salt $[(C_8H_{17})_3N^+CH_3]Cl^-$. This salt is itself quite soluble in nonpolar(organic) media owing to the presence of long hydrocarbon chains. When this PTC is dissolved in $CHCl_3$ and the solution shaken with aqueous NaOH, some of the OH^- ions in the aqueous phase will be partitioned (pulled) into the organic phase by the PTC in exchange for its own Cl^- ions, which are transferred back into the water. Hydroxide ion in chloroform is a powerful base, and under these conditions it can remove a proton from the solvent to give $-CCl_3$

which in turn decomposes to the reactive electrophilic intermediate CCl_2 (dichlorocarbene). If an alkene (e.g., styrene) is present in the organic phase, the carbene adds to it and the product of the reaction is a dichlorocyclopropane.

The ability to increase the range of reactivity of a species by transferring it from one phase to another is a powerful tool in chemical synthesis. There are, however, two drawbacks to the use of phase-transfer catalysts: (1) the PTC itself is generally expensive; and (2) a PTC is potentially dangerous in that it will, by its very nature, catalyze the transfer of chemicals into human tissue. The potential health hazard of using a PTC must, however, be counterbalanced by the synthetic efficiency that follows from its employment since without the addition of a PTC, many heterogeneous reactions are limited to the interfacial regions of contact and are consequently slow.

Ultrasound helps improve the liquid–liquid interfacial area through emulsification, which is important for viscous films containing gas-filled bubbles and cavitation bubbles. Gas-filled bubbles within the film, oscillating because of ultrasound and mobilized by acoustic streaming, entrain some of the film. Simultaneously, cavitation bubbles spray solvent on the film that covers the pulsing gas bubble. The pulsing action of the gas bubble is therefore disrupted and the liquid is scattered on its surface, leading to highly dispersed emulsions. Very fine emulsions greatly increase the reactive interfacial area and allow faster reactions at lower temperatures. An example of this would be the ultrasonically enhanced saponification of wool waxes by aqueous sodium hydroxide using *tetra-n*-heptylammonium bromide as a PTC.

There have been a large number of reports on the use of ultrasound in phase-transfer catalysis. In several cases the use of ultrasound has enabled cheaper phase-transfer agents to be used. For example, ultrasound has a pronounced effect on the rate of saponification of carboxylic esters. Thus, methyl-2,4-dimethylbenzoate and sodium hydroxide solution in the presence of an aliquot gave a 94% yield of the acid after sonication for 1 h compared with only 15% yield of the acid after refluxing for 1.5 h. Insonation allowed the saponification of commercially important wool waxes to be carried out at much lower temperatures than is usual. This also led to improvements in the color of the products.

Significant increases in turnover numbers are reported for the hydroformylation of alkenes using a water-soluble rhodium catalyst in the presence of ultrasonic fields (30–40 kHz). Thus using a 1:1 ratio of CO to H_2 at 2.5 MPa, 1-hexene and an aqueous solution containing $HRh(CO)[P(C_6H_4SO_3H)_3]_3$ yields aldehydes with a turnover number of 11.34 in ultrasonic fields compared with only 3.24 with stirring at 500 rpm. In another example, increased yields of products were obtained under ultrasonic irradiation in the PTC alkylation of the isoquinoline derivatives using 50% aqueous NaOH as a base. Efficient mixing is not easy to achieve for this system under normal reaction conditions because of the viscosity of the aqueous base. In the specific case of alkylation with benzyl chloride, ultrasound plus $[Et_3NCH_2Ph]$ +

Cl^- achieves 60% yield in 20 min compared with only 50% in 2 h with stirring at 25°C (6 h).

The above examples indicate that ultrasound can aid in any liquid–liquid phase-transfer reaction for the transformation of organic pollutants from the aqueous phase. More work in this area needs to be carried out.

5

GAS–LIQUID–SOLID CAVITATION CHEMISTRY

5.1. INTRODUCTION

In this chapter we briefly evaluate the effects of cavitation on the gas–liquid–solid reaction. While in principle three-phase systems can be subjected to hydrodynamic cavitation, it is clear that a three-phase flow through an orifice or a pressure expansion device may lead to some operational drawbacks. The literature for the application of hydrodynamic cavitation to three-phase reactions is therefore sparse. Similarly, the application of optical cavitation to three-phase systems may be difficult to control owing to the presence of the solid phase. Our discussion here on the effects of cavitation on gas–liquid–solid reactions will therefore be restricted to acoustic cavitation. The general principles should, however, be applicable to other types of cavitation as well.

When ultrasound is passed through a fluid medium, two important phenomena occur. First, there is acoustic streaming caused by nonlinear coupling of the first-order acoustic waves. These waves produce a stirring effect and in the vicinity of the surfaces, a reduction in the thickness of diffusion layers, thereby increasing the fluid–solid mass transport. Second, the ultrasound produces cavities, some of which implode and cause high temperatures. The imploding cavities are estimated to have radii of about 200 μm and lifetimes of less than 2 μs. The implosion generates high-energy shock waves and in the vicinity of the surfaces, the bubble collapse is nonspherical and produces high-velocity microjets of solvent, which impinge on the surface with velocities estimated to be in excess of 100 ms^{-1}.

This phenomenon can result in the removal of oxide layers from metals, thus providing clean surfaces. In the case of powdered reactants, the particles can also be set into motion at speeds of up to 100 ms^{-1} and undergo collisions that can markedly change their morphology. The jet as well as the shock waves from the cavity implosion erode solid surfaces, remove nonreactive coatings, and fragment

brittle powders. Reactions can also be facilitated by the high temperatures and pressures associated with cavity implosions near surfaces. The chemical reactivity of solid surfaces, which depends upon crystalline form and crystal size within a particle, and the purity and chemical composition of the metal, as well as the shape and size of the particle, can thus be altered by acoustic streaming and cavitation.

The extreme conditions generated by cavitation near surfaces can also be utilized to induce reactivity in "unreactive" metals. Johnson (1966), for instance, examined reactions among carbon monoxide, molybdenum, and tantalum, as well as other comparable metals. Conventional techniques require pressures of 100 to 300 atm and temperatures of 200 to 300°C to form metal carbonyls. Using ultrasound, however, formation of metal carbonyls can proceed at room temperature and pressure.

In general, both acoustic streaming and cavitation may lead to improved reactivity of solid reagents by:

removal of passivating surface coatings
creation of surface defects, which because of reduced coordination may lead to reactive sites
reduction in particle size, thereby increasing the reactive surface area
improvements in mass transport

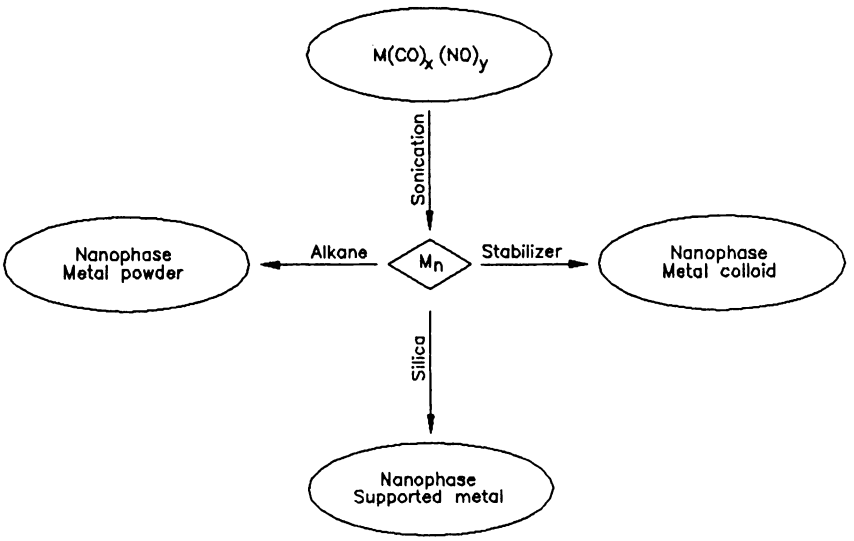

Figure 5.1. Sonochemical synthesis of various forms of nanostructured materials. $n = 100–1000$. (From Peters, 1996, with permission.)

TABLE 5.1a. Sonochemical Reactions Involving Alkali Metals[a]

lithium:

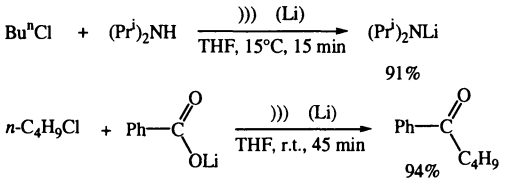

sodium:

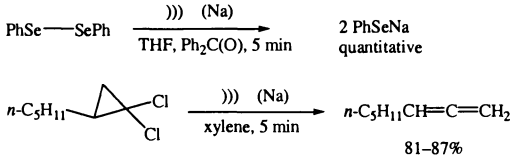

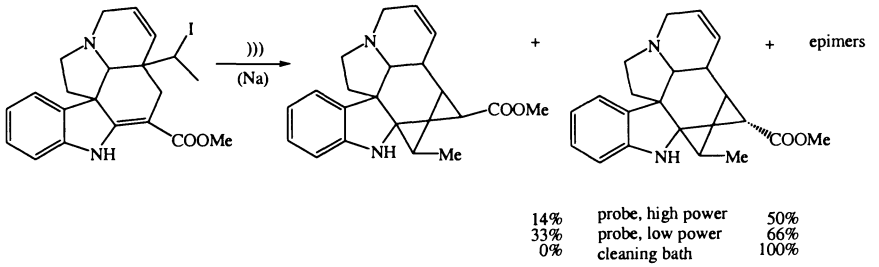

potassium:

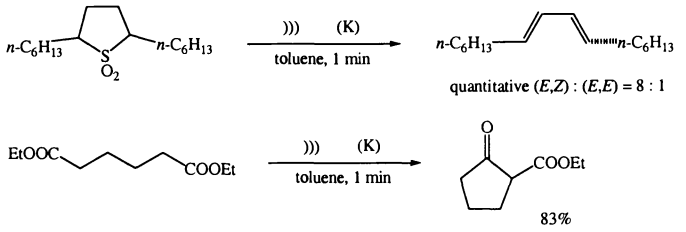

[a]From Peters (1996) with permission.

Ultrasound is a useful tool in nearly every case where a liquid and a solid must react. Furthermore, since ultrasound can radiate through large volumes of liquid, it is well suited for industrial applications.

In a recent review Peters (1996) gave an excellent treatment of the application of ultrasound to the material reactions. As shown in Figure 5.1, he articulated the

TABLE 5.1b. Sonochemical Reactions Involving Group II, III, IV Metals[a]

magnesium:

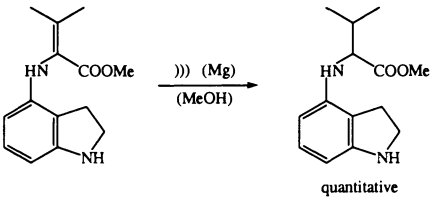

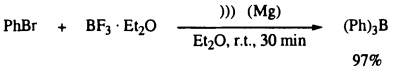

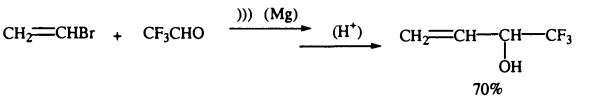

aluminum:

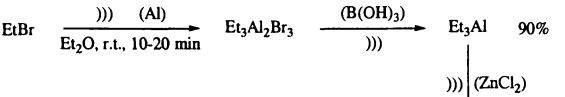

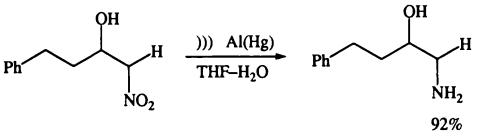

indium:

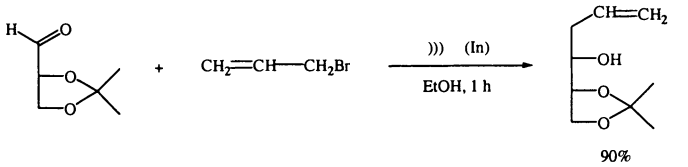

tin:

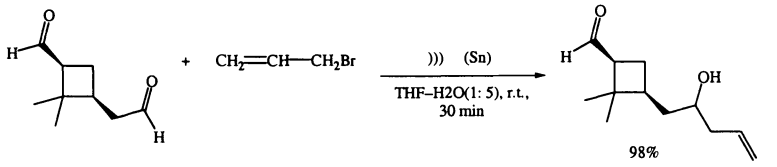

[a]From Peters (1996) with permission.

TABLE 5.1c. Sonochemical Reactions Involving Transition Metals[a]

zinc:

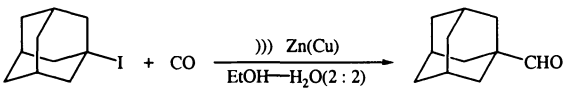

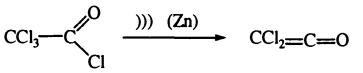

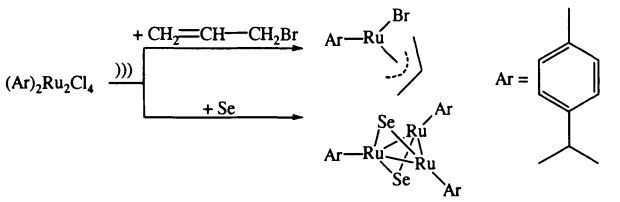

samarium:

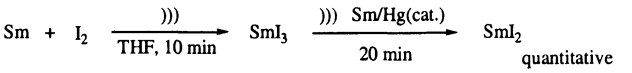

nickel:

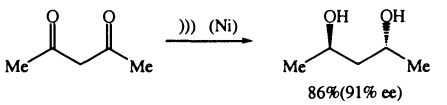

mercury:

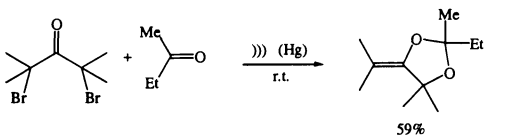

cadmium:

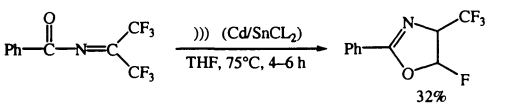

copper:

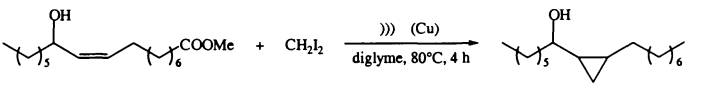

[a]From Peters (1996) with permission.

TABLE 5.2. Application of Ultrasound to Nonradical Catalyzed Polymerizations[a]

ring-opening polymerization:

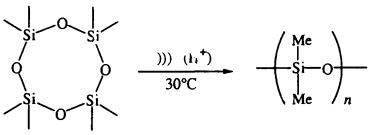

organometallic catalyzed polymerization:

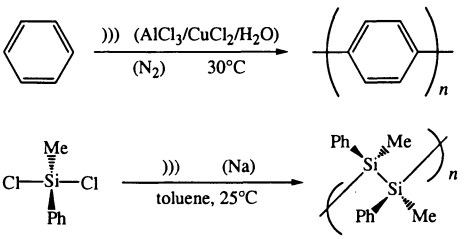

[a]From Peters (1996) with permission.

sonochemical synthesis of various forms of nanostructured materials from Mn where n =100–1000. Several examples of sonochemical reactions involving alkali metals; group II, III, and IV metals; and transition metals described by Peters are given in Tables 5.1a, 5.1b, and 5.1c, respectively. An application of ultrasound to nonradical catalyzed polymerization is shown in Table 5.2.

5.2. GENERAL EFFECTS OF ULTRASOUND ON GAS–LIQUID–SOLID REACTIONS

There are a number of reasons for rate enhancement or change in product distribution during gas–liquid–solid reactions in the presence of ultrasound. Some of these are briefly described in the following section.

5.2a. Surface Cleaning

There are two types of reactions involving metals: (1) one in which the metal is a reagent and is consumed in the process and (2) one in which the metal functions as a catalyst. The sonochemistry of solid surfaces in liquids is best exemplified by the reactions of active metals such as lithium, magnesium, zinc, and aluminum. Ultrasonic irradiation of reaction mixtures consisting of these metals provides better control at lower temperatures and produces relatively higher yields. The

chemistry of these metals is very difficult to control. Traces of water, oxygen, or nitrogen can react at the surface to form protective coatings. Increasing the reactivity of the protected surface by direct heating, however, can result in undesirable explosions. Ultrasound can keep the surface clean and allow the reaction to proceed evenly at reduced ambient temperatures. Excellent yields and improved reliability can be achieved for many reactive metals in large-scale industrial applications. The removal of inhibiting impurities and the pitting of the surface increases the number of active sites available to reagents, and the accelerated flow of liquid from acoustic streaming counters the local depletion of reagents at the active sites. It is also possible to optimize both the frequency and the ability to focus sound beams to perform "site-specific" reactions, e.g., selective cross-linking on the surface.

Surface contaminants can be classified according to their ability to withstand cavitational effects, their binding strength to the surface to be cleaned, and their mode of interaction with the solvent. For metals in the forms normally used in chemical reactions (i.e., powders, dispersions, chips, and wires), the common surface inhibitors are dust, grease films, oxide films, and products of reactions with incidental agents such as sulfur, chloride, and other halogens. Most surface films are broken down in a liquid by cavitation and acoustic streaming. In addition, vibration of the particle causing stress in the coating can lead to film fracture and removal. Jet cleaning occurs as a pulsating cavitation bubble moves over the contaminant film, cleaning "paths" that trace its journey. These liquid jets are generated during the division of large unstable bubbles into smaller ones on the surface.

Apart from these mechanical reasons, in some cases chemical reactions promoted by ultrasonic waves must also be considered as an important cleaning mechanism. For example, metal oxide films may be susceptible to aqueous solvents, depending on the pH of the system. For organic solvents, free-radical side reactions may promote the removal of oxide, sulfide, or halide impurities. Oxidation or reduction by electron transfer between intermediates formed during the course of a chemical reaction and surface impurities is also feasible. In many cases, the cleaning effect alone is insufficient to explain the extent of the sonochemically enhanced reactivity. In such cases sonication serves to sweep reactive intermediates, or products, clear of the metal surface and thus presents a renewed, clean surface for reaction. This sweeping effect would not be as effective under normal mechanical agitation.

Surface cleaning by acoustic streaming is most important when the contaminant film is soluble in the solvent. This mechanism differs sharply from mechanical agitation because it rapidly exchanges the solvent at the surface, reducing the thickness of the boundary layer. Higher frequencies lead to greater flow rates because of increased absorption of acoustic energy and are recommended for loosely bound contaminants. More tightly held inhibitors require cavitation, and thus lower frequencies are more efficient.

Electron microscopic examination of ultrasonically assisted cleaned surfaces reveals pitting of the surface of the metal, which acts to expose new surface to the reagents and to increase the effective surface area available for reaction. The pitting is thought to be caused by two possible processes: (1) the implosion of cavitation bubbles formed from seed nuclei on the surface or (2) microstreaming of a jet of solvent onto the surface when a cavitation bubble collapses in the solvent close to it.

The reactions of solids with soluble reagents that yield poorly soluble products cover the reactive surface of the solid and thereby hinder a fresh supply of reagent. In these reactions ultrasound is considered to improve mass transport by the continuous cleaning of the surface of the solid reagent. A good example of such a reaction is the neutralization of sulfuric acid with calcium oxide grains. Calcium sulfate (gypsum) is produced that passivates the surface of the calcium oxide. Ultrasonic irradiation leads to a faster increase in pH than with stirred reactions, especially when larger calcium oxide grains are used. The increased rate observed under ultrasonic irradiation is attributed to the continuous cleaning of the surface of the calcium oxide grains.

5.2b. Morphological Changes in Metal Catalysts

The effects of ultrasound on particle morphology, surface composition, and catalyst reactivity have been investigated by Casadonte and Doktycz (personal communication). They discovered that catalysts such as nickel, copper, and zinc powders irradiated with ultrasound show dramatic changes in surface morphology. Individual surfaces are smoothed and particles are consolidated into extended aggregates. Ultrasound can remove the oxide coating on a nickel catalyst, thus improving its reactivity. Ultrasonic irradiation increased the effectiveness of nickel powder as a catalyst more than 100,000 times. The nickel powder is as reactive as some special catalysts currently in use, yet it is nonflammable and less expensive.

5.2c. Cavitation Erosion

Cavitation erosion is predominantly mechanical in nature and has two possible sources: the shock wave of isolated imploding cavities attached to the surface and the jet impact generated by clusters of cavities collapsing near the surface. The most popular theory is that erosion of metals results from asymmetric collapse of single bubbles attached to, or very near, the surface, which produces shock waves and liquid jets of sufficient force to deform the surface of the metal. There is also a cascading effect; i.e., the asymmetric collapse promotes erosion, which in turn enhances asymmetric collapse, and so on. It should be noted that cavitation erosion can also affect the surface of the acoustic horn.

5.2d. Shape, Size, and Specific Area of Particle

It has been shown that ultrasonic horns that deliver high-power ultrasound can break down solids and increase their specific surface area. As a result, higher reaction rates are observed in subsequent reactions. For example, the increased rate of the Ullman reaction in the presence of ultrasound has been shown to be partly due to the breaking down of the copper powder to an average size of 25 μm. Similarly, the particle size of various inorganic solids has been reduced from 60–90 to 5–10 μm.

In gas–liquid–solid reactions involving solids dispersed in liquids, the overall reactivity will depend upon the available reactive surface area. The difference when using powders (metallic or nonmetallic) is that ultrasonic pitting can lead to fragmentation and a consequent reduction in particle size. One interesting aspect of such reductions is that for a particular set of experimental conditions there appears to be an optimum size for the reduction beyond which ultrasound has no further effect. This is generally considered as a stable particle size. The force needed to crush a particle is generally inversely proportional to the particle diameter. One important benefit of a reduction in particle size and a simultaneous surface activation is the possibility of substituting sonication for the use of a phase-transfer catalyst as a means of assisting solid–liquid reactions.

The major factors responsible for the increase in the reaction rates of nonmetallic solids are probably: (1) an increase in surface area of the solid reagent from cavitation-induced particle size reduction and (2) improved mass transport of liquid reagent to the solid surface via surface streaming. Augmenting the effects of increased surface area should be the improved "refresh rate" at the surface of the solid that results from acoustic streaming. As mentioned earlier, this effect is different from mechanical mixing because the flow rates at the surface are increased by the motion of the particle, which is caused by its absorption of sound or hydrodynamic energy.

5.2e. Improved Mass Transport

Dispersion of solids in liquids is also improved when carried out in a cavitating liquid. For example, the successful dispersion of mica, gypsum, and hematite in water, producing colloidal or semicolloidal solutions, was reported as far back as 1938. This technique is now widely used for the peptization of gels and gel-like substances in favor of mechanical methods, and is commonly used in the preparation of drugs, dyestuffs, and preceramics. With the exception of a reduction in size of the suspended particles and the increased stability of the suspension, the properties of the ultrasonically dispersed materials were usually the same as those produced by the conventional techniques of heating, mixing, and/or vigorous

shaking. There are numerous potential applications to synthesis; an ultrasonically dispersed $TiCl_3$ in polyolefins results in improved Ziegler–Natta catalysis.

Ultrasonic waves do not act directly on molecular diffusion, but can induce convective motion in the medium and as a result decrease the thickness of the diffusion boundary layer. This leads to an increase in the transport velocity of matter and thereby to acceleration of the diffusion-controlled reactions. There are many ways ultrasound may induce convective transport near the solid–liquid interface. One important factor is assumed to be acoustic streaming, which is defined as the time-independent flow of fluid induced by a sound field. It can be divided into two general types: first, the quartz or sound wind that is associated with the plane acoustic waves in the volume of an attenuating medium, and second, acoustic microcurrents, also called *microstreaming* or *microstirring*, which are associated with the interaction of a sound field with a boundary or a surface. These microcurrents can be described as a circulatory motion of the medium near the phase separation boundary, and they are responsible for the acceleration of some multiphase reactions. Acoustic streaming can occur in the absence of cavitation. Experiments showed that resonant gas bubbles resting on a boundary are also a very efficient source of microstreaming. Finally, microjets that are formed when a cavitation bubble collapses near a solid surface and that have a velocity over 100 ms^{-1} may also induce convective transport. Cavitation-induced cold fusion studies can substantiate this hypothesis.

5.2f. Mechanisms for Gas–Liquid–Solid Cavitation Reaction

In gas–liquid–solid systems, cavitation reactions follow an ionic mechanism. Even if the ionic pathways, from a purely chemical component aspect, are not influenced by hydrodynamic turbulence or sonication, mechanical effects such as microstreaming, which are purely physical in nature, are still present and will be responsible for enhancement in rates and yields. This class of reactions is sometimes referred to as "false" sonochemistry, since the role of ultrasonic waves is similar to that of a highly efficient agitation process. Since no "chemical" role is involved, no sonochemical switching is expected.

Several types of cavitation reactions contain the characteristics of both of the above two categories of reaction. A liquid–solid system that can react by involving a SET mechanism will be subject to both the mechanical and the chemical effects of sonication. Other examples of mixed reactions are the effects of ultrasound on photochemical, phase-transfer, or enzyme-catalyzed reactions. In all of these cases, more than one type of chemistry simultaneously occurs during the reaction process. Some examples of sonochemical switching are shown in Table 5.3.

TABLE 5.3. Examples of Sonochemical Switching[a]

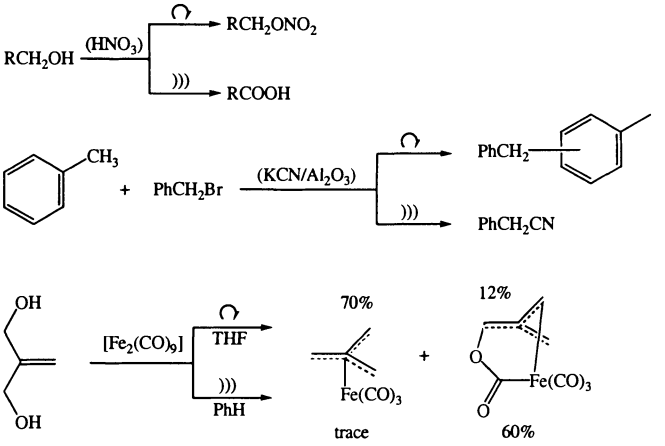

[a]From Peters (1996) with permission.

5.3. SPECIFIC ROLE OF ULTRASOUND ON GAS–LIQUID–SOLID REACTIONS

For heterogeneous reactions involving catalyst reagents, ultrasound may be beneficial to five distinct phases:

in catalyst or reagent preparation
in catalyst or reagent activation
during catalyst induction
during reaction with substrate
in catalyst regeneration

Here we examine each of these cases separately. Several applications of ultrasound to metals and nonmetallic solids are shown in Table 5.4. Some practical examples of gas–liquid–solid organic syntheses that are enhanced by ultrasound are briefly described in Table 5.5. Finally, a few examples of catalysts used for ultrasonically assisted waste conversion reactions are given in Table 5.6.

5.3a. Catalyst and Reagent Preparation

Several reports (Pugin and Turner, 1990; Lindley, 1992) indicate that the use of ultrasound during the preparation of solid catalysts leads to improvements in catalytic activity compared with catalysts prepared by chemically similar method

TABLE 5.4. Applications of Ultrasound to Metals and Nonmetallic Solids[a]

Material	Applications of Ultrasound
Metals	Production of amorphous, nanosized metal powders and nanocolloids
	Preparation of activated and supported metals used as catalysts
	Agglomeration of metals, formation of metal carbides
	Electroplating and spray pyrolysis to form metal layers
	Crystallization
	Metal welding, machining, soldering, casting, sonocleaning
	Organometallic sonochemistry
Solids	Impregnation of catalysts on solid supports
	Preparation of fine particles and colloids
	Particle size reduction, cavitation erosion
	Surface treatment
	Agglomeration and crystallization
	Intercalation of guest molecules into host inorganic layered solids
	Dispersion, dyeing, sieving
	Heterogeneous sonochemistry

[a]From Peters (1996) with permission.

but using only mechanical agitation. The use of ultrasound to enhance rates of crystallization was reported as early as 1927. Since then there has been considerable increase in activity in the field, particularly in the area of crystallization of metals and alloys. With acoustic fields below the cavitation level, acoustic streaming is effective in increasing mass transport to the growing crystals, which can lead to an increased rate of crystal growth, provided the degree of supersaturation is low. At high degrees of supersaturation, the concentration gradient near the growing crystal is high, so that the acoustic streaming has little effect on crystal growth rate. For acoustic intensities above those required for cavitation, increases in the rates of nucleation and crystallization may be observed; this often results in crystals with a smaller particle size and narrower particle size distribution.

The crystal structure of ultrasonically produced crystals is often different than conventionally produced crystals because as they tend to show less dendritic growth, which gives rise to crystals with a more equiaxial form. This can happen if the bubble contents are adiabatically expanded during the expansion cycle of the acoustic wave, which gives rise to a localized cooling in the vicinity of the bubble and an increase in the degree of supersaturation. Following bubble collapse, the increased supersaturation leads to the formation of germ nuclei, which are dispersed throughout the medium. The crystals produced in this manner have higher purity and fragrance value. Some examples are diphenyl oxide and phenyl and methyl ether.

TABLE 5.5. Practical Examples of Gas–Liquid–Solid–Cavitation Reactions[a]

Reaction	Time	Yield (%)	Scale of operation
1. Two-step condensation of substituted phenol with nitro olefin	2–4 h	36-85	Laboratory
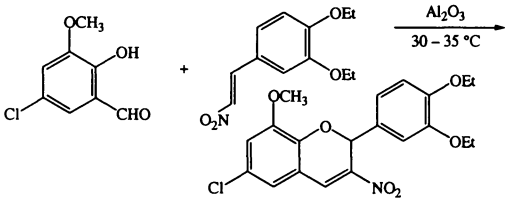			
2. Conversion of benzyl bromide to cyanide		67	Laboratory
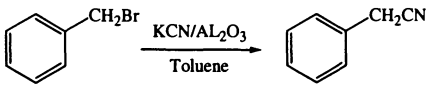			
3. Conversion of benzyl bromide to acetate	24 h	80	Laboratory
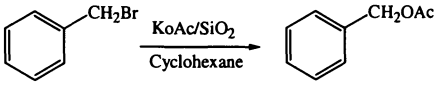			
4. Oxidation of unsaturated alcohols with MnO_2 to corresponding aldehyde	20 min	73	Laboratory
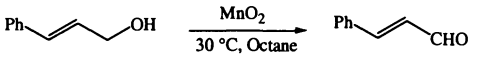			
5. Reduction of heteroatom halogen bonds	4.5 h (approx.)	98	Laboratory
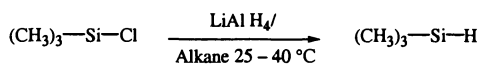			
6. Ether formation of the phenol group in a 5-hydroxy chromone	0.5-1.5 h	80-100	Laboratory
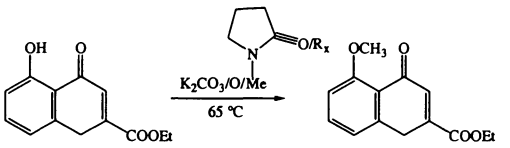			

[a]From A. B. Pandit and V. S. Moholkar, "Harness cavitation to improve processing," *Chem. Eng. Prog.* (July 1996), 57–69. Reproduced with permission of the American Institute of Chemical Engineers. Copyright © 1996 AIChE. All rights reserved.

The effects of ultrasound in zeolite synthesis have been investigated recently (Lindley, 1992). Zeolites are microporous tectosilicates with giant three-dimensional lattices built up from AlO_4 and SiO_4 tetrahedra. Zeolites are usually prepared hydrothermically by heating aqueous solutions of sodium silicate and sodium

TABLE 5.6. Examples of Catalysts Used for Environmentally Relevant Conversions[a]

Catalyst	System
Cu, Pt metals, silica gel, Cr_2O_3/Al_2O_3, Cr_2O_3 gel, MnO_2 gel, $CaCO_3$, NiO, Cr_2O_2/Al_2O_3	Decomposition of H_2O_2
Platinum metals	Oxidation of ethanol
Cr_2O_3/MoO_3	Oxidation of methanol
Mn acetate	Oxidation of acetaldehyde

[a]From Perkins (1990) with permission.

aluminate at temperatures from 25 to 300°C for several days to a few hours. In the synthesis of zeolite NaA, ultrasound leads to substantial reductions in nucleation time and overall completion times (Table 5.7) and it also produces crystals of smaller particle size (Figure 5.2). Crystallization in the presence of seeds also leads to particle size reductions in the presence of ultrasound, which seems to support a liquid phase nucleation process in which ultrasound aids the dissolution of the seeds to yield germ nuclei that are dispersed throughout the medium as a result of cavitation. Ultrasound has also been reported to be of value in the hydrothermal synthesis of A-type zeolites by enabling cheap natural minerals such as kaolin to be used as the aluminosilicate source.

The use of ultrasound during the precipitation of an $FeTe_{0.85}MoO_x$ catalyst for the oxidation of alkenes from aqueous solution has resulted in catalysts with increased specific surface area and thereby an increased catalytic activity. Similar results have been reported (Perkins, 1990) for the precipitation of a mixed chromium–molybdenum catalyst for the oxidation of methanol. However, application of the ultrasound after the precipitation was complete led to agglomeration, a reduction in surface area, and loss of activity.

TABLE 5.7. Synthesis of Zeolite NaA at 85°Ca

Ultrasonic system	Seeded (S) Unseeded (U)	Nucleation time (h)	Completion time (h)
Cleaning bath (50 kHz,150 W)	U	3	7
Control	U	4	9
Cleaning bath	S	0.75	5
Control	S	2.5	7
Probe[b]	U	1	3.5
Control	U	5	10

[a]From Lindley (1992) with permission.

[b]A Sonics and Materials, Vibracell system, 500 W.

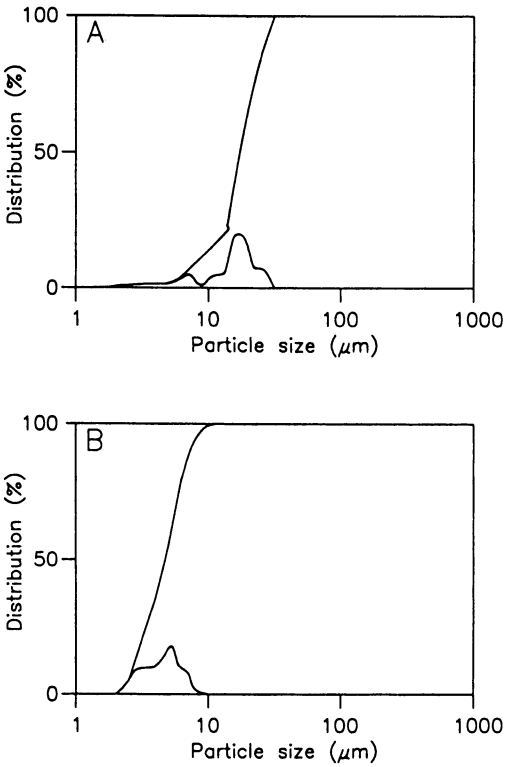

Figure 5.2. Particle size distribution of zeolite NaA. (A) mechanical stirring and (B) ultrasound. (From Lindley, 1992, with permission.)

Platinum blacks prepared by reduction of aqueous solutions of platinum metal salts with formaldehyde have been shown to give up to a three-fold increase in activity in the decomposition of hydrogen peroxide and the oxidation of ethanol compared with blacks produced with mechanical stirring at 1000 rpm (Perkins, 1990). In addition, platinum blacks produced in the presence of ultrasound have shown a 62% increase in surface area and a 98% increase in magnetic susceptibility. These differences were interpreted in terms of an increase in the amount of atomic phase present, which was shown to be more catalytically active than the crystalline metal. It is interesting that the most active platinum blacks were obtained at high frequency (3 MHz), whereas, as shown in Table 5.8, with palladium the highest activity was obtained at low frequency (20 kHz). In all cases the ultrasonic intensity was quite low.

Further sonication of crystallized platinum blacks, however, led to a 38% reduction in surface area and a 50% increase in crystal size. These results clearly indicate

TABLE 5.8. Effects of Ultrasound on the Activity of Platinum and Palladium Blacks (the activity of blacks obtained nonultrasonically is 1.0)[a]

	Pt black			Pd black		
Catalytic process	3 MHz	548 kHz	20 kHz	3 MHz	548 kHz	20 kHz
Decomposition of H_2O_2	2.6	1.75	1.35	1.0	2.0	3.2
Oxidation of ethanol	1.4	0.84	0.74	.79	1.35	2.4

[a]From Perkins (1990) with permission.

that the ultrasound is most effective during the crystallization process. This is probably due to an increase in the nucleation rate caused by the dispersion of crystallization centers throughout the medium. Similarly, sonication (25 kHz, 0.3 W cm^{-2}) during the precipitation of cobalt and nickel oxalates leads to a reduction in particle size, lower porosity, increased specific surface area, and increased bulk density. Chromium–molybdenum oxide catalysts precipitated in ultrasonic fields followed by calcination show enhanced activity in the oxidation of methanol compared with a catalyst prepared with mechanical stirring.

The literature reports (Perkins, 1990) indicate that an application of ultrasound (90 kHz) during the precipitation of silica gel can lead to 18% reductions in surface area and 30% reductions in pore volume. Surprisingly, this gel showed increased activity in the decomposition of hydrogen peroxide. Electron microscopy of the gel revealed a large increase in the number of surface cracks, which are claimed to be the active centers for this reaction. Similar effects were reported for the decomposition of hydrogen peroxide over a series of alumina-supported metal oxides (Table

TABLE 5.9. Alumina-Supported Catalysts for H_2O_2 Decomposition[a]

Catalyst	$E^{\ddagger}$ (kcal mol^{-1})	Log A	Surface area (m^2g^{-1})	Rate constant at 50°C (h^{-1} g^{-1})
Al_2O_3	—	—	220	—
Cr_2O_3/Al_2O_3				
Ultrasound	14.8	10.73	135	4.17
Normal	13.3	9.5	108	3.37
MnO_2/Al_2O_3				
Ultrasound	7.0	5.85	120	13.0
Normal	5.64	4.84	107	10.6
Co_2O_3/Al_2O_3				
Ultrasound	7.9	5.6	125	1.8
Normal	7.0	4.94	105	1.6

[a]From Perkins (1990) with permission.

5.9). These results suggest that sonication produced both an increase in number and a change in the type of active sites. Cr_2O_3 gels precipitated in the presence of ultrasonic fields showed a 30% increase in activity for the decomposition of hydrogen peroxide. This increase in activity was attributed to an increase in both the specific surface area and the surface concentration of Cr(VI) species. An application of ultrasound during the preparation of calcium chromium hydrochloride gel catalyst resulted in a 30% more active catalyst toward the decomposition of H_2O_2. Ultrasound increased the specific area of the catalyst and decreased the activation energy for peroxide decomposition. Nickel carbonate precipitated from a basic solution of nickel nitrate in the presence of ultrasound exhibited a 25% increase in activity toward peroxide decomposition and a 16% increase in surface area. Precipitation of calcium carbonate in an ultrasonic field also increased its activity by 30%.

Amorphous Metals. Platinum metal (Pt, Pd, Rh) blacks prepared by reduction of aqueous solutions of soluble salts in the presence of low-intensity ultrasound have shown up to a 62% increase in surface area and increased activity for the decomposition of hydrogen peroxide compared with those prepared without ultrasound.

Recently a novel method for the synthesis of amorphous iron has been described (Perkins, 1990). In this method, $Fe(CO)_5$ in decane is irradiated at 0°C with high-intensity ultrasound (20 kHz, 100 W cm^{-2}) for 3 h under argon. The amorphous iron produced by this method showed ten times greater activity in the catalysis of the Fischer–Tropsch conversion of carbon monoxide and hydrogen to low molecular weight hydrocarbons at the low reaction temperature of 200°C and > 30 time activity in the dehydrogenation of cyclohexane to benzene compared with 5 μm crystalline iron powder. The production of amorphous iron was critically dependent on the solvent vapor pressure, the thermal conductivity of the dissolved gas, and the ratios of specific heats of the dissolved gas.

Intercalation. Spectacular improvements in the rates of intercalation of guest molecules into layered inorganic solids have also been reported in the literature (Perkins, 1990; Lindley, 1992). The time for intercalation of *n*-hexylamine into TaS_2 has been reduced from 50 h under thermal conditions to 0.25 h under sonochemical conditions. The major sonochemical effect was a reduction in particle size of the host solid from 75 to 5 μm. The copper-exchanged montmorillonite produced in the presence of ultrasound showed reduced particle size and increased activity for the decomposition of hydrogen peroxide. More work in this area is needed.

Impregnation of Catalysts and Reagents on Supports. In recent years the use of catalysts and reagents impregnated on high surface area supports such as silica gel, kieselguhr, molecular sieves, alumina, and celite has been greatly increased.

The use of such systems has led to substantial rate and yield enhancements, and in several cases the combined use of ultrasound and supports has led to improvements in the reactivity of a number of inorganic reagents and catalysts for organic reactions.

The use of ultrasound to facilitate the impregnation of reagents on supports has been investigated since 1964. Ranganathan *et al.* (1971) reported that sonication for 1 h of aqueous suspensions of various metal oxides (Cr_2O_3, MnO_2, Co_2O_3) and alumina prior to drying and calcination yielded catalysts with higher dispersity of metal oxide and higher activity in the decomposition of hydrogen peroxide. Similarly, reduction of aqueous ammonium hexachloroplatinate solution containing a suspension of silica gel in an ultrasonic field (440 kHz, 5 W cm^{-2}) gave an 80% increase in surface area of the metal compared with those prepared in a mechanically stirred vessel.

5.3b. Effects of Ultrasound on Catalyst–Reagent Activation

The extreme turbulence within liquids caused by cavitation has considerable effect on the surfaces of solid particles suspended within the liquid. These changes may arise as a result of bombardment of the surface of solvent microjets and shock waves, or as a result of high-energy interparticle collisions driven by cavitational forces. In some cases the interparticle collisions between metal particles are of sufficient energy to cause local melting and fusion of the colliding particles. In the case of hard metallic reagents and catalysts, such as copper and nickel powders, ultrasonic pretreatment causes removal of the passivating oxide coating on the surface (Lindley, 1992). The particle size for a copper powder was reduced from 86 to 23 μm and its original rough surface became smooth after 1 h of sonication. This sonicated copper showed enhanced activity in the Ullmann coupling of activated aryl halides. Similarly, ordinary 5-μm nickel powder, which had a very low activity as a catalyst for alkene hydrogenation, became activated after sonication for 1 h in pentane. The rate of hydrogenation with the sonicated nickel is comparable to that of active forms of nickel such as Raney nickel.

Scanning electron microscopy study indicates that sonication can make a marked change in surface morphology. A prolonged sonication increases agglomeration, which can decrease the reaction rate. The most striking effect of ultrasound on the activation process was revealed by auger electron spectroscopy. The initial nickel powder was coated in a thick oxide layer that extended to a depth of 250 Å; however, after sonication for 1 h, most of the oxide layer was removed (Lindley, 1992).

Insonation of Raney nickel has been shown to increase its activity in the catalysis of hydrogen/deuterium exchange in carbohydrates and glycosphingolides. Extensive surface studies revealed that the acoustic field increases and develops catalytic sites, removes passivating impurities, and causes an elemental redistribution within the bulk catalysts. Insonation (20–500 kHz, 4–20 W cm^{-2}) of a $TiCl_3$ Ziegler–Natta

catalyst suspended in octane leads to a reduction in particle size from 15–40 μ to 0.1–5 μ. This catalyst gives rise to crystalline polymers with a more uniform molecular weight distribution than those obtained without ultrasonic treatment. Similar results are reported for other Ziegler–Natta catalysis.

The activation of nonmetallic inorganic catalysts and reagents by ultrasound is well documented. The technique ranks alongside other methods of activation, such as phase-transfer catalysis and the use of high surface area supports. In many cases the combination of ultrasound and the other techniques gives enhanced results. For example, as shown later, the combination of phase-transfer catalysis and ultrasound has been successfully exploited in liquid–solid systems. The results shown in Table 5.10 for the bromination of napthalene using $CuBr_2$ on alumina illustrate the combined effects of ultrasound and high surface area supports.

Model for the Ultrasonically Assisted Chemical Activation of Metal Surfaces. A model for the ultrasonic activation of metal surfaces is shown in Figure 5.3. This model is based on the premises that any metal surface (1) has an unreactive surface layer, (2) needs the creation of initiation sites for catalyst activation, and (3) will experience corrosion of the catalyst when the reagent is added. The rate of activation will depend on the last two items.

Unreactive Surface Layer. A reasonable assumption is that oxide layers are generally present on unreactive metals used in organic synthesis. The surface may

TABLE 5.10. Bromination of Napthalene Using $CuBr_2/Al_2O_3$ at 76°C in CCL_4[a]

Run	Reagent preparation	Ultrasound irradiation	Relative initial rate	100% conversion time[b]	% yield[c]	
					1-Br	2-Br
1	$CuBr_2$ and Al_2O_3 without prior mixing	No	0.33[d]	—	55	—
2	$CuBr_2/Al_2O_3$[e]	No	1.00	180	91	9
3	As in run 2	Yes	1.40	100	89	11
4	As in run 2	Yes[e]	1.8	100	86	14
5	Aqueous suspension of $CuBr_2$ and Al_2O_3 insonated for 1 h then as in run 2	No	1.8	60	87	13

[a]From Lindley (1992) with permission.

[b]Minutes.

[c]Yields calculated from gas-liquid chromatography data.

[d]Calculated after a 2-h induction period.

[e]In chlorobenzene

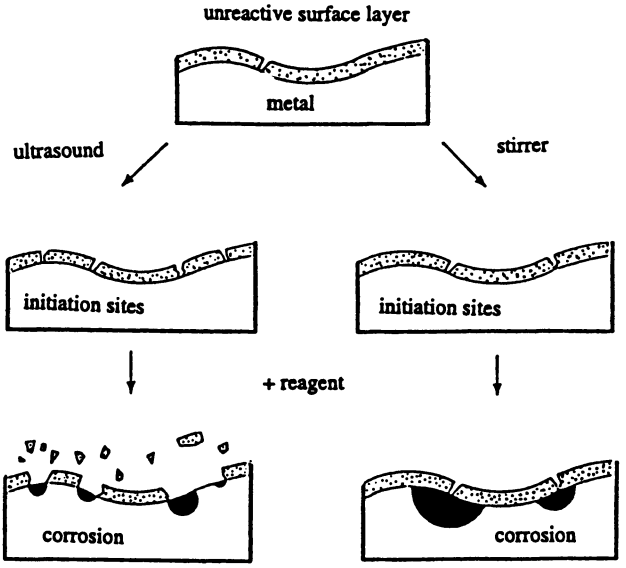

Figure 5.3. Model for the ultrasonically assisted chemical activation of metal surfaces. (From Pugin and Turner, 1990, with permission.)

already have a few initiation sites, that is, specific sites where the reaction can start. These may be cracks in the unreactive layer and dislocations on the metallic surface.

Creation of Initiation Sites. Initiation sites may be created by cavitation near the surface or by interparticle collision or friction. These processes can cause localized erosion and plastic deformation. Sonochemistry and tribochemistry both follow very similar phenomena. While instantaneous high temperatures and sonoluminescence are associated with imploding cavity bubbles, local heating of the solid and luminescence have been identified in tribochemical processes. The reaction with a small amount of iodine indicates that ultrasonic pretreatment indeed creates active sites where the iodine is quickly consumed. However, with a larger amount of iodine, the rate of reaction that leads to corrosion and activation of the metallic surface seems to be rate determining and considerably accelerated by ultrasound.

An SEM study indicates that in the first stage of the reaction, initiation is characterized by the formation of isolated corrosion pits. The initiation occurs readily at dislocations that can be produced mechanically. The number of initiation sites is not changed by chemical activation. Thus, initiation appears to occur at sites that are determined by the surface structure of the metal rather than by the nature of the initiating reagent. As the reaction proceeds, the pits grow in size until they overlap and lose their individual identity. If the rate of formation of pits is large

compared with their subsequent growth, that is, the rate of reaction of the reagent with the metal, then a large number of small pits can be observed. If however, a reaction is carried out with the same amounts of reagents and the rate of formation of pits is small compared with their subsequent growth, then a few large pits are expected.

The results of Pugin and Turner (1990) clearly show that approximately four times the number of pits were produced on manganese samples that were corroded in the presence of ultrasound generated with an ultrasonic cleaner or with a horn, than on a sample that was reacted with stirring without ultrasonic pretreatment. Also, the size of most pits generated in the ultrasonic reactions was less than 1 nm, while those from the stirred reaction were significantly larger and ranged between 2 and 4 nm. These findings can be discussed using the model shown in Figure 5.4. Numerous small pits found in the sonicated reaction suggest that the rate of formation of initiation sites is fast compared with the rate of corrosion. Since the ultrasonic reaction is much faster than the stirred reaction and generates more initiation pits, it can be concluded that low-intensity as well as high-intensity ultrasound creates initiation sites at a higher rate.

Ultrasonic pretreatment of manganese in the absence of reagent followed by reaction with stirring yields samples with about three times the number of pits than those in samples that were produced just with stirring. The size distribution of the pits lies somewhere between those observed in acoustic and in mechanically stirred reactions. These results clearly demonstrate that low- as well as high-power ultrasound can create initiation sites in the absence of a controlling agent.

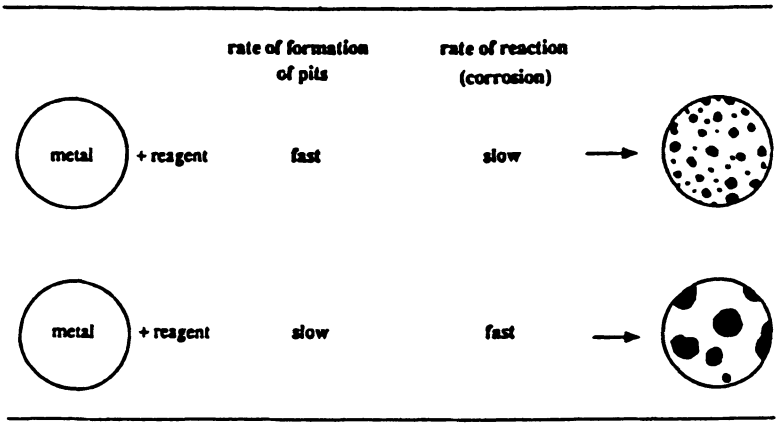

Figure 5.4. Illustration of two limiting types of pitting. (From Pugin and Turner, 1990, with permission.)

Corrosion. When a reagent is added to a metal, the reaction starts, solid reagent is consumed, that is, corrosion takes place, and the area of the activated surface grows. The initial rate of this reaction correlates to the number of initiation sites. The corrosion takes place underneath the unreactive surface layer. In a stirred reactor, this may cause severe mass transfer problems to occur because the unreacted surface layer remains intact. Ultrasound can accelerate the process of corrosion by accelerating the rate of reaction and also by breaking away particles of the unreactive surface layer that were undetermined by previous chemical corrosion. The rate of the activation of a metal surface depends not only on the number of initiation sites but also on the rate at which the reagent reacts with the metal. In this reaction, solid reagent is consumed, that is, corrosion occurs, which results in a larger area of activated surface.

5.3c. Catalyst Induction Period

There is no official definition of the term "induction period" (Figure 5.5). It has been described as "the time interval between initiation and actual reaction" or "time of acceleration of a chemical reaction from zero to a maximum rate."

Very little is known about the effects of pretreatment of metals with low-intensity ultrasound generated in ultrasonic cleaners. It was shown (Pugin and Turner, 1990)

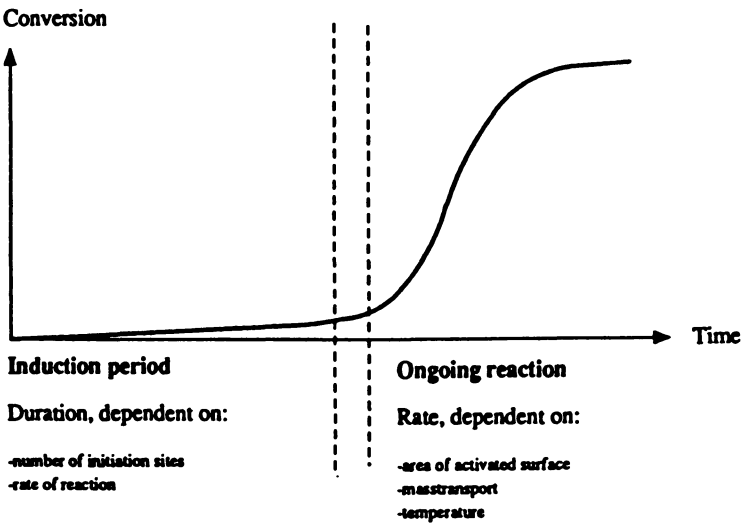

Figure 5.5. Typical course of a reaction with an elemental metal. (From Pugin and Turner, 1990, with permission.)

that the presonication of magnesium turnings in an ultrasonic cleaner did not reduce the induction period observed in the formation of a Grignard agent.

The literature indicates that the most dramatic effects on induction periods are observed with highly reactive reagent–metal combinations. Ultrasound leads to shorter and more reproducible induction periods. The mechanisms proposed are the creation of new initiation sites (through cavitation or interparticle collision) and the increase of the rate of corrosion (by microstirring and the removal of an unreactive surface layer). The results suggest that in most cases it is corrosion that is rate limiting, rather than the availability of the initiation sites. As a method of activation, ultrasound has many advantages, including (1) chemical activation or special preparation of the metal for its activation becomes unnecessary in many cases, (2) less absolute conditions may be used, and (3) side reactions can be reduced by activation at lower temperatures.

In large-scale industrial applications, exothermic reactions with long and unpredictable induction periods are difficult to control, especially when excessive amounts of reagents or high temperatures are used to initiate the reaction. The advantages of ultrasound as described above may be applicable to such-large scale reactions because significant effects are apparent even with very low ultrasonic intensities. A cyclopropanation reaction using zinc metal has been successfully performed with ultrasound on a medium scale. It is also possible that with the application of ultrasound, less hazardous continuous reactors rather than batch reactors may be developed.

5.3d. Reactions with Continuous Ultrasound

There are a large number of reports on the sonochemical enhancement of reactions involving catalysts and reagents where ultrasound has been used continuously. The continuous application of ultrasound during catalysis is claimed to give improvements in mass transport, the rate of production and renewal of active sites, and the desorption of products and poisons from the catalyst surface. It is not evident, however, that the ultrasonic conditions have been optimized, since in some cases presonication of the catalyst or reagent is just as effective as continuous sonication. In several cases, prolonged periods of sonication may lead to agglomeration and loss of active surface. Continuous ultrasound is of benefit in those situations where the reaction products form an insoluble coating on the solid catalyst or reagent and when the interphase mass transport is important. In liquid–liquid systems, continuous ultrasound is often necessary to produce emulsions, thus increasing the interfacial surface area.

There have been several reports of the sonochemical enhancement of reactions of aromatic aldehydes such as the Cannizzaro, Michael additional, Claisen–Schmidt, and Wittig–Horner reactions catalyzed by a solid barium hydroxide catalyst prepared by calcination of commercial $Ba(OH)_2 8H_2O$. In a mechanistic

study of the Wittig–Horner reaction (Perkins, 1990; Lindley, 1992), the active catalytic sites were identified by selective site poisoning of the unhindered strong base centers. Infrared studies indicate that in the thermal Wittig–Horner reaction, the aldehyde substrate is adsorbed, whereas under sonochemical conditions it is not. Small amounts of water have a dramatic effect on yields in both the thermal and sonochemical reactions; this is considered to be related to the stabilization of the crystalline lattice. By contrast, the sonochemical Cannizzaro reaction is found to occur at reducing sites on the barium hydroxide catalyst.

There are numerous reports of the use of ultrasound during hydrogenations over a variety of catalysts. For example, hydrogenation of acrylic acid over platinum black at 25°C proceeds with a three-fold increase in rate at low-power ultrasonic fields (400 kHz, 5 W cm^{-2}) compared with stirring at 1000 rpm. Up to 100-fold increase in the rate of hydrogenation of soya bean oil with copper chromite or Nysel catalysts are reported using ultrasound in a flow reactor. There are a number of ultrasonically enhanced hydrogenations using *in situ*-generated hydrogen from compounds such as formic acid (Pd/C catalyst), hydrazine (Pd/C catalyst), and water (Zn/Ni catalyst). Although the gas phase is chemically inert in these reactions, it plays a vital role in the cavitation process, which leads to activation of the catalyst and to the generation of hydrogen radicals that are believed to be important in these reactions. Substantial improvements are observed for the Pd/C-catalyzed hydrosilation of alkenes in the presence of low-intensity ultrasound, which enables the reactions to occur at 30°C; this is the lowest temperature ever reported for such Pd/C-catalyzed hydrosilations.

The effects of ultrasound on reactive surface area and corrosion patterns were discussed earlier. The literature shows that in reactions with manganese or lithium, the use of ultrasound may lead to different corrosion patterns. This may result in a different surface area of the metal. Temperature changes induced on solids in an ultrasonic field have been investigated, and experimental results and theoretical considerations show that they do not exceed a few degrees Celsius. Kinetically controlled reactions would thus be unaffected by ultrasound unless the latter affects the surface area or character of the catalyst. Improved mass transport seems to be the most probable explanation for the ultrasonic acceleration by a factor of 2 to 4 of the reaction of cyclopentyl bromide with magnesium. With more viscous solvents, where mass transport problems become more pronounced, even larger ultrasonic effects would be expected.

5.3e. Effects of Ultrasound on Catalyst Regeneration

The ability of ultrasound to clean surfaces has been exploited in the area of catalyst regeneration. Thus a brass catalyst used in the production of acetone from isopropanol is regenerated to 83% of its original activity by insonation (18–22 kHz, 6–20 W cm^{-2}) in a bath containing a solution of sulfuric acid, nitric acid, and sodium

dichromate. Nonultrasonic treatment leads to only 63% regeneration. Insonation is reported to completely restore the surface area, porosity, and activity of a palladium alumina catalyst used for the removal of nitrogen oxides from waste gases. A nickel–molybdenum hydrocarbon cracking catalyst is regenerated by oxidation in air followed by insonation in low-viscosity oil. Similarly, a TiO_2-V_2O_5 catalyst for denitrification of flue gases is reactivated by insonation in water.

5.4. CASE STUDIES

5.4a. Cavitation Effect on Heterogeneous Catalytic Oxidation

Cyclohexane Oxidation in the Presence of Catalysts that Had Undergone Preliminary Ultrasonic Treatment. When chromium, lead, and copper oxides, plus a mixed cobalt oxide, were preliminarily subjected to ultrasonic radiation (in cyclohexane) for periods of 5, 10, 15, and 20 min, a substantial increase in the subsequent oxidation reaction rate was recorded. However, the existence of ultrasound during the reaction decreased the rate of oxidation by a factor of 1.5–2.1, depending on the catalyst. This decrease in the reaction rate when using these pretreated catalysts may be explained by the fact that when chromium, lead, and copper oxides, plus the mixed cobalt oxide, are under continuous influence of the ultrasonic field during the reaction, an activated catalyst intensifies the mass-exchange processes of the reactants, labile particles, and products of the reactions that occur on the catalyst surface, in a manner such that the net effect is to reduce the rate of the oxidation reaction. Similar results were also obtained for the reaction $S + Na_2SO_3 \rightarrow Na_2S_2O_3$.

Figure 5.6 shows the dependence of the cyclohexane oxidation rate on the period of ultrasonic irradiation of a Co_3O_4 catalyst measured at 413 K. For this catalyst, the reaction rate reaches a maximum value after an initial sonication time of 5 min; with prolonged treatment for periods of 10, 15, and 20 min, the rate decreases slightly to finally reach a constant value. While similar results were obtained for the oxides of chromium, lead, and copper, the oxidation rates in these cases did not show maxima with respect to the preliminary treatment time.

Measurement of the specific surface areas of the catalysts, after initial sonication treatment, showed that with an increase in irradiation time, their specific surface areas decreased by 4–7%, depending on the nature of the oxide used. The decrease in specific surface area with increasing exposure to ultrasound appears to be connected to the relative change in the number of micro- and macropores on the surface of the catalyst particles. Despite the fact that an increase in initial sonication time results in a greater number of active centers on the catalytic surface, the reduction in specific surface areas is caused by the coagulation of the catalyst particles. The insensitivity of the cyclohexane oxidation may be due to "trapping"

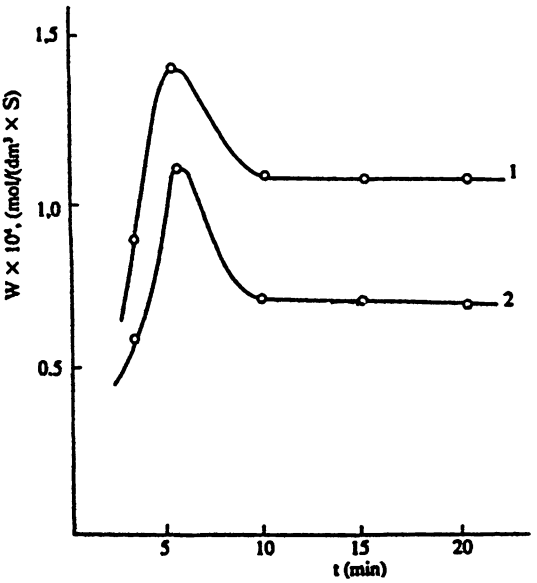

Figure 5.6. The dependence of the rate of the catalytic oxidation of cyclohexane on the period of preliminary ultrasound treatment of the mixed-oxide catalyst Co_3O_4, showing the effect of the gaseous atmosphere that was used: 1, treatment in an oxygen atmosphere; 2, treatment in an argon atmosphere. $T = 413$ K, $P = 10^6$ Pa. (From Mokry and Starchevsky, 1993, with permission.)

of the substrate within the deeper micropores of the catalyst, which leads to a partial high-temperature carbonization reaction of the organic species during the reaction.

The nature of the gaseous atmosphere has a great influence on the resultant activity of a catalyst that has been previously exposed to ultrasound. In particular, after pretreatment in an oxygen atmosphere of the mixed cobalt oxide, Co_3O_4, in cyclohexane, the rate of the subsequent catalytic oxidation process was 1.2–1.4 times greater than that determined for the system in which the catalyst had been treated in the presence of argon (Figure 5.6). This increase in catalytic activity of the oxide may be partially explained by an initial saturation of the surface layers that are in contact with the oxygen. Another important parameter in this pretreatment process is the reaction temperature. Figure 5.7 shows the relationship between the rate of cyclohexane oxidation and the pretreatment time of the Co_3O_4 catalyst at temperatures of 413 and 303 K. This reduction in temperature led to a decrease in the reaction rate by a factor of 1.7–1.9.

Role of Ultrasound During Heterogeneous Chemical Oxidation. One of the reasons for the limited application of heterogeneous catalysts in liquid-phase oxidations of organic compounds is their low activity compared with homogeneous

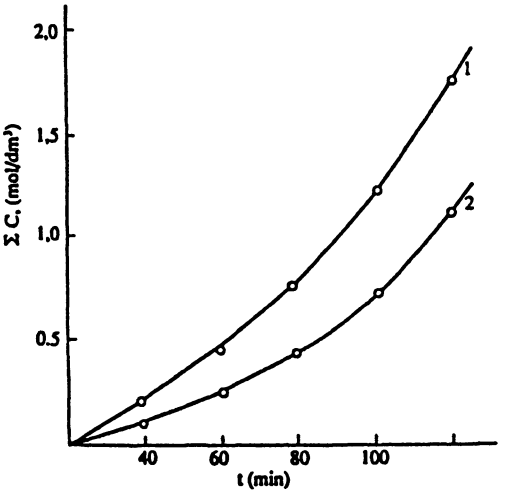

Figure 5.7. The dependence of the concentration of products of the catalytic oxidation of cyclohexane on the period of preliminary ultrasound treatment of the mixed-oxide catalyst, Co_3O_4, showing the effect of the pretreatment temperature: 1, sonication at 413 K; 2, sonication at 303 K. (From Mokry and Starchevsky, 1993, with permission.)

catalysts. Thus, for example, the maximum rate of cyclohexane oxidation at 413 K in the presence of a catalyst such as Co_3O_4, is 3×10^{-5} mol/(dm^3·s), which is only 1.5–2 times greater than the auto-oxidation rate, while in the presence of $CoNf_2$ the rate is 1.4×10^{-4} mol/(dm^3·s). The activity of the catalysts decreases according to the following sequence: Co_3O_4>Cr_2O_3>PbO_2>CuO.

As shown in Figure 5.8, for a Co_3O_4 catalyst in the presence of an ultrasonic field, the cyclohexane oxidation rate increased by some 8–11 times. Similar results were obtained for other catalysts. A comparison of the oxidation rate for a Co_3O_4 catalyst in the presence of an ultrasonic field versus the performance of the same catalyst that had been preliminarily subjected to ultrasound is given in Figure 5.9. These results indicate superior performance of the catalyst in the presence of an ultrasonic field. Similar results were obtained for other catalysts. The results indicate that in addition to an increase in the reaction rate, the composition of the reaction mixture in all cases also changes: in the presence of Co_3O_4 and PbO_2 the quantity of cyclohexanol in the oxidate mixture increases, while the use of Cr_2O_3 leads to an increase in the amount of cyclohexane, and for an acoustic-chemical reaction catalyzed by CuO, increased amounts of acid products are obtained. The hydroperoxide concentration in all of these cases is reduced by a factor of 1.5–2.0. The same sequence of activity for the various catalysts, as described above, is maintained when ultrasound is applied to the system.

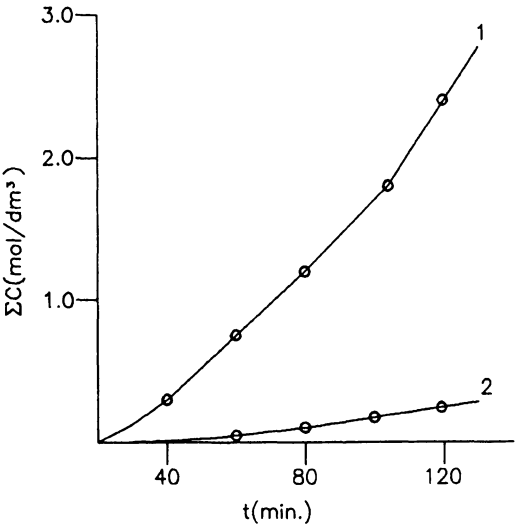

Figure 5.8. Increase in the concentration of reaction products from the oxidation of cyclohexane, as a function of time, when carried out in the presence of Co_3O_4 catalyst for both sonicated (curve 1) and nonsonicated (curve 2) samples. All measurements were carried out at 413 K at a pressure of 10^6 Pa, using catalyst concentrations of 0.027 mol/dm^3. (From Mokry and Starchevsky, 1993, with permission.)

The surface area of these catalysts decreased between 4 and 7% with ultrasonic irradiation. However, the catalysts that were used retained their high catalytic activity for successive experiments *in the absence of an ultrasonic field.* The most active, i.e., Co_3O_4, preserved its activity even after 6 months of prolonged storage

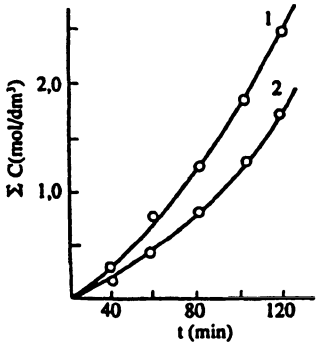

Figure 5.9. Increase in the concentration of reaction products from the oxidation of cyclohexane, as a function of time, carried out using a Co_3O_4 catalyst. Experiments were carried out in the presence of an ultrasonic field (curve 1), and using oxides that had been preliminarily subjected to ultrasound (curve 2). All measurements were carried out at 413 K at a pressure of 10^6 Pa, using catalyst concentrations of 0.027 mol/dm^3. (From Mokry and Starchevsky, 1993, with permission.)

remote from the reaction area. Consequently, as a result of the effect of ultrasound, significant changes appear to take place in the bulk structure of the catalysts.

Hydroperoxide decomposition is one of the most important stages of the overall cyclohexane oxidation process. The overall hydroperoxide decomposition constant, k_p, for a sonicated system is approximately 1.5–2.0 times greater than that found in a nonsonicated system: i.e., the resulting hydroperoxide concentration in the oxidate mixture obtained after heterogeneous catalytic oxidation with the application of ultrasound is 1.5–2.5 times lower than that found in the corresponding nonsonicated system. Values of the various kinetic constants of the heterogeneous catalytic decomposition process of cyclohexyl hydroperoxide obtained under various experimental conditions are given in Table 5.11.

In summary, therefore, the beneficial influence of ultrasonic cavitation on liquid-phase, heterogeneous-catalytic, cyclohexane oxidation processes is closely connected with the formation of additional centers of activity on the catalyst surface; these participate in the initiation and the degenerated chain-branching stages of the oxidation reaction.

5.4b. Cavitation Effect on Liquid–Solid Phase-Transfer Reactions

Sonications can have some direct effect on the phase-transfer catalyst. In the case of liquid-solid phase-transfer reactions, ultrasound can help the rate by preventing

TABLE 5.11. Values of Kinetic Constants of the Heterogeneous Catalytic Decomposition Process of Cyclohexyl Hydroperoxide, Obtained under Various Experimental Conditions[a]

T(K)	k(s^{-1})	K(dm^3/mol)	$k_p(=k\,K)^b$	Experimental conditions(dm^3/mol s)
348	0.32	53.1	17.0	No ultrasonic field
333	0.26	60.1	15.6	
348	0.51	56.4	28.8	Ultrasonic field, 22 kHz
333	0.43	62.1	26.7	
348	0.48	61.2	29.4	Catalyst subjected to ultrasonic field (freq. 22 kHz) for 5 min
333	0.37	66.7	24.7	
348	0.49	54.8	26.9	Ultrasound field of 44 kHz
333	0.41	63.2	25.9	
348	0.47	61.8	29.04	Catalyst subjected to ultrasonic field (freq. 44 kHz) for 5 min
333	0.34	67.1	22.8	

[a]From Lindley (1992) with permission.

[b]k_p includes the concentration of the catalyst.

solid agglomeration or by increasing surface area by disintegration of solids. Rate enhancements have been reported in several solid–liquid heterogeneous substitutions involving the use of PTC. In several instances the use of ultrasound has enabled less expensive PTC reagents to be used. For example, the efficiency of N-alkylation of amines with alkyl halides in toluene in the presence of solid KOH using the inexpensive and nontoxic PEG methyl ether as PTC is markedly increased with ultrasound. With benzyl and phenyl groups of amines and halides, the yield is 98% in 1 h at 25–50°C under sonication, compared with only 70% after 48 h in the absence of sonication. In the absence of PTC, however, there was no reaction under sonication. This result emphasizes that the increase in reactivity is not simply a matter of increasing interfacial contact area. In the case of auto-oxidation of 4-nitrotoluene in the presence of O_2 using KOH and PEG 400 as PTC, sonication not only reduces reaction time but also affects the selectivity of such reactions.

Ratoarinoro *et al.* (1995) examined the effects of ultrasound emitter type and power in a Michael reaction: the addition of ethyl malonate to chalcone in toluene under solid–liquid phase-transfer conditions. The reaction was catalyzed by solid potassium hydroxide (KOH) in association with trimethylbenzyl ammonium chloride (TMBA) as a phase-transfer catalyst with toluene as a solvent; only KOH and TMBA were in the solid suspended phase. All the experiments by Ratoarinoro *et al.* (1995) were performed at 20 KHz ultrasound frequency and ambient conditions. The particle size of KOH decreased rapidly, whatever the initial particle size, and then decreased more slowly for longer sonication times. After 15 min the mean particle size was 15–20 μm, independent of an initial size up to 240 μm. Sonication thus clearly increased the solid surface area of the catalyst. This resulted in a dramatic increase in the reaction rate: an equilibrium yield was obtained in 2 min, while it required 1 h with mechanical stirring. A minimum power input corresponding to the cavitation threshold was required. However, since the reaction was over in 2 min, there was probably only little advantage in increasing the power beyond this minimum value. At a smaller power per unit volume of reactor, the cleansing bath was least effective; both cup and horn and horn systems for the acoustic input were equally effective. Since the mechanism of the reaction exclusively involves ionic species, it is likely that the observed effects resulted from the physical phenomena.

Contamine *et al.* (personal communication) showed that when the Michael addition reaction was carried out with a TMBA phase-transfer catalyst, ultrasound improved the reaction rate by a factor of 15 compared with a classical mechanical stirrer, but the same magnitude of improvement was achieved by an Ultraturrax (very fast mechanical stirrer). On the other hand, as shown in Figure 5.10, in the absence of any phase-transfer agent, ultrasound significantly enhanced the reaction rate at all operating conditions, whereas an Ultraturrax at the same power was much less efficient, and there was almost no reaction with conventional mechanical stirring.

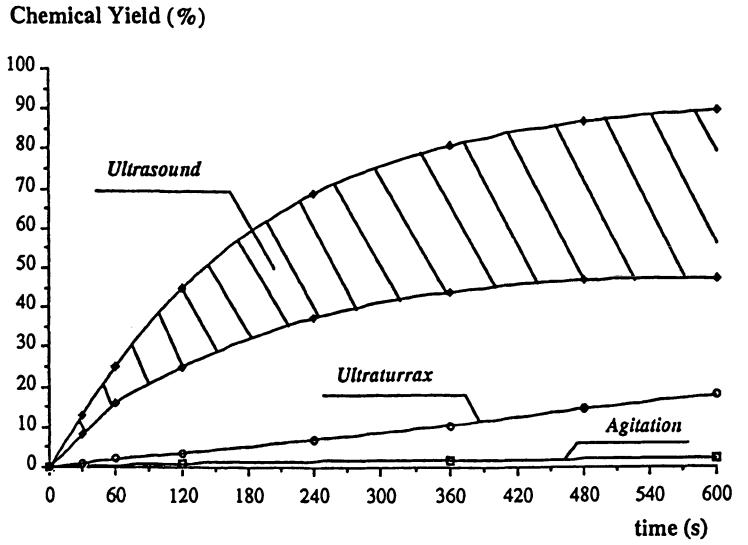

Figure 5.10. Michael addition (system 2): chemical yield versus time, without phase-transfer catalyst, under different stirring conditions: mechanical stirring (26 rd/s), ultraturrax (1570 rd/s), and ultrasound (power inputs: 2–200 W). (From Contamina *et al.*, personal communication.)

Hagenson *et al.* (1994) evaluated the role of ultrasound on the synthesis of benzyl sulfide from benzyl chloride and sodium sulfide in a suitable organic solvent. They showed that ultrasound was very effective in enhancing the reaction rate in a variety of operating conditions. All ultrasound experiments were carried out at 20 kHz and an intensity of 150 W/cm^2. Sekhar (personal communication) examined the solid–liquid reaction between sulfur and sodium sulfite, forming thiosulfate. Shankar (1988) and Starks and Liotta (1978) demonstrated that the rate of this reaction can be significantly enhanced with the use of a phase-transfer catalyst. Sekhar (personal communication) showed that the predispersion of the solid sulfur and sonication of the reaction mixture enhanced the rate of reaction significantly compared with that in the presence of stirring alone. The results were obtained at various catalyst and reactant concentrations. A typical effect of sonication on the rate for PTC reaction is shown in Figure 5.11.

The above examples indicate that ultrasound can aid in many liquid–solid phase-transfer reactions for the transformation of a variety of organic compounds. More work in this area needs to be carried out.

5.4c. Cavitation Effect on Gas–Liquid–Solid Biological Reactions

Biological organisms are often the only sources for certain industrially important products that are used as biological catalysts, pharmaceutical drugs and adjuvants,

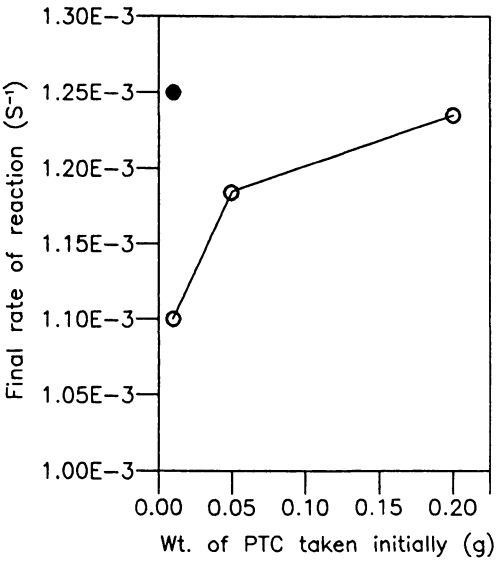

Figure 5.11. Effect of PTC loading on the final rate of reaction. ■ with sonication. (From Sekhar, personal communication.)

food sources and additives, and diagnostic reagents. Bioprocessing involves the conversion of a raw material substrate into a product using microbial fermentation of enzymes. It is also concerned with the recovery of by-products, their separation from the fermentation broth, and their purification. The use of biological systems for effecting organic transformations has attracted a great deal of interest over the past few years. Many organic pollutants from water can be treated by an enzyme catalyst. A number of organic transformations such as those listed in Table 5.12 indicate that ultrasound enhances the rate of many enzyme-catalyzed reactions.

TABLE 5.12. Examples of Enzyme-Catalyzed Organic Transformation Improvement by Acoustic Cavitation[a]

Increased activity by 200% at 5 kW/m^2 acoustic intensity for α-amylase and glucoamylase on porous polystyrene and α-chymotrypsin on agarose; probably caused by improved mass transfer processes.
Improved breakdown of yeast cell wall as in the production of the methyl ester of ganoderic acid via cyclization of squalene; maximum conversion efficiency at 0°C, 2 h; acoustic treatment at 40 W/cm^2 intensity.
Increased conversion of 2,3-oxidosqualene lanosterol by more than twofold using baker's yeast (*Saccharomyces cerevisiae*) as a source of sterol cyclase.

[a]Data taken from Mason (1991) and Mason and Lorimer (1988).

Cell disruption is a necessary step for the release of intracellular products that are not secreted by the cells. When the intracellular components to be released are of a delicate nature, the disruption procedure must be capable of fine control to maintain a balance between efficient disruption and product integrity and activity (Hetherington *et al.*, 1991). Cell disruption is generally carried out immediately after the fermentation step and hence controls all further downstream processing. It is the unit operation in which the maximum product loss occurs both by virtue of a low percentage recovery and by deactivation. While the most commonly used equipment is the high-pressure homogenizer (HPH) and the bead mill, in general, the equipment used should be selected mainly on the basis of the type of cells to be lysed and the specifications of the final product.

A key factor in economic production of industrially important microbial components is an efficient large-scale cell disruption process. As mentioned earlier, for the large-scale disruption of micro-organisms, mechanical disintegrators such as high-speed agitator bead mills (Limon-Lason *et al.* 1979), high-pressure industrial homogenizers (Edebo, 1960), or high-intensity ultrasonic generators (Hughes *et al.*, 1971) are often employed, although with these equipment, disruption is a high-cost, energy-intensive unit operation. The typical energy efficiencies of the current methods are in the range 5–10%; 90–95% of the dissipated energy is lost in the form of the heat. An energy-efficient cell disruption can be carried out by hydrodynamic as well as acoustic cavitations. Save *et al.* (1994,1997) showed that proteins released during acoustic and hydrodynamic cavitations are similar. Furthermore, during hydrodynamic cavitation more protein is released with a larger discharge pressure. A typical comparison of probe and bath acoustic systems for an enzymatic reaction is given by Mason (1990b).

Saksera and Nyborg (1970), Sakai *et. al.* (1977), and Sarkari *et al.* (personal communication) also compared the performance of hydrodynamic cavitation with that of ultrasonication to achieve an efficient cell disruption. They examined the effects of both hydrodynamic and acoustic cavitations on cell lysis using baker's yeast as microbial biomass. Baker's yeast is commercially produced from a strain of *Saccharomyces cerevisiae*. The experimental measurements were carried out for various concentrations of yeast and various conditions for hydrodynamic and acoustic cavitations.

The results of these studies indicate that there is an optimum discharge pressure for each setup that uses pressure as means of disrupting cells. This optimum discharge pressure is very high in the case of the high-pressure homogenizer. Thus even though 100% lysis can be obtained in a high-pressure homogenizer for a concentration of 0.1% of yeast suspension compared with a hydrodynamic cavitation setup, the pressure required is very high. Also, in the case of hydrodynamic cavitation, an operation at high pressures decreases the extent of lysis. Thus, in order to get maximum lysis, one should operate the equipment at its optimum pressure. An increase in the time of exposure to lysis increases the release of protein

in all cases except that of the high-pressure homogenizer, in which material subjected to too many passes does not increase the amount of protein released, but only produces more fines.

In the case of acoustic cavitation, a study by Sarkari *et. al.* (1999) found that the nature of the equipment chosen has a major impact on the extent of cell disruption. Thus, in order to get a maximum protein release, one should use the ultrasound bath directly. Since proteins are affected by high temperatures, it is important to control the bulk temperature during cavitation. This can be done in hydrodynamic cavitation by injecting cooling water in the cavitation chamber. In the case of an ultrasonic bath, the direct introduction of ice is not possible and hence the experiment must be frequently stopped to prevent overheating of the suspension.

In order to obtain maximum lysis, it is necessary to work with an optimum concentration of yeast suspension; in the case of all cell disruption units this can be considered to be 1%. Cavitational activity was definitely involved in the lysis of yeast cells. In terms of protein released per unit power consumed, it can be concluded that a hydrodynamic cavitation setup is more efficient than a high-pressure homogenizer. The study by Sarkari *et al.* (1999) concluded that hydrodynamic cavitation can be used on a large scale for the disruption of yeast cells at an optimum concentration of 1%, with efficient temperature control in order to preserve the activity of the desired protein and recover products of commercial interest from a very valuable source yeast.

5.4d. Cavitation Effect on Photo-oxidation Reactions

Complete mineralization of organics upon UV irradiation of aqueous organics in the presence of TiO_2 has been reported for aliphates and aromatics such as polychlorinated biphenyls and dioxins. Photodegradation (with or without TiO_2) may provide a safe and efficient means to destroy a variety of organic pollutants in groundwater and process water. Power ultrasound can aid this efficient process.

Johnston and Hocking (1993) reported ultrasonically accelerated photocatalytic conversions of pentrachlorophenol, 3-chlorobiphenyl, 2,4-dichlorophenol, and 4-chlorophenol. Some typical results illustrating the rate enhancements by high-intensity (>10 W cm^2) 20 kHz frequency ultrasound at 35°C bulk temperature for 2,4-dichlorophenol and 3-chlorobiphenyl are given in Figures 5.12 and 5.13, respectively. The authors postulated the following reasons for the reaction rate enhancement:

- Cavitation causes a localized increase in temperature and pressure.
- Microstreaming cleans or sweeps the TiO_2 surface, allowing more active sites.
- There is an increase in mass transport of reactants and products.
- There is an increase in surface area due to fragmentation or pitting of the TiO_2 powder.

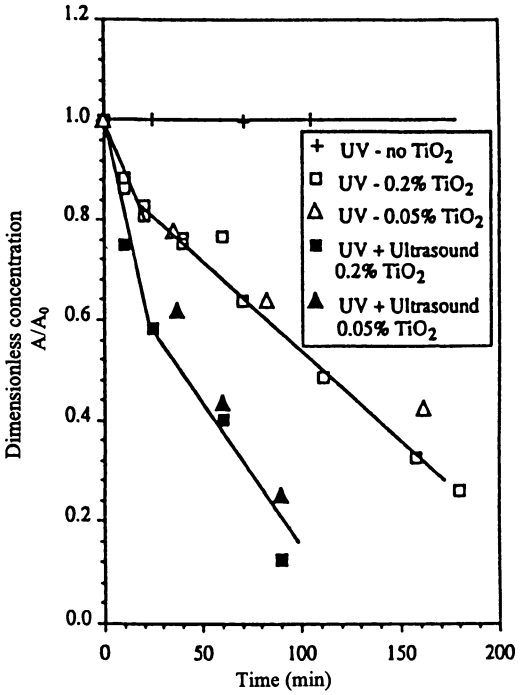

Figure 5.12. 2,4-Dichlorophenyl degradation with lower catalyst concentration, as measured by UV spectral analysis (510 nm). (From A. J. Johnson and P. Hocking, "Ultrasonically accelerated photocatalytic waste treatment," in *Emerging Technologies in Hazardous Waste Management III*, pp. 106–118, D. W. Tedder and F. Pohland, eds., Copyright © 1993, American Chemical Society. Reproduced with permission.)

- Bulk cavitation induced reactions between radical intermediates and organic compounds.
- There are direct reactions between organic substances and photogenerated surface holes and electrons.

While these reasons apply in general to all similar ultrasonically assisted TiO_2-catalyzed photodegradation reactions, a further analysis of the data led the authors to conclude that the process of homogeneous cavitational collapse does not contribute significantly to the enhanced degradation rates. Cavitation improves mixing, but on a macroscopic level it is only as effective as a high-speed stirrer. On a microscopic level, mass transport is improved because of microstreaming. If surface adsorption of the substrate is an important first step in reactions with hydroxyl radicals (adsorbed or free), then ultrasonic irradiation may aid this process and reaction as a result of cavitational collapse in proximity to the semiconductor

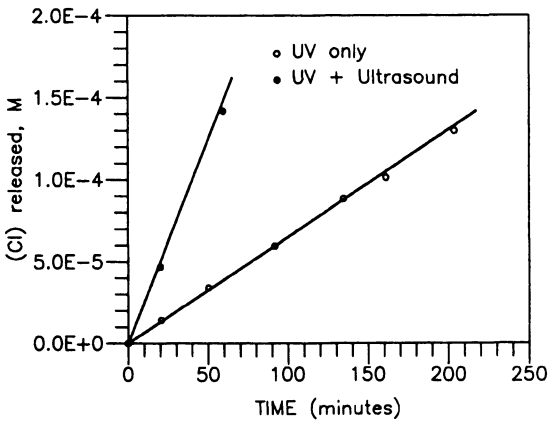

Figure 5.13. Degradation of 3-chlorobiphenyl as measured by choloride release. (From A. J. Johnson and P. Hocking, "Ultrasonically accelerated photocatalytic waste treatment," in *Emerging Technologies in Hazardous Waste Management III*, pp. 106–118, D. W. Tedder and F. Pohland, eds., Copyright © 1993, American Chemical Society. Reproduced with permission.)

particle. This would generate local high temperatures and pressures for the enhancement of reactions between the radical and substrate. Also, impingement of a jet solution at the particle may result in cleaning of the catalyst surface, allowing more effective adsorption and radical production as well as improved transport rates for reactants and products. The origin of the ultrasonically assisted rate enhancement appears to be mainly acoustic and/or cavitational effects at the semiconductor/solution interface during UV irradiation.

The results of this study indicate that more work on combined ultrasound and photo-oxidation-driven removal of organic pollutants from water should be pursued in the future.

5.4e. Cavitation-Induced Microfusion

Benson (1995) describes an interesting study carried out by Roger Stringham and Russ George of E-Quest Sciences, Inc. of Palo Alto, California, in which an ultrasonic cavitation "microfusion" device was created to melt palladium foil by delivering only 100 W of power in ultrasonic waves impinging on the foil under heavy water (D_2O). The ultrasonic waves create cavitation bubbles that drive a new type of nuclear reaction inside the metal. This vaporizes the foil material and appears to release energy that many observers believe to be obtained from nuclear reactions under the cold conditions. Moreover, underwater melting occurs within minutes of startup. It can be reproduced essentially every time with 100% reproducibility.

In this process, palladium, titanium, or another metal target is immersed in heavy water and the target is bombarded with high-intensity sound waves (generally with a frequency of 20 kHz). These generate cavitation bubbles that collapse close to or on the palladium surface. Instead of collapsing and disappearing from the fluid, the bubbles actually collapse into the metal surface. Photomicrographs show that the bubbles form a funnel-shaped jet, which injects the contents of the bubble into the metal lattice. The advantage of the ultrasonic technique is that it is highly effective in rapidly packing deutrons into the lattice of metal atoms. A schematic of the E-Quest microfusion reactor is shown in Figure 5.14. A schematic of cavitation bubble formation and collapse in an acoustic system is given in Figure 5.15. Three features of bubble behavior are shown in the top part of this figure.

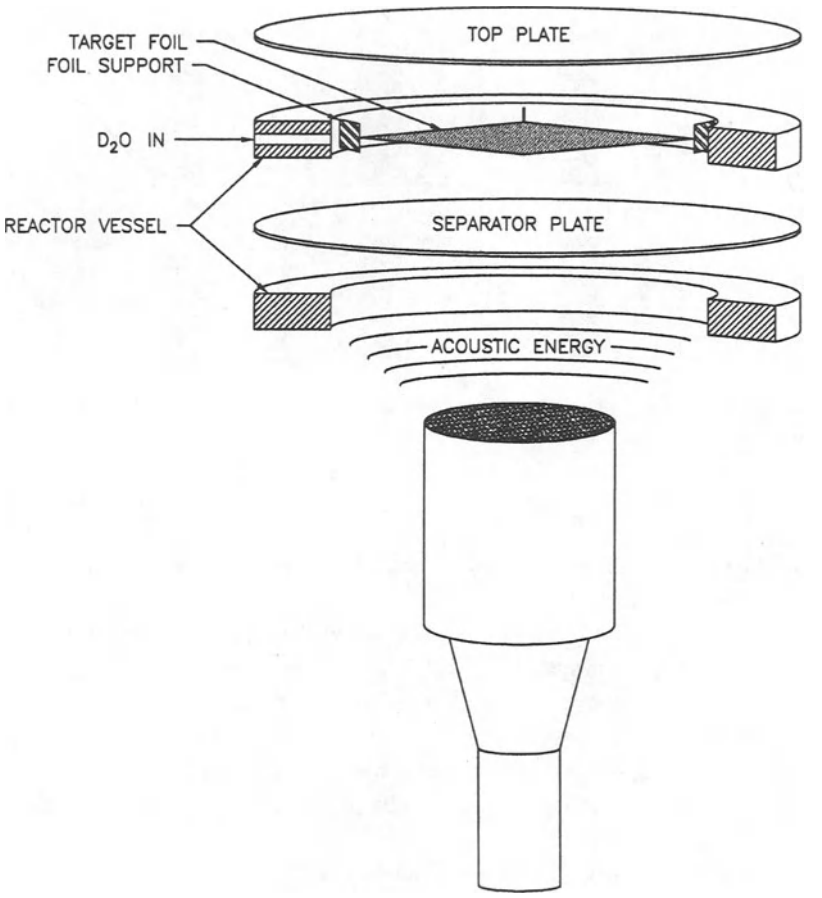

Figure 5.14. Schematic of E-Quest microfusion reactor. (From Benson, 1995, with permission.)

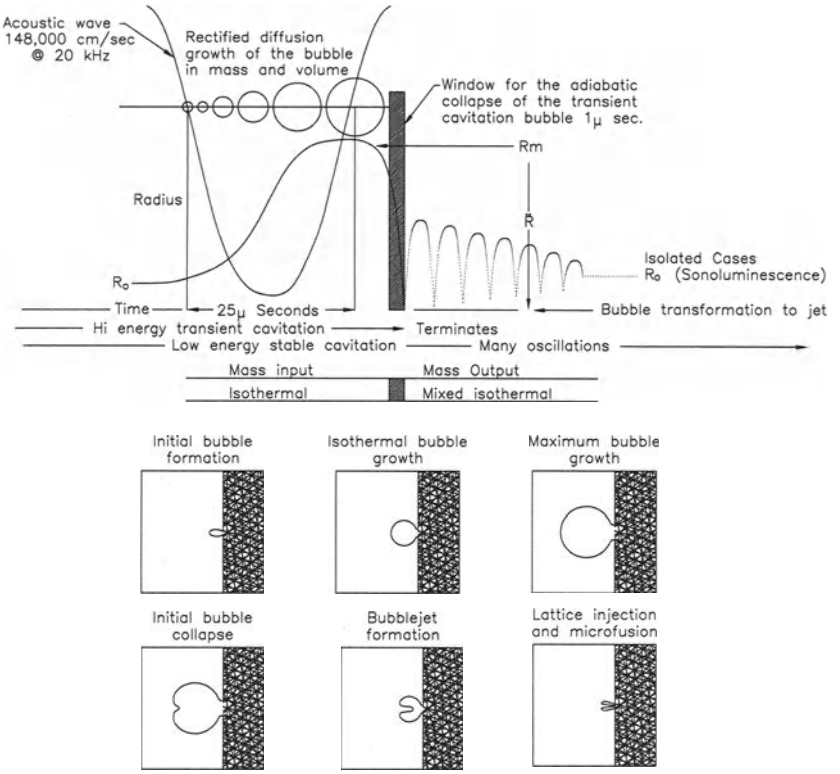

Figure 5.15. Schematic of cavitation bubble formation and collapse. (From Benson, 1995, with permission.)

1. The rate of change of bubble shell radius during one acoustic cycle is shown by the dotted line.
2. The two different types of cavitation are shown in the top part of the figure: A stable cavitation system, which sometimes manifests itself as sonoluminescence, is a many-cycle event. A transient cavitation system, which forms the bubble jet, is a one-cycle event.
3. The isothermal growth of the bubble by mass and radius (rectified diffusion) and its adiabatic collapse are shown by the increasing volume.

The bottom part of Figure 5.15 shows a schematic of the bubble formation, growth, and collapse during microfusion. A detailed economic assessment for the large-scale application of this process is under investigation.

6

CAVITATION REACTORS

6.1. INTRODUCTION

In this chapter we describe various types of reactors for hydrodynamic, acoustic, and optical cavitation reaction processes. Laboratory as well as commercial reactors are examined. The purpose of these reactors can be one of the following:

- to evaluate the feasibility of the cavitation process for a given chemical transformation
- to examine either the intrinsic kinetics of the chemical conversion or the effect of various scaleup variables on the reactor performance
- to evaluate the commercial viability of the cavitation conversion process

The hydrodynamic cavitation reactor is perhaps simplest to design and operate. It is often used to demonstrate the feasibility of the cavitation conversion process under either laboratory or large-scale conditions. The optimization of the reactor can be carried out in a relatively straightforward manner. The reactor is, however, not particularly useful for examining the intrinsic kinetics of the cavitation conversion process. Since hydrodynamic cavitation generates lower cavitation intensity, the reactor is generally part of a hybrid process (see Chapter 9) involving a hydrodynamic cavitation reactor and another advanced oxidation reactor.

The acoustic cavitation reactor is very complex to design and scale up. It can be used to demonstrate the viability of a process at both the laboratory and commercial scale. With a very careful design, it can also be used to study the fundamental kinetic behavior of the acoustic cavitation conversion process. Numerous designs are available to handle a variety of reaction conditions for such a study. The reactor is, in general, very difficult to model and scale up. The availability of high intensity in the acoustic cavitation conversion process would allow this type of reactor to be operated as a standalone or with other advanced oxidation processes.

The optical cavitation reactor is generally useful for a detailed and fundamental study of cavitation bubble dynamics or the kinetics of the cavitation conversion process. Since in this type of reactor single or multiple bubbles can be generated under a controlled environment, the reactor is a useful tool for fundamental studies. The reactor can also be used to evaluate the feasibility of a particular cavitation conversion process at a laboratory scale. It is, however, not very useful for a large-scale, commercial operation. In the following sections, we briefly examine various types of hydrodynamic, acoustic, and optical cavitation reactors.

6.2. Hydrodynamic Cavitation Reactors

In a flowing system, the liquid velocity varies locally and cavities can occur at the points of highest velocity and low pressure. In a hydrodynamic cavitation reactor, which mainly consists of a pump and an orifice downstream of its discharge, the cavities are generated by the reduction of pressure near the orifice. This phenomenon can be explained as follows:

If the liquid is flowing through an orifice, the reduction in the cross-section of the flowing stream increases the velocity head at the expense of the pressure head. During the reexpansion of the flow, the fluid stream gets separated at the lower end of the orifice and eddies are generated. The creation and motion of the eddies cause a permanent pressure loss, and full pressure recovery does not take place. The static pressure at the vena contracta is lower than the bulk pressure downstream of the flow. However, as velocity is increased, the pressure at the vena contracta decreases further. At a particular velocity, the pressure may actually fall below the vapor pressure in the liquid, causing the generation of the cavities.

A reactor using the above-described principle is shown in Figure 6.1. Here the cavitation number (see Chapter 1) can be altered by opening the valve partially or fully. Also, a bypass is provided to control the flow rate. The principal parameters that affect the fluid pumping cost are irreversible loss in pressure head and turbulence and friction loss. Because of its simple construction and operation, the design and maintenance of a hydrodynamic cavitation reactor is relatively easy. Also, since all the parameters affecting the performance of the reactors can be appropriately quantified, the opportunities for an immediate scaleup are high.

Cavitating conditions and hence the outcome of cavitation can be easily manipulated in this type of reactor. The knowledge of the effects of the geometrical and physical parameters such as discharge pressure, orifice-to-pipe diameter ratio, and the size of the pipe downstream of the orifice on bubble behavior have been well quantified. This allows manipulation of the pressure and temperature pulses to create a specific reaction or a physical effect. The reactor system shown in Figure 6.1 can be operated at both high flow rates and high pressure. A schematic diagram of the cavitation nozzle is shown in Figure 6.2.

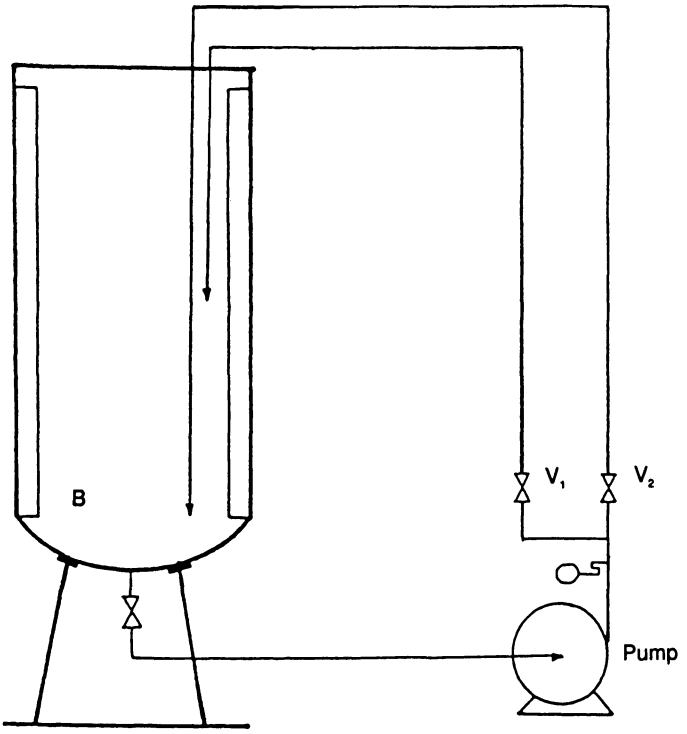

Figure 6.1. Setup for hydrodynamic cavitation. (From A. B. Pandit and V. S. Moholkar, "Harness cavitation to improve processing," *Chem. Eng. Prog.* (July 1996), 57–67. Reproduced with permission of the American Institute of Chemical Engineers. Copyright © 1996 AIChE. All rights reserved.)

One advantage of a hydrodynamic cavitation reactor is that it allows the external introduction of a gas or steam bubbles. Air or steam bubbles of required sizes can be introduced in the flow at a vena contracta downstream of the orifice and thus the pressure pulse amplitude can be manipulated. The cavitation is produced at the shear layer, and the liquid evaporated at the vena contracta downstream of the orifice is proportional to the area of this shear layer. This fact allows a designer to control the bubble population in the flow. By changing the shape of the orifice (making it triangular, hexagonal, etc.), the area of this shear layer can be varied (obviously it is lowest for a circular orifice) and hence the rate of vaporization and the bubble or cavity population can be controlled.

Moholkar and Pandit (1997) reported a simulation of bubble and cavity behavior under the influence of turbulence.They showed that bubble behavior in hydrodynamic cavitation under the influence of turbulence closely resembles that reported for acoustic cavitation. Bubble behavior similar to that observed in acoustic

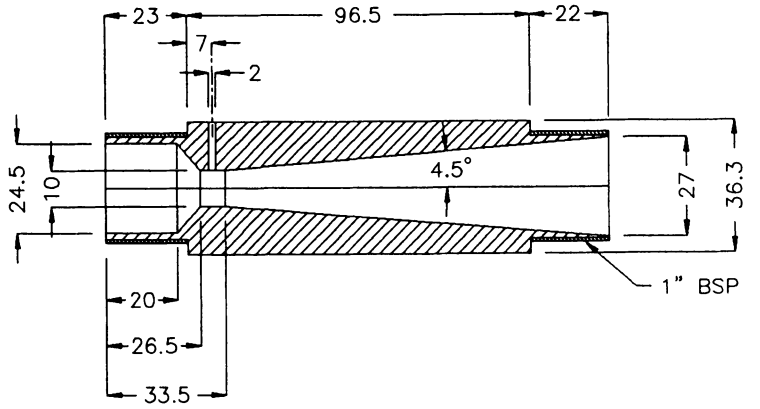

Figure 6.2. Schematic diagram of cavitation nozzle (all numbers are in mm).

cavitation can be obtained in a hydrodynamic cavitation reactor by simple modifications of the orifice. If a rotating valve is installed in place of a permanent orifice, the bubbles that are formed at the shear layer experience a sinusoidally varying pressure field rather than a linear one. Also, if two or three orifices are installed one after the other downstream of the pump, then the bubbles that are generated at the shear layer experience a highly fluctuating pressure field and the collapse is more violent, giving rise to large temperature and pressure pulses of magnitudes comparable to those under acoustic cavitation. High-pressure hydrodynamic cavitation generally involves multiple orifices in series. For the reactions that require fixed catalyst beds (for example, tetralin preparation by hydrogenation of naphthalene), hydrodynamic cavitation can be achieved by throttling the reactant stream through the gaps between the orifice pellets, which act as orifices. In reactions where a slurry is to be handled (for example, nitrobenzene to aniline reduction by hydrogenation with a catalyst), slurry pumps can be used. However, the discharge pressures should be very high in such cases compared with the gas–liquid systems.

In a hydrodynamic cavitation reactor, a large volume downstream of the orifice is affected by the cavitation as a result of the large bulk fluid motion. Pressure pulses produced by the oscillations are relatively small in size but are very large in number compared with those produced in acoustic cavitation reactors. Cavitation occurs at the shear layer in bulk and hence erosion problems are less severe. Cavitation is also uniform throughout the reactor owing to the high level of turbulence. Thus, reactions that require relatively milder conditions of temperature and pressure can be carried out efficiently in a hydrodynamic cavitation reactor. Energy input requirements per unit of reactant volume are low because of the higher volumes of reactants treated with it. Studies on the hydrolysis of fatty oils carried out by Joshi

and Pandit (1993) and on polymerization by Chivate and Pandit (1993) reveal that hydrodynamic cavitation can be far more energy efficient than acoustic cavitation. Save *et al.* (1994) also demonstrated that hydrodynamic cavitation is an order of magnitude more energy efficient than acoustic cavitation in the mechanical disruption of yeast cells for the extraction of intracellular proteins.

In summary, better control over cavitating conditions and less geometric sensitivity allows better reliability, predictability, and control of a hydrodynamic cavitation reactor. However, this reactor also has some drawbacks, some of which can be stated as follows:

- The pressure recovery downstream of the orifice in this reactor is very poor. The permanent pressure head loss is inversely proportional to the ratio of the orifice to the pipe diameter (typically pressure loss is about 73% of the pipe differential for an orifice-to-pipe diameter ratio of 0.5). Therefore, pumping costs for this reactor run very high, especially when a mixture of solid and liquid is handled. In order to produce high temperature and pressure pulses, the discharge pressure of the pump needs to be very high.
- The magnitudes of the pressure pulses produced by oscillations of the bubbles (under a linear pressure recovery profile) are not very high. Specifically, only reactions occurring at up to 10–15 atm and temperatures up to 300°C can be conducted efficiently in such reactors, but the ones requiring high temperatures and pressures would be difficult to process. Furthermore, the performance of a hydrodynamic cavitation reactor is quite low for viscous reacting mixtures. In such cases cavitation is difficult to produce and the cost of pumping viscous materials is very high, both of which affect the economy of the process.
- The heating of the cavitating medium is relatively high in this type of reactor. Therefore, cushioning of the cavities reduces the cavitation intensity.

6.2a. High-Pressure Homogenizer

As indicated above, in hydrodynamic cavitation, bubbles are formed in the region of highest velocity and low pressures. These cavities then collapse in the region of high hydrostatic pressures as they travel with the liquid. Hydrodynamic cavitation is generally used in food and pharmaceutical industries for homogenizing purposes as well as for bacterial and yeast cell disruption studies.

A high-pressure homogenizer that produces hydrodynamic cavitation can be an alternative to ultrasonic equipment. Recent studies by Prasad-Naidu *et al.* (1994) and Shirgaonkar and Pandit (1997) for KI oxidation carried out in a high-pressure homogenizer indicate the formation of I_2 under some experimental conditions. The decomposition of KI to liberate iodine is a classic reaction for assessing the severity of cavitation. If significant cavitation and subsequent bubble collapse are occurring

in the system, then KI should decompose to liberate iodine. On the other hand, no iodine is liberated if the cavitation intensity is low.

Shirgaonkar and Pandit (1996, 1997) examined this reaction system in the high-pressure homogenizer shown in Figure 6.3. Some typical results for iodine liberation, as measured by absorbance in a UV spectrophotometer, are given in Figure 6.4. The results shown in this figure indicate that the high-pressure homogenizer at 5000 psi discharge pressures is indeed operating under high-intensity cavitation conditions. Below a 5000-psi discharge pressure, cavitation is negligible because very little iodine is liberated. It is interesting that yeast cell disruption rates also show an identical trend (Figure 6.5), i.e., not much disruption below a discharge pressure of 5000 psi, but considerable cell disruption (measured on the basis of protein absorbance) at 5000 psi. Figure 6.5 also indicates that a further increase in the pressure (i.e., to 7000 psi) reduces the amount of protein absorbance.

The results described here indicate that severe cavitation conditions can be generated in a high-pressure homogenizer, which is basically a hydrodynamic cavitation device. It is well known that KI decomposes readily under acoustic cavitation. Thus, conditions similar to acoustic cavitation can be generated hydrodynamically. This study also suggests that one of the major causes for the disruption of yeast cells in a high-pressure homogenizer is the strong cavitation (Shirgaonkar and Pandit, 1996, 1997). The study also proves that cavity behavior in hydrodynamic cavitation with strong turbulence will be very similar to that observed in acoustic cavitation. The cavity behavior changes from stable oscillating to transient with the inclusion of a turbulence pressure field in the hydrodynamic cavitation reactors.

Some typical reactions that can be carried out in a hydrodynamic cavitation reactor are given in Table 6.1. A number of oxidation reactions described in Chapters 4 and 5 can also be carried out in a hydrodynamic cavitation reactor as long as temperature and pressure requirements are not excessively large. Various large-scale applications of hydrodynamic cavitation reactors are discussed in Chapter 9.

6.3. ACOUSTIC CAVITATION REACTORS

The steps generally followed in an acoustic cavitation reactor are shown in Table 6.2. The design of the power ultrasound equipment and the reactor needs to be such that overall energy consumption is efficient. The acoustic cavitation reactor system thus involves the elements listed in this table.

The technology for ultrasound generation is well developed (Mason, 1990b). An efficient design of transducers and horns is very important for overall success and cost effectiveness of the ultrasonic process. The nature of the reaction media can not only affect the life of transducers and horns but also determines the nature of

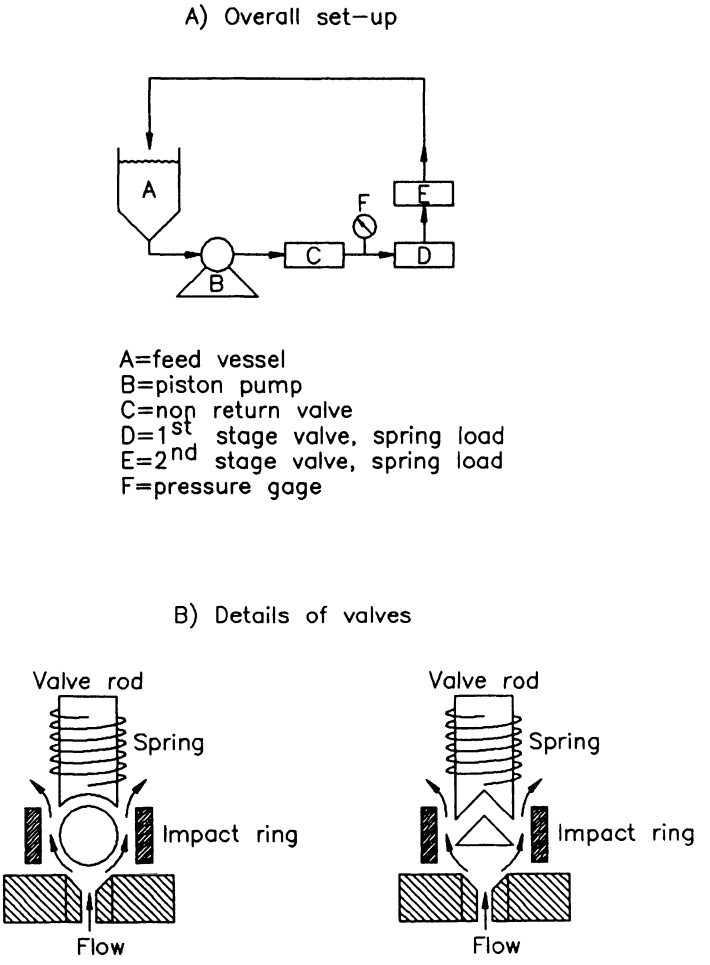

Figure 6.3. High-pressure homogenizer setup. (From A. B. Pandit and V. S. Moholkar, "Harness cavitation to improve processing," *Chem. Eng. Prog.* (July 1996), 57–67. Reproduced with permission of the American Institute of Chemical Engineers. Copyright © 1996 AIChE. All rights reserved.)

the cavitation field and the resulting cavitation chemistry. The most important steps for the efficiency of the sonochemical process are the conversion of electrical energy to acoustic energy and the conversion of acoustic energy to the generation of an effective cavitation field and contacting pattern for the chemical reaction.

In this section we evaluate various types of acoustic cavitation reactors. The reactors contain two basic elements: transducers and horns and the reactor vessel itself, where cavitation and subsequent acoustic cavitation reactions occur. We

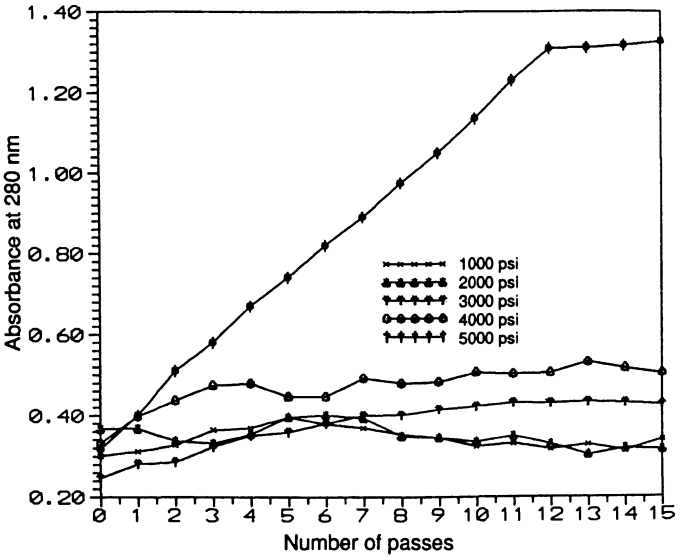

Figure 6.4. Effect of pressure (HPH) KI = 5%, CCl_4 = 25 ml on conversion. (From Shirgaonkar and Pandit, 1997.)

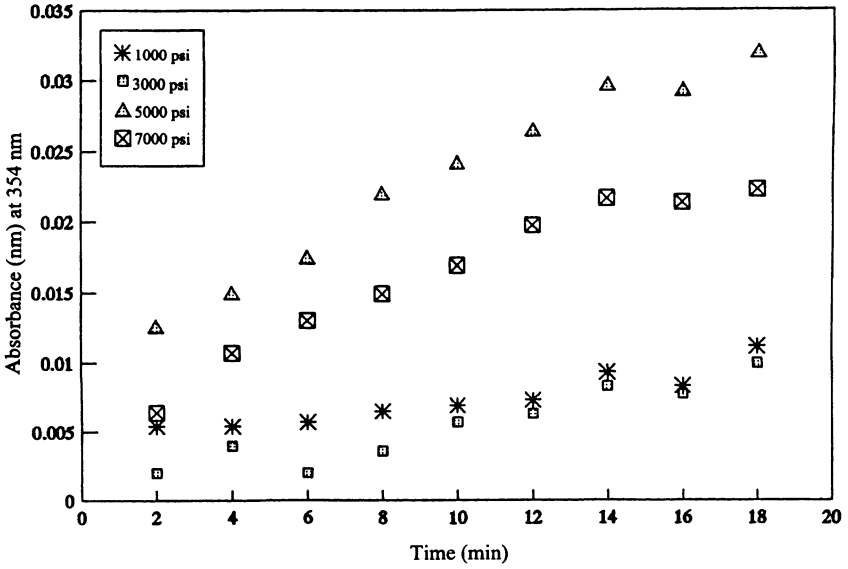

Figure 6.5. Effect of pressure on 1% yeast suspension. (From Shirgaonkar and Pandit, 1996, 1997.)

TABLE 6.1. Chemical Processes for Hydrodynamic Cavitation

Description of process	Temperature (°C)	Pressure (atm)
Hydrolosis of fatty acids such as Kerdi oil, etc.	250–300	3–15
Cyclohexane formation by hydrogenation of benzene.	170–230	25
Tetralin preparation by hydrogenation of naphthalene.	400	25–30
Hydrogenation of mesityl oxide followed by its reduction to MIBK and further reduction to 4 methyl pentane-2-ol.	step(1) 30 step(2) 50 step(3) 150–200	1 3 10
Sorbitol production by large-scale hydrogenation of *D*-glucose.	140	30–70
Nitrobenzene to aniline reduction by hydrogenation with catalyst.	300–475	5–15

evaluate both of these elements. Both laboratory and large-scale vessels as well as scaleup issues are briefly discussed.

6.3a. Transducers and Horns

A transducer is a device capable of converting one form of energy into another. Ultrasonic transducers are designed to convert either mechanical or electrical energy into high-frequency sound. There are three main types of transducers: gas driven, liquid driven, and electromechanical.

TABLE 6.2. Steps for Energy Conversion in Acoustic Cavitation Chemistry[a]

Power supply
↓
Ultrasound generator
↓
Transducers and horns
↓
Reaction media
↓
Cavitation field
↓
Contacting pattern
↓
Gross chemical effect

[a]From Martin (1992) with permission.

The gas-driven transducers are simply whistles with high-frequency output. Dog whistles and sirens are two examples. These transducers can be used to break down foams, agglomerate fine dusts, and accelerate drying processes; however, they have no significant chemical applications because it is not possible to achieve a sufficiently high intensity in airborne ultrasound by this method. Liquid-driven transducers (i.e., a liquid whistle) can be used to produce efficient homogenization. The majority of the chemical effects observed when using whistle-type transducers for the sonication of nonhomogeneous reactions can be attributed mainly to the generation of very fine emulsions rather than the ultrasonic irradiation itself.

Two main types of electromechanical transducers are based on either piezoelectric or magnetostrictive effects. The latter refers to changing in the dimension of a suitable ferromagnetic material (e.g., nickel or iron) by applying a magnetic field. A magnetostrictive transducer is usually in the form of a rod or bar acting as the magnetic core within a solenoid. The application of a varying current to the coil produces a variation in the dimensions of the bar. More recently, the nonmetallic ferrite materials ($NiFe_2O_4$, $ZnFe_2O_4$, and $PbFe_2O_4$) have become important because of their negligible eddy current losses. The advantage of this transducer is that a vastly greater driving force can be applied than with a piezoelectric device. The major disadvantage is that the useful frequency range is restricted to below 100 kHz. Ceramics are also widely used in the new transducers.

Transducers used in modern power ultrasonic systems are often based upon prestressed piezoelectric design. In the construction shown in Figure 6.6, a number of piezoelectric elements, normally two or four, are bolted between a pair of metal end masses. The piezo elements would be of polarized lead titanate zirconate composition, which exhibits high activity coupled with low loss and aging characteristics. They are ideally suited to form the basis of an efficient and rugged transducer. Since ceramics have poor thermal capacity and low tensile strength, a number of their elements are clamped between two low acoustic impedance metal end masses; either titanium or aluminum is generally used for this purpose. The assembly would be designed so that the overall length is a half-wave at the required frequency of operation.

As shown in Figure 6.6, in a typical transducer, two piezo elements are positioned near the point of maximum stress in a half-wave resonant assembly. The elements are arranged so that they are mechanically aiding and electrically opposing. The assembly is clamped together by means of a high tensile bolt. Transducers constructed in this way can have potential efficiencies of 98% and will handle power transfers on the order of 500–1000 W when employed in a continuous operation mode. Maximum peak-to-peak displacements at the transducer radiating face would be on the order of 15–20 μm when operating at a frequency of 20 kHz (Neppiras, 1980).

The design of power ultrasound equipment for high-intensity cavitating duty may require multiple transducers. Some technical challenges for this case are

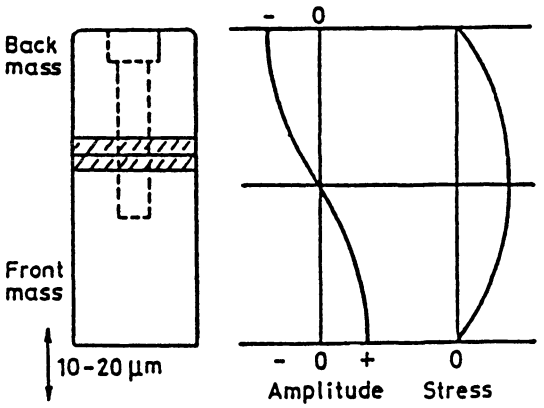

Figure 6.6. Sandwich transducer operating at 1–200 kHz. (From J. P. Perkins "Power Ultrasound," Ch. 4 in T. J. Mason, "Sonochemistry: The uses of ultrasound in chemistry," 1990 with permission.)

transducer mounting
coupling to the liquid load
controlling the interaction between the transducers within the reactor medium and between each other through the hardware
ensuring reasonable transducer life
design flexibility for the selective removal of transducers for maintenance

The vibrating motion generated by the transducers is normally too low for practical use and so it is necessary to magnify or amplify this motion. This is done by a horn, which is a resonant element in the compression mode. Normally these are half a wave length long, but the length can be increased by screwing one horn into another and so on. This method is, however, not often used.

The most popular designs and the amplitude and stress curves of each of these designs are shown in Figure 6.7. The stress discontinuity in the case of the stepped horn requires great care in machining since any marks in the nodal region will create "stress raisers," causing metal fatigue in high-magnification horns. The materials for acoustic horns require: (1) low acoustic loss; (2) chemical inertness; (3) high dynamic fatigue strength; and (4) resistance to cavitation erosion. These are satisfied by: (1) titanium alloy; (2) aluminum; (3) aluminum bronze; and (4) stainless steel, in that order; titanium alloys are superior to the other three. Aluminum alloys are too soft for the irradiation of liquids, and the last two will result in end amplitudes reduced by factors of 0.75 and 0.5 compared with titanium alloys for a given power group in the transducer. The horns made of materials (3) and (4) will become hot and transfer heat to the reaction, an undesirable side effect.

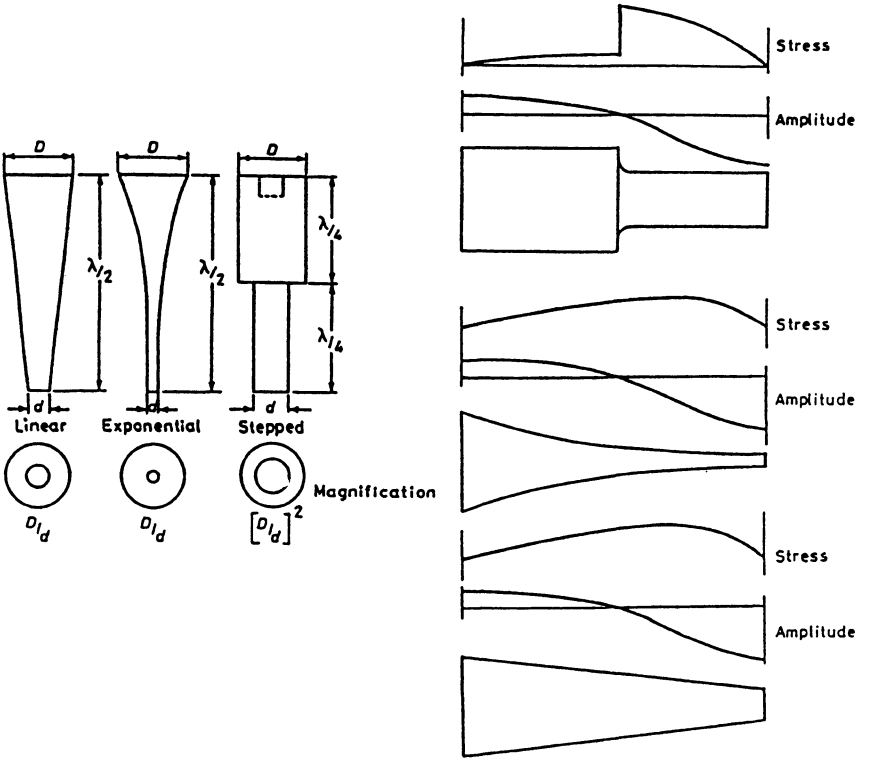

Figure 6.7. Amplitude and stress curves for three popular horn designs. (From Mason, 1990b, with permission.)

6.3b. Measurements of Acoustic Power

In industry, equipment is designed to perform a particular application and vibrational levels are invariably predetermined. A meter indicating relative power supplied to the transducer is common, but this does not normally indicate actual watts. Certain equipment, such as "ultrasonic experimentry," measures a transducer amplitude. It would seem sensible therefore that a number of acoustic parameters should be monitored, which would ensure that:

- Acoustic conditions are consistent over a period of time.
- The results obtained are comparable with those of other workers and are based upon some absolute values.

- Eventually both desirable and undesirable products can be accurately correlated to the acoustic inputs.

There are two basic parameters that should be known: the operational frequency and the acoustic intensity in the treated sample. Frequency is not normally critical within 5–10%. Acoustic power is more difficult to measure. The rated power of the generator cannot be used as an indication of acoustic power, since the power transferred will depend upon how heavily the transducer is loaded (this is a function of horn magnification) and the area of the horn immersed in the reaction medium. There are three possible approaches to the determination of acoustic power:

Calorimetric Method. This is simply the calculation of power input by measuring the rate of temperature rise in the system while taking into account its thermal capacity. This is a rather cumbersome and impractical method and seldom used.

Measurement of Vibrational Amplitude. This is the direct measurement of the amplitude at the working face of the horn, and will give a parameter that is at least proportional to the acoustic power, given by the relation

$$P_{ac} \alpha \frac{1}{2} \rho c \xi^2 \tag{6.1}$$

where P_{ac} = acoustic power, ρ = density of load, c = load sound velocity, and ξ = transducer amplitude. P_{ac}, by this method, can be continuously monitored but it cannot really be considered a reliable method since c and ξ in a cavitating medium cannot easily be determined.

Amplitude offers a very sensitive measurement of acoustic change. It changes as the horn is immersed further into the reaction medium, i.e., as it becomes more loaded. In addition, it will warn of any changes in acoustic transmission caused by dirty interfaces between transducer and horn or horn and tip, total or partial fatigue in the horn, fatigue in the coupling stud between transducer and horn tip, and transducer faults.

A combination of the calorimetric method and measurement of vibrational amplitude might well be the most useful method of monitoring power and therefore control. The measurement of amplitude gives an indication of the acoustic power output rather than the electrical power into the transducer. Generally an 80% efficiency for the conversion of electric power into acoustic power is considered to be a very desirable number.

Measurement of the Real Electrical Power to the Transducer. The real electrical power to the transducer can be converted to acoustic power if the overall acoustic transfer efficiency is known. The use of a wattmeter to measure electrical power to the transducer can, in certain circumstances, lead to a measurement of the true

acoustic power transmitted to the sonicated sample. This can certainly be true of probe systems used for sonochemical treatment. The method, however, is not always very reliable. If the system is driven in a controlled manner, then one can derive the transmitted acoustic power from the unloaded and loaded electrical powers. While introducing the acoustic power, if different horns are used with the same transducer, the transmitted acoustic power would be similar as long as the gain-to-area ratio is kept the same for each horn. The energy density can be varied by selecting the appropriate probe end areas. It should be pointed out, however, that some limitations to these measurement techniques do exist. For example, if the gain-to-area product is made too large, the electrical control system will be unable to handle it and the system will either stall out or the horn will exceed its dynamic fatigue limits and fracture.

In summary, the measurement of either amplitude or electrical power, or both, can offer a valuable means of checking the acoustic performance of a system and of monitoring the acoustic power transmitted.

6.3c. Methods for Measuring Amplitude

Microscopic Measurements. One can measure amplitude by examining the end of a free transducer with a metallurgical microscope with a 15× calibrated eyepiece and a 10× objective, allowing measurement down to ~5 μm. Since most transducers will generate amplitudes of at least 10 μm and this value is amplified by the horn, quite accurate measurements can be made.

Continuous Monitoring. The ability to measure amplitude with a microscope is clearly impracticable during a sonochemical experiment. A method is required that provides continuous monitoring with a display. There are two possible approaches: electromechanical and purely electrical.

Electromechanical. The alternating stress in a resonant element is at a maximum in the center. If a strain gauge is bonded to the center of such an element, then the output from this will be proportional to the displacement or amplitude of vibration. This output signal can be rectified and displayed, for example, on a meter, which can be calibrated by the use of a microscope. It is also possible to derive a purely electrical signal that is proportional to transducer displacement and eliminate the use of the strain gauge. Using this method, it should only be necessary to calibrate the meter once since any subsequent change in transducer amplitude due to loading will be accompanied by a proportional change in strain in the transducer–acoustic system. While the method has some attractive features, in practice it is not often used.

Purely Electrical. Electrical methods of measurement can be contained within the ultrasonic generator. Essentially this is a power amplifier that converts energy

at the main frequency to energy at a chosen ultrasonic frequency. Because of the very narrow operating frequency band of the transducer, it is essential that the amplifier track any changes in resonant frequency of the system.

The same electrical signal used to display amplitude can be fed back into the amplifier and this will enable the power generated to follow any frequency changes in the transducer–acoustic system. This is very important because the resonant frequency of the transducer decreases as it becomes warm and lengthens. Another desirable feature of this method is that it can be used to limit the transducer amplitude and thus ensure that it does not damage itself or the coupled resonant elements by overstress.

6.3d. Hydrophones

Hydrophones measure pressure pulses at any time interval and for a range of frequencies. These instruments are used to measure pressure pulses from 10 kPa to over 100 MPa, depending on the frequency and number of cycles per pulse. High power ultrasound fields can be extremely difficult to characterize, often because of the cavitation events that occur. Not only can the cavitation activity cause damage to the measuring sensor being used, but the bubble populations generated can also scatter the acoustic signal produced by the source under investigation. Furthermore, the oscillating bubbles present will produce their own acoustic signatures, and resolving these from the signal produced by the source can be a complex process. A choice of suitable hydrophone is therefore very important.

Some typical hydrophones are sold by Bruel and Kjaer of Denmark (types 8103, 8104, 8105 and 8106). These hydrophones are individually calibrated waterborne-sound transducers that have a flat frequency response and are omnidirectional over a wide frequency range. Out of the four types of hydrophones, type 8103 is suitable for laboratory and industrial use and particularly for the acoustic study of marine animals or for cavitation measurements. Hydrophone type 8103 is a small-size, high-sensitivity transducer for making absolute sound measurements over the frequency range 0.1 Hz to 180 kHz with a receiving sensitivity of –211 dB for 1 V/u Pa. It has a high sensitivity relative to its size and good all-around characteristics, which make it generally applicable to laboratory, industrial, and educational use. The 8103's high-frequency response is especially valuable when making acoustic investigations of marine animals and in measuring pressure-distribution patterns in ultrasonic cleaning baths. It is also useful for cavitation measurements. Figure 6.8 indicates the major features of the 8103.

There are several other types of hydrophones and other measurement instruments in the market. A brief summary of the various high power measurement techniques is given in Table 6.3. The details of these techniques are provided by Hodnett and Zequiri (1997). The two most commonly used hydrophones are the needle type (see Figures 6.9 and 6.10) and fiber optic hydrophones. Needle-type ceramic probes can

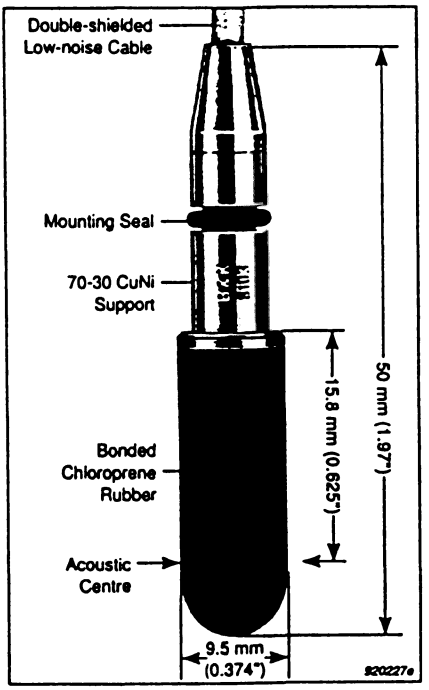

Figure 6.8. Hydrophone type 8103 (Bruel and Kjaer of Denmark) (from technical documentation of hydrophone types 8103, 8104, 8105, and 8106). (Reprinted from *Ultrasonic Chemistry*, **4**, M. Hodnett and B. Zequiri, eds., "A strategy for the development and standardization of measurement methods for high power/cavitating ultrasonic fields: review of high power field measurements," pp. 273–288, 1977, with permission from Elsevier Science.)

be fairly robust devices and are usually of high sensitivity. However, they can suffer from unpredictable structure in both their frequency and their directional responses owing to radial resonance modes, reflections, and mode conversions in the active element and backing material. Typically, hydrophones of this type are constructed with active elements of diameters 0.4–0.6 mm. Fiber optic devices partially alleviate the difficulties associated with manufacturing sensors with small active elements and usable sensitivities. Fiber optic devices also allow a replaceable tip. Further details on these and other types of hydrophones are given by Hodnett and Zequiri (1997).

6.3e. Sonochemical Reactor Geometries

Basically, there are three methods of introducing ultrasound in a reactor: (1) immerse a reactor in a tank of sonicated liquid (e.g., a vessel in a cleaning bath);

TABLE 6.3. Summary of Key Measurement Techniques for High-Power Ultrasound Fields[a]

	Device					
Property	Membrane hydrophone	Needle hydrophone	Discrete thermal probe	Multielement thermal probe	Fiber-optic hydrophone	Interferometric methods
Physical effect	Piezoelectricity	Piezoelectricity	Thermal absorption	Thermal absorption	dn/dp	Membrane or pellicle movement
Parameter	Acoustic pressure	Acoustic pressure	Sata acoustic intensity (relative)	sata acoustic intensity (relative)	Acoustic pressure	Particle displacement or velocity
Spatial resolution	40μm	75μm	10μm	Spatially averaging	0.1mm	50μm
Bandwidth	100MHz	30MHz	Dependent on absorbing material	Dependent on absorbing material	Potentially >3 GHz	Up to 100 MHz
Sensitivity	20 nV Pa^{-1}	40 nV Pa^{-1}		0.1 mV Jm^{-3} (increase as f^2)	4 nV Pa^{-1}	60 nV Pa^{-1}
Pressure range	Up to 100 MPa	Up to 100 MPa	Not proven	Not proven	50 MPa	Potentially large
Comment	Can be damaged by cavitation. Expensive	Can be damaged. High sensitivity. Frequency response unpredictable	Cheap. Easy to use. Subject to cavitation erosion damage in high-intensity fields, and perhaps shielding and streaming effects	Can be subject to cavitation damage in high-intensity fields: Patent refers to device suitable for use in 20 kHz fields only	Upper frequency limit determined only by wavelength of light used	High-power capabilities not yet fully tested

[a]Reprinted from *Ultrasonic Chemistry*, **4**, M. Hodnett and B. Zequiri, "A strategy for the development and standardization of measurement methods for high power/cavitating ultrasonic fields: review of high power field measurements," pp. 273–288, 1997, with permission from Elsevier Science.

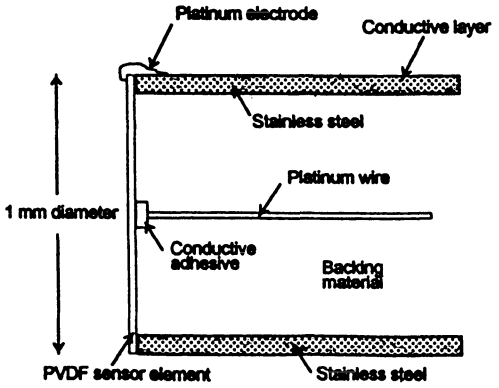

Figure 6.9. Schematic construction of PVDF needle-type hydrophone. (Reprinted from *Ultrasonic Chemistry*, **4**, M. Hodnett and B. Zequiri, eds., "A strategy for the development and standardization of measurement methods for high power/cavitating ultrasonic fields: review of high power field measurements," pp. 273–288, 1977, with permission from Elsevier Science.)

(2) immerse an ultrasonic source directly into a reactor medium (e.g., a probe dipped into a reaction vessel); and (3) use a reactor constructed with ultrasonically vibrating walls. A cup-horn sonicator is a design somewhere between (1) and (2) in which cell disruption is carried out and the contamination of the titanium horn is avoided. Besides these three, whistle reactors are used for reactions requiring emulsification. Some sonoreactors employ immersible transducers. A number of novel sonochemical reactor designs have been evaluated in Europe. Some of these reactors are used for laboratory-scale as well as large-scale operations.

One of the basic parameters in ultrasonic engineering is power density, which can be defined as the electric power into the transducers divided by the horn

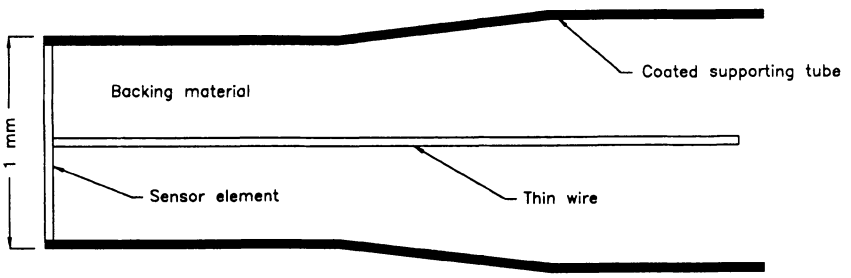

Figure 6.10. Schematic representation of ceramic needle-type hydrophone. (Reprinted from *Ultrasonic Chemistry*, **4**, M. Hodnett and B. Zequiri, eds., "A strategy for the development and standardization of measurement methods for high power/cavitating ultrasonic fields: review of high power field measurements," pp. 273–288, 1977, with permission from Elsevier Science.)

radiating surface area. For a modern piezoelectric transducer, a low-density system uses a power density at the transducer face of the order of 1–2 W cm^{-2}. For a probe system, the power density can be of the order of 100 W cm^{-2}. For a transducer attached to the walls, the level of intensity will depend on the mechanical strength of the walls and other attachments. The intensity experienced by the fluid will be somewhere in between cases (1) and (2). In both of these cases the working frequencies are of the order of 20–80 kHz. The probe system allows greater vibrational amplitudes, energy densities, and control of energy densities within the reactor. Both of these systems and their modifications are described in detail below.

The Ultrasonic Cleaning Bath. The simple ultrasonic cleaning bath is by far the most widely available and cheapest source of ultrasonic irradiation for chemical reactions (Figure 6.11). While this is one of its main advantages, there are several other positive points, including its ability to provide a fairly even distribution of energy in the immersed reaction vessel. No special adaptation of reaction vessels is required; i.e., a conventional apparatus can be transferred directly into the bath. This means that an inert atmosphere or pressure can be readily achieved and maintained throughout a sonochemical reaction. In general, it is desirable to use flat-bottomed glassware since this permits more efficient transfer of the ultrasonic energy (which is radiated from the base of the tank) from the bath water into the reaction. Round-bottomed vessels tend to deflect or reflect a larger fraction of the sound energy away from the reaction mixtures they contain. Despite its ready accessibility, there are some severe limitations to the general use of this equipment. These limitations are outlined in Table 6.4.

Local ultrasound intensity in an ultrasonic cleaning bath is strongly affected by:

liquid level in the ultrasonic cleaner
solvent level in the reaction flask
position of the reaction flask

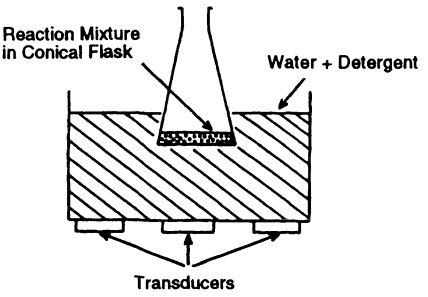

Figure 6.11. Ultrasonic cleaning bath. (From Perkins, 1990, with permission.)

TABLE 6.4. Limitations on Use of Ultrasonic Cleaning Bath[a]

The amount of energy that reaches the reaction is low, normally between 1 and 5 W cm^{-2}. For liquid–solid systems, mechanical agitation of the reaction mixture during sonication is required.
All baths operate at frequencies and powers dependent upon the transducers employed. Direct comparisons between studies done in different baths is difficult.
The use of water limits the upper temperatures of operation to below 100°C. A change in the medium also results in a change in energy transfer from transducer to reaction vessel.
There is poor temperature control unless the system is operated under thermostatic conditions. Any cooling system will interfere with the clear passage of ultrasound through the bath. It is important to record the temperature *inside* the reaction vessel since this will always be a few degrees above that of the bath itself due to ultrasonic heating.
The precise position of the reaction vessel in the bath, both vertically and horizontally, is important. Naturally the same glass vessel should be used each time if reproducible results are required since the thickness of the glass base will affect the power transfer into the reaction system.

[a]From Mason (1990b) with permission.

ultrasonic power delivered by the ultrasonic cleaner (if standing waves can form, the local ultrasound intensity does not necessarily increase with increasing ultrasound power)
presence of solid particles

In the cases where low-intensity irradiation is needed, batch treatment could be as simple as using a large-scale ultrasonic cleaning bath as the reaction vessel. However, the tank should be constructed of a material that is inert toward the chemicals involved. An appropriate grade of stainless steel may be adequate or in some cases a plastic tank could be used. In the latter case, however, the transducer would need to be bonded onto a stainless or titanium plate and this assembly then bolted to the tank. A useful variant of this, and indeed one that offers greater flexibility in use, is the sealed, submersible transducer assembly. With either system, some form of additional (mechanical) stirring would almost certainly be needed.

Bath-type reactors may also be used in a flow system. In this case the reacting liquids could be continuously fed into an ultrasonic tank with outflow over a weir toward the next process. Such treatment could be intensified by recycling or by connecting a number of such sonicated tanks in line.

Large-scale ultrasonic cleaning bath reactors may employ externally mounted transducers fixed to the walls of the reactor vessel (Figure 6.12). This approach has been successfully adopted by the ultrasonic cleaning industry, which manufactures large, multiliter cleaning baths for industrial use. From a sonochemical viewpoint,

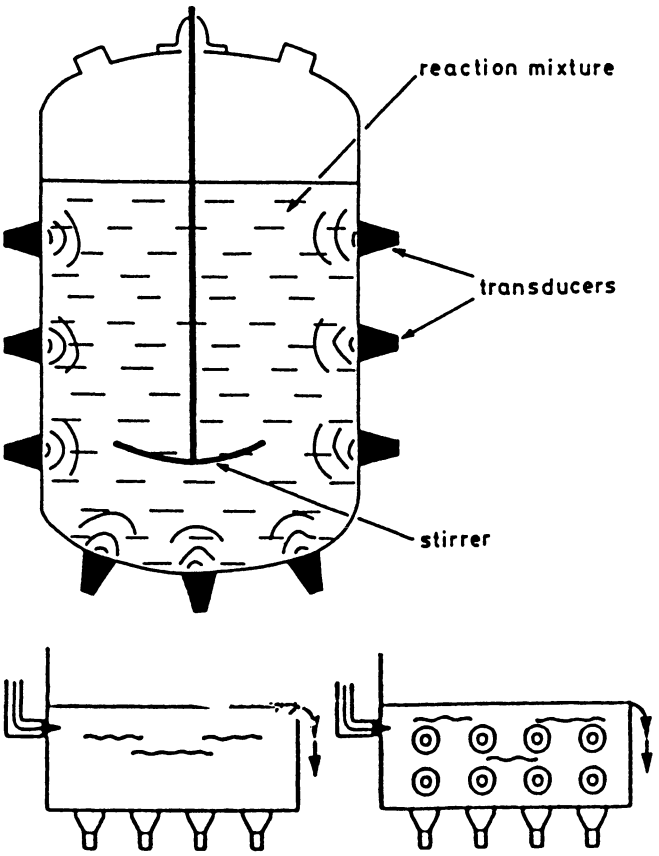

Figure 6.12. Various configurations of "cleaning bath" reactor employing wall-mounted transducers. (From Perkins, 1990, with permission.)

there are a number of advantages and disadvantages associated with this approach; these are briefly listed in Table 6.5.

The following analysis of a typical chemical reactor indicates the number of transducers and the operating power required to achieve a production-scale sonoreactor: A 3-m high, 1.5-m diameter cylindrical reactor vessel has an internal volume of 5 m^3 and a surface area (bottom and sides) of 16 m^2. A typical 20-kHz transducer (as used in the cleaning bath industry) has a diameter of 6 cm and a surface area of $3 \times 10^{-3} m^2$. Thus, for 100% coverage of the vessels, you would need 5700 transducers; for 10% coverage, 570 transducers. At 10% coverage, each transducer has to irradiate 9 liters of reaction mixture (cf. a cleaning bath with 6 liters/transducer). Fifty watts are required to operate each transducer to produce a

TABLE 6.5. Advantages and Disadvantages of the Large-Scale Cleaning Bath Reactor

Advantages	Disadvantages
No contamination of the reagents by erosion of the ultrasonic source	A low-intensity, nonuniform field throughout the vessel
The reaction vessel may be operated under pressure without the need for elaborate sealing of the ultrasonic source	Bulk heating of the reaction mixture (not always desirable)
	Transducer must be "glued" to the outside of the vessel to achieve efficient coupling of the ultrasonic energy with the reaction. This is usually difficult to achieve and would probably involve significant alterations to the existing capital equipment.

power density of 1–2 W cm^{-2} at the transducer face. Thus, 570 transducers will require 30 kW and 30 generators to operate. These figures illustrate the potential cost of the ultrasonic component of a large-scale cleaning bath sonoreactor.

Sonoreactors Employing Immersible Transducers. For many years, the manufacturers of ultrasonic cleaners have offered the submersible transducer as an alternative to the bath as a means of batch sonication (Figure 6.13). In essence, this system permits any bath (vessel) to be converted into an ultrasonic cleaning bath. The advantage of this is clearly convenience in vessel size. Immersible transducers are widely used throughout the ultrasonic cleaning industry because the units are relatively cheap, readily available, and can be retrofitted to most large vessels. Most immersible units consist of a series of ultrasonic transducers mounted within a steel box; all the necessary wiring is connected to the transducers through suitable piping. To irradiate the desired fluid, the units are simply dipped into the liquid and switched on. The attraction of using this approach for large-scale sonochemistry is, therefore, obvious: the required number of immersible units are placed within the vessel to irradiate the reaction mixture. They can be designed to fit into any existing reaction vessel and are capable of withstanding organic solvents. As with cleaning bath systems, however, this reactor requires mechanical stirring. The advantages and disadvantages of this reactor are summarized in Table 6.6.

The feasibility of this approach can be demonstrated by, once again, considering a 3-m high cylindrical reactor with an internal diameter of 1.5 m. The internal volume is 5 m^3 and the surface area is 16 m^2 (Figure 6.14). A typical immersible transducer unit has the following dimensions: 0.7 × 0.25 × 0.1 m. This unit would usually contain 32 transducers. The surface area of this unit is 0.18 m^2 and it has a volume of 0.019 m^3. To get 570 transducers into the vessel, just as illustrated for the cleaning bath reactor, one would need 18 units. These units would have a surface area of 3 m^2 and occupy 20% of the vessel wall area. Similarly, their total volume

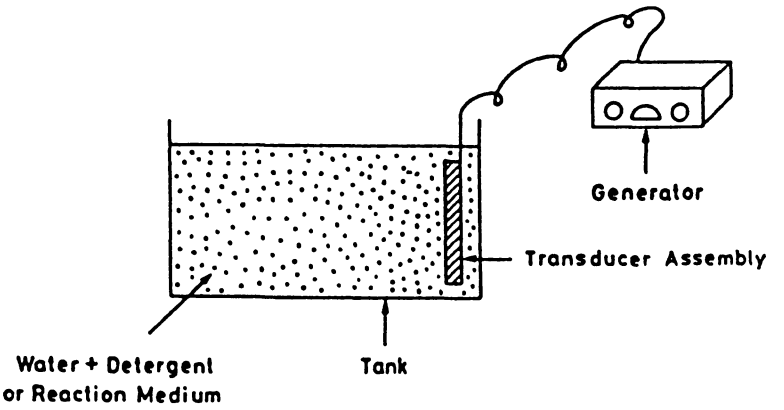

Figure 6.13. Submersible transducer. (From Mason and Berlan, 1992, with permission.)

is 0.3 m^3 or 1/15th of the vessel volume. Thus the insertion of immersible transducers into a chemical reactor leads to a significant proportion of the internal volume being occupied; this, coupled with the major problems over insulation and protection of the units during use, tends to detract from the initial attractiveness of this approach. The cost of the immersible approach would be similar to the cost of a cleaning bath reactor.

The Cup-Horn System. This piece of equipment may be envisaged as a small but powerful ultrasonic bath. In effect, it uses a specially designed inverted horn to irradiate a small cup of liquid (normally water) into which the reaction vessel is dipped (Figure 6.15). Circulating coolant through the specially designed horn assists in maintaining temperature stability. As a result of its design, it has several

TABLE 6.6. Advantages and Disadvantages of the Large-Scale Immersible Transducer Reactor

Advantages	Disadvantages
Higher ultrasonic intensities than those obtained for cleaning bath reactors	Erosion of the metallic transducer cover
Retrofit situation—they can be used without any permanent modification of the reaction vessel	Nonuniform field within the reaction vessel
	"Intrusive"—they would interfere with stirrers, cooling pipes, and other pieces of equipment within the reactor vessel
	Sealing of the transducers and electrical supply from the corrosive reaction mixtures

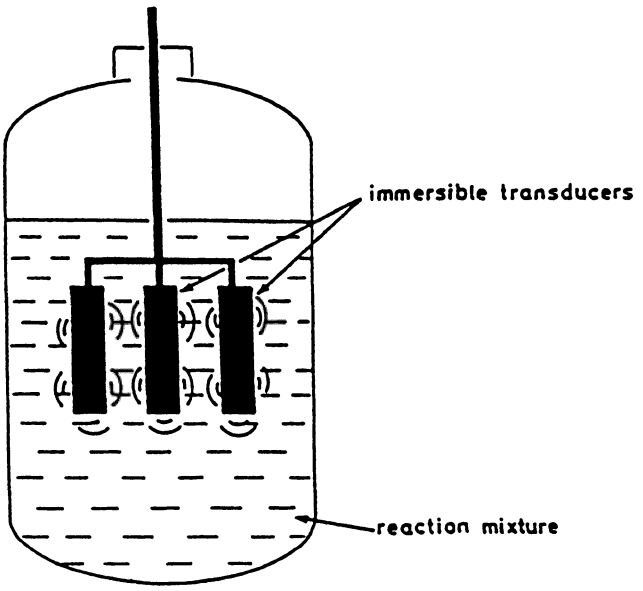

Figure 6.14. Large-scale sonoreactor employing immersible transducers. (From Mason, 1990b, with permission.)

major advantages over a simple ultrasonic bath; however, a number of disadvantages, including its applicability to a small-size reaction vessel, still remain.

The major advantages of the cup-horn system include good temperature control because water of a constant temperature can be circulated through the bath system. Since the irradiation source is a modified sonic horn, the power can be better controlled. The possibility of radical formation in the reaction vessel is lowered because of the reduced intensity of sonication, which is transmitted through the water in the cup, and any fragmentation of metal from the tip of the probe into the reaction is eliminated.

Besides its applicability to only small-size reaction vessels, the other major disadvantages of the cup-horn sonicator are that the power is greatly reduced compared with that of a sonic horn and this device is only largely available for 20-kHz horns. The vessel is useful for studying the kinetics of sonochemical reactions.

The Ultrasonic Probe System. In order to increase the amount of ultrasonic power available to a reaction, it is desirable to introduce the energy directly into the system. The simplest method of achieving this is to introduce the ultrasonically vibrating tip of a sonic probe into the reaction media itself (Figure 6.16). The metal

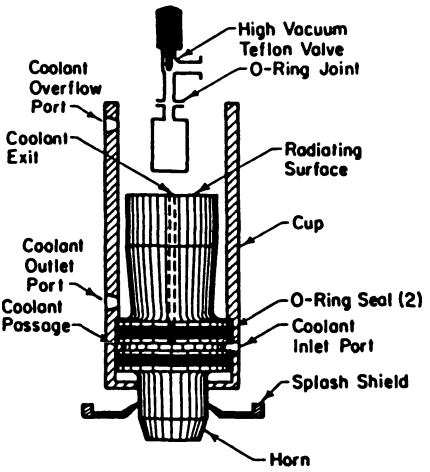

Figure 6.15. Cup-horn sonicator; modification of a design from heat systems-ultrasonics. (From Mason, 1990b, with permission.)

probe represents the part of the sonic horn that amplifies the small vibrations of the piezoelectric crystal to a larger amplitude. This is frequently seen as the most obvious method of scaling up sonochemical reactions because the probes can be dipped into a reaction mixture by insertion through a suitable port in the top of the vessel. This retrofit, coupled with the high intensities generated by the probe, are the main advantages of this approach.

The ultrasonic power delivered by a horn is directly related to the magnitude of the vibration of the tip. This can readily be controlled by the electrical power input to the transducer and so the precise power of the system can be regulated. Maximum powers of several hundred W cm^{-2} can be easily achieved (depending on the size of the unit). Ultrasonic streaming from the tip of the probe is often sufficiently powerful to provide efficient bulk mixing. Most modern units have a pulse facility that allows the operator to sonicate reactions repeatedly for fractions of a second. This gives adequate time for cooling between sonic pulses. With such systems the probe (horn) can be tuned to give optimum performance. This is important in terms of reproducibility of results. Modern equipment is normally fitted with an automatic frequency regulator.

As with all systems that operate using piezoelectric transducers, the optimum performance is obtained at a fixed frequency. For most commercial probe systems this is 20 kHz, and although it is possible to drive them at their overtones (i.e., 40 or 80 kHz), the power dissipation at overtones of the fundamental frequency of the system is very much reduced. To operate successfully at different frequencies, it is best to purchase amplifier-horn systems tailored to individual requirements. As with

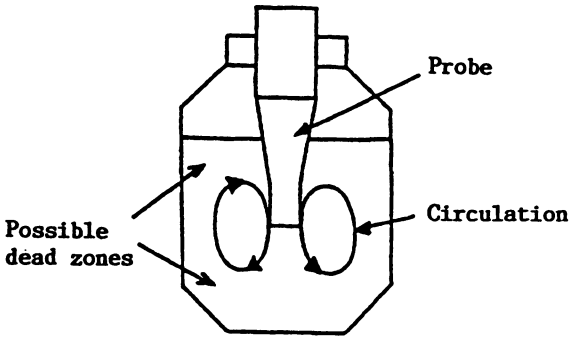

Figure 6.16. Probe batch reactor. (From A. B. Pandit and V. S. Moholkar, "Harness cavitation to improve processing," *Chem. Eng. Prog.* (July 1996), 57–67. Reproduced with permission of the American Institute of Chemical Engineers. Copyright © 1996 AIChE. All rights reserved.)

baths, there is a problem with accurate temperature control unless precautions are taken. The use of specially designed reaction vessels [e.g., a Rosett cell (Figure 6.17)], alleviates much of this difficulty. The temperature within the reaction vessel should be continuously monitored.

Owing to the high intensity of irradiation in the reaction close to the tip, it is possible that radical species may be produced which could interfere with the normal course of reaction. The cavitation that is the source of chemical activation is also the source of a common problem with probe systems, tip erosion, which occurs despite the fact that most probes are fabricated of very hard titanium alloy. There are two unwanted side effects associated with erosion: (1) metal particles eroded from the tip will contaminate the reaction mixture; and (2) the physical shortening of the horn causes a loss of efficiency (eventually it will become too short to be tuned). The latter problem is avoided by the use of screw-on tips to the probe in the form of studs; this eliminates the need for a costly replacement of the whole horn. Special seals will be required if the horn is to be used in reactions involving reflux, inert atmospheres, or pressures above (or below) ambient. Generally, this system is suitable only for small batch reactions although multiple probes can handle larger volumes.

The possible use of sonic probes in large-scale sonochemistry is illustrated by considering the 5-cm^3 cylindrical reaction vessel (see Figure 6.18). The largest commercially available sonic probe is a 2.5-kW unit with a 5-cm diameter probe tip; the transducer and probe are 45 cm long and 10 cm in diameter. Assuming the 2.5 kW rating to be correct, then the maximum operating intensity at the probe tip is 120 W cm^{-2}. The volume of irradiation of this probe (at this intensity) is probably 0.001 m^3 or 1/5,000th of the reactor volume. One therefore needs a multiple array of probably 10 or more probes. The cost of this, however, would be significantly

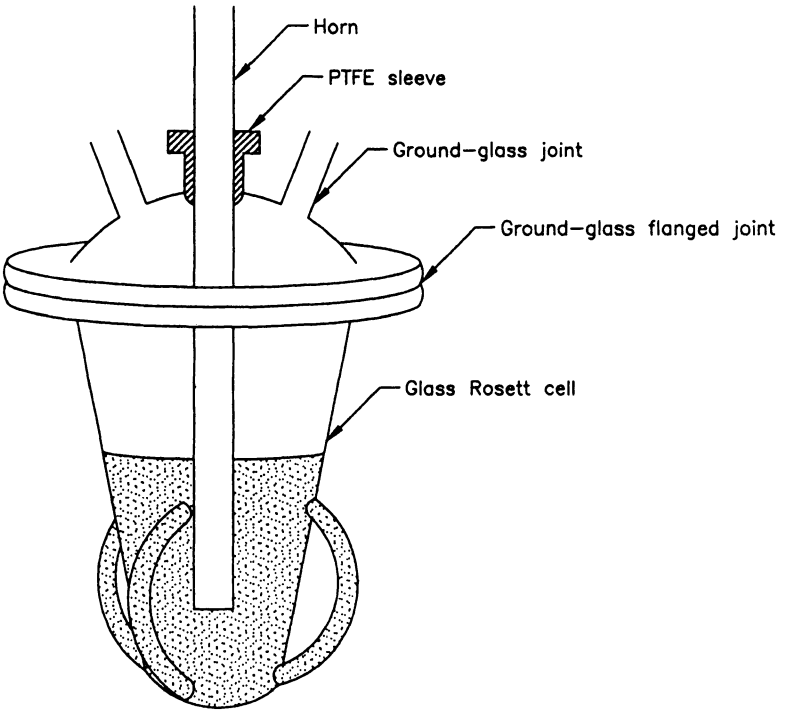

Figure 6.17. Rosett cell reactor. (From Mason and Lorimer, 1988, with permission.)

less than that associated with either the cleaning bath or immersible transducer approach. Thus, provided a suitable method of circulating the reagents through the zones of high ultrasonic intensity at the probe tip is employed, sonic probes are the most attractive method of ultrasonically enhancing large-scale sonochemical reactions on a batch basis. The advantages and disadvantages of the large-scale sonic probe reactor are briefly summarized in Table 6.7.

Flow Systems. The probe system also can be used with a continuous flow (see Figure 6.19), and this is regarded as the best approach for industry because it offers several benefits, as described below. The simple flow cell is an excellent means for processing relatively large volumes. Flow systems are generally regarded as the best approach to industrial-scale sonochemistry. One method is to couple the probe transducer into a flow pipe by means of a T-section (see Figure 6.20). A number of such transducers could be employed in this manner to give extended treatment time. For larger scale operations where high-intensity ultrasound is required, the sonic horn is best utilized as part of a flow loop outside of the main reactor. This permits

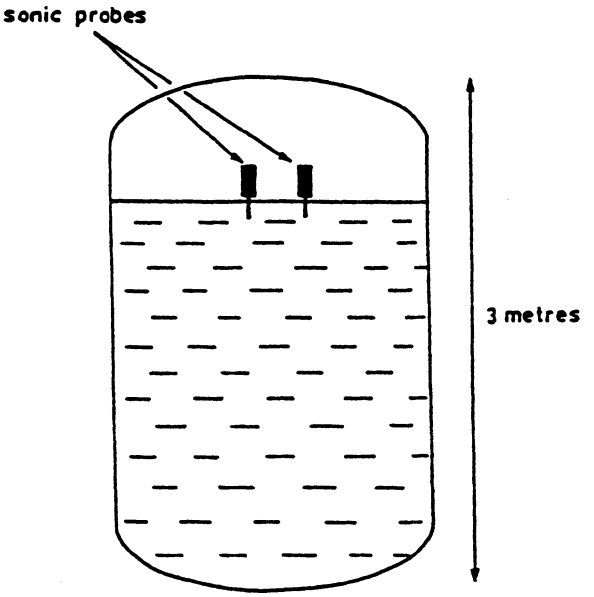

Figure 6.18. Large-scale sonoreactor incorporating sonic probe (to scale). (From Mason, 1990b, with permission.)

the continuous processing of large volumes. Temperature control is provided through the circulating reaction mixture. This reactor also allows the residence time of the reacting system in the flow to be varied by changing the flow rate. The reactor carries the general disadvantages of the probe system, i.e., tip corrosion and potential production of radicals. Pumping is required for circulation to the flow cell and so is not suitable for either very viscous reaction media or heavily particulate

TABLE 6.7. Advantages and Disadvantages of the Large-Scale Sonic Probe Reactor

Advantages	Disadvantages
Retrofit approach	Erosion of the probe tip; frequent replacement of probe may be needed
	Only a small proportion of the total reaction volume is irradiated with high-intensity ultrasound; reaction yield sometimes passing through a maxima with respect to the intensity of irradiation (high-energy intensity may enhance side reactions)
	Insulation of the ultrasonic transducer from the chemical environment above the reaction mixture
	Stalling of the probe in reaction mixtures of high viscosity

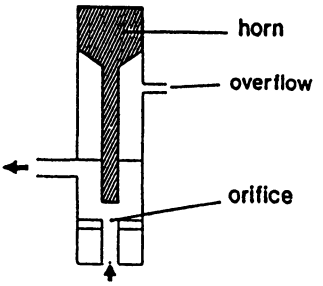

Figure 6.19. Flow cell. (From Mason and Berlan, 1992, with permission.)

systems. Although the flow cell will produce liquid movement via streaming, it is normal to employ a circulating pump to force liquid reactants across the probe in the opposite direction.

An alternative arrangement would involve a number of probes inserted through the walls of a pipe, allowing a much longer sonochemical treatment zone. Such a system will suffer from the same problems as the individual flow cell except that the system will continue to function even if one or two probe units fail. The advantages and disadvantages of these systems are described in Table 6.8.

Because of the ready availability of the large sonic probes, utilization of this equipment for large-scale sonochemistry operating on a continuous basis is a distinct possibility in the near future. The success of the approach is obviously dependent on the suitability of the chemical reaction for operation on a continuous basis.

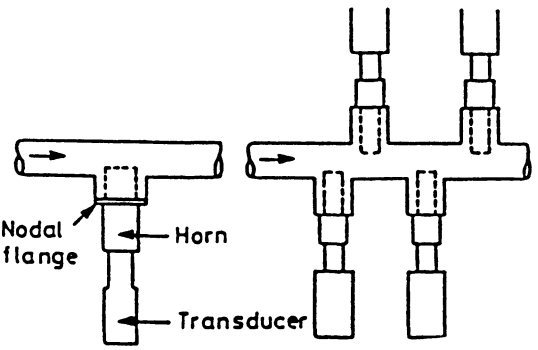

Figure 6.20. Large-volume treatment using high-intensity process. (From Mason, 1990b, with permission.)

TABLE 6.8. Advantages and Disadvantages of Flow Systems with Sonic Probes

Advantages	Disadvantages
High-intensity fields are generated within the flow cell; there are commercially available units that can process up to 250 liters/h	Sealing of reactor/probe joints particularly for the operation of high-pressure reactions
The flow cells can be used in series if required	Erosion of the probe tip and flow cell during operation
A flow cell could be retrofitted to an existing reactor loop	Degradation of the reagents due to the high ultrasonic fields at the probe tip

Specialized Laboratory-scale Reactors Involving Probe Systems. Although it is possible to simply dip the probe into a reaction medium contained in a standard round-bottomed flask or even a beaker, chemical reactions often require a vapor-tight apparatus, the slow addition of reagents or inert atmospheres, high pressure and temperature, the presence of a solid catalyst, or special circumstances due to the nature of the reaction. To cater to these constraints, specialized sonochemical reactors have been developed and some these are briefly described below.

1. The design of a glass Rosett cell with a flanged lid (see Figure 6.17) allows the irradiated reaction mixture to be sonically propelled from the end of the probe around the loops of the vessel and thus provides both cooling (when the vessel is immersed in a thermostat bath) and efficient mixing. A polytetrafluroethylene sleeve provides a vapor-tight fit between the probe and the glass joint. As an alternative to this, an ordinary reaction vessel can be adapted for sonic mixing by providing an indentation on its base to disperse the acoustic waves as they are reflected from the base (Figure 6.21).

2. Many hydrogenation reactions operate under high pressure. There may also be some intrinsic advantages in running other types of catalytic reactions under high pressure. A typical apparatus for pressurized sonication is illustrated in Figure 6.22.

3. Special types of laboratory reactors have been developed to study Belousov–Zhabotinsky oscillating reactions. Rapid fluctuations in meter readings due to the formation and removal of cavitation bubbles require a change in experimental method. These include electronic separation of the rapidly fluctuating signal, measurement of optical density after instantaneously switching off ultrasound, and using specially designed cuvettes. The oxidation-reduction potential has turned out to be almost insensitive to cavitation processes. Three types of reactors, depending on the required ultrasonic frequency, have been developed. A probe reactor for a 22-kHz frequency is illustrated in Figure 6.23.

4. Luche (1987, 1988, 1991, 1992, 1993) and Luche *et al.* (1983, 1984, 1989) have carried out extensive investigations into sonochemical preparations of organometallic species and has designed a reactor containing a support on which the

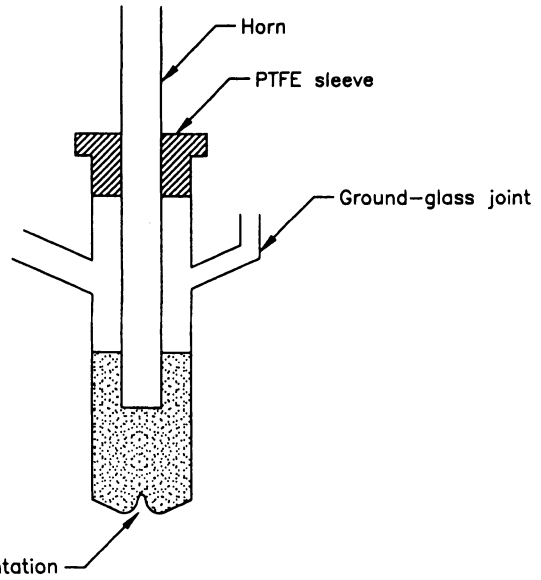

Figure 6.21. Indented-base reactor. (From Mason and Lorimer, 1988, with permission.)

lithium can be placed at a fixed distance from the horn (Figure 6.24). This type of reactor can be used to examine any gas–liquid–solid sonochemistry at the laboratory scale.

Whistle Reactors. Whistle reactors (see Figures 6.25(a) and (b), have been extensively used for homogenization in the food industry. This system is already available for large-scale processing since it is practical, robust and durable, and requires low maintenance. Although ideal for liquid processing, it can also be used for solid–liquid systems. This type of reactor is useful when the reactor requires efficient emulsification, homogenization, or dispersion as an essential requirement for promoting reactivity. Typical applications include processing of fruit juices and tomato ketchup. The underlying mode of action, since it involves flow-induced vibration of a steel blade, immediately suggests the problem of erosion by particulate matter—the sandblasting effect. It seems likely that the liquid whistle could find applications in large-scale sonochemistry involving noncorrosive materials.

The major disadvantage of this system is that, in general, whistle reactors do not generate a very high intensity of sonication, and so ultrasonically initiated and driven reactions will not have high conversions in such reactors. The optimum frequency of blade vibration (designed for 20 kHz) relies upon rapid pumping of the reaction mixture, which is clearly not possible for viscous materials. The reactor

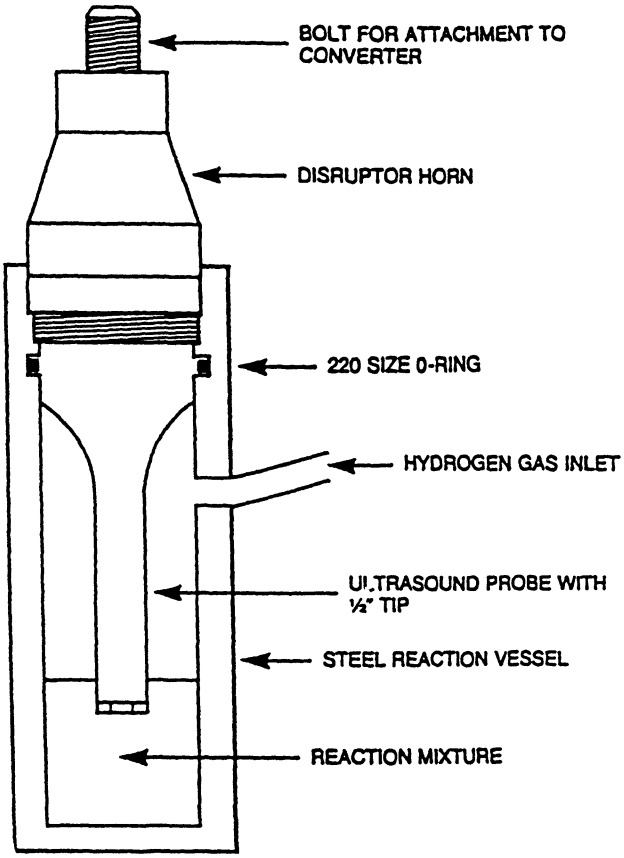

Figure 6.22. Apparatus for pressurized sonication. (From Suslick, 1986a, with permission.)

can be used as a flow system and, as such, has immediate possibilities for relatively straightforward scaleup. With no moving parts required to produce sonication, the system is rugged and durable. A special type of the whistle reactor, namely the Galton whistle, is schematically shown in Figure 6.25(b).

Flow Reactors with Wall-Mounted Transducers. Probe systems, by their very nature, will suffer from erosion of the horn tip and in the long term this could prove expensive in terms of downtime for repair and replacement. A simple solution to the problem is the use of radially positioned transducers surrounding the flow pipe itself, i.e., a tube reactor (see Figures 6.26 and 6.27). This type of reactor can be used for laboratory-scale as well as large commercial-scale processes. This reactor provides the greatest hope for the general use of ultrasound in sonochemistry. Since

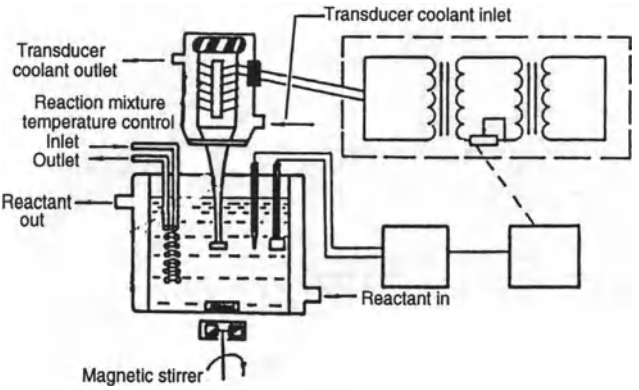

Figure 6.23. Experimental setup for the study of the action of ultrasonic waves with 22 kHz frequency and modulated ultrasonic waves on the Belousov–Zhabotinsky oscillating reaction. (From Mason, 1990b, with permission.)

the system has, as of yet, received no real commercial trial, its advantages and disadvantages are somewhat difficult to identify, although some are listed in Table 6.9. The diameter of the tube is at least an inch or two, based upon the need to physically fit transducers around its perimeter. Much larger diameter tubes can be used and so high flow rates and viscous materials can be handled with no problems of flow blockage. The ultrasonic energy is focused toward the middle of the tube,

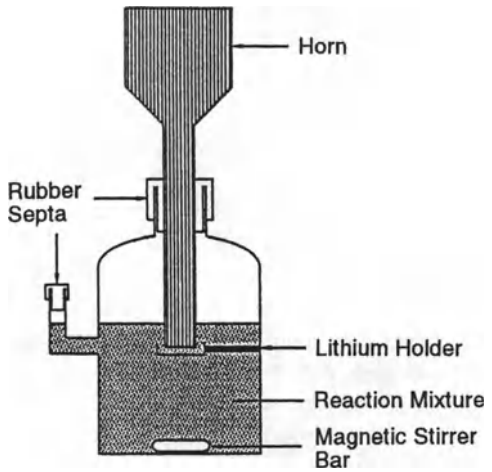

Figure 6.24. Reaction vessel designed to investigate the influence of ultrasound on the preparation of organolithium reagents. (From Mason, 1990b, with permission.)

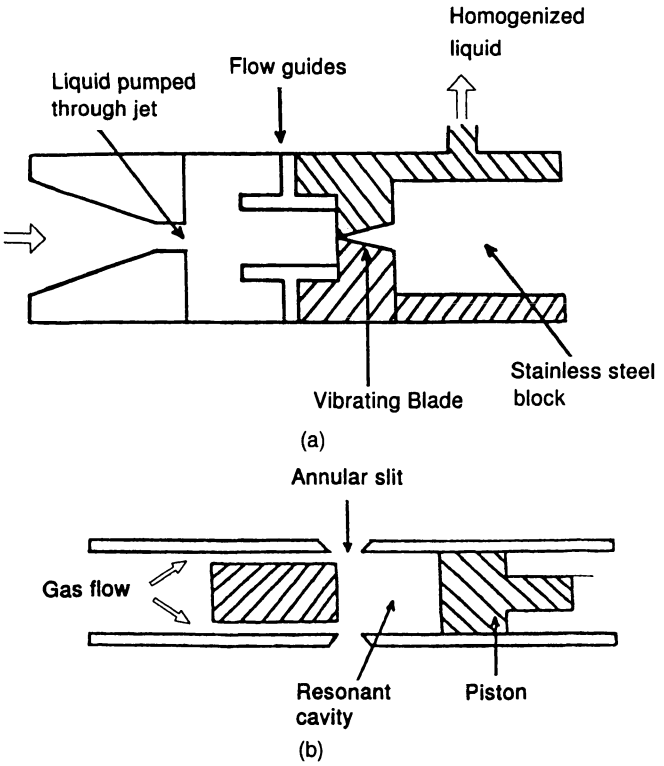

Figure 6.25. Whistle reactors. (a) Conventional whistle reactor and (b) Galton whistle. (Conventional whistle reactor reproduced from Perkins, 1990, with permission. Galton whistle reproduced from A. B. Pandit and V. S. Moholkar "Harness cavitation to improve processing," *Chem. Eng. Prog.* (July 1996), 57–67. Reproduced with permission of the American Institute of Chemical Engineers. Copyright © 1996 AIChE. All rights reserved.)

with much lower power at the inner surface. In this way erosion problems are reduced. The system can easily be fitted to existing pipework, thereby requiring minimal disturbance of the existing technology.

High-intensity treatment does not automatically include the use of probes. If the application involves particle size reduction, then the choice may well be the reverberatory ultrasonic mixing system as developed by the Lewis Corporation (Figure 6.28). This system (sometimes called a nearfield acoustic processor) can be visualized as two sonicated metal plates that enclose a flow system. In effect, the plates can be regarded as the bases of two ultrasonic baths facing each other and separated by only a few centimeters. Under these conditions any liquid flowing between the plates is subject to an ultrasonic intensity greater than that expected from simply doubling a single plate intensity. The ultrasound reverberates and is magnified in its effect. Figure 6.28 also suggests the existence of a standing wave

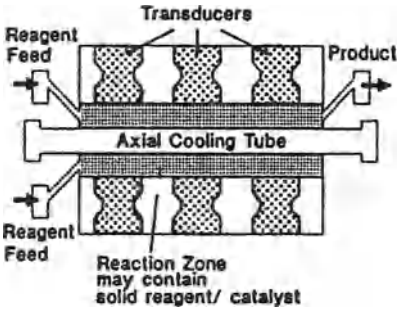

Figure 6.26. Cylindrical reactor. (From A. B. Pandit and V. S. Moholkar, "Harness cavitation to improve processing," *Chem. Eng. Prog.* (July 1996), 57–67. Reproduced with permission of the American Institute of Chemical Engineers. Copyright © 1996 AIChE. All rights reserved.)

pattern (depending on the spacing). The system is already used for such applications as particle size reduction and the extraction of oil from oil shale, and thus could easily be applied to sonochemical reactions. An additional benefit is that with vibrating plates of the size of table tops, the system can cope with very large throughputs of material, allowing an examination of the small residence time of the reaction.

The basic idea behind this approach is the attachment of suitable transducers to the external wall of a pipe through which the reaction mixture is flowing. The reagents then experience an ultrasonic field during their residence in the irradiated zone. Some reactions will require one slow pass through this zone whereas others may require many, possibly fast, passes through the zone. The dimensions of the irradiated zone depend on the number of transducers employed, the intensity at which they are operating, and the diameter of the pipe. Despite the disadvantages listed in Table 6.9, this approach has been successfully adopted in the ultrasonic

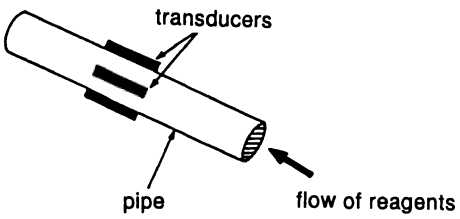

Figure 6.27. Flow systems incorporating wall-mounted transducers. (From A. B. Pandit and V. S. Moholkar, "Harness cavitation to improve processing," *Chem. Eng. Prog.* (July 1996), 57–67. Reproduced with permission of the American Institute of Chemical Engineers. Copyright © 1996 AIChE. All rights reserved.)

TABLE 6.9. Advantages and Disadvantages of Flow Systems with Wall-Mounted Transducers

Advantages	Disadvantages
It is nonintrusive, so there is no contamination of the reagents	Mechanical problems are associated with the mounting of flat transducers on the walls of cylindrical pipes; curved transducers are, however, now available
A relatively small number of transducers are required, probably less than 50. This, in turn, leads to the overall cost being much lower than, for example, the cleaning bath approach	The acoustic intensity achievable within the fluid is critically dependent on the dimensions of the pipe
There is the possibility of retrofitting the transducers to existing continuous reactor systems	Circulation of solid reagents, such as magnesium turnings, through the irradiated zone

processing techniques employed by the food industry. It should be noted, however, that many large units operate at much lower ultrasonic intensities than those generally required for sonochemical reactions.

For all flow systems, pumping is required for circulation and so they are less suitable for viscous or heavily particulate reaction mixtures. One solution is to use pipes (which can be of different cross-sectional geometries) to introduce ultrasound into the flowing system through the vibrating pipe walls. The length of such a pipe must be accurately designed so that a null point exists at each end and it can then be retrofitted to existing pipework. Such systems are capable of handling high flow rates and viscous materials. A cylindrical resonating pipe will provide a focus of ultrasonic energy in the center of the tube, as will a hexagonal pipe. Thus, relatively low power at the perimeter inner surface will give high energy in the center, which reduces erosion problems at the emitting surface. However, in engineering terms,

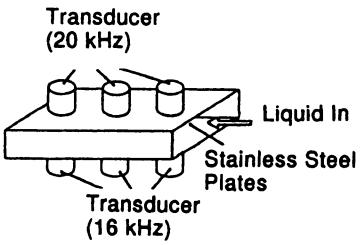

Figure 6.28. Reverberatory ultrasonic reactor (nearfield acoustic processor). (From A. B. Pandit and V. S. Moholkar, "Harness cavitation to improve processing," *Chem. Eng. Prog.* (July 1996), 57–67. Reproduced with permission of the American Institute of Chemical Engineers. Copyright © 1996 AIChE. All rights reserved.)

the cylindrical cross-section pipe suffers from the disadvantage that the attachment of transducers to the curved outside surface walls is not as simple as attachment to the planar walls of a hexagonal pipe. One approach is to use a fluid coupling medium.

Cylindrical tube reactors with transducers directly bonded to the outer surface have been developed by a number of groups. The Battelle resonating pipe is 6 in. in diameter, operates at 25 kHz, and has been used for the degassing of oils. The cylindrical reactor (see Figure 6.26) developed at the University of Milan has a central core through which a coolant can be passed. In this system, a cooling pipe is placed in the focal region of acoustic energy and this acts as both a temperature control and a coaxial reflector of the sound waves. The reactor volume is then the annular space between the resonating pipe and the cooling core. As shown in Figure 6.29, the cylindrical pipe reactor can be a polygon-type reactor. In this type of reactor, the diameter of the cylindrical tube inside the outer hexagonal tube (on whose surfaces the transducers are physically bonded) has certain dimensional limitations. However, a tube with a much larger diameter can be used, surrounded by an outer tube and a coupling fluid through which ultrasound energy is supplied to the system. Thus very large throughputs can be handled without any blockage. Also, the coupling fluid can be circulated in this case and thus used for cooling. In

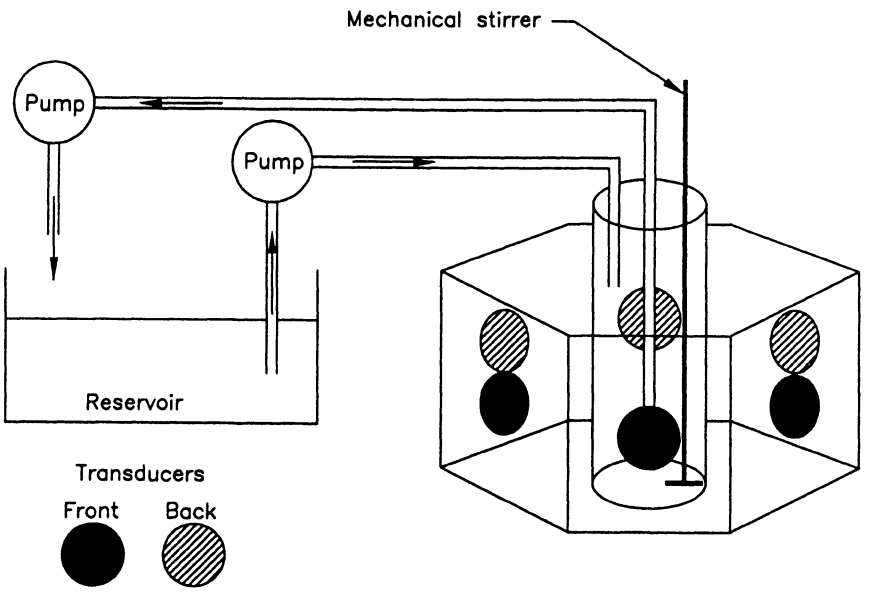

Figure 6.29. Hexagonal cross-section sonicator. (From A. B. Pandit and V. S. Moholkar, "Harness cavitation to improve processing," *Chem. Eng. Prog.* (July 1996), 57–67. Reproduced with permission of the American Institute of Chemical Engineers. Copyright © 1996 AIChE. All rights reserved.)

this type of system, the engineering problems of bonding the piezoelectric transducer to the pipe surface are eased because each of the six faces of the pipe is flat. Potential applications include ultrasonic pasteurization, crystallization, degassing, dispersion, and emulsification.

Branson Sonochemical Reactor. The Branson sonochemical reactor (see Figure 6.30) provides a simple solution to the problem of vibrating pipe walls. This modular system is made up of units that consist of a pair of 20-kHz probe-type sonicators (each 1800 W) mounted on either side of a pipe containing the reaction mixture. The ultrasonic energy from these transducers is coupled to the pipe by means of a fluid that can be used in batch or continuous mode. As with all probe-based designs, this system suffers from erosion of the horn tip and in the long run may incur expensive downtime for repair and replacement. In addition, the flat transducer is mounted on a curved surface and therefore coupling is not ideal. The acoustic wave may form a standing wave pattern in the tube; thus the length of the tube must be such that the ends are at an antinode of the sound wave length in the unit.

The Vibrating Tray. This device was first designed by Lewis Corporation and is similar in operation to a bath system for processing of coal or metal ores (see Figure 6.31). The block of transducers is bonded to the lower surface of the tray and vibrations are transmitted along its length. The tray assembly must be suspended on plastic supports so that the ultrasonic vibrations are not absorbed through the

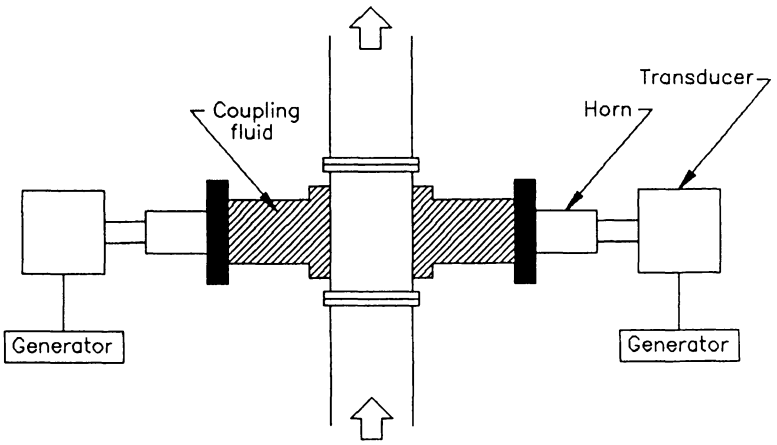

Figure 6.30. Branson sonochemical reactor. (From A. B. Pandit and V. S. Moholkar, "Harness cavitation to improve processing," *Chem. Eng. Prog.* (July 1996), 57–67. Reproduced with permission of the American Institute of Chemical Engineers. Copyright © 1996 AIChE. All rights reserved.)

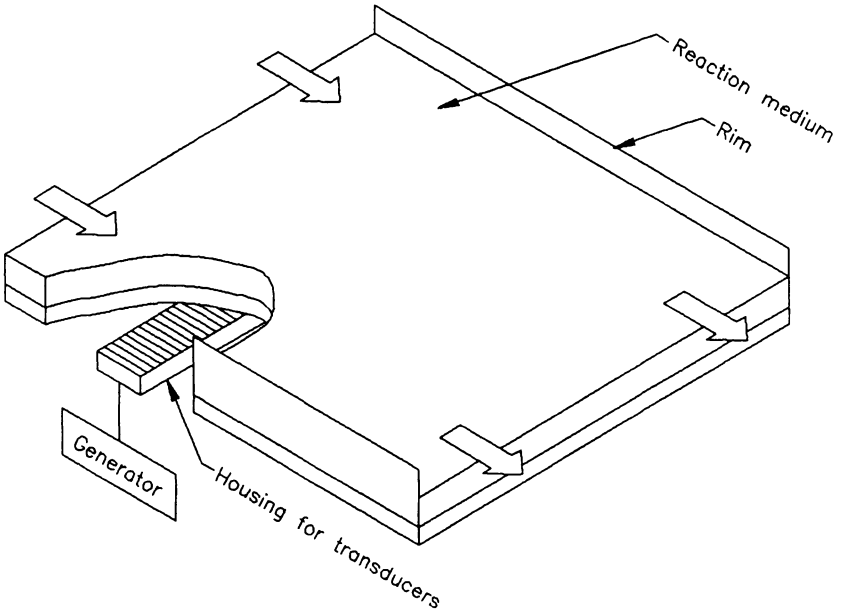

Figure 6.31. The vibrating tray. (From A. B. Pandit and V. S. Moholkar, "Harness cavitation to improve processing," *Chem. Eng. Prog.* (July 1996), 57–67. Reproduced with permission of the American Institute of Chemical Engineers. Copyright © 1996 AIChE. All rights reserved.)

medium. The vibrating tray is generally used in open-air conditions and can be used for large-scale operations as well. It is extremely robust.

Novel Sonochemical Reactors. There have been a number of novel developments in the design of sonochemical reactors, some of which might be considered spinoffs from the ultrasonic cleaning industry. Four new types are discussed below, the first three of which can basically be classified as potential components for a tube reactor system.

Telsonic Tubular Resonator (Switzerland). This consists of a hollow, gas-filled tube sealed at one end and driven at the other by a standard piezotransducer [Figure 6.32(a)]. This device looks like a conventional probe system, but is significantly different in that the sealed end is at a null point and the ultrasound is emitted radially at half-wavelength distances along its length. There is the potential to unblock the end and use the system as a flow tube. Since it was designed and marketed for cleaning, there is currently no information on its potential for chemical applications.

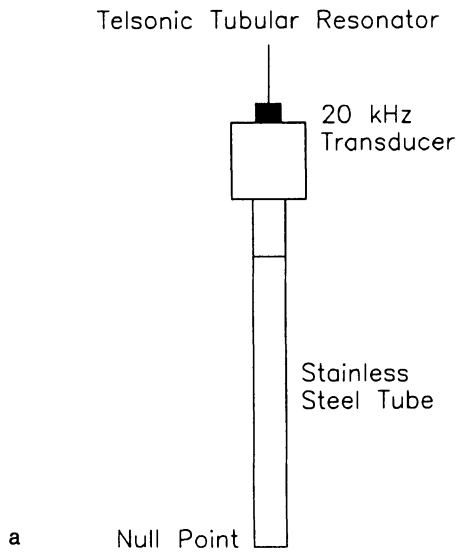

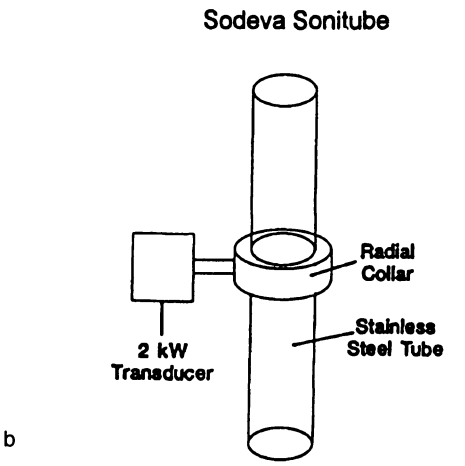

Figure 6.32. Novel sonochemical reactors. (From A. B. Pandit and V. S. Moholkar, "Harness cavitation to improve processing," *Chem. Eng. Prog.* (July 1996), 57–67. Reproduced with permission of the American Institute of Chemical Engineers. Copyright © 1996 AIChE. All rights reserved.) (a) Telsonic tubular resonator. (b) Sodera Sonitubi. (c) Martin Walter push-pull. (d) Undatim ortho reactor. (From Mason, 1992, with permission.)

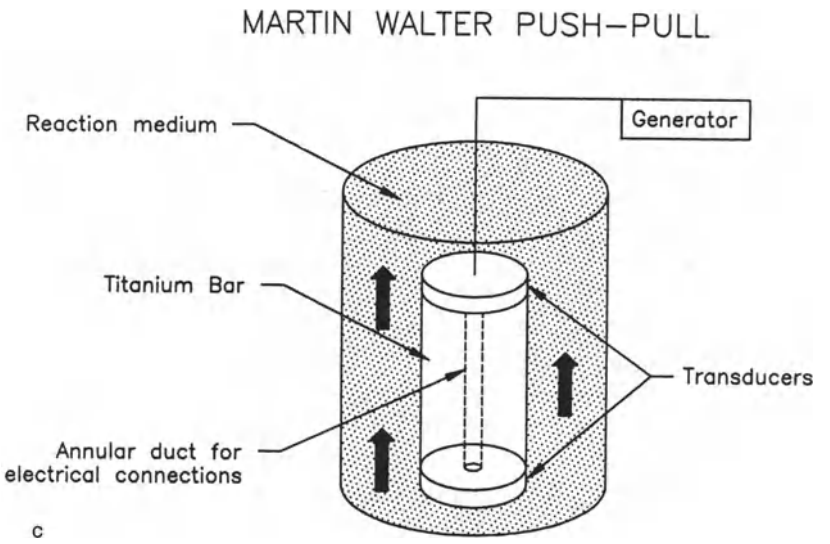

Undatim Orthoreactor

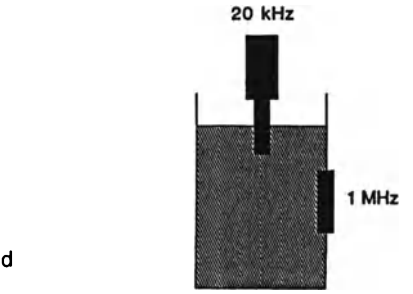

Figure 6.32. (cont.)

Sodeva Sonitube (France). This is also a radially emitting hollow tube, but the tube is open ended and the method for ultrasonic input is somewhat different. In this design, a transducer horn system is coupled directly to an annular collar, which acts as a cylindrical resonator [see Figure 6.32(b)]. The collar is screw fitted to take one or two stainless steel pipes accurately machined so that the remote end is a null point and may be further coupled to other pipework. At an operating length of 1.2 m and an internal tube diameter of 42 mm, the unit can be driven at 2 kW per 1.2 m with 80% efficiency. The maximum resonance power then operates on the flowing

liquid at half-wavelength distances along the tube. An advantage of both this system and that of Telsonic is that when the steel tubing becomes eroded it can be easily replaced.

Martin Walter Push–Pull (Germany). This reactor [see Figure 6.32(c)] consists of a cylindrical bar of titanium (cut to a precise number of half-wavelengths of sound) with opposite piezoelectric transducers banded to each end and connected through a center hole. Because of the combined oscillations of the transducers, the metal bar expands and contracts up to half of the wavelength of the sound in the material. This is called the *concertina effect.*

The major advantage of this system is that it can be retrofitted coaxially in an existing pipe network. The efficiency of the system can be increased by coupling it with a tube reactor operating at a different frequency, thus giving an enhanced sonication to annular flow.

Such ultrasonic options, however, pose a number of problems related to effective scaleup and industrial implementation. In particular, few data are available to the designer for an effective scaleup. In addition, the severe erosion encountered during operation can only be overcome by using titanium or nickel alloys as construction materials. This obviously adversely affects the economics of scaleup.

Undatim Orthoreactor (Belgium). The principle of operation for this device originates from some studies published by Margulis in the Russian literature Margulis (1969, 1974, 1975a, 1975b, 1976a, 1976b, 1976c, 1976d, 1980, 1981, 1985) and developed by Undatim in Belgium. In a small reactor, two ultrasonic fields are introduced at right angles to each other [Figure 6.32(d)]. The transducer operating in the megahertz range generates an ultrasonic field that gives efficient mass transfer. This field also enhances the cavitational effects produced by the higher energy transducer operating in the kilohertz range. The principle of combining orthogonal irradiation at different frequencies promises significant improvements over irradiation at a single frequency.

Reactors Using Frequencies Outside Ultrasound Power. The wavelength of sound in a material is governed by the frequency and the velocity of sound in that material. Consider the consequences of using different sound frequencies on reactor design. The transducers employing the higher frequency are much smaller. Unfortunately such devices would provide far less power and penetration than those in the kilohertz range. For small-volume treatment, however, it is possible to focus the acoustic energy by using a transducer with a concave emitting face and provide a localized high-energy region. Chemically the reactions at 1 MHz would be expected to generate shorter-lived bubbles, giving more radical diffusion into the bulk liquid. There would be more efficient mass transfer to surfaces and less erosion damage.

Since sonochemistry is connected with cavitation, one should consider any sound frequency that engenders cavitation. Perhaps this precludes frequencies above 20 MHz, beyond which it is thought that cavitation cannot occur, although this range can be of interest in terms of acoustic streaming and mass transport. In cavitation terms, however, only the audible sound range should be mainly considered. It is quite clear that one of the most important parameters that change as the frequency is reduced is the elongation in resonant wavelength in a metal bar. This can be used to advantage in the case of 200-Hz (audible) sound transmitted through steel. In this case one might imagine the simplest concept for scaleup—a giant probe system with a 12-m bar of steel as the horn. Although the whole device may be enormous, there is a mechanical benefit from the large- (6 mm) amplitude vibration at the tip. Such a giant probe system can be used in large-scale applications such as grinding of ores or sawing. When applied to sonochemical processes, the immediate possibilities include large-scale mixing and the destruction of hazardous waste.

In the case of infrasound frequencies, the resonance lengths become unmanageably long—for 20 Hz in titanium it is 127 m. Here we can take another approach and utilize a short length (say 10 cm) of metal rod, which will behave like a piston when subjected to a vibration at this frequency. Such a device has been described by Margulis (1985b), with the piston driving into a reaction mixture contained in a tube. The system is sealed through a plastic collar that transmits the vibrations. The net result of an infrasound energy input is the generation of large deformed bubbles with diameters approximately 1 cm across. These have been shown to fragment with the emission of sonoluminescence. Although the sonochemistry for such a system has not yet been widely researched, the scaleup potential is clear, particularly for processes involving mixing.

Powerful transducers suitable for this application are currently being used in the metallurgical industry to dramatically assist in the cold drawing of metal pipes. Sonication of the dye used permits a lower number of passes to be used for diameter reduction and significantly reduces the power required to draw a tube through it. The engineering problems associated with the construction of such tube reactors constructed using this principle have already been solved and so the transfer of this technology to a chemical plant should be straightforward.

Loop or Recycle Reactor. The size of the cavitation reaction zone is limited in both gas–liquid and gas–liquid–solid systems. Therefore, in scaling up batch reactors for industrial applications, some form of two-zone layout can be very appropriate. Practically, this will take the form of an internal or external loop reactor: This type of reactor can also be suitable for continuous flow schemes if it is operated in a "feed and bleed" mode.

The use of a loop or a recycle reactor (Figure 6.33) has a number of advantages: the problem of penetration range is overcome; the residence time of reagents in the actively insonated part can be controlled; and a modular approach can be taken to

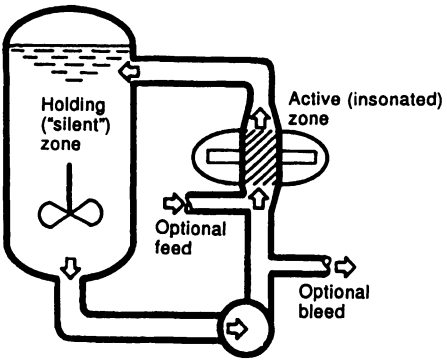

Figure 6.33. Loop reactor for sonochemistry. (From Mason, 1992 and Martin and Ward, 1992, with permission.)

the design, installation, and maintenance of the power ultrasound module, which can also be used alone in the laboratory if so desired.

A number of questions, however, need to be addressed in the design of such a recycle or loop reactor. The effects of the volume ratio between the cavitated and "silent" parts on the performance of the entire reactor loop need to be established. The effect of recirculation flow rate or the effects of the relative and absolute residence times in the cavitated zone need to be evaluated. With regard to the cavitation reactor chamber, the main design issue is the operation and performance of instrumentation for the cavitation, which may be multiple transducers for acoustic cavitation (it can also be multiple orifices in hydrodynamic cavitation, or multiple lasers for optical cavitation if the concept is applied to these types of cavitation). However, serious consideration needs to be given also to maintainability, as well as to the potential acoustic and flammability hazards of industrial operation.

In a loop reactor in which the reagents are recirculated, it is apparent that the benefits of insonation will be reduced as the relative volume of the silent zone increases with respect to that of the insonated zone. The modular design of the insonator makes scaleup straightforward, but the challenge is to achieve real economies of scale by maximizing the effectiveness of the insonated zone. The best results can be obtained in the following circumstances:

- The residence time of the limiting reagent in the insonated zone is optimized by control of flow rate.
- The limiting reagent, such as the solid in a heterogeneous reaction, is retained in and around the insonated zone; thus the limiting reagent is continuously insonated or at least its effective residence time is much greater than for the

other reagents. This strategy has been successful in the case of the Barbier reaction, where the lithium reagent can be retained in a cage within the insonated zone.

- One or more of the reagents remains activated for a period of time after it has passed through the insonation zone, or that is to say, it retains a "memory" of insonation. The memory effect on reactor performance is discussed further in Chapter 7.

One of the important scaleup parameters for the loop reactor is the relationship between the power distribution or intensity, measured in units of power flux, and the total power effectively deposited (i.e., the power that generates cavities) in a given volume. This subject for the loop reactor is discussed in Chapter 8. While this discussion is restricted to acoustic cavitation, in general, the concept of a loop reactor can be applied to other types of cavitation reactors.

Harwell Ultrasonic Reactor. Harwell Laboratories in Didcot, UK have developed a flow reactor (see Figure 6.34) that is capable of generating high intensities

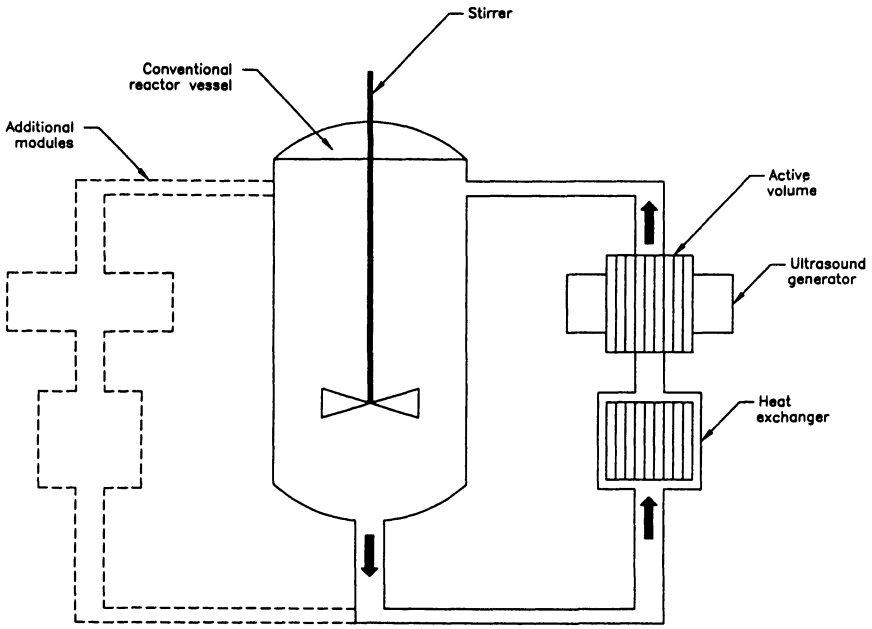

Figure 6.34. Harwell sonochemical reactor. (From A. B. Pandit and V. S. Moholkar, "Harness cavitation to improve processing," *Chem. Eng. Prog.* (July 1996), 57–67. Reproduced with permission of the American Institute of Chemical Engineers. Copyright © 1996 AIChE. All rights reserved.)

with a power rating up to 1500 W. This reactor is supposed to create no cavitational damage to the walls while providing high-energy insonation to the contained material. It can be used as a static unit (up to 4-liter capacity) for trial, but can be easily incorporated in a flow loop handling 230 liters/h. If the reaction itself requires less residence time, higher throughput may be possible. Reported results indicate that increasing its size provides a significant improvement in the efficiency of this reactor. Its advantages are

- Although the problem of localization of acoustic energy exists, because the reaction zone in this case is surrounded by transducers, irradiation of the reactions from several directions can remove this problem.
- Good control of residence time in the cavitation zone can be achieved by pump loop action.
- It is relatively simple to retrofit to existing conventional reactors.
- Scaleup is straightforward because of the modularity of the active region.

6.3f. Qualitative Considerations for Reactor Choice, Scaleup, and Optimization

When deciding on the type of the reactor required for a particular chemical process, the first question that must be addressed is whether the cavitation enhancement is the result of an improved mechanical process (due to enhanced mixing). If this is the case, then cavitation pretreatment of a slurry may be all that is required before the reacting system is subjected to a conventional-type reaction and the scaleup of the pretreatment vessel would be a relatively simple task.

If, however, the effect is truly based on cavitation chemistry, then cavitation must be provided during the reaction itself. The scientific database from the laboratory study should typically provide the parametric window found to be most effective at the laboratory scale and the cause-and-effect relationships between the ultrasonic parameters and the observed results. The first step is to try to understand the mechanisms of interaction from the observed phenomena so that the desired cavitation field can be created on a larger scale to promote similar interactions. The important scaleup consideration is then to establish the optimum conditions for the reaction in terms of the variables that influence cavitation. In this analysis, the nature of the reaction will also have an impact on the suitability of the given reactor.

Both chemical and physical properties of the reaction medium will dictate the required level of the cavitation power. High-viscosity media with low vapor pressure will require higher energy to produce cavitation. The presence of entrained or evolved gases will facilitate cavitation, as will the presence or generation of solid particles. External parameters such as those listed in Table 6.10 are important when attempting to optimize the reaction conditions. The effect of overpressure on a reaction has been investigated by Crum (1980) and Crum and Hansen (1982), and

TABLE 6.10. Factors that Influence Cavitation[a]

Viscosity and vapor pressure of the medium
Presence of gases or solid particles
Overpressure
Reaction temperature
Cavitation number or acoustic power and frequency
Size and geometry of chemical reactor

[a]From Mason and Berlan (1992) with permission.

the influences of reaction temperature and applied power are reported by Luche (1991, 1992a, 1998). For many years frequency was not thought to be influential in cavitation chemistry; however, the use of 500-KHz irradiation has significantly greater effect on the generation of hydrogen peroxide from water than 20 kHz (Luche 1987, 1991, 1992b, 1998; Luche *et al.* 1983, 1984, 1989). In addition, the size and the geometry of the chemical reactor will affect the efficiency of the cavitation process.

Besides the factors outlined in Table 6.10, an efficient coupling of the acoustic energy to the material that will provide a transmission path for the ultrasonic energy is also very important. This is usually a major step and requires a thorough understanding of the nature of high-frequency elastic wave propagation and radiation from pipe, plate, or channel-shaped chemical reactors. The important factors that need to be analyzed are

- mechanisms of cavitation and their interaction with reactor material
- high-frequency wave propagation in structures
- acoustic coupling and mode of excitation
- transducers and power generator technology
- integration of ultrasonics into the process system

While the above knowledge base is difficult to quantify, it is essential for the successful development of reliable and predictable large-scale cavitation conversion technology.

Both continuous and batch processes are used in commercial scale. For high throughput, continuous processes are usually more desirable. However, a batch process is often selected in cases where:

The residence time is relatively long.
There is a need for more precise control of the ingredients.
Backmixing is not desirable.

Several different products are made in essentially the same setup.
Production volume is relatively small and a continuous process is not economic.

The challenges associated with coupling acoustic energy to a batch or a continuous process depends to a great extent on the size and the geometry of the reactors. When the size of the reactor or structure is not very large compared with the wavelength of a desirable mode of ultrasound in that structure, it is usually possible to integrate the acoustic source with the reactor. However, temperatures above 200°C, cooling or heating jackets, and extremely corrosive conditions that may limit additional stress due to acoustic vibration are some of the conditions that continue to be challenges to successful integration of ultrasonic energy into the material to be processed.

Intense levels of acoustic energy can be generated in a cylinder, a channel, or a platelike structure. Cylindrical acoustic reactors have been designed for sizes ranging from 50 to 250 mm. Channel or platetypes of acoustic applicators can be designed for a wide range of cross-sections of dimensions, typically between 50 and 1000 mm. Several of the structures could be coupled either in series or parallel to handle longer residence times or higher throughput, respectively. The acoustic intensity levels and the intensity profiles in the working volume can be controlled to promote desirable effects, e.g., cavitation, nonlinear oscillations of microbubbles, degassing, agglomeration of particles, shear thinning, dispersion, compaction, and microstreaming.

The choice of acoustic transducers and generators depends on the frequencies, intensity levels, and the intensity distribution desired to promote the expected benefits. Both piezoelectric and magnetostrictive transducers have potential applications, depending on the environment, e.g., temperature, pressure, or wet or dry. Acoustic power generators with a delivery capacity up to 30 kW are commercially available. If more power is necessary, several of these generators can be operated in parallel. Prudent and judicious integration of the acoustic system with the process system is a major step toward scaleup. There are many challenges associated with this and the key step is to integrate the emerging technologies of acoustic energy conversion, coupling them to structures and controlling the energy profile for effective and efficient interaction.

6.4. LASER CAVITATION REACTORS

High light intensities are needed to produce cavities in liquids. This can be achieved using ruby, a neodymium glass laser, or any other laser used in nuclear fusion studies, provided the liquid under study is transparent enough for the wavelength of the laser. A typical laboratory experimental setup for a laser cavitation reactor is shown in Figure 6.35. In a study by Lauterborn (1980a), a single-stage

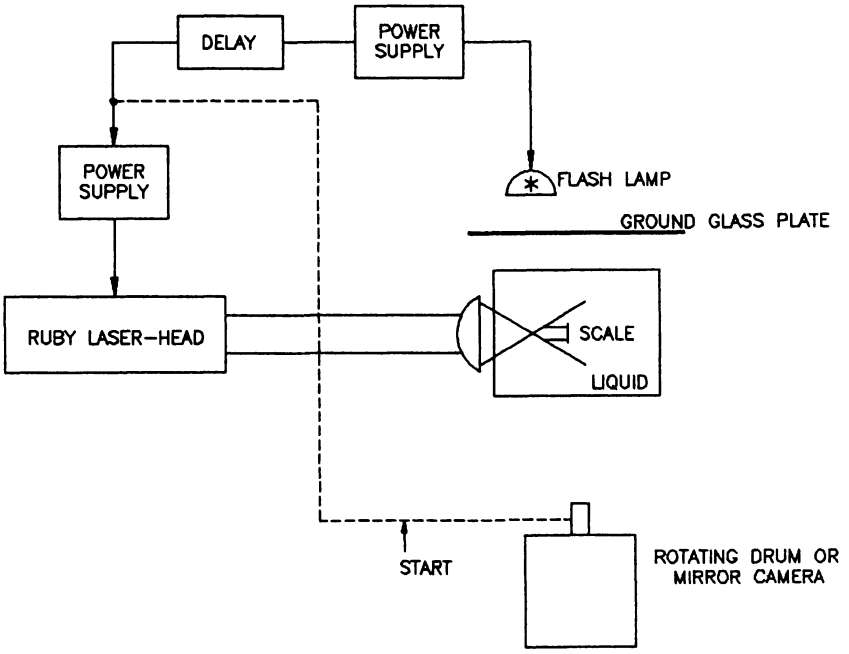

Figure 6.35. Block diagram of experimental setup. (Reproduced from W. Lauterborn, "Cavitation and coherent optics in underwater acoustics," *Cavitation and Inhomogeneities in Underwater Acoustics*, pp. 3–12, Springer-Verlag, New York, 1980, with permission.)

ruby was Q-switched by a Kerr cell and delivered light pulses of up to 1 J total energy at a pulse duration of about 30 to 50 ns. The beam diameter was about 1 cm. The light was focused into the liquid (mostly water) with a single lens of short focal length (44 mm when submerged in water). The cavity or the cavities appeared at, or in the vicinity of, the focal point. They were diffusely illuminated by a flash lamp through a ground-glass plate and photographed by a Beckman–Whitley model 330 rotating mirror camera that allowed framing rates of up to a million frames/s. This apparatus was used to examine cavity oscillations in the bulk of the liquid (water and silicon oil), cavity dynamics near plane boundaries and at air/liquid interfaces, and the dynamics of the interacting cavities (Lauterborn, 1972, 1973, 1974, 1976, 1977; Lauterborn and Bolle, 1975, 1977). The investigations showed that one peculiar dynamic feature, namely jet formation, pervades all dynamics.

Holography can be used to achieve multiple breakdowns in a liquid for cavity interaction studies. Such studies are of great importance in connection with noise emission and erosion problems in both hydrodynamic and acoustic cavitations. In

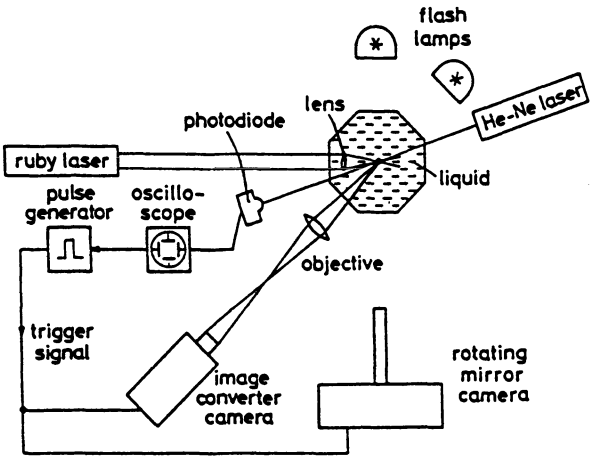

Figure 6.36. Block diagram of the experimental setup for high-speed photography of laser-induced cavities with triggering from the cavity itself. (Reproduced from W. Lauterborn, "Cavitation and coherent optics in underwater acoustics," *Cavitation and Inhomogeneities in Underwater Acoustics*, pp. 3–12, Springer-Verlag, New York, 1980, with permission.); also shown in Lauterborn (1977).

order to examine cavity interaction dynamics, reproducible cavity configurations are needed. It seems that laser cavitation is the only method that allows complex investigations of this kind. The holographic method illustrated in Figure 6.36 is appealing because the experimental setup is simple. Only the focusing lens in Figure 6.37 is replaced by an appropriate hologram, which is in this case is also called a *holographic lens*. Such a lens can be regarded as a generalization of a usual lens because the incoming light beam is focused into different points in space. This method for generating multiple cavities requires the use of phase holograms

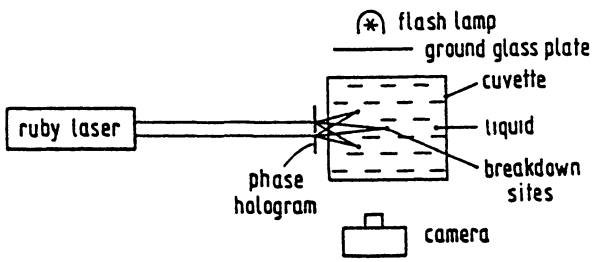

Figure 6.37. Setup for multiple cavity generation in liquids by holographic focusing. (Reproduced from W. Hentschel and N. Lauterborn (1980). "Holographic generation of multi-bubble systems," in *Cavitation and Inhomogeneities in Underwater Acoustics*, N. Lauterborn (ed.), pp. 47–53, Springer-Verlag, New York, with permission.)

because of high light intensities. The method has been used to examine multiple cavities in water and silicon oil (Lauterborn, 1980a).

6.5. SOME ADDITIONAL CONSIDERATIONS FOR FLOW REACTORS

Mason (1991) and Pandit and Moholkar (1996) have given excellent state-of-the-art reviews on the operation of the flow systems. Some general thoughts on the large-scale flow systems can be summarized as follows:

1. For gas–liquid or gas–liquid–liquid systems that require a large interfacial area, one should consider the use of low-intensity liquid whistles. These are used in the industry as emulsifiers, but they can also be used as a flow system.

2. As indicated above, a variety of cleaning baths are available that can be adapted to flow systems. For example, a reaction vessel immersed in a cleaning bath can be operated in flow mode. Alternatively, external transducers can be attached to the walls of the reactors. While this configuration allows the use of high temperatures and pressures, only low-intensity ultrasound can be provided to the vessel contents.

3. The region in which cavitation occurs is important in the design of a large-scale reactor. Good acoustic cavitation is normally observed up to a few centimeters from the wall of the transducer. Furthermore, cavitation damage to the reactor wall is not desirable. Because of these reasons, a recycle or loop flow reactor provides an attractive alternative when only part of the liquid content is being cavitated at any given time.

4. A cavitation section of a loop or a straight flow reactor generally takes the form of a tube. As shown earlier, the simplest of these is a standard pipe with ultrasonic probes inserted through T-joints at intervals. The main problems with this kind of sonicator are the tip erosion and uniform distribution of cavitation. In the Bronson sonochemical reactor, a coupling fluid is used in conjunction with the horns; the coupling fluid is chosen in such a way that it does not cavitate, but merely transmits energy to the wall.

5. Transducers generally do not make good contact with the curvature of a pipe. To overcome this problem, both pentagonal and hexagonal pipes have been employed. Here the energy can be focused without severe cavitation damage to the wall. However, the energy is focused near the center line and less cavitation occurs near the walls. Thus the uniformity of the cavitation cannot be ensured.

6. Tube reactors can also be modified in two different ways. In one case there are two coaxial tubes in which the reaction mixture is passed through the inner tube, whereas the coupling fluid (noncavitating) is passed through the outer one. In the second configuration, the coolant can be passed through the inner tube and the reagent passed through the outer one. In each case the transducers are mounted in the outer tubes; solids can also be handled by such reactors.

6.6. HEALTH AND SAFETY ASPECTS OF LABORATORY REACTORS

Generally, hydrodynamically produced cavitation is safe and does not create noise of any consequence. If the flow rates are very high, however, the noise of the pump may be a problem. Care must also be taken if the operation requires either high pressure or slurry. In these cases, safe operation of the pumps needs attention. Cavitation effects produced during the sonication of a liquid sample generate a wide spectrum of noise (Figure 6.38). This noise is radiated into the atmosphere and consideration must therefore be given to the health and safety aspects associated with the use of ultrasound. Laser cavitation will require careful monitoring of the laser beams, particularly if multiple cavities are required.

There are two ways of guarding against radiated noise: acoustic earmuffs or an acoustic screen around the apparatus. The second solution would take the form of a box lined with a proprietary sound-absorbing material. This approach can be used also for a high-flow hydrodynamic cavitation process. For acoustic cavitation, the transducer and treatment sample would be housed within the box. A 6-mm thick Perspex door would permit observation of the sonication process. A well-fitted door is essential to reduce the noise leakage. Noise levels in excess of 100 dBa would not be uncommon at a distance of 1 m when processing small samples at 20 kHz without acoustic screening. It is certainly possible to reduce these levels to 75 dB by a well-designed screening box. For hydrodynamic cavitation, similarly the entire unit (i.e., pump, cavitation chamber, and associated pipelines) can be enclosed in a soundproofed box.

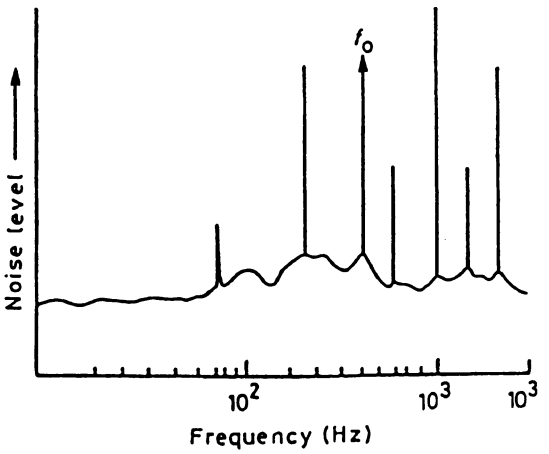

Figure 6.38. Cavitation noise spectrum. (From Mason, 1996, with permission. Redrawn from R. Esche, *Acustica* 2, Akus Beih, 1952.)

6.7. INTEGRATION OF CAVITATION INTO EXISTING SCALED-UP PROCESSES

Industrial chemists have become interested in using cavitation to enhance their chemical processes because it has the potential to make considerable economic savings during production. In addition to the obvious chemical benefits, such as increased rate of reaction, improved yield, the switching of reaction pathways, and the induction of new reactions, there are a number of process benefits for the manufacturer. These include

- milder operating conditions; lower operating temperatures and pressures mean less product degradation and lower capital investment
- easier process control; hydrodynamic cavitation can be controlled by bypassing the cavitation chamber; "on-off" control of the ultrasound means that the effects of the ultrasound can be easily controlled and laser cavitation can be easily switched off if desired
- lower purity feedstocks
- smaller batch sizes
- increased throughput

These process benefits depend on the nature of the reaction and the requirement of the intensity of the cavitation. Hydrodynamic cavitation will require lower energy consumption, but it will also be in general less effective in process improvement. Acoustic cavitation will be more effective, but it will usually require an ultrasonic intensity greater than 50 W cm^{-2}. Laser cavitation will be extremely energy intensive and can be justified only in very special cases.

6.8. CONCLUDING REMARKS

In this chapter we briefly described various types of laboratory as well as commercial-size cavitation reactors. Hydrodynamic cavitation reactors are perhaps easiest to scale up; however, in these reactors intensities are low and therefore conversion will also be low. A commercial unit of any size in this case should be possible. If necessary, a number of modules can be operated in parallel. The acoustic reactors can be operated at laboratory as well as commercial scale. The scaleup in this case is much more difficult. The feasibility as well as the reliability of a large-scale operation depends on the operability and the life of the transducers. Longer lasting transducers will enhance the commercial viability of the cavitation conversion process. The laser cavitation reactors are largely used to examine the behavior of cavities or the kinetics of the cavitation conversion process under controlled operating conditions. At present they are too expensive for the commercial operations.

7

MODELS FOR CAVITATION REACTORS

7.1. INTRODUCTION

In Chapter 6 we evaluated various types of hydrodynamic, acoustic, and laser cavitation reactors used in laboratory as well as pilot and commercial-scale operations. These reactors and the associated technologies available for the generation of cavities (by hydrodynamic, acoustic, or laser means) indicate the feasibility of the cavitation conversion processes. While there are many problems that need to be solved, in principle the chapter demonstrated the feasibility of cavitation reaction engineering technology.

In this chapter we address the issues dealing with the reliability, predictability, scaleup, and optimization of cavitation reactor performance. Generally, this is achieved by developing a suitable model for the reactor. Because of the complex nature of the cavitation conversion process, the development of a generalized reactor model is a very difficult task and as yet has not been achieved. At the very best, a model can be developed for a specific reaction process, although this will also require appropriate simplifying assumptions for both the chemistry and the physics of the process. In general, the development of a cavitation reactor model will require the following steps:

1. Development of an intrinsic kinetic model for the reaction. As shown later, the reactions occur both in the cavities and in the surrounding liquid film. Both of them have to be appropriately accounted for to develop a generalized kinetic model for the reaction system.
2. Characterization and modeling of cavity distribution as a function of time and energy input. The model must also include the mechanism of cavity collapse and the energy released to induce a chemical reaction.
3. Steps 1 and 2 need to be suitably combined to develop a model that also includes the energy input to generate the cavities. The model can then be used not only to predict the reactor performance under various system conditions

but also to give guidelines for the appropriate reactor scaleup and optimization.

In order to achieve what is outlined in the above three steps, a considerable amount of experimental work is needed. Once it has been established in the laboratory that the desired physical and chemical changes take place through cavitation chemistry, the laboratory tests should include complete characterization of the hydrodynamic, acoustic, or laser equipment used in the study, i.e., hydrodynamic, electrical, or optical power consumed; actual power dissipated; number and size of the cavities generated and collapsed; likely pressure pulses generated in the hydrodynamic, acoustic, or laser equipment for the chosen driving pressure recovery rate or frequency; and the likely chemistry associated with it.

The important results to be expected from a laboratory study are the kinetic rate constants for various reactions as a function of net energy input. An analysis of the rate of product formation is an essential step. The model should emphasize a quantitative relationship between the reactor performance and various scaleup parameters. The model should also include the characterization of the cavitating conditions existing in the laboratory test rig and an exploration of the possibility of generating similar cavitating conditions by means other than sonication, i.e., hydrodynamic, spark gap discharge, laser, or particle-induced cavitation.

The reaction paths and associated kinetics for a variety of gas–liquid and gas–liquid–solid cavitation reactions were discussed in Chapters 4 and 5. Here we examine a few models for cavitation reactors. We first examine an approach proposed by Prasad–Naidu *et al.* (1994) for the gas–liquid cavitation reactor. While this approach is complex, the concept is applicable to a variety of cavitation reactions. We then examine methods of identifying the distribution of cavities and their collapse. These methods will be particularly important in an assessment of cavity distribution and the reaction zone in reactors of various scales. We then examine a pseudo-empirical method, namely, the cavitation yield model, that can be used to predict and scaleup reactor performance under the same energy requirements. The model can also indicate the energy efficiency of various cavitation conversion processes. Finally, we briefly evaluate the effect of "retained activation" on the performance of a loop or recycle reactor. This memory effect presents a special issue in any modeling effort involving a recycled reactor system.

7.2. GENERAL CONSIDERATIONS FOR A GAS–LIQUID CAVITATION REACTOR MODEL

A model for a gas–liquid cavitation reactor has to take into account the following processes: (1) the dynamics that lead to the high temperatures and pressures in the bubble to produce reactive intermediates as well as pyrolysis products, (2) the rate

at which the reaction products and other intermediates are released into the surrounding liquid medium, and (3) the rate at which the heat and mass transfer from bubble collapse are transferred into the surrounding liquid and the reactions between the transferred and produced intermediates and other species present in the liquid medium.

7.2a. Bubble Dynamics

The dynamics of a bubble are dominated by inertial forces since the Reynolds number for the flow is high. One can therefore use the Rayleigh–Plesset equation (see Chapter 2) for the purely radial motion of a bubble in inviscid liquids. The work done by the hydrodynamic or acoustic field goes toward increasing the kinetic energy of the liquid and toward doing work on the gas bubble. The assumption of an incompressible liquid becomes invalid toward the last stages of the bubble motion, and corrections for the compressibility of the liquid need to be incorporated. In general, the Rayleigh–Plesset equation can be integrated to find the radius of a bubble at any time, provided the initial velocity and bubble size are specified. The radius of the bubble increases as the acoustic pressure falls and should decrease as the pressure increases. The bubbles will not oscillate in this manner, but will collapse due to instabilities. Since the Rayleigh–Plesset equation cannot predict instabilities, a condition for the bubble collapse needs to be specified. Generally, it is assumed that the bubble collapses when the velocity of its wall reaches the velocity of sound in the surrounding liquid. Since this value of velocity is high and the bubble size is small, this assumption is generally considered to be reasonable.

With the above set of assumptions, Figure 7.1 shows a typical result obtained by integrating the bubble dynamics equation (Prasad-Naidu et al., 1994). For the conditions shown in the figure, the radius of the bubble slowly increases from 2 to about 40 μm in about 20 μs. After that, the bubble size decreases rapidly to 30 μm and from there instantaneously (in a microsecond) to about 2 μm and below. While the growth process is isothermal, the shrinkage is adiabatic. Three regimes—growth, oscillation, and collapse—that can be articulated from such a diagram are shown in Figure 7.2. Such bubble dynamics calculations form a basis for modeling cavitation reactors. The applications of these concepts to a batch gas–liquid cavitation reactor are described in Section 7.3. The reactions in a collapsing bubble occur in both the core and the liquid film surrounding the bubble core (see Figure 7.3). The nature of the reactions occurring in the core and the film is discussed below.

7.2b. Pyrolysis Reactions in the Bubble

The temperatures and pressures generated in a bubble during collapse are generally very high. Hydrodynamic cavitation involves a somewhat lower intensity

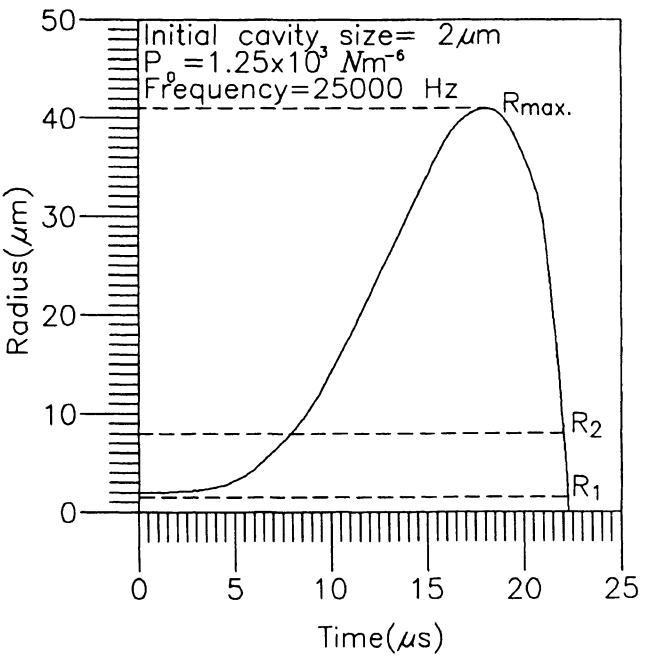

Figure 7.1. Radius of bubble during growth and collapse under sinusoidal pressure wave (initial cavity size = 2.0 μm, $P_s = 1.38 \times 10^5$ N/m^2 and frequency = 25,000 Hz) (Reprinted from *Chem. Eng. Sci.* **49**, D.V. Prasad–Naidu *et al.* "Modeling of a batch sonochemical reactor," pp. 877–888, copyright 1994, with permission from Elsevier Science.)

of energy release during bubble collapse and therefore comparatively lower temperatures and pressures at the point of collapse. Acoustic cavitation involves more intense energy release and thus can create plasma-level temperatures and pressures. Laser cavitation will similarly create very high temperatures and pressures. In modeling a cavitation reactor, it is important to include all pyrolysis reactions for the components present in the bubble. Sometimes an assumption of equilibrium at the final adiabatic temperature and pressure is made, but this is normally considered to be a restrictive assumption. The modeling process requires knowledge of the bubble composition at the point of collapse. Once again, the application of these concepts to two specific reactions is discussed in Section 7.3.

7.2c. Free Radical Reactions in the Liquid Film

When a bubble collapses, the content of the mass (which includes reactive species as well as products) and heat are released into the surrounding liquid. The bulk

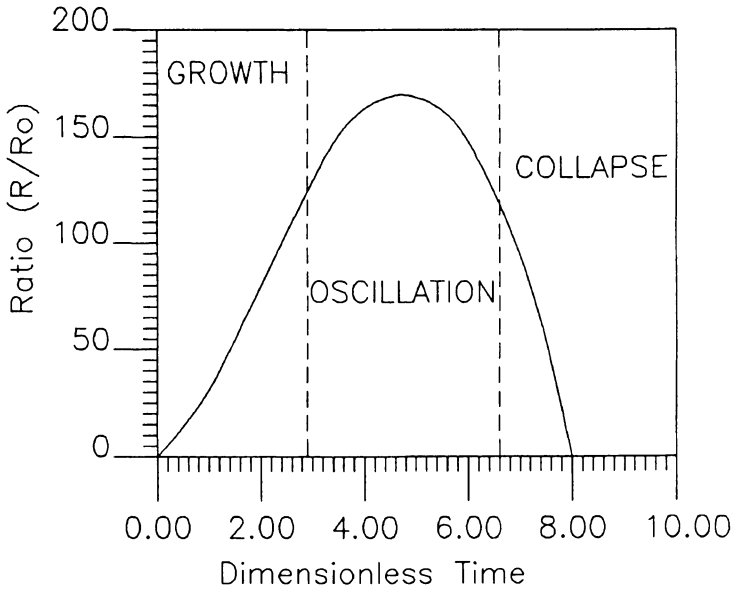

Figure 7.2. Radius history of bubble oscillation in sonic bath (description of various regimes).

liquid is generally assumed to be well mixed. While in reality mass and heat diffusion takes place in the liquid film surrounding the collapsing bubble, often it is assumed that the contents are instantaneously released into the surrounding liquid. This assumption is quite a drastic one because the fragments can cool and the composition could change. It is also possible that the reactive intermediates diffuse out of a bubble as they form. Generally, free radical reactions could occur in the film surrounding the collapsing bubble. If the assumption of instantaneous release is accepted, then the amounts of products released by the bubbles are the same as the amounts calculated to be present in the bubble before its fragmentation using a free energy minimization procedure (Anbar and Pecht, 1964b).

If the number of bubbles collapsing per unit volume per unit time, N, is known, the amount of reactive content being released per unit time per unit volume of the liquid is $N \times n_b$ where n_b is the amount of all products present in the collapsing bubble. The mass balances for these species and those present in the liquid can be easily written for a batch reactor. One can assume that the reactor is well mixed and hence the bubble contents released upon fragmentation are instantaneously mixed with the rest of the liquid. If the kinetics of these reactions are known, the model is then complete. Some details of the modeling of a batch acoustic reactor are given in the next section.

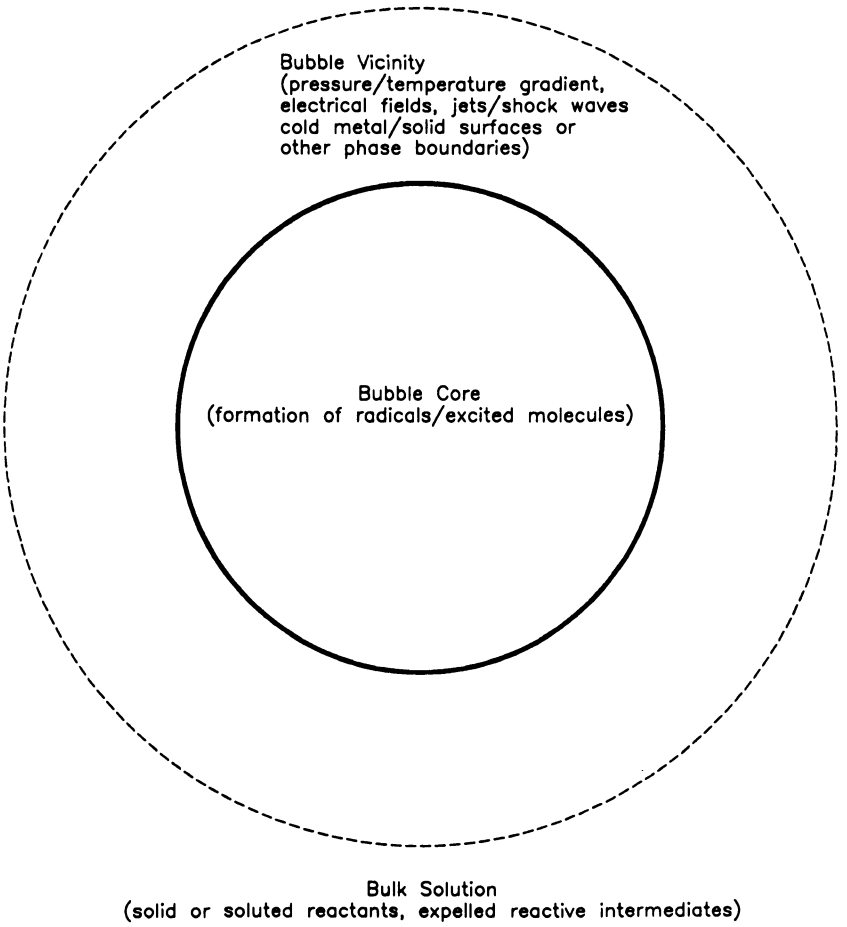

Figure 7.3. Reaction sites of a collapsing cavitation bubble. (Reprinted from *Chem. Eng. Sci.* **49**, D.V. Prasad–Naidu *et al.* "Modeling of a batch sonochemical reactor," pp. 877–888, copyright 1994, with permission from Elsevier Science.)

7.3. MODELLING A BATCH GAS–LIQUID ACOUSTIC REACTOR

A model for a gas–liquid reaction in a batch reactor has been developed by Prasad-Naidu *et al.* (1994). The reaction considered is the formation of I_2 from KI solution. When a solution of KI is sonicated in a cleaning bath or through an ultrasonic horn, measurable quantities of I_2 are liberated. While a number of investigators have qualitatively studied this reaction, the most comprehensive study has been conducted by Hart and Henglein (1985). They irradiated aqueous solutions

of KI in a batch reactor with 300 kHz ultrasound under argon, oxygen, and Ar–O_2 mixtures of varying composition. They found the products formed to be I_2 and H_2O_2. They also conducted experiments in the presence of ammonium molybdate which catalyzes the oxidation of the iodide ion by H_2O_2 to iodine. Their main findings with regard to formation of I_2 from KI are:

- The rate of liberation of iodine increases with KI concentrations, but for a given KI concentration it remains constant with time.
- Different rates of iodine formation are obtained when different gases such as N_2, O_2, and Ar are used.
- When mixtures of Ar and O_2 are used as dissolved gases in the KI solution, the reaction rate passes through a maximum at an intermediate composition. The model of Prasad-Naidu *et al.* (1994) tries to explain such results quantitatively according to the following general framework.

7.3a. Physical Description

The physical description of the cavitation process upon which the model is developed is as follows: The cavities undergo three stages: formation, growth, and collapse. The reactions take place in the well-stirred liquid during the collapse stage. The KI solution is assumed to have a large number of nuclei in the form of small bubbles or a gas entrapped in the crevices of the reactor wall. When the liquid medium is subjected to ultrasonication, these nuclei grow and collapse. Most of them grow and collapse as transient cavities if the frequencies employed are lower than 100 kHz (Arakeri and Chakraborty, 1990). These cavities grow and collapse in about one acoustic cycle. The actual phenomena of heat and mass transfer during the growth and collapse of a bubble are very complex. The authors have, therefore, used a simple analysis by Flynn (1964).

In this analysis, the entire growth phase and a part of the collapse phase are assumed to be isothermal whereas the rest of the collapse phase can be treated as adiabatic. The transition from isothermal to adiabatic during the collapse phase is assumed to occur when the internal gas pressure becomes equal to the vapor pressure of the liquid at the bulk temperature. The adiabatic collapse phase is assumed to end when the bubble wall velocity reaches the sonic velocity in the liquid medium. During the adiabatic collapse phase, the temperature and pressure inside the bubble increase due to compression, producing extreme conditions. This can result in the formation of free radicals from the water vapor and oxygen (if oxygen is present in the dissolved gas). Here the authors assume that at the end of the collapse phase the amounts of reactants, products, and free radicals present in the system can be calculated without considering the detailed kinetics of the reactions taking place in the gas phase.

The radicals released into the medium undergo several reactions, one of them being the oxidation of iodide ion. The mechanism of the mixing of these radicals in the liquid phase and their subsequent reactions are uncertain. Although the reactions are fast and may be controlled by the diffusion, the presence of microjets and shock waves creates significant mixing. Furthermore, upon collapse, a bubble may fragment and produce a number of bubbles. In the absence of a clear picture, the model assumed complete mixing in the vessel. Thus, the model involves the following set of assessments:

growth and collapse of the cavity
evaluation of temperature and pressure at the end of the collapse
calculation of equilibrium compositions in the gas phase at the end of the collapse phase
material balances for various species in the liquid phase in which the gas contents are assumed to mix instantaneously

7.3b. Model Equations and Analysis

Expansion and collapse are governed by the bubble dynamics equation, normally referred to as the Rayleigh–Plesset equation, and are given by Plesset (1949):

$$R\ddot{R} + 3/2\dot{R}^2 = 1/\rho_L[P_L - P_\infty] \tag{7.1}$$

The liquid pressure at the bubble surface is related to the inner pressure by

$$P_L(R) = P_i - \frac{2\sigma}{R} - \frac{4\mu}{R}\left(\frac{dR}{dt}\right) \tag{7.2}$$

Here P_i is the internal pressure of the bubble and is equal to $P_g + P_v$, the sum of the partial pressures of gas and vapor, respectively. Although the gas partial pressure changes inside the bubble as its radius changes, the amount inside the bubble remains the same. Hence

$$P_g = P_{g0}(R_0/R)^{3\alpha} \tag{7.3}$$

The external pressure is time varying and is characteristic of the acoustic field applied. Thus

$$P_\infty = P_b - P_a \sin\omega t \tag{7.4}$$

Substituting Eqs. (7.2), (7.3), and (7.4) in Eq. (7.1) and rearranging, we obtain

$$d^2R/dt^2 = 1/\rho_L[P_{g0}(R_0^{3\alpha}/R^{3\alpha+1}) + P_v/R - 2\sigma/R^2 -$$

$$- (P_b - P_a \sin\omega t)/R] - \frac{3}{2}(\dot{R})^2 \tag{7.5}$$

where $\dot{R}$ represents dR/dt.

Equation (7.5) indicates that the bubble dynamics equation depends on α, the value of which differs for isothermal and adiabatic phases. Thus, for the isothermal phase, we solve Eq. (7.5) with the following initial conditions and by setting $\alpha = 1$ and $P_v = P_s$.

$$\text{At } t = 0,\ R = R_0 \text{ and } \dot{R} = 0 \tag{7.6}$$

The end of this phase also means the beginning of the collapse phase. Following Flynn (1964), the collapse phase begins when P_g becomes equal to P_s. The value of the bubble radius R at the beginning of the collapse phase is readily calculated from P_s by

$$P_g = P_s = P_{g0}(R_0/R_2)^3 \tag{7.7}$$

During the second stage, no heat or mass transfer is permitted between the bubble and its surroundings. Therefore the pressure and volume of the bubble during this phase were related using the adiabatic gas laws. The bubble dynamics equation for $R < R_2$ becomes:

$$\frac{d^2R}{dt^2} = 1/\rho_L[2P_s(R_2^{3\alpha}/R^{3\alpha+1}) - 2\sigma/R^2 - (P_b - P_a \sin\omega t)/R] - \frac{3}{2}(\dot{R})^2 \tag{7.8}$$

The bubble collapse is assumed to end when the bubble wall velocity reaches the velocity of sound in the liquid medium. Its size then is denoted by R_f. The initial gas pressure P_{g0} is related to initial cavity size by

$$P_s + P_{g0} = P_b + 2\sigma/R_0 \tag{7.9}$$

The temperature and pressure at the end of collapse are calculated from R_2 and R_f as

$$T_f = T_2(R_2/R_1)^{3(\gamma-1)} \tag{7.10}$$

and

$$P_f = P_2(R_2/R_1)^{3\gamma} \tag{7.11}$$

Since the change in moles due to reactions in this case was found to be negligible (< 3%), the moles in the bubble are

$$n_w = 4/3\pi R_2^3 P_s / R_g T \tag{7.12}$$

Prasad–Naidu *et al.* (1994) calculated various parameters, such as γ and σ for appropriate compositions. They found the collapse temperatures to fall between approximately 2100 and 3200 K, whereas the pressures varied between 80 and 120 bar.

These temperature and pressure profiles were then used along with the bubble compositions (at R_2) to evaluate the equilibrium compositions at R_f. This was done by calculating the composition leading to the minimization of free energy, through the SOLGASMIX program (Eriksson, 1975). The program yields as output the equilibrium compositions and fugacities of various species for any given temperature, pressure, and input concentrations. The expected products are also provided, which in the case of water were H_2O, the constituents of the gas O_2,H, OH, and HO_2. The calculations showed significant formation of hydroxyl radicals ($\sim 10^{-3}$ mol of OH per mole of water).

The radicals provided by the SOLGASMIX program are released into the liquid phase, which is assumed to be well mixed. The reactions taking place in the liquid are given by Hart and Henglein (1985) as

$$2KI + 2OH \xrightarrow{k_1} 2KOH + I_2$$

$$OH + OH \xrightarrow{k_2} H_2O_2$$

$$2HO_2 + 2KI \xrightarrow{k_3} 2KOH + I_2 + O_2$$

$$HO_2 + HO_2 \xrightarrow{k_4} H_2O_2 + O_2$$

$$2O + 2I^- + 2K^+ 2H_2O \xrightarrow{k_5} I_2 + O_2 + 2KOH + H_2$$

If sonication is carried out in the presence of the catalyst ammonium molybdate, H_2O_2 can also oxidize the iodide as

$$H_2 + 2KI \rightarrow 2KOH + I_2$$

Based on this set of reactions, Prasad–Naidu *et al.* (1994) derived the following material balance equations:

$$\text{Hydroxyl radicals: } dC_A/dt = nC_A - k_2C_A^2 - k_1C_AC_B \tag{7.13}$$

$$\text{iodine: } dC_c/dt = \beta_1 k_1 C_A C_B + \beta_2 k_4 C_B C_D + \beta_3 k_5 C_B C_E \tag{7.14}$$

$$\text{Hydroperoxyl radicals: } dC_D/dt = nC_D - k_3C_D^2 - k_4C_DC_B \tag{7.15}$$

$$\text{Oxygen atoms: } dC_E/dt = nC_E - k_5C_EC_B \tag{7.16}$$

Equations (7.13) to (7.16) have some interesting implications. The rate at which the radicals are released into the liquid phase, or nC_i, reaches a steady state soon after sonication begins. Thus it is possible that concentration of radicals reaches a quasi-steady state, i.e., $d\overline{C}_i/dt = 0$. If simultaneously C_B is sufficiently large, it can be assumed to be constant during the experiment and therefore the rate of iodine liberation also reaches a quasi-steady state. Thus, the model can easily explain the key features of the findings by Hart and Henglein (1985).

The model requires the number of collapsing cavities per unit time. The authors have found this from experiments conducted with ammonium molybdate in which all OH goes into the formation of iodine. The n was found by them to be 2.6445×10^{10}/liter-s. They found the values of the rate constants by using the data with air as dissolved gas. Their predictions in the presence of air, nitrogen, and oxygen are compared with their data in Figures 7.4 and 7.5(a) and (b), respectively. As shown, the agreement is quite good. The most interesting feature of this model is its ability to predict the maximum when oxygen–argon mixtures are employed. These predictions, along with the data, are presented in Figure 7.6. The predictions are shown for two R_0 values, 2.0 and 2.5 μm. Though the rates are not predicted very well, the model does predict the maximum at about the same oxygen–air composition.

The real phenomena occurring in even the simple reaction outlined above are rather complex. At best the present model, while providing significant progress toward the modeling effort, is only a reasonable approximation of the real phenomenon and captures only its gross features. The model neglects heat transport and cannot explain the influence of gas thermal conductivity on H_2O_2 formation, which has been experimentally observed. The number of nuclei were determined from experiments that may not be feasible for other reactions. The fate of the bubble is sensitive to the initial radius R_0. The model, however, does not provide a foolproof method of assessing this. Even though the collapse phase lasts for less than half a microsecond, the model assumes with success that thermodynamic equilibrium is attained. While this assumption appears reasonable in light of good experimental fit, more work on model systems for which the kinetics are known needs to be done so that we have a more solid foundation for the assumption.

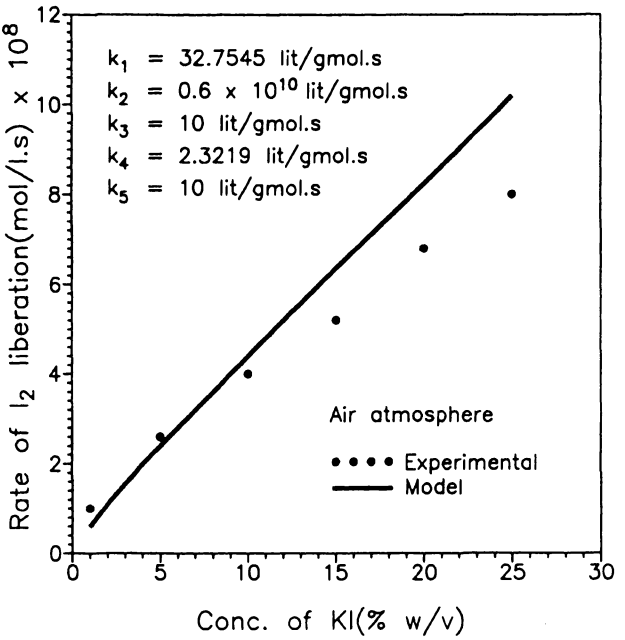

Figure 7.4. Comparison of predicted and observed rates of iodine liberation under air atmosphere. (Reprinted from *Chem. Eng. Sci.* **49**, D.V. Prasad–Naidu *et al.* "Modeling of a batch sonochemical reactor," pp. 877–888, copyright 1994, with permission from Elsevier Science.)

An interesting modification of the above-described reaction is the decomposition of CCl_4 in water in the presence of KI. Gandhi (1997), Rajan (1997), and Rajan *et. al.* (1998) showed that the sonolysis of KI solution containing CCl_4 as a separate phase results in the formation of I_2, but shows characteristics that are different from those observed when KI solution alone is sonicated. They also noted that the rates of iodine production in this system have been observed to be greater by nearly two orders of magnitude than those observed in the absence of CCl_4. In the presence of CCl_4, the rate becomes independent of KI concentration, the effect of a gas atmosphere becomes less pronounced, and the rate becomes time dependent. Furthermore, the average rate passes through a maximum as the dispersed-phase holdup is increased. The main reactions in the bubble are

$$CCl_4 \rightarrow CCl_3 + Cl$$

$$CCl_4 + 2H_2O \rightarrow CO_2 + 4HCl$$

The main reactions in the liquid phase are

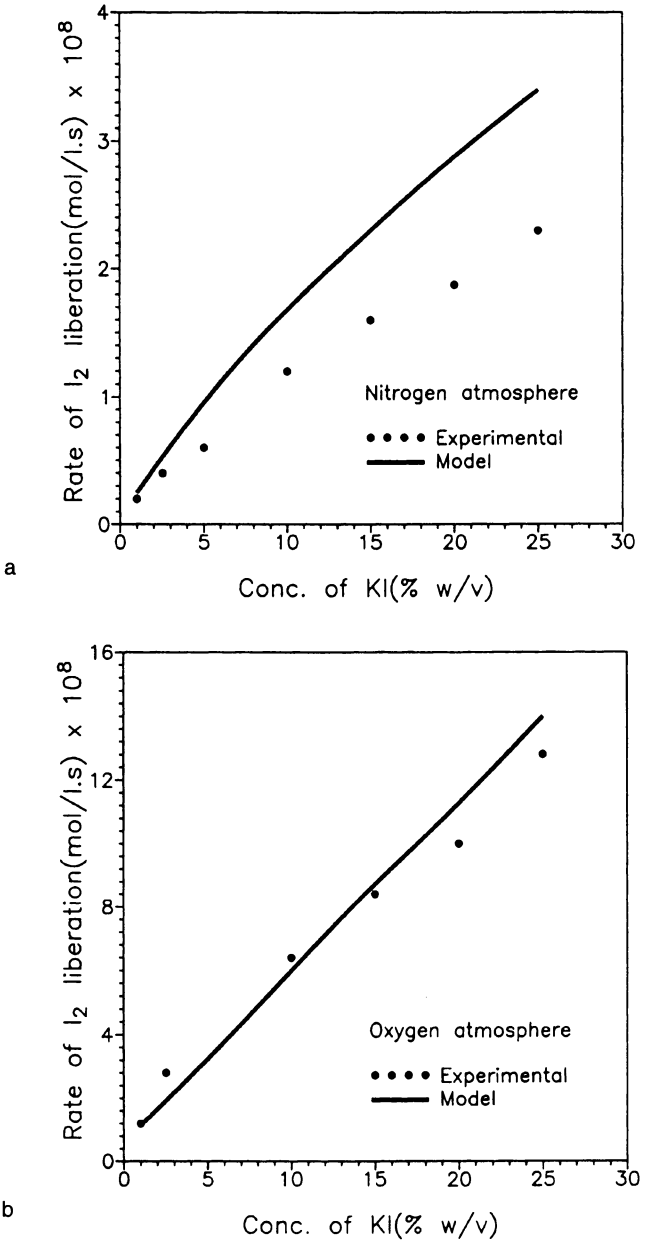

Figure 7.5. Comparison of model predictions and observed rates of liberation of iodine (a) under N_2 atmosphere and (b) under O_2 atmosphere. (Reprinted from *Chem. Eng. Sci.* **49**, D.V. Prasad–Naidu *et al.* "Modeling of a batch sonochemical reactor," pp. 877–888, copyright 1994, with permission from Elsevier Science.)

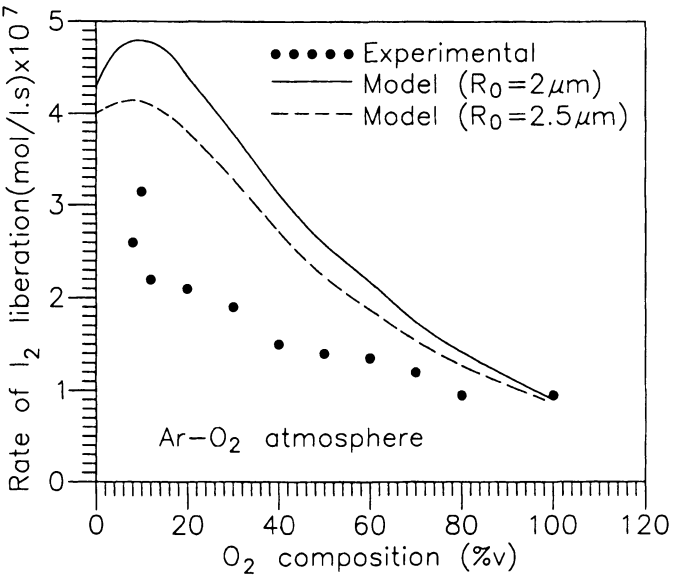

Figure 7.6. Comparisons of rates under Ar–O_2 atmospheres. (From Gandhi, 1997, with permission.)

$$Cl + Cl \rightarrow Cl_2$$

$$Cl_2 + H_2O \rightarrow HOCl + HCl$$

$$2KI + HOCl + HCl \rightarrow 2KCl + I_2 + H_2O$$

$$2KI + HOCl \rightarrow KCl + KOH + I_2$$

When the same model was applied to this reaction system, chemical reaction equilibria calculations showed that the chlorine produced was much greater than the hydroxyl radicals, and the model (Rajan, 1997) was able to account for the rate of decomposition of CCl_4 and production of iodine. The significant increase in the oxidation rate has been found to be due to release of Cl_2, Cl, and HOCl, which act as a separate source of reactants to yield I_2. Since all these quantitatively react in the reactor with KI, the rate becomes independent of KI concentration. The gas atmosphere was found to change continuously because of the formation of CO_2 and O_2. This results in a change in the composition of gas bubbles with time, which reduces the effect of the initial gas atmosphere used. The presence of a dispersed phase reduces the number of bubbles because of attenuation and scattering, but increases them owing to interfacial cavitation, thus yielding a maximum at a specific

holdup. Figure 7.7 shows the comparison between the model predictions and observations of Bhatnagar and Cheung (1994). As shown, the model captures the basic features of reaction behavior. The destruction of CCl_4 considered here is an example of the use of ultrasound in the destruction of polluting agents. As shown by Jensen (1996), the use of cavitation in the destruction of water pollutants is gaining more popularity. The model described above should be workable for other pollutants as well (Price, 1992).

The weakest part of the model is the assumption about the state of mixing in the reactor. Although the assumption of complete mixing works reasonably well, the reactions are so fast that the time scale of mixing is likely to be much larger than the time scale of various reactions. Future work needs to relax this assumption. Since no other gas–liquid reactors or gas–liquid–solid reactors are modeled in detail as yet, the study by Prasad–Naidu *et al.* (1994) provides a significant basis for expanding future work. In a recent study Sochard *et al.* (1997,1998) presented a model for homogeneous reaction in the presence of ultrasound. The model assumed uniform pressure but considered interfacial heat and mass transfer. The model equations were solved numerically using an orthogonal collocation method that included Chebychev polynomials for special integration together with the Gear method for time integration. As before, thermodynamic equilibrium was assumed at the end of the bubble collapse. The influence of physicochemical properties of

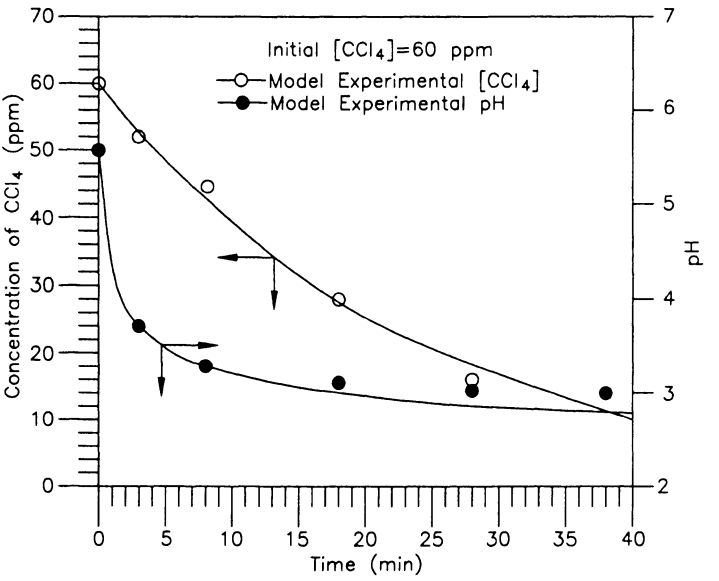

Figure 7.7. Decomposition of aqueous CCl_4 under sonication. (From Gandhi, 1997, with permission.)

gas and liquid and experimental conditions on maximum temperature and free radical concentration was derived. These authors found good agreement between theoretical predictions and experimental measurements for the effects of frequency and temperature on the production of free radicals in the bubble at the end of the collapse phase (see Figure 7.8).

Gas–liquid–solid reactor modeling is very important and is more complex, because cavitation in this case may or may not directly influence the reaction rate. At present a general model to predict the effect of cavitation on the gas–liquid–solid reaction rate does not exist.

One of the most difficult and important elements in modeling a cavitation reactor is the appropriate characterization of the cavities (either alone or in the form of clusters) and the extent of the reaction zone under a variety of operating conditions. This subject is discussed further later in this chapter.

7.3c. Further Improvements in the Model

The model proposed by Prasad–Naidu *et al.* (1994) and Gandhi (1997) assumes a uniform cavitational intensity or activity in the entire reaction bulk. Visual observations of the ultrasonic bath and the mapping of the mean pressures within the fluid bulk give a completely different picture. These observations indicate that the active cavitation zone is restricted to certain locations in the bath and that the mean pressure varies substantially with the location in the bath. These variations are due to the geometric arrangements of the ultrasonic transducers used for a particular bath to distribute the total energy.

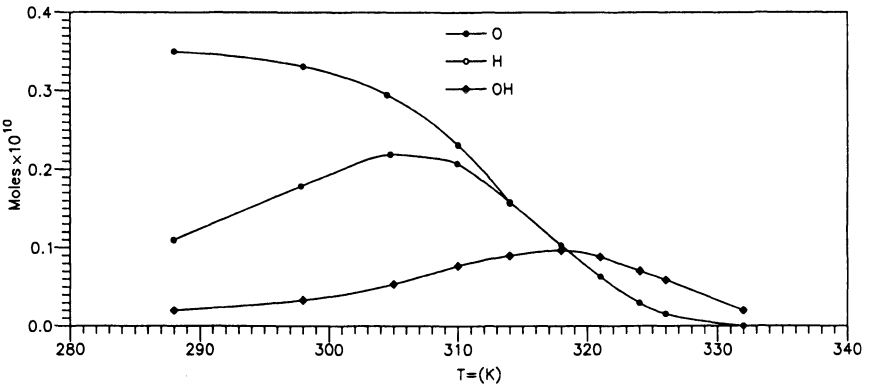

Figure 7.8. Amount of free radicals formed at the maximum compression of the steady-state oscillations of a 100-μm bubble driven at an acoustic pressure amplitude P_a = 1 bar and a frequency of 20 kHz, versus the liquid bulk temperature. (From Sochard et al., 1997, with permission.)

The observed reaction yields in such a case strongly depend on the positioning of the reactor in the cavitating media. The situation is relatively simple if a single transducer is used as an ultrasonic power source. This is, however, not always possible owing to the limitations of each transducer in terms of maximum deliverable power. Again, the results will be quite reproducible on a laboratory scale if the total reaction volume is quite small compared with any cavitational zone volume at any location in the bath (usually it is a few cubic centimeters), but the results are likely to be different if the reactor volume is substantially larger than the cavitational zone volume.

One possible way out of this impasse is to map the pressure fluctuations with dynamic pressure transducers and represent this pressure pulse in terms of frequency amplitude spectrum by performing fast Fourier transform (FFT) on this pulse. This frequency–amplitude spectrum will vary, depending on the location of this dynamic pressure transducer or hydrophone. The next step is to solve the Rayleigh–Plesset equation for a single cavity (or a cluster of cavities). The cavity behavior obtained from the solution of this equation is then split into three regimes: growth (the cavity grows), oscillations (the cavity passes through the same diameter twice, i.e., during growth and collapse), and collapse. This cavity behavior occurs at different frequencies: low frequency for growth, intermediate frequency for oscillation, and high frequency for collapse. Thus, if the measured amplitude–frequency spectrum shows a large number of high-frequency components, then that zone can be attributed to the collapsing cavities producing a maximum cavitational effect and so on.

This picture is too simplistic because all the processes occur simultaneously and only a maximum probability for an event (i.e., growth, oscillation, or collapse) can be ascertained. Thus the reactor or a particular zone in the reactor is likely to be cavitationally more active if it shows the maximum probability of collapsing cavities. The larger the number of such zones in any reactor, the better the performance that can be expected in terms of cavitational-assisted transformations. The model described here is not predictive in terms of identifying from the first principle the zones of cavity formation, growth, oscillation, and collapse, but useful scaleup and design information (i.e., the location of multiple sources) can be obtained by this analysis. More details of this analysis are given in Section 7.4. A survey of the literature indicates that researchers who have used the local pressure measurements in a bath to locate their reactants have maximum success compared with those who have positioned the reactant randomly and have reported poorly reproducible results.

Visual observations also indicate that the cavities often do not exist individually, but in the form of clusters, depending on the intensity and frequency of cavitation, the nature of the gas and liquid, etc. Photographs show vapor clouds that are actually a cluster or aggregate of cavities. The important difference between individual cavity behavior and the behavior of the cluster in relation to the driving

time-dependent pressure field was discussed in Chapters 2 and 3. Nevertheless, it is worth pointing out here the importance of shielding effect on reactor performance.

The models of Prasad–Naidu *et al.* (1994) and Gandhi (1997) largely depend on the composition of the thermodynamically equilibrium species for a cavity collapsing in a specific manner, and they have shown that these reactive species are produced in different concentrations if the cavity collapse conditions are different. As discussed earlier, an isolated cavity is influenced by the driving time-dependent pressure field, whereas a cavity surrounded by other cavities, as in the case of clusters, is influenced by the behavior of the cavities on the periphery of this cluster. A cavity within a cluster is insensitive to the pressure changes in the reaction media. Thus an isolated cavity behaves completely differently than a single cavity in a cluster in an identical time-dependent pressure field. The size of the cluster depends on many parameters, such as nucleation, zone of sonication, or width and length of shear layers (hydrodynamic cavitation), and hence the behavior of an individual cavity in isolation and in a cluster can give completely different concentrations of reactive species generated as a result of collapse.

It is clear from this discussion that the proper characterization of the reaction zone, estimating nucleation in terms of probability, and using a cavity cluster instead of a single cavity would be some of the steps in the right direction for further development of the modeling effort.

7.4. CHARACTERIZATION OF THE REACTION ZONE

As indicated in the above-described model and its analysis, the most important step in the development of a cavitation reactor model is the proper characterization of the nature of the cavity and its distribution in the reaction chamber. Since imploding cavities are the sites for reactions, their size, number, and locations are needed to formulate appropriate chemical reactions as well as mass balances for the relevant chemical species. The proper mathematical characterization of the location and the distribution of the imploding cavities or cavity clusters is extremely difficult because this process is at best random and very little quantitative knowledge is available on the relationship between the cavitation (hydrodynamic, acoustic, or laser) energy imparted to the reaction medium, and the size, number, and distribution of cavities generated from it. It is also more difficult to *a priori* identify the nature of the cavities (i.e., whether a particular cavity is in a growth, oscillation, or implosion mode). In the absence of such knowledge, the scaleup of the reactor can only be done on a qualitative or an empirical basis. In this section, we first outline a physical picture for the nature and the distribution of a cavity in various types of cavitation reactors. Then we present an analysis for cavity distribution based on the probability density function.

Knowledge of the reaction zone is very important for a reactor scaleup. Numerous attempts have been made to enlarge the reaction zone. In a hydrodynamic cavitation reactor, cavities can be formed in different shear layers. The major shortcoming of the ultrasound equipment lies in its directional sensitivity, i.e., the effects due to cavity oscillation collapse pertain to a very small area near the ultrasound horn or transducer because cavities do not travel far from the point of inception. This means that the entire liquid volume is not cavitated. Furthermore, the life of the cavities is very short, of the order of a few microseconds. There is a need to characterize ultrasonic equipment in terms of its directional sensitivity. A few attempts to alleviate this problem associated with ultrasound instrument have been made by using a tubular reactor with a transducer attached to each of its surfaces, thus trying to concentrate the ultrasound intensity at the center of the core. Multiple transducers have also been used. Uniform cavitation can be generated throughout the system by irradiating the system with the same frequency as the resonant frequency of the reactor, but such a technique fails when the volume of the reactor is too large and resonant frequencies are below the sonic limit. In order to appropriately design and operate a cavitation reactor, it is necessary to map the cavitational intensity and hence the energy required for cavitation.

In hydrodynamic cavitation, the cavity distribution will generally follow the flow streamlines, which depend on the reactor size and geometry and the degree of turbulence downstream of the orifice. While the concentration of the cavities is generally higher near the point of expansion, unlike the case in acoustic cavitation, the reaction zone in this case generally covers a larger portion of the reactor volume. An appropriate design of the vessel is once again important for uniformity in the cavity distribution. In optical cavitation, the fate of the cavity will generally depend on the prevailing fluid mechanics surrounding the cavity.

The topics covered here form the basis for significant future work that needs to be done in this area. Cavitation reaction engineering will become a truly reliable, predictable, and scalable technology with a proper quantitative understanding of the nature of the cavity, along with its number and time-space distribution. More research in this area is strongly encouraged.

7.4a. Physical Description

The typical cavity radius obtained in the case of an acoustic or hydrodynamic cavitation reactor is on the order of 5 μm or so. This cavity when formed will first grow and then will undergo a violent collapse or oscillation, depending on its location in the acoustic or hydrodynamic field. From the simulation reported by Moholkar and Pandit (1997), it is clear that the contribution to the overall cavitation effect by both smaller and larger bubbles is significant. Smaller bubbles (on the order of 5–10 μm) grow larger (specifically about 150–200 times their original size) before a transient collapse. Since the time of the collapse of the bubble is very

small, heat transfer during the process is negligible and the collapse can be assumed to be completely adiabatic. The pressure and temperature pulse produced are directly proportional to the ratio of the maximum radius of the bubble just preceding the collapse. The pressure and temperature pulses produced by smaller bubbles are very high, but the zone of influence of these pulses is very small because it is proportional to the size of the bubble itself. The reverse is the case for larger bubbles. Here, since the growth of the bubble prior to a transient collapse is quite small, the magnitude of the pressure pulse produced after a transient collapse is low. The zone of influence of this pressure pulse is, however, quite large owing to the larger initial bubble size.

As indicated in an earlier section, the entire radius and pressure pulse history of a bubble can be divided into three regimes: (1) growth, (2) oscillation, and (3) collapse (see Figure 7.2). These regimes are associated with certain ranges of the pressure for a cavity of specific size in a sonic field of a specific intensity at the bubble boundary in the bulk liquid. Just as in acoustic cavitation, the cavities also go through growth, oscillation, and collapse regimes in hydrodynamic cavitation. The driving force in this case is the turbulence field created by the flow expansion. The cavities generally follow the flow streamlines, but in some circumstances they could leave the streamlines and move toward the walls. The degree of turbulence affects the intensity of the bubble collapse. In optical cavitation, the cavities are formed at the points of laser impact and they grow, oscillate, and collapse based on the surrounding pressure field.

Every bubble is associated with some natural oscillation frequency and the pressure pulses it gives out are at that frequency if its size at the end of one oscillation cycle is unchanged. Now as the bubble grows, the natural oscillation frequency of the bubbles decreases since it is inversely proportional to the size of the bubble and the reverse happens during the collapse phase. An assumption of independent oscillation of a single cavity can be made and collective oscillations of the bubble can be neglected. Thus the knowledge of the pressure pulses obtained at various frequencies can be translated to identify various regimes of operation, namely, growth, oscillation, and collapse. Each of these regimes is characterized by the pressure pulse given out by the bubble at the stage of oscillation. From simulations, it was found that when the pressure in the liquid near the bubble boundary was between 1 (at the start) to 0.5 atm, the cavity was in the growth stage. When the pressure was between 0.5 and 0.02 (the lowest during the entire life cycle), the bubble was in the oscillation regime. The cavity was at this point at its largest size and the pressure at this point started increasing abruptly. Any pressure above 1 atm indicates that the bubble has started collapsing. Therefore 0.5 atm can be taken as the crossover pressure from a growth to an oscillation regime and the threshold between an oscillation regime and a collapse regime can be taken as 1 atm.

This physical picture forms the basis upon which a quantitative model for cavity behavior and distribution can be developed. One such model and its analysis is described in the following section.

7.4b. Reaction Zone based on Probability Density Function

One method for the determination of the reaction zone is the statistical analysis of cavitational intensity as measured by the probability density function of bubble oscillation or collapse. The above-described physical model forms the basis for the determination of the probability of a bubble residing in a particular regime. Such a probability distribution provides a good appraisal of various regimes since the collapse of a cavity is an entirely random process. The two commonly used methods for analyzing random signals are the spectral density function (SDF) based on the frequency of random signals and the probability density function based on the amplitude of the signals.

The probability density function for any parameter relates the possible values of a parameter to the probability that they will be observed in a real system. The probability of a particular event in a system occurring within a specified time interval is defined as the degree of belief held by the person providing the data that the quantitative system characteristic will have a value in a particular interval under specified conditions of measurement. In such assessments the probability associated with a value of a parameter corresponds to the relative frequency with which randomly sampled values would lie in different intervals of the allowed range of values in the limit as the number of samples goes to infinity.

In a study carried out by Moholkar (1996), as shown in Table 7.1, seven different locations in a bath were chosen to evaluate the pressure and frequency signals. The pressure signals were measured by pressure transducers (PCB Inc.), which were made of piezoelectric crystals. The charge generated by the transducers was fed to

TABLE 7.1. Locations of the Pressure Measurements in the Bath[a]

	Coordinates of the location of pressure transducers in the bath		
Transducer No.	X (cm)	Y (cm)	Z (cm)
1	6.9	7.0	0.3
2	5.2	4.0	0.3
3	9.8	2.8	0.3
4	8.7	9.1	0.3
5	12	10.8	0.3
6	3.0	2.9	0.3
7	3.3	11.9	0.3

[a]Data from Moholkar (1996).

a charge amplifier and the output of the amplifier (voltage) was fed to an FFT-based Lecroy oscilloscope. The amplitude of the pressure pulse felt by the transducer can be calculated by converting the voltage reported by the oscilloscope into the charge actually generated and later converting the charge into the pressure pulse with the help of the calibration graphs provided by the transducer suppliers.

The FFT of the input signal was obtained and voltages for different frequencies were noted in the range of 2 to 152 kHz. The frequencies beyond 152 kHz were neglected because of the limitations of the transducers. As shown in Table 7.1, the distance of the transducers from the bottom of the reactor (designated as Z) was kept at 3 mm. This distance was chosen because of early collapse of the bubbles and it is generally believed that cavitational effects are observed only in the close vicinity of the oscillating surface.

A statistical analysis of the pressure signal was made in order to determine the probability of the bubble residing in three (i.e., growth, oscillating, and collapse) regimes. This is expected to provide a good appraisal of the regimes since the cavity collapse is an entirely random process. The pressure pulse values (i.e., the voltage values) were divided into certain ranges, such as 0–2 mV, 2–4 mV, and 4–6 mV (i.e., up to 0.5 atm) in a growth regime and so on as given in Table 7.2. The values of the voltages obtained at different frequencies were sorted according to these ranges and the number of pulses falling in one particular range were calculated. This number divided by the total number of pulses thus gives the probability of bubbles oscillating in one regime assigned to that range. In this way voltages from 0 to 6 mV were assigned to the growth regime, those 6 to 12 mV were assigned to the oscillation regime, and those 12 mV and up were assigned to the collapse regime.

For an average of fifty runs, the distributions of the number of pressure pulses and probability as a function of voltage range for seven different locations were obtained by Moholkar (1996). A typical probability distribution for one such location is shown in Figure 7.9. It is clear from the figure that the bubbles in this location were predominantly in the growth and oscillation regimes. These and other similar results indicated that cavitational intensity decreases rapidly with an in-

TABLE 7.2. Voltage Ranges and Regime Specifications[a]

Voltage Range (mV)	0–2	2–4	4–6	6–8	8–10	10–12	12–14	14–16	16–18	18–20	20–on
Pressure (atm)	0.2	0.4	0.5	0.8	1.0	1.2	1.5	1.8	2.0	2.4	2.5
Regime[b]	G	G	G	O	O	O	O	C	C	C	C

[a]Data from Moholkar (1996).

[b]G = growth, O= oscillation, and C = collapse.

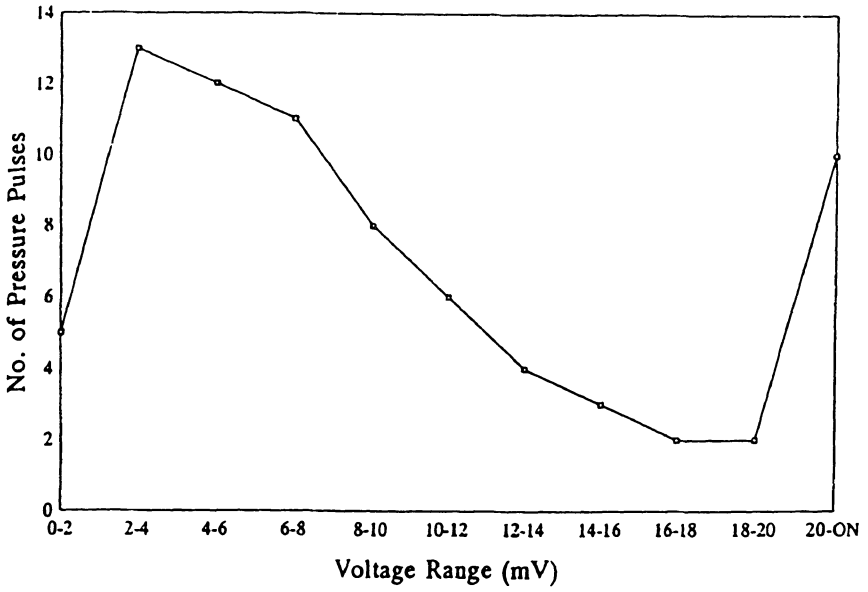

(A)

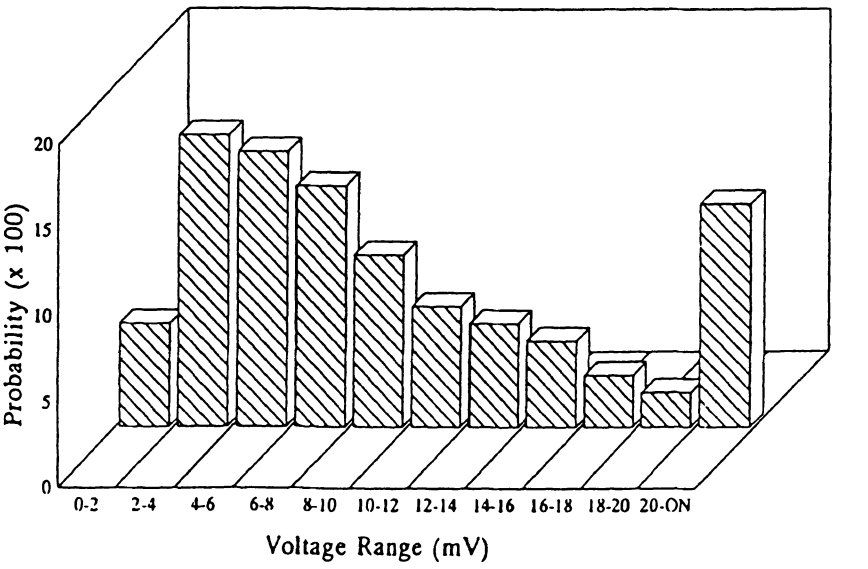

(B)

Figure 7.9. Typical (A) pressure pulse and (B) probability distributions.

crease in distance from the transducer to the bulk. The phenomena of cavity growth, oscillation, and collapse are random and two consecutive runs of the same time interval may yield entirely different results. In Moholkar's study, the number of cavities collapsing per unit time was far higher than those either growing or oscillating per unit time.

The entire reactor can be mapped to find the probability of bubble growth, oscillation, and collapse. Their overall probabilities based on the results described in Figure 7.9 and similar results for other positions are shown in Figure 7.10. The probability density distribution thus provides a powerful tool for identifying cavity behavior and therefore the nature and number of reaction sites in a cavitation reactor. The study also indicates that if collapsing cavities are concentrated at one location, different arrangements of transducers or reactor vessels should be explored.

In summary, it is generally known that a statistical analysis (such as a probability density function) of the pressure signals from an ultrasonic bath gives a very realistic picture of the distribution of cavitation intensity in the bath. If the probability density function peaks on collapse at a particular location, the bath is assumed to be highly efficient at that location, but if we want to distribute collapsing cavities, different arrangements of transducers or reactor vessels should be explored. If, on the other hand, the probability density function does not show peaks at all locations in the ultrasonic bath, then stirring is recommended to ensure a uniform residence time of the mixture in the cavitation zone. If a reaction vessel is to be kept in a bath, it should be placed at locations where the probability density function shows peaks in the oscillation regime. The alignment of the transducers should be such that at all locations the probability function peaks in the collapse

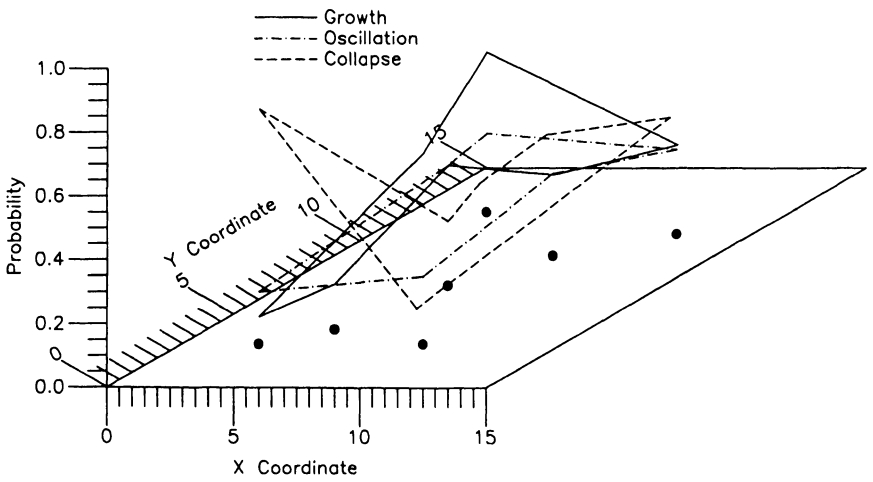

Figure 7.10. Overall probability distribution in a bath (all regimes). (From Moholkar, 1996.)

regime. Although this method suffers from severe limitations, such as collective oscillations of the cavities interfering with the resultant pressure amplitude obtained from the collapse of a single cavity, it forms a good basis for identifying the nature and extent of the reaction zone. While this discussion of PDF has been restricted to acoustic reactors, the concepts can be similarly applied to hydrodynamic and optical cavitation reactors.

In a recent study, Romdhane *et al.* (1997) evaluated the effects of different parameters on the intensity profiles of the ultrasonic wave. The space and time distributions of the ultrasonic intensity were measured using a thermoelectric probe. The results showed that ultrasound propagation is influenced by the presence of cavitation bubbles, the flow regime, and the presence of solid particles. Some typical results illustrating the effects of acoustic frequency and power, solids concentration, and the presence of mechanical stirring on the intensity profile are shown in Figures 7.11 and 7.12. In these figures, the intensity is represented in terms of the difference between the steady-state probe temperature T_{eq} and the medium temperature T_0. The results clearly indicate that a larger concentration of solids and the presence of mechanical stirring results in a decreased intensity away from the surface of the probe. Both solids and mechanical stirring thus have a homogenization effect.

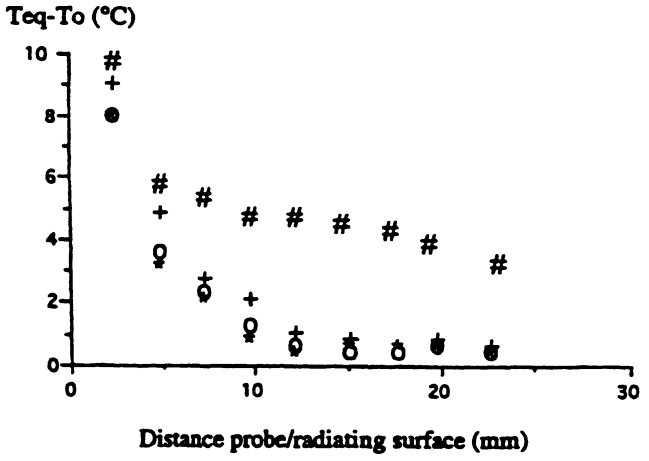

Figure 7.11. Intensity profile measured along the central axis of a horn (f = 40 kHz, power = 29 W) for different solid-to-volume ratios, ϕ, of the liquid. #, Pure water; +, ϕ = 0.4 kg/m^3; o, ϕ = 1.6 kg/m^3; *, ϕ = 3.2 kg/m^3. Measurements were made in a flask (volume = 2500 cm^3) in which the height of the distilled water was fixed at 16 cm. The solid (Japanese pearls) was maintained in suspension using magnetic stirring. (Reprinted from *Ultrasonics Sonochemistry*, **4**, M. Romdhane *et al.*, "Experimental study of ultrasound attenuation in chemical reactors," pp. 235–243, 1997, with permission from Elsevier Science.)

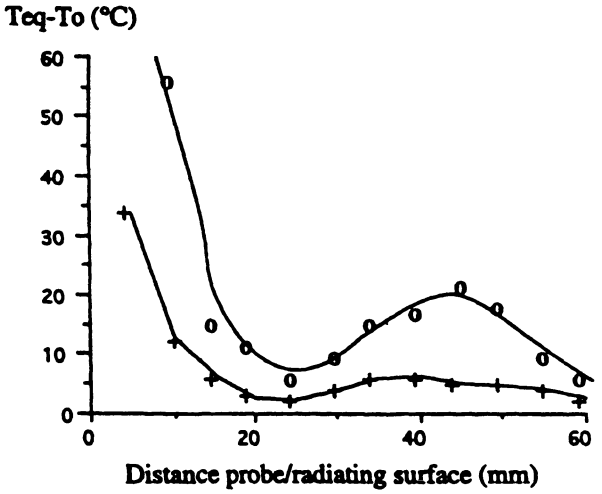

Figure 7.12. Influence of agitation on the intensity profile measured along the central axis of a horn ($f = 20$ kHz, power = 15 W): o, stagnant water; +, medium agitated by magnetic stirring. Measurements were made in a flask (volume = 2500 cm^3) in which the height of the distilled water was fixed at 16 cm. (Reprinted from *Ultrasonics Sonochemistry*, **4**, M. Romdhane *et al.*, "Experimental study of ultrasound attenuation in chemical reactors," pp. 235–243, 1997, with permission from Elsevier Science.)

7.5. REACTOR DESIGN AND SCALEUP BASED ON THE CONCEPT OF CAVITATION YIELD

The previous section showed the complexities in modeling a cavitation reactor. Besides the size, number, and distribution of cavities, the reactor model requires an appropriate energy balance. This would require knowledge of the percentage of energy that goes toward cavitation and subsequent chemical reactions, both of which are difficult to model and predict (see Chapter 8), which has not been successfully achieved so far. Because of these difficulties, an alternative approach to evaluate reactor performance that alleviates the detailed energy considerations has been proposed in the literature. A new concept of cavitation yield has been used to evaluate design and scaleup options for a cavitation reactor. In this new concept, the efficiency of a cavitation reactor can be defined in terms of cavitation yield as

$$\text{cavitation yield} = \text{measured effect/cavitation power} \tag{7.17}$$

The measured effect is the amount of product generated in a fixed time. The cavitation power is the energy entering the reactor and is not, for example, the same as the electrical power consumed during acoustic cavitation. This can be assessed in a number of different ways, depending upon the nature of the cavitation. For

hydrodynamic cavitation, hydrodynamic pressure loss would give a good starting point. For acoustic and laser cavitations, this can be assessed by calorimetry, which measures the initial temperature rise of the system when the acoustic or laser irradiation is first switched on. For acoustic power, units can be quoted either as the energy emitted at the surface of the acoustic device in W cm^{-2} or the energy dissipated in the bulk of the sonicated medium (in W cm^{-3}). In general, however, cavitation power is strongly related to the operating cost of the cavitation reactor. Several options for cavitation power are further discussed in Chapter 8.

This method of evaluating reactor performance has so far only been used for acoustic reactors. Suslick (1989,1995) applied the concept to three types of acoustic systems using the reaction system for formation of I_2 from a KI solution. Some details of this study are described in Chapter 8 and will not be repeated here. Since cavitation yield is a measure of energy efficiency of the cavitation process, this parameter can be used as a measure for the appropriate reactor scaleup. For an acoustic cavitation process, the above analysis indicates that a probe reactor is generally very energy efficient. Large-scale processes are generally continuous and may not use probe reactors. Cavitation yield can be used as a measure for scaleup particularly when the large-scale reactors are different from the laboratory ones.

Suslick (1989,1995) examined the application of this concept to scaling up reactors for dry as well as liquid–liquid phase-transfer reactions. Based on this concept, he showed that for a dry phase-transfer reaction, a hexagonal bath in a continuous mode can be scaled up to a cavitation yield equivalent to a laboratory-scale cup-horn reactor. For a liquid–liquid phase-transfer reaction, he considered the conversion of an organic chloride to a nitrile in a reaction medium of water–toluene using an alkali metal cyanide and a phase-transfer catalyst. For this case the analysis indicated the liquid whistle to be an excellent economic choice for scaleup of processes of this type in that it is very inexpensive and has low electric energy demand. With a processing volume of 4 m^3 h^{-1}, the whistle reactor can produce 300 tons/year of the nitrile. The cavitation yield can thus be used as a vehicle for determining the appropriate scaleup.

7.6. MEMORY EFFECT IN A LOOP CAVITATION REACTOR

As indicated in Chapter 6, the concept of a recycle or loop cavitation reactor has significant commercial viability because such a reactor can be scaled up from laboratory to commercial scale without significant alteration in the basic configuration of the reactor. While the specifics in this chapter are for the acoustic recycle reactor examined by Martin and Ward (1992), the concept in general can be applied to other types of cavitation reactors. The reactor has a number of advantages: the problem of penetration range for acoustic and laser cavitations is overcome; the residence time of reagents in the actively cavitated part can be controlled; and a

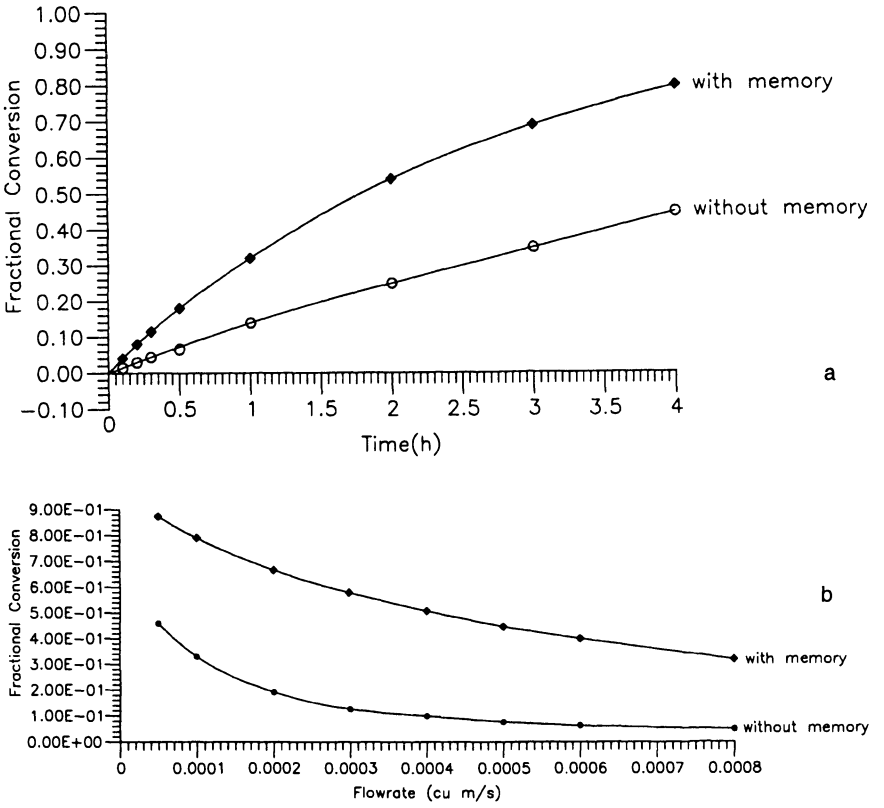

Figure 7.13. Performance of (a) batch and (b) continuous reactors with and without retained activation (memory). (From Martin, 1992, and Martin and Ward, 1992, with permission.)

modular approach can be taken to the design, installation, and maintenance of the cavitation reactor module, which can also be used alone in the laboratory if so desired.

The modeling of a recycle reactor requires the incorporation of the retained activation into the reactor performance. For this reason, it is important to consider which types of sonochemical reaction mechanisms are likely to be most susceptible to retained activation (i.e., "memory effect") and, therefore, to efficient scaleup. Proposed mechanisms can be divided into electrical, physical "hot spot," and mechanical.

It is reasonable to expect that the effects of the electrical and "hot spot" mechanisms will be too short lived to lead to retained activation, unless their effect is either to modify the course of the reaction or to generate active species that are

self-propagating to a significant extent. However, mechanical activation, resulting, for instance, from surface damage or cleaning, could be retained for many seconds and minutes.

A model to take account of memory effect on loop reactor performance is described by Martin and Ward (1992) and Martin (1993). The model incorporates memory effect in the model equations by assuming an exponential decay of the first-order rate constant with time, from k_{1_s} to k_1 for instance, from the point at which activated material leaves the cavitation reaction chamber. Figure 7.13(a) illustrates the effect of activity retention for a first-order reaction on the conversion-time profile in a batch reactor. Similarly, Figure 7.13(b) illustrates the results for a continuous reactor. In both cases, the volume, v, of the insonated zone was assumed to be 4 liters and the "silent" volume, V, was assumed to be 1.0 m^3. The results clearly indicate that the memory effect is significant in the conversion-time profile for both batch and continuous reactors. The extent of the memory effect on reactor performance will depend on the nature of the cavitation reaction mechanism.

7.7. CONCLUDING REMARKS

In this chapter we briefly examined some qualitative, quantitative, and semiempirical considerations for evaluation of cavitation reactor performance. The subject is rather complex and considerable future work is needed. The work should largely be focused on integrating the production and distribution of cavities with their implosion and the resulting chemistry. Only through such an integrated model can cavitation chemistry be controlled and optimized by adjusting the independent system parameters that affect the distribution and implosion of the cavities. While in the absence of a sophisticated model, the performance of various types of cavitation reactors can be qualitatively compared using the cavitation yield model; this model is not predictive. The probability density function of cavity clusters would be a good starting point for the development of a sophisticated model.

8

ENERGY EFFICIENCY AND THE ECONOMICS OF THE CAVITATION CONVERSION PROCESS

8.1. INTRODUCTION

The objective of this chapter is to briefly outline energy efficiency and various economic considerations involved in converting the cavitation chemistry observed in a laboratory-scale operation into a commercially viable technology. First we examine the energy efficiency of the steps (see Table 8.1) involved in the cavitation conversion process. The overall economics (particularly the operating costs) of the cavitation conversion depend very much on the efficiency of the individual steps; energy efficiencies of the equipment are briefly outlined in Table 8.2. Various models for determining the energy efficiency of the cavity implosion are evaluated. A cavitation yield model that correlates overall reactor performance to the total energy consumption is evaluated. Finally, the energy efficiencies of cavitation

TABLE 8.1. Steps for Energy Transformation

Hydrodynamic cavitation → pump → C[a] → T[b]
Acoustic cavitation → freq. generator → transducer → C → T
Optical cavitation → laser → C → T

[a]C = Efficiency of single bubble or cluster cavitation.
[b]T = Efficiency of thermochemical conversion.

TABLE 8.2. Energy Efficiency of Cavitation Equipment

Hydrodynamic cavitation

Equipment	Energy efficiency (%)	Range of flow rate (m^3/h)
Pump (low pressure) (centrifugal pump)	50–70	>10
Pump (high pressure) (displacement pump)	20–40	<10

Acoustic cavitation

Frequency generator	Energy efficiency (%)	Range of power
Low frequency (<1 MHz)	45–70	$P < 200$ W
	<45	1 kW > P > 200 W
High frequency (>1 MHz)	>70	$P < 1$ W

Transducers[a]

Piezomagnetic

Coupling factor	Feroxcube 7A1	Feroxcube 7A2	Kearfert N-51	Nickel	Alfenol 13 $Fe_{0.87}Al_{0.13}$
K	0.25–0.30	0.21–0.25	0.32–0.40	0.15–0.31	0.25–0.32

Piezoelectric

f_R / f_M (resonant freq. / nat. mech. resonant freq.)	Coupling factor, K[b]
1.0	0.0
0.8	0.6
0.6	0.8
0.4	0.92

Optical cavitation[c]

Type of laser	Wavelength (μm)	Efficiency (%)	Energy (J)	Pulse duration (ns)	Pulse repetition	Spectral width (nm)
Nd-YAG	1.06	0.1	0.02	10–25	$100\ s^{-1}$	0.5
GaAs	0.9	4	10^{-4}	100	$100\ s^{-1}$	2.0
Ruby	0.694	0.013	7	3	$20\ min^{-1}$	0.04
Nd-glass	0.530	0.04	20	20	$12\ h^{-1}$	0.9

[a]Data from Mason (1966).

[b]K→1 indicates electrical energy conversion to mechanical energy over a wide frequency range with good efficienty.

[c]Data from Thyagarajan and Ghatak (1981).

conversion processes are compared with those of other advanced oxidation processes.

Second, this chapter compares the economics of the cavitation conversion process with those of other advanced oxidation processes. The comparison is largely illustrated with sample calculations and case studies. It should be pointed out that a comparison based on economics is not always definitive in making a final

judgment on the value of a cavitation technology for a specific application. In some situations cavitation technology may provide a complex but favorable enhancement of the process that would not otherwise be possible. The final decision on the application of this technology for a specific purpose will depend on the value it brings to the process.

8.2. EFFICIENCY OF ENERGY TRANSFORMATION

8.2a. Steps for Energy Transformation

A successful and economical design for a cavitation reactor requires an effective conversion of mechanical, electrical, or optical energy into the energy required to break chemical bonds. The steps generally followed for this conversion were previously shown in Table 8.1. The first major step is the conversion of mechanical, electrical, or optical energy into the energy required for the formation of cavities. For hydrodynamic cavitation, this is the local pressure reduction sufficient to form cavities. For acoustic cavitation, it is the acoustic energy required to form cavities. Finally, for optical cavitation, it is the optical energy required to rupture liquid film to produce cavities. Once cavities are formed, their implosion and the energy released from the implosions are of major importance.

In a hydrodynamic cavitation reactor, the pressure loss through expansion is the major source of energy loss. The associated pumping cost is a major issue for the economics of the process. There is also energy loss associated with the formation and implosion of the cavities. While both capital and operating costs for hydrodynamic cavitation are lower than those for acoustic cavitation, the intensity of the cavitation chemistry is also lower in the former case. The commercial applications of hydrodynamic cavitation are discussed in great detail in Chapter 9.

As indicated in Table 8.1, the overall energy efficiency for the conversion has three components: (1) the efficiency of the equipment, such as a pump, frequency generator, transducer, or laser; (2) the energy efficiency associated with the formation and implosion of the cavities or cluster of cavities; and (3) the energy efficiency associated with the transformation of the energy released from cavity implosion to the energy required for the chemical transformation. For the three types of cavitations considered here, these three types of energy efficiency are shown separately in Table 8.1. The letters C and T denote the energy efficiency associated with steps (2) and (3), respectively.

In hydrodynamic cavitation, there is a substantial energy loss in the fluid pumping process. The loss depends on the flow rate as well as the pressure level. Different pressures and different flow rates will require different types of pumps. The energy efficiency associated with cavity implosion in hydrodynamic cavitation will depend on the level of turbulence in the flow. For example, orifices with small diameters

will cause larger pressure drops but also larger turbulence downstream, which will allow a larger amount of energy to be released during the cavity implosion. In an acoustic reactor, there will be electrical and heating losses as electrical input drives the mechanical motion of the transducer through the generator. In turn, the transducer motion must be transferred to the liquid medium, which involves coupling losses. While the technology for ultrasound generation is well developed, a good design of transducers and horns is important for an efficient conversion of electrical energy to acoustic energy and thereby for the success and cost effectiveness of the ultrasonic process.

The nature of the reaction media can not only affect the life of transducers and horns but it also determines the nature of the cavitation field and the resulting sonochemistry. Acoustic energy produces cavitation and chemical effects; however, the generation of cavitation bubbles also involves heating losses. The efficiency of the conversion of acoustic energy to the generation of an effective cavitation field is important. Finally, there will be attenuation of sound energy through the medium by bubbles or suspensions. Also, energy will be absorbed (and reflected) from stirrers, baffles, cooling coils, or any other devices in the reaction vessel. All of these energy losses should be evaluated in a large-scale-process because they affect the economics of the process. For optical cavitation, the energy associated with the generation of laser light and the transformation of laser energy into the formation of a cavity are major issues. This type of cavitation is generally too expensive for commercial applications.

8.2b. Equipment Efficiency

The efficiency of the cavitation conversion process very much depends on the efficiencies of the cavitation equipment involved. A brief summary of the equipment efficiency for the three types of cavitation processes is given in Table 8.2. For commercial operations, along with energy efficiency, the durability (i.e., life) of the equipment is important. Significant progress in this direction has been made over the past few decades.

8.2c. Energy Efficiency for the Cavity Implosion

The basic physical phenomenon underlying cavitation chemistry is the nucleation, growth, and collapse of microbubbles, or clusters of microbubbles, giving rise to very high temperature and pressure pulses. These high temperature and pressure pulses are responsible for the physical and chemical effects of cavitation. The degree of cavitation intensity depends on two factors: the amplitude of the pressure variation and the frequency of the pressure variation. The literature on cavitation chemistry described in Chapters 4 and 5 has shown that the yields of chemical reactions can pass through maxima with a variation in either frequency or pressure.

It is also known that chemical yields can be improved significantly by choosing a driving frequency for the acoustic power input that matches the natural oscillation frequency of the reactor, thereby obtaining a resonance effect. A little work, however, is done to determine the optimum cavitating conditions (defined in terms of frequency and intensity of pressure waves) for the maximum energy efficiency for the cavity implosion.

In order to choose among the frequencies of operation in a cavitation reactor, it is necessary to assess the variation in the efficiency of the reactor (defined as the energy output due to cavitational collapse divided by the energy dissipation rate required to collapse the cavity) with the variation in the operating frequency. In this definition of efficiency, it is assumed that the energy required to cavitate the liquid is small compared with the energy required to collapse the cavity.

The following paragraphs outline a method for analyzing the energy efficiency of a cavity implosion. The analysis uses the first principles of fluid mechanics and numerical simulations to study the variation in energy input and output rates for the cavity implosion with the operating frequency. A wide range of frequencies (from 50 Hz to 100 MHz) have been examined. This range covers the hydrodynamic cavitation reactor (typically operating between 50 and 1000 Hz), acoustic cavitation reactor (operating between 20 kHz and 1 MHz), and optical cavitation reactor (operating between 1 and 100 MHz). The intermediate frequencies between hydrodynamic and acoustic cavitation are also analyzed. The analysis is based on the following assumptions:

1. In hydrodynamic cavitation, two extreme cases are analyzed based on the position of the cavity after its inception. In the first case, the cavity is assumed to escape the shear layer after its inception. In the second case, the cavity remains in the shear layer after its inception, as a result of which maximum growth is restricted by inertial and surface tension forces defined in terms of a critical Weber number. In reality, some cavities escape the shear layer while others remain within the layer. The percentage between these two paths is extremely difficult to estimate.
2. In acoustic cavitation, the acoustic field is assumed to be uniform.
3. The analysis is based on a single bubble (isolated cavity). No bubble–bubble interaction is considered.
4. The bubble is assumed to collapse when the bubble wall velocity exceeds the velocity of sound in the liquid media.
5. The optical cavitation analysis follows the same mechanism for the bubble collapse as that used for acoustic cavitation.

Energy Input Calculations. The energy dissipation rates were calculated for hydrodynamic, intermediate, and acoustic cavitation frequencies. An algorithm for the calculations is given below.

Hydrodynamic Cavitation. In a hydrodynamic cavitation reactor, the cavitation inception criterion is given by the cavitation number, which is defined as

$$\sigma_c = (P_2 - P_v)/(1/2)\rho V_o^2 \tag{8.1}$$

Here P_2 is the recovered discharge pressure, P_v is the vapor pressure, V_o is the orifice velocity, and ρ is the density of the cavitating medium. The value of the cavitation number is assumed to be equal to one, indicating that the pressure at the vena contracta is equal to the vapor pressure. Thus for any value of recovered P_2, the required orifice velocity can be estimated as explained below.

The orifice velocity is calculated for an assumed recovery pressure. For this orifice velocity, the pipe velocity (V_p) is calculated by assuming the pipe diameter to be 1 in. (which is typical of our laboratory reactor). The orifice-to-diameter ratio is assumed to be 0.5. From the charts of permanent pressure loss versus orifice-to-pipe diameter ratio, the discharge pressure from the pump is calculated corresponding to the recovery pressure P_2. The discharge from the pump (Q) is then calculated by multiplying the velocity through the pipe by the area of a cross-section of the pipe. The product of the discharge and the pressure head loss gives the total energy dissipated in the system. This energy is dissipated in a zone extending approximately eight pipe diameters downstream of the orifice in which the pressure recovery takes place.

Acoustic and Optical Cavitations. In acoustic cavitation, the threshold frequency required to generate and collapse the cavities is obtained from the graph of threshold intensity (I) vs. frequency (f) reported by Mason (1991). This intensity multiplied by the area of the transducers through which it is transmitted gives the power input to the system in watts. Typically, the acoustic intensity is supplied from either an ultrasound horn or a bath. Here we consider the case of an ultrasound horn. The diameter of a horn is typically 1 cm (area 0.78 cm^2). The threshold intensity multiplied by the area of the horn gives the power input. The optical cavitation is simulated by extending the acoustic cavitation for a high-frequency range (>1 MHz).

Energy Output Calculations. The energy output rates under different types of cavitation were examined by evaluating bubble behavior from the numerical simulation. An initial bubble radius of 10 μm is taken for simulation to be typical of the values reported in the literature. The expansion and collapse of the bubble is governed by the bubble dynamics equation,

$$Rd^2R/dt^2 + (3/2)(dR/dt)^2 = (1/\rho)(P_{g0}(R_0/R)3\gamma - 2\sigma/R - 4\mu R(dR/dt) - P_\infty) \tag{8.2}$$

Here R is the instantaneous radius of the bubble, dR/dt is the bubble velocity, d^2R/dt^2 is the bubble wall acceleration, P_{g0} is the initial pressure inside the bubble, ρ is the density of the cavitating medium, and P is the time-varying pressure in the bubble environment. The specific assumptions in this equation are as follows:

1. Only one bubble is considered at a time; collective oscillations of the bubble (i.e., cluster effects) and bubble–bubble interactions are neglected.
2. The liquid is assumed to be incompressible.
3. The bubble content is assumed to obey the ideal gas law.
4. The growth of the bubble is assumed to be isothermal while the collapse is adiabatic, i.e., heat and mass transfer effects in the collapse phase of the bubble are neglected.
5. The program is terminated (i.e., the bubble is assumed to collapse) at a point when the bubble wall velocity exceeds 1500 m/s, (the velocity of sound in water).
6. The intensity of the acoustic field in case of acoustic cavitation is assumed to be uniform and constant.
7. In hydrodynamic cavitation, two separate sets of assumptions can be made:
   the cavity escapes the shear layer after its inception
   the cavity remains in the shear layer after its inception, as a result of which the maximum growth is restricted by inertial and surface tension forces defined in terms of a critical Weber number. The results are described here with both of these assumptions.
8. The initial conditions of the simulation are as follows:

$$\text{At } t = 0, R = R_0 \text{ and } dR/dt = 0.$$

The value of P in both acoustic and hydrodynamic cavitation can be estimated in different ways. This can be explained as follows:

Hydrodynamic Cavitation. The pressure variation in hydrodynamic cavitation is linear, with turbulent pressure fluctuation superimposed over it. The stepwise procedure for the calculation of the P in hydrodynamic cavitation as a function of time or distance downstream of the orifice is given below:

1. First, knowing the values of the orifice and pipe velocities, the time for pressure recovery is obtained from Newton's law (8.3).
2. To estimate the turbulent fluctuation velocities and the eddy frequency, the assumption of isotropic turbulence is made. In isotropic turbulence, the power input per unit mass is given as

$$P_M = -(3/2)d(v')^2/dt \tag{8.3}$$

3. Power input per unit mass can be obtained by dividing the net energy input estimated as permanent pressure loss by the mass of water in the zone of pressure recovery.
4. To estimate the turbulence length scale, a Prandtl eddy model is used. According to this model, the length is given as

$$l = 0.08\ \mathrm{d} \tag{8.4}$$

where d is the diameter of the conduit. Here d is taken as the average of orifice and pipe diameters. With this, the turbulent velocity and the frequency of turbulent velocity fluctuations are estimated as

$$P_M = (v')^3/l \tag{8.5}$$

$$f = v'/l \tag{8.6}$$

5. The local pressure without turbulence can be estimated on the basis of linear pressure recovery as

$$P_\infty = P_v + (P_2 - P_v)t/\tau \tag{8.7}$$

where τ is the pressure recovery time. Using this mean pressure, the local mean velocity at a particular point downstream of the orifice is calculated. The turbulent velocity fluctuations have been superimposed on it assuming that a sinusoidal velocity variation in the instantaneous velocity is given as

$$v_{tn} = v_t + v'\sin(2\pi ft) \tag{8.8}$$

This instantaneous velocity is used to estimate the local static pressure using Bernoulli's equation of the following form:

$$P_t = P_v + 1/2\ \rho \times V_o^2 - 1/2\ \rho V_{tn}^2 - \Delta P \tag{8.9}$$

The following parameters for bubble growth and collapse can thus be obtained:

the time for the bubble growth
the time for the bubble collapse
the minimum pressure reached in the bubble during oscillation
the pressure in the bubble at a point when its bubble wall velocity exceeds 1500 m/s

Acoustic Cavitation. In acoustic cavitation, the variation in pressure is taken as sinusoidal. Here P is written as

$$P_\infty = P_0 - P_A \sin \omega t \tag{8.10}$$

where P_0 is the bulk pressure (atmospheric), P_A is the maximum pressure amplitude, and ω is the angular frequency of ultrasonic irradiation given as

$$\omega = 2\pi f \tag{8.11}$$

The maximum acoustic pressure amplitude is calculated from the threshold intensity of the ultrasound field for the frequency. It is given as

$$P_A = (2I\rho_L C)^{1/2} \tag{8.12}$$

where I is the acoustic intensity (W/cm^2), ρ_L is the density of the cavitating medium, and C is the velocity of sound in the cavitating medium.

Stability Criterion for the Bubbles. A solution of the Rayleigh–Plesset equation often shows significant bubble growth, on the order of 10 to 100 times their original size. A bubble, however, may not be stable at such a stage and its stability may be evaluated based on a Weber number stability criterion. The Weber number is defined as

$$\text{We} = u^2 \rho d_{\max} / \sigma \tag{8.13}$$

where u is the bulk fluid velocity in the cavitation medium, $d_{\max}$ is the maximum stable bubble diameter, ρ is the density of the cavitating medium, and σ is the surface tension. For a stable bubble, the Weber number should be either less than or equal to one.

For acoustic cavitation, the bulk velocity is defined as u = frequency of the horn × amplitude of oscillation of the horn. For hydrodynamic cavitation, u is the same as the turbulent fluctuation velocity, v', and its calculation was explained in detail in the section on hydrodynamic cavitation. When solving the Rayleigh–Plesset equation, the Weber number criterion has to be applied at every stage.

Energy Balance During Bubble Lifetime. Apfel (1981) has given an energy balance during bubble oscillations. The energy stored in the bubble is released after its collapse. The work done by the bubble during its growth minus the work done by the bubble during its collapse is stored in the bubble as potential energy, which is released after its collapse. Consider a bubble of initial radius R_0 pulsating in an

incompressible fluid of density ρ. The radius of the bubble varies with time according to the relation,

$$R = R_0 + \xi_b \tag{8.14}$$

Here we assume that the pressure variation and the radial displacement ξ_b are in phase. As the bubble pulsates, the surrounding liquid is set into motion. If the frequency is low, it will move as if it is incompressible. This means that at any time t the total volume that is displaced outward through any spherical surface of constant radius R is independent of r. Thus the volume of displacement is $4\pi R^2\xi_b$, at any arbitrary value of R at that time. Assuming ξ_b is small compared with the equilibrium radius R_0, we set $R \cong R_0$ and obtain

$$\xi/\xi_b = R^2/r^2 \tag{8.15}$$

Thus the displacement in the liquid varies inversely with r^2. It follows that the velocity dR/dt also varies inversely with r^2. The assumption of incompressible flow on which these inverse-square laws are based is valid for a distance r smaller than the wavelength λ for sound waves in the liquid.

The kinetic energy of the mass of the liquid surrounding a pulsating sphere of radius r is given by $1/2\ M_{\text{eff}}(dR/dt)^2$ where M_{eff} is the effective mass felt by the bubble given by three times the mass of the liquid that would fill the sphere,

$$M_{\text{eff}} = 3\rho(4\pi/3)R^3 \tag{8.16}$$

This kinetic energy minus the energy dissipated at the surface due to viscous effects is equal to the work done by the surface tension σ and internal and external liquid pressures, P_i and P_0, respectively. Extending this equation over the entire bubble life cycle, assuming isothermal growth and adiabatic collapse, we have,

$$1/2M_{\text{eff}}(dR/dt)^2 - \int_{R_0}^{R}(-4\mu/R\ dR/dt)4\pi R^2 dR = \int_{R_0}^{R_1}(P_0 + 2\sigma/R_0)(R_0/R)^3 4\pi R_2 dR$$

$$- \int_{R_1}^{R_2}[(P_0 + 2\sigma/R_0)(R_1/R_2)^{3y} - 2\sigma/R]4\pi R^2 dR \tag{8.17}$$

$$= 4\pi(P_0 - 2\sigma/R_0)R_0^3 \ln R_1/R_0 - \{[4\pi(P_0 - 2\sigma/R_0)R_1^3/3(1-\gamma)[(R_2/R_1)3(y-1) - 1]$$

$$- 4\pi\sigma R_1^2[(R_2/R_1)^2 - 1]\} \tag{8.18}$$

Here R_0 is the initial radius, R_1 is the maximum radius during growth, and R_2 is the radius when the bubble wall velocity crosses the sonic velocity in the cavitating liquid. The equation of bubble dynamics was solved for the conditions in both acoustic and hydrodynamic cavitation. Representative radius and pressure pulse history diagrams of the bubble oscillations are shown in Figure 8.1 (for case 1) for hydrodynamic cavitation and in Figure 8.2 for acoustic cavitation. The parameters for all the simulations are given in Table 8.3.

Results and Discussion. For hydrodynamic cavitation, as mentioned earlier, we investigated two limiting cases for the cavity path. The results shown in Table 8.4 indicate that a cavity residing in the shear layer dissipates much less energy than a cavity escaping the shear layer. This is because the growth of a cavity residing in the shear layer is restricted by inertial and surface tension forces (critical Weber number) rather than the surrounding pressure field.

The calculated values of work stored in the bubble, the maximum and minimum radius ratio (at a bubble wall velocity of 1500 m/s) R/R_0, the corresponding pressures in the bubble, and the life-time of the bubble are given in Table 8.5. For frequencies exceeding 100 kHz, the bubble undergoes two or more oscillations before a violent collapse. For the conditions described in Table 8.5, the cumulative work stored in the bubble for each oscillation is estimated. The fact that the work stored in the bubble goes on decreasing with frequency implies that the energy output of the reactor per bubble also decreases with increasing frequency.

The variations of energy output per bubble vs. frequency are shown in Figures 8.3(a) and (b) for hydrodynamic cavitation cases 1 and 2, respectively and in Figure 8.4 for acoustic cavitation. Here we see that the curve of output vs. frequency shows two peaks, one each in an acoustic and a hydrodynamic cavitation regime. This indicates that the energy output per bubble is not directly proportional to the frequency of operation. Therefore these results are useful in deciding the optimum frequency for the cavitation reactor, i.e., one at which the output from each bubble is maximum. In the case of a very high frequency (>1 MHz), the output again increases because of multiple oscillations resulting from a single bubble.

The energy efficiency of the reactor can be defined as energy output per bubble divided by the total energy input to the reactor per unit volume. The energy efficiencies of hydrodynamic cavitation reactors as functions of frequency for cases 1 and 2 are shown in Figures 8.5(a) and (b) and in Figure 8.6 for acoustic cavitation. It can be inferred from the figures that the efficiency of the hydrodynamic cavitation reactor decreases as the frequency goes up, while the efficiency of the acoustic cavitation reactor shows two peaks, one each at 20 and 100 kHz, and passes through a minimum at 50 kHz.

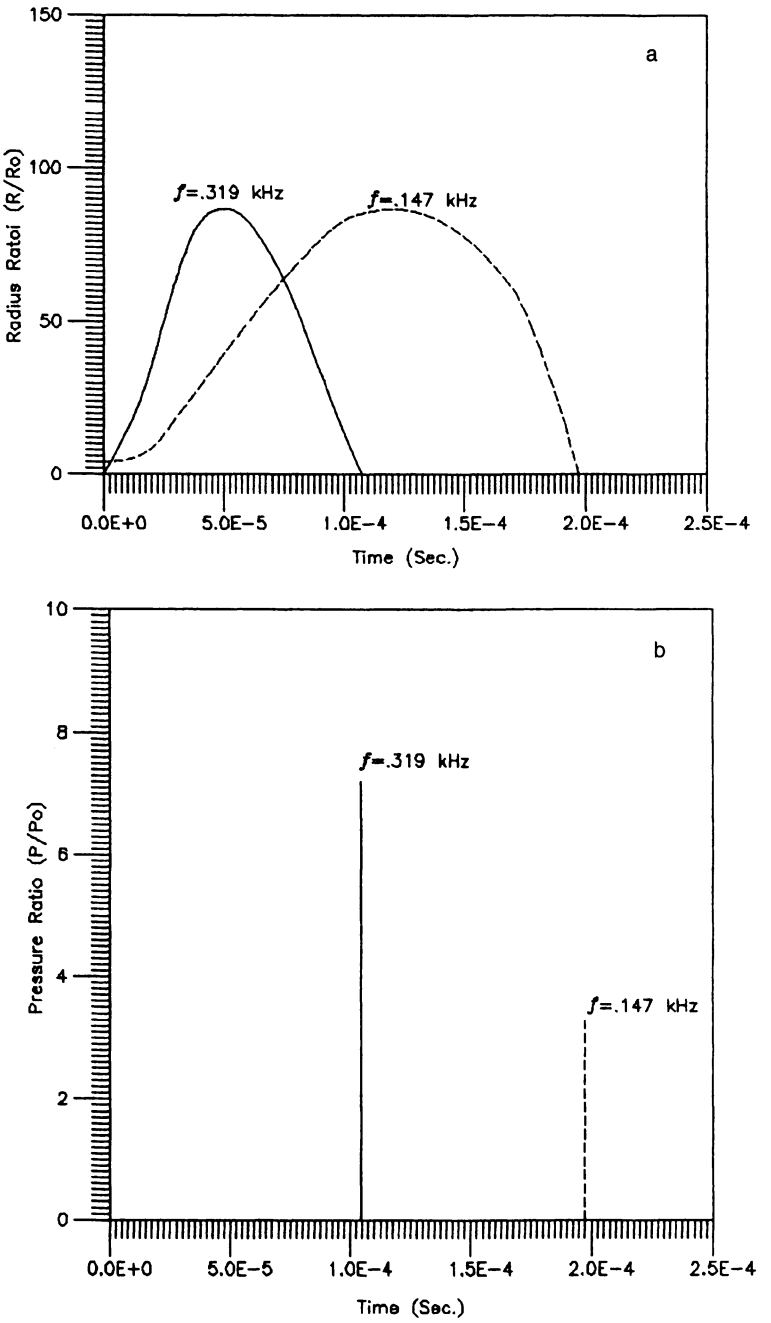

Figure 8.1. Representative radius (a) and pressure (b) versus time profiles for hydrodynamic cavitation.

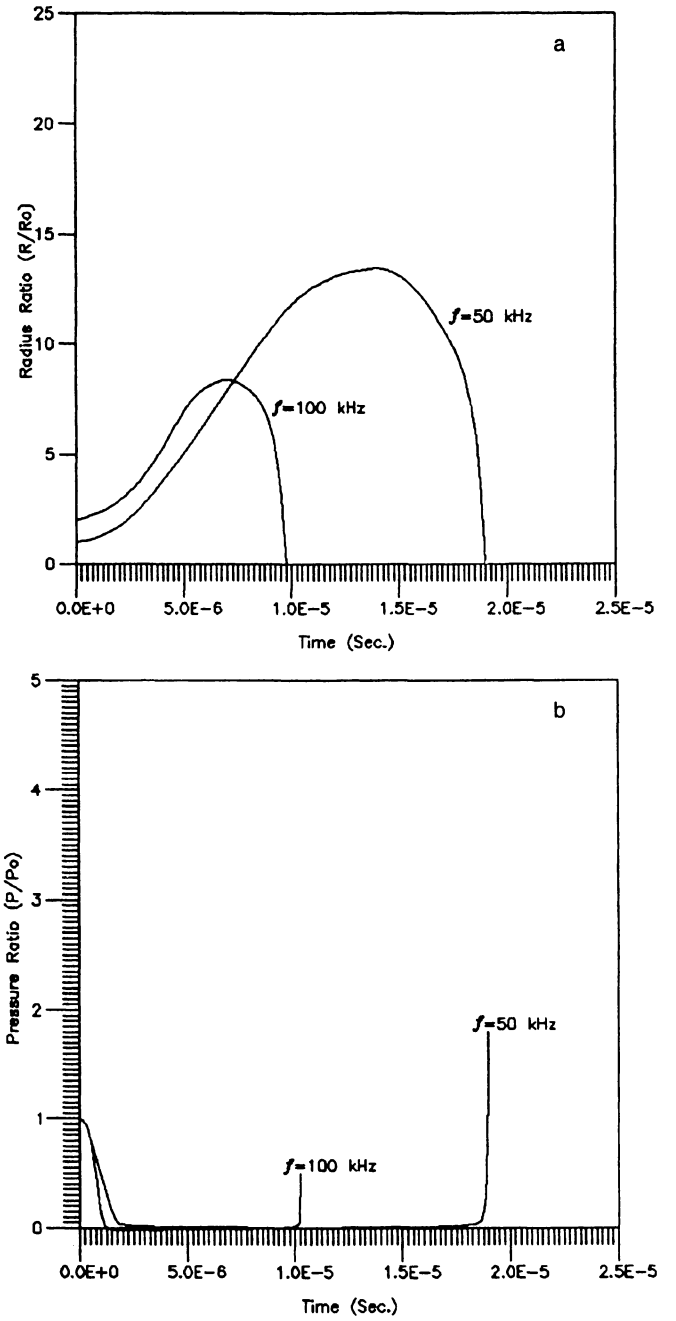

Figure 8.2. Representative radius (a) and pressure (b) versus time profiles for acoustic cavitation.

TABLE 8.3. Conditions for Simulation Results

Type of cavitation	Frequency (kHz)	Intensity/Recovery (W cm^{-2}/atm)	Initial bubble radius (mm)
Hydrodynamic	0.147	10	0.01 (case 1) 1.87×10^{-4} (case 2)
Hydrodynamic	0.208	20	0.01 (case 1) 9.36×10^{-5} (case 2)
Hydrodynamic	0.319	50	0.01 (case 1) 3.7×10^{-5} (case 2)
Hydrodynamic	0.452	100	0.01 (case 1) 1.87×10^{-5} (case 2)
Hydrodynamic	0.748	300	0.01
Intermediate	2	2	0.01
Intermediate	5	3	0.01
Intermediate	10	4	0.01
Intermediate	15	4.5	0.01
Acoustic	20	5	0.01
Acoustic	50	6	0.01
Acoustic	100	10	0.01
Acoustic	250	20	0.01
Acoustic	500	50	0.01
Acoustic	1000	500	0.01
Acoustic	10,000	500	0.01
Acoustic	50,000	500	0.01
Acoustic	100,000	500	0.01

Here we have made an attempt to determine how energy input and output of a reactor varies with the operating frequency. As we mentioned earlier, the energy output rate is a function of bubble behavior in the given atmosphere. Therefore it is necessary to study bubble behavior under a range of frequencies generated by a

TABLE 8.4. Maximum Bubble Radius Reached During Hydrodynamic Cavitation (Weber Number Criteria)[a]

Frequency (kHz)	Max. bubble size (μm)
0.147	1.8731
0.208	0.9359
0.319	0.3742
0.452	0.1871

[a]Maximum size cavity can grow if it stays in the shear layer.

TABLE 8.5. Details of the Simulation Results

Case	f(kHz) (case)	Max (R/R_0)	Min (R/R_0)	τ (s)	Min. pressure (atm)	Max. Pressure (atm)	W (J)	Energy input (J)	Efficiency per bubble
1	0.147	170.25	0.86	3.594E–4	8.218E–11	0.3659	9.1575E–9	56.1386	1.63E–10
2	0.147	1.0976	0.94	1.198E–4	5.491	10.51	6.075E–15	56.1386	1.19E–16
1	0.208	172.11	4.52	3.049E–4	7.851E–11	3.413E–4	9.3484E–9	134.922	6.93E–11
2	0.208	1.1	0.94	8.416E–5	11.00	20.94	1.5719E–15	134.922	1.17E–17
1	0.319	173.23	7.47	1.984E–4	7.642E–11	4.151E–5	9.4281E–9	347.374	2.71E–11
2	0.319	1.0969	0.938	5.382E–5	27.44	52.15	2.535E–16	347.374	7.3E–19
1	0.452	173.55	9.86	1.414E–4	7.583E–11	1.29E–5	9.4474E–9	700.47	1.35E–11
2	0.452	1.0968	0.939	3.695E–5	54.88	80.51	6.433E–17	700.47	9.18E–20
1	0.748	91.43	3.78	4.996E–5	1.119E–9	7.258E–4	8.1406E–9	1286.285	6.33E–12
1	2	180.25	8.32	3.931E–4	4.163E–10	1.585E–4	9.2114E–9	6.10E–4	1.51E–5
1	5	91.47	4.44	1.685E–4	7.085E–9	2.19E–3	8.0084E–9	3.94E–4	2.03E–5
1	10	53.19	2.64	8.805E–5	6.826E–8	0.01903	7.0469E–9	2.75E–4	2.57E–5
1	15	37.75	1.89	5.98E–5	2.859E–7	0.07721	6.439E–9	2.10E–4	3.07E–5
1	20	29.91	1.51	4.56E–5	7.558E–7	0.1961	6.0264E–9	1.78E–4	3.39E–5
1	50	13.42	0.6747	1.896E–5	2.148E–5	5.743	4.6058E–9	8.87E–5	5.19E–5
1	100	8.45	0.414	1.0236E–5	1.484E–4	58.6039	3.7858E–9	7.98E–5	4.74E–5
1	250	4.59	0.1638	4.7216E–6	1.89E–3	2164.04	2.7041E–9	7.37E–5	3.67E–5
1	500	3.23	0.1571	4.0101E–6	8.186E–3	2569	2.3838E–9	1.56E–4	1.53E–5
1	1,000	3.38	0.09	3.777E–6	6.769E–3	25970	2.752E–9	1.47E–3	1.87E–6
1	10,000	1.12	0.27	2.387×10^{-6}	0.1	30.18	7.3301×10^{-10}	1.47E–3	4.99E–7
1	50,000[a]	1	0.354	2.069×10^{-6}	0.16	10.36	1.3207×10^{-9}	1.47E–3	8.98E–7
1	100,000[a]	1	0.3721	1.984×10^{-6}	0.18	8.447	1.216×10^{-9}	1.47E–3	8.27E–7

[a]This bubble first undergoes compression before expanding. For optical cavitation (freq. >1 MHz) we have dondensed only the first oscillation for the efficiency calculation because the bubble undergoesseveral oscillations at identical frequencies. The final efficiency results would be identical even if multiple oscillations were considered.

variety of pressure transducers. In the present analysis it is also assumed that the cavity of the specified size already exists and the energy required to generate such a cavity has been neglected.

The analysis presented here will enable the designer to determine the optimum frequency or an optimum range for acoustic and hydrodynamic cavitation reactors for a particular application. Although the total efficiency of the reactor will depend on the actual number of cavities that get generated and collapse per unit of time (which in turn depends on whether the cavitating medium is aerated or any gas is bubbled through it during cavitation), the energy output per bubble is an indication of the reaction intensity of the cavitation reactor.

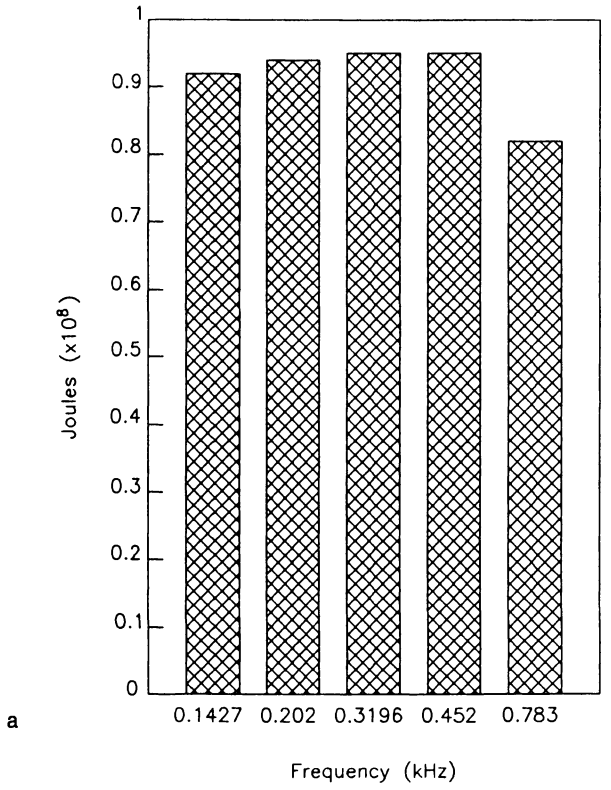

Figure 8.3. Hydrodynamic cavitation. Energy output per bubble vs. frequency. (a) case 1 and (b) case 2.

8.2d. Cavitation Yield Model

One gross method for assessing the energy efficiency of the cavitation conversion process is to define the term "cavitation yield" as

cavitation yield = measured effect/cavitation power

The measured effect is the amount of product generated in a fixed time. The cavitation power is the energy entering the reactor and is not necessarily the same as electrical power consumed. This can be assessed by calorimetry, measurement of the initial temperature rise in the system, such as when the ultrasonic irradiation is first switched on or when hydrodynamic cavitation first begins. Ultrasonic power units can be quoted as either the energy emitted at the surface of the ultrasonic device in W cm^{-2} or the energy dissipated in the bulk of the sonicated medium (in W cm^{-3}). Various methods for determining the power input in the acoustic vessel are described in a later section. Hydrodynamic energy loss can be computed in terms of pressure loss in the orifice. Optical energy can be computed in terms of energy input by the laser.

For every reaction system, cavitation yield exhibits an optimum with respect to the cavitation power. For example, Contamine *et al.* (personal communication) presented the data shown in Figure 8.7, which indicate that for KI oxidation as well as the Michael reaction, the conversion per unit power input has optimum values.

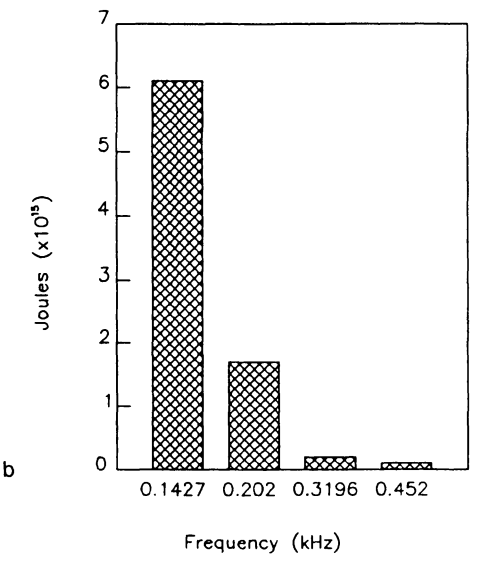

Figure 8.3. (cont.)

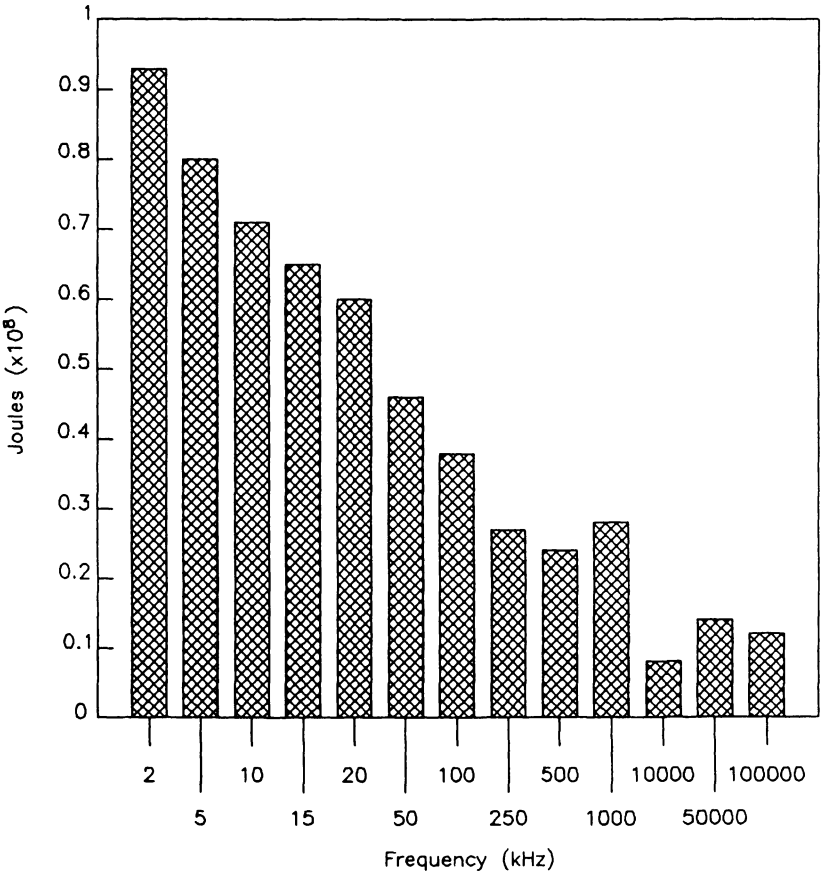

Figure 8.4. Acoustic cavitation. Energy output per bubble vs. frequency.

Similar results were reported by Ratoarinoro *et al.* (1995) for Michael addition of diethyl malonate with chalcone. In this system, toluene was used as solvent and potassium hydroxide as catalyst. While the optimum values of the cavitation yield may depend on the nature of the reaction and the reactor, they may form the basis for the appropriate reactor scaleup.

Application to Acoustic Reaction. When the cavitation yield model is applied to an acoustic reaction, it is generally described as a sonochemical yield model. The efficiency of the energy input in the sonochemical reaction depends upon a number of parameters, such as the nature of the reaction vessel, the position of the ultrasonic probe within the reaction medium, and the method of ultrasound input to the reaction media. Contamine *et al.* (personal communication) examined the effects

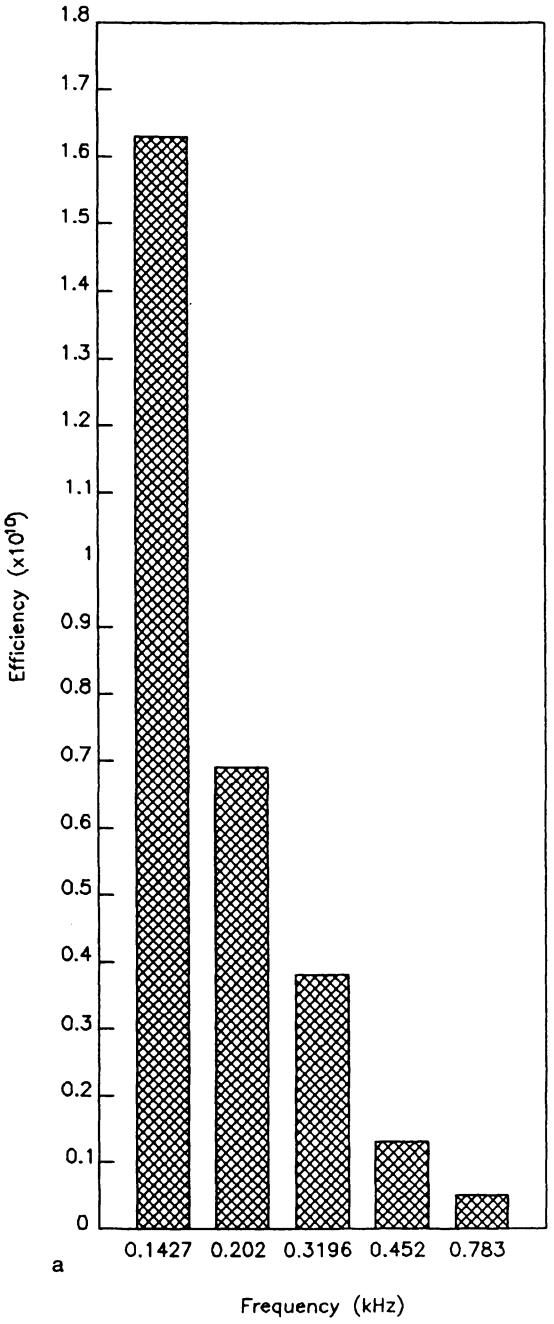

Figure 8.5. Hydrodynamic cavitation. Energy efficiency vs. frequency. (a) case 1 and (b) case 2.

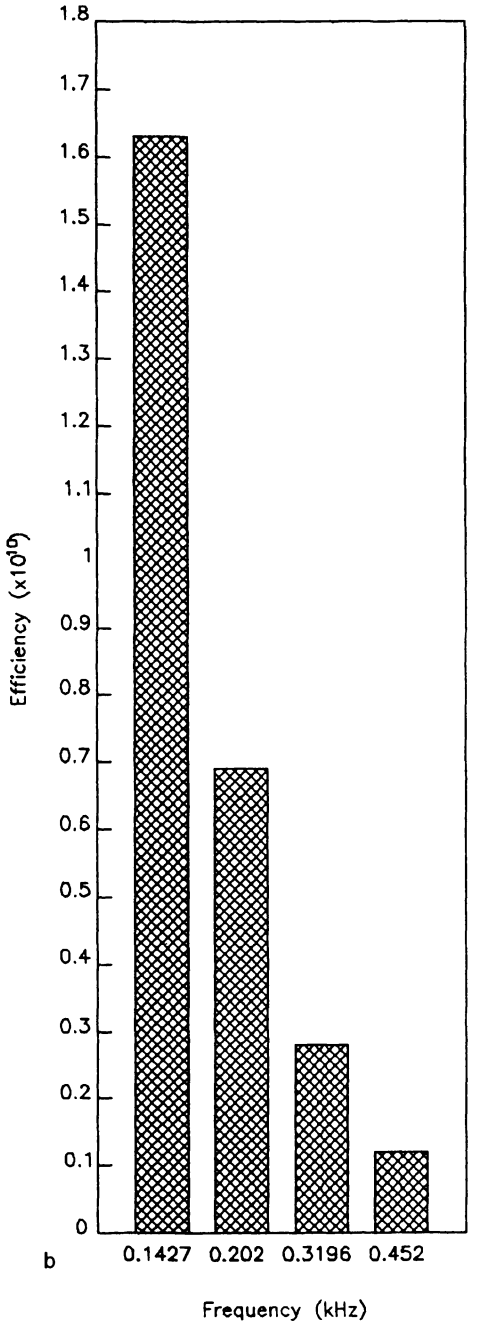

Figure 8.5. (cont.)

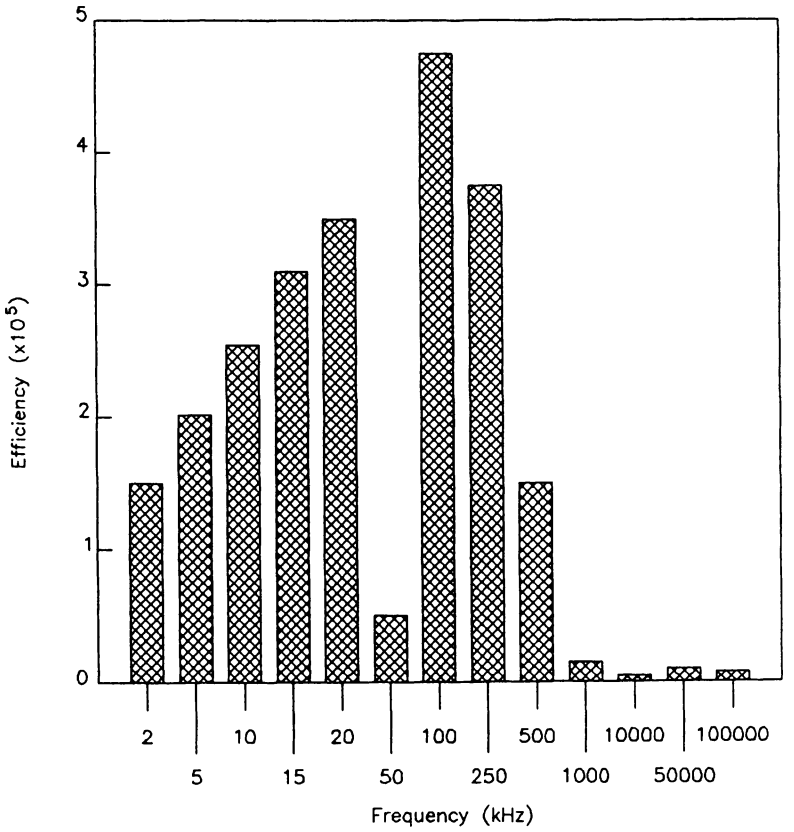

Figure 8.6. Acoustic cavitation. Energy efficiency vs. frequency.

of these parameters on sonochemical yield for the iodine liberation reaction. Three different types of reactor systems: a reactor immersed in a cleaning bath, a reactor with an immersed ultrasonic probe, and a reactor with the sonication through the walls were examined. Some details of the study are given below.

Reactor Immersed in a Cleaning Bath. For this type of reactor, a comparison was made of the efficiency of three differently shaped vessels in a Kerry Pulsatron 55 cleaning bath (35 kHz) filled with water containing 5% Decon 90 detergent at 25°C. The calorimetric measurements revealed that the maximum energy was transmitted into a volume of 55 cm^3 using a 100-cm^3 round-bottomed flask. The results for iodine liberation were, however, quite different. By far the most efficient result was obtained using a 250-cm^3 conical flask containing a 55 cm^3 reaction mixture. When the results were combined to obtain a measure of cavitation yield, the combination

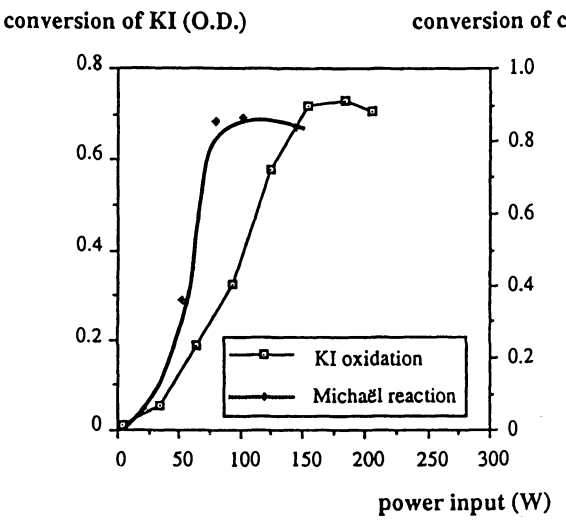

Figure 8.7. Relationships between KI oxidation and Michael addition reaction conversion and acoustic power input (liquid height 4.4 cm; sonication; 900 s). (From Contamine *et al.*, personal communication, with permission.)

of 55 cm^3 reaction volume and a 250-cm^3 conical flask gave the best results. This result can be rationalized in terms of the larger base area of the vessel, which gives a better transmission of energy, and the depth of the liquid in the vessel, which is related to the wavelength of sound in the medium. The optimum result is shown in Table 8.6.

Ultrasonic Probe Immersed in the Reactor. For this evaluation, a Sonics and Materials VC600 sonicator system (20 kHz) was used to irradiate a 27.4-cm^3 reaction volume. In this situation, the results show that for a fixed volume, the most efficient result is obtained using the horn with the largest tip diameter. This can be explained in terms of the improvement in energy transfer through a larger face of the irradiating source. The optimum result is described in Table 8.6.

TABLE 8.6. Comparison of Sonochemical Yields for Different Reactors[a, b]

Probe (1.2-cm tip, 27.5 cm^3 reagent).	35
Tube reactor (1500 cm^3 reagent)	14
Bath (250 cm^3 conical, 55 cm^3 reagent)	10

[a]From Mason and Berlan (1992) with permission.

[b]Sonochemical yield quoted in grams of iodine (liberated after 5 min) per watt ($\times 10^{-5}$).

Sonication Through the Walls of a Reactor. For this study, a small Branson pentagonal tube reactor sealed at one end and with a volume of 1500 cm^3 operating at 40 kHz was first used as a reaction vessel. The pentagonal tube was then filled with water containing 5% detergent (Decon 90), and a series of glass tubes containing the reaction mixture were inserted to serve as reactors. The effects of the change in cross-section of these tubes on the efficiency of the reaction reveals an optimum cross-sectional diameter of 26.5 mm, which is almost as efficient as using the pentagonal vessel itself as the reactor. This result is almost certainly related to the distance from the irradiating face to the glass wall of the inserted tube and the wavelength of sound in the water used as coupling fluid. This optimum result is given in Table 8.6.

Comparison of Sonication Methods. The optimum values of the sonochemical yield obtained in these three different types of reactors are compared in Table 8.6. It is clear from these results that the order of effectiveness for the three methods is probe system > pentagonal reactor > dipped reaction vessel. The life of the transducer in a probe reactor, however, may be smaller than the one imbedded on the tube walls or the one used in ultrasonic bath reactors. It must, however, be emphasized that this cavitation (or sonochemical in this case) yield comparison is only valid for the particular instruments used and the sonochemical reaction chosen as a model. If an attempt is made to expand this scheme to include other reactors, care must be taken to ensure similar irradiation conditions. The irradiation frequency affects the radical reactions of the type used in odometry, and other external parameters may also have a significant influence on the sonochemical yield. For some types of sonochemical reactions, it might be advisable to find another model reaction for estimating sonochemical yield. One possible reaction is polymer degradation, which relies on the shear forces produced on cavitational collapse and is not significantly influenced by the sonochemical generation of free radicals. A scaleup of the optimum sonochemical yield obtained for the probe reactor generally requires careful consideration of the details of the reactor design.

Appropriate Power Measurement in Sonochemistry. Ratoarinoro *et al.* (1995) examined various ways of measuring power input in sonochemistry. They concluded that the choice of reference power measurements is of great importance when reporting results in sonochemistry. Great care should be taken when taking into account the generator-displayed power. The generator input and output electric powers, adequately measured, can both be used as references. The electrical power is important from an economics point of view, because it determines the energy cost; on the other hand, the output measurement is also interesting as the phase shift is determined, which is important for good tuning of the generator.

The relationship of power to the chemical yield depends on the volume of the liquid. This means that the sonochemical yield, which can be defined as the

chemical yield divided by the electrical power input, depends on the acoustic load. It appears to be increased with the load, with a possible optimum value (see Figure 8.8). In a recent study by Hagenson and Doraiswamy (1998) and one by Hagenson *et al.* (1994), optimum values of the liquid–solid mass transfer coefficient with respect to power input were similarly observed for two levels of liquid height (see Figure 8.9). Ratoarinoro *et al.* (1995) also found that the specific dissipated power (i.e., dissipated power per unit volume) was almost independent of the liquid height (see Figure 8.10), that is, of the volume. This dissipated sonic power is linearly correlated with the electrical power input or output, and the measurement of these different powers is important in order to make sure that every part of the ultrasound device works well. Their measurements should be carried out at regular intervals to ensure reproducible results.

One of the important scaleup parameters is the relationship between the power distribution or intensity, measured in units of power flux, and the total power effectively (i.e., cavitationally) deposited in a given volume. Here we apply this question on an area-specific parameter to one that is volume-specific, as outlined by Martin and Ward (1992) and Martin (1993). While the analysis is given for acoustic cavitation, it can be adopted for laser cavitation.

Because of the nature of the transducers in acoustic cavitation, the source of the ultrasound field will typically be a circular surface vibrating with frequency f and amplitude a as shown in Figure 8.11. An intensity $I = I_o$ is delivered by the radiating face, defined by

$$I = 2\pi^2 \rho f^2 a^2 c \tag{8.19}$$

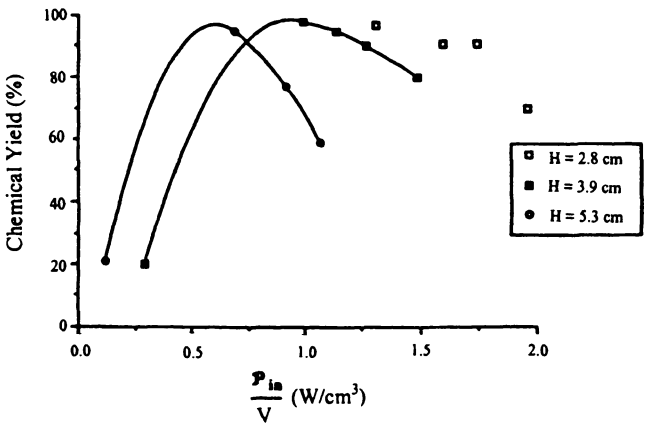

Figure 8.8. Chemical yield versus generator specific input power for different liquid heights. H = □, 2.8; ■, 3.9; ○, 5.3 cm. (Reprinted from *Ultrasonics Sonochemistry*, **2**(1), F. Ratoarinoro *et al.*, "Power measurement in sonochemistry," pp. 543–547, 1995, with permission from Elsevier Science.)

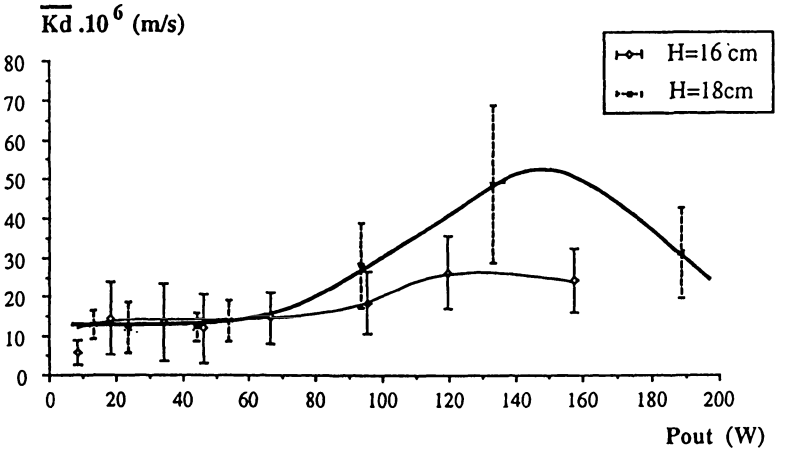

Figure 8.9. Relationship between liquid–solid mass transfer coefficient and acoustic power input at two different liquid levels. (Data from Hagenson *et al.*, 1994, and Hagenson and Domaiswamy, 1998.)

and energy is dissipated largely through a main lobe of the ultrasound field subtending an angle from the normal. Intensity falls off with distance from the radiating face by cavitational dissipation and beam spreading until the intensity falls below the threshold intensity for cavitation: beyond this threshold distance, cavitation is absent and energy is wasted in heat. In practice, at the frequencies most used

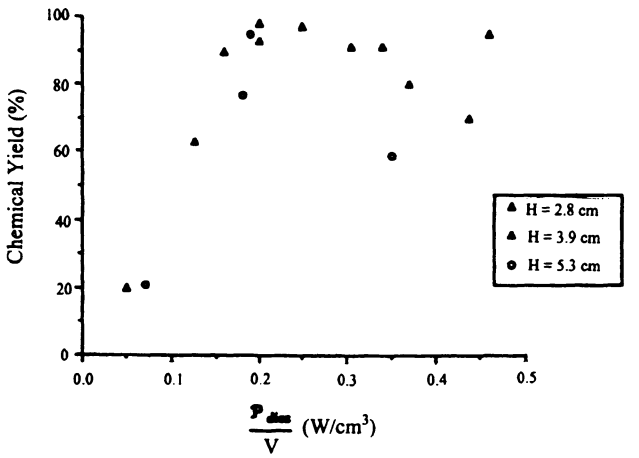

Figure 8.10. Chemical yield versus specific dissipated power for different liquid heights. H = △, 2.8; ▲, 3.9; ○, 5.3 cm. (Reprinted from *Ultrasonics Sonochemistry*, **2**(1), F. Ratoarinoro *et al.*, "Power measurement in sonochemistry," pp. 543–547, 1995, with permission from Elsevier Science.)

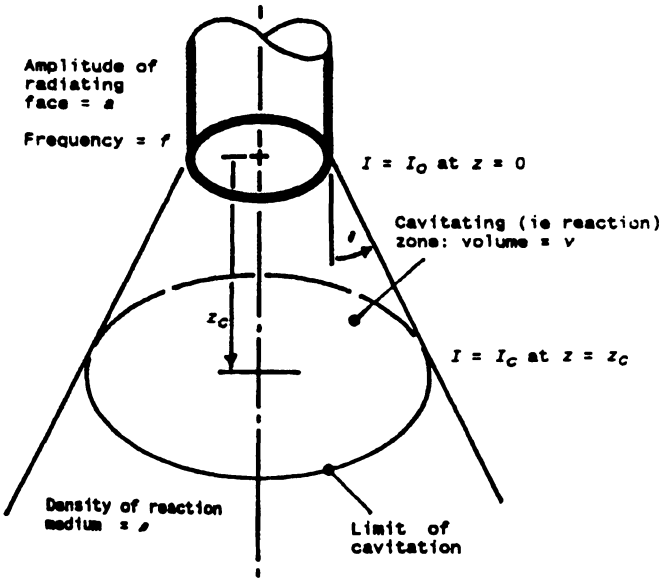

Figure 8.11. Intensity, power dissipation, and volume of the "active" cavitation zone. (From Martin and Ward, 1992, and Martin, 1992, with permission.)

for sonochemistry, 20–50 kHz, the effective range is a few centimeters, or at best a few tens of centimeters. If Λ is the attenuation constant, it can be shown using appropriate assumptions that the power dissipated in the cavitating zone is given by

$$P = \int_0^{z_c} \pi(r_0 + z\tan\theta)^2 \Lambda I_{(z)} dz = \pi I_0 r_0^2 (1 - e^{-\Lambda z_c}) = P_0(1 - e^{-\Lambda z_c}) \qquad (8.20)$$

The power so dissipated can in turn be related to the measured conversion by means of an empirical constant.

Looking at the above analysis, it can be seen that intensity, power distribution, and actively cavitating volume can in principle be correlated, at least for a single source; some uncertainties still remain regarding the interaction of multiple sources. However, the range of cavitationally effective ultrasound is limited even in gas–liquid systems, and will be more so in the many gas–liquid–solid systems of interest to sonochemists. Therefore, in scaling up batch reactors for industrial applications, some form of two-zone layout as indicated by the loop reactor is most appropriate.

Other Considerations. Sonochemical yield is a rather gross method for evaluating the energy efficiency of the sonochemical conversion process. In essence it is expected that in order to optimize a sonochemical yield there will be an optimum value for almost all the variables that influence cavitation. In addition, one might expect that these optima will be very precise so that great care will be needed when scaling up sonochemical processes.

The use of sonochemical yield for reactor scaleup, however, has some inherent difficulties. For the same power input per unit volume of the reactor, we do not get the same value of the sonochemical yield for two reactors of different sizes, even if geometric similarity is maintained. The reason for this is the highly nonlinear nature of the phenomena associated with cavitation. Whereas reasonably uniform cavitation may be possible on the laboratory scale, the same cannot be achieved on a larger scale, where the cavitation occurs only in a limited zone of the reactor.

At present, attempts are being made to identify different geometries and configurations that can give reasonably uniform acoustic intensity in the sonication zone. However, methods are not available for predicting the performance of a larger reactor from experiments in a small batch reactor. Matters become more complex if a continuous reactor is to be designed based on the data collected on a batch system.

When gas–liquid–solid reactions are involved, the particles undergo pitting and breakage during cavitation. Perhaps the particles can be sonicated in the absence of reaction and the resulting particles used during the reaction. This may produce no significant breakage during sonication. However, for such reactions, the increase in mass transport may not be the same for small and large reactors.

A further interesting feature has been introduced by Martin and Ward (1992), who discovered the memory effect in such reactors. When a catalyst or a solid reactant gets sonicated, its surface gets partially cleaned and its activity increases. However, this activity does not fall to zero when the particle leaves the sonicator zone. It retains this activity for some time to come. While these authors considered an exponential decay of the memory, the effects may be more complex and need to be investigated further, possibly through pulse sonolysis. It is possible that the memory effects last for a period shorter than the average residence time in the stirred vessel. To ensure that only spent particles go to the sonicated zone, it might be better to have a stirred sectionalized column that will act as several stirred vessels connected in series. The memory effect in a loop reactor is further described by Martin and Ward (1992) and in Chapter 7.

When a reactor consists of packed particles, these particles seriously scatter the ultrasound, thereby making a reactor scaleup based on the sonochemical yield model more difficult. The passage of fluidized particles through the sonicator offers a smaller alteration, but the sonicated zone might have to be enlarged for the proper scaleup.

Finally, we have no control over the rate of nucleation. A small and a large reactor might have different rates of nucleation. It is necessary to study the nucleation phenomena and try to find external nucleation sites that can be introduced as well. Alternatively, a stage might be introduced in the loop in which the reactants can be saturated with an inert gas. This will introduce a uniform nucleation rate with time as otherwise the contents slowly get degassed, thereby affecting nucleation. Ultrasonic reactors with the best potential for scaleup using the sonochemical yield model are listed in Table 8.7.

While the above discussion is largely restricted to the sonochemical reaction, similar principles should be applied to hydrodynamic or optical cavitation. At present, however, there is no detailed literature available on this topic.

8.2e. G-Method for Energy Efficiency

In a recent study, Thoma *et al.* (personal communication) compared the performance of sonochemical conversions with other methods of conversion using a conversion efficiency concept from radiation chemistry commonly reported as the G method. They used this method to evaluate the efficiency of removal of a contaminant from an aqueous system in order to assess the economic suitability of the process for industrial application. The G method is based on the parameter G, which is defined as the number of molecules converted (reacted) per 100 eV input to the system. While the basis for the input to the system may be debatable, Thoma *et al.* (personal communication) used the energy drawn from the electrical outlet as the energy input. Thus all inefficiencies associated with conversion of electrical energy to sonic energy to chemical energy are included. Furthermore, in acoustic cavitation, the G value will be concentration dependent since the likelihood of the contaminant conversion in an environment with an essentially constant molar concentration of hydroxyl radicals (assuming that the radical mechanism is a dominant one) will be directly proportional to the contaminant's molarity. It is therefore important to note the concentration of the reactant and applied power level when reporting the G efficiency.

A comparison of the G efficiencies for acoustic cavitation and other oxidation processes was outlined by Thoma *et al.* (personal communication). In the case of

TABLE 8.7. Ultrasonic Reactors with Potential for Scaleup[a]

Submersible transducer
Probe system with flow cell
Tube reactor (circular cross-section)
Near-field acoustic processor (NAP)

[a]From Mason and Berlan (1992) with permission.

supercritical water oxidation, estimates of both the heating and high-pressure pumping energy requirements were included; it was assumed that the heating requirements were mitigated by preheating the feed with the treated effluent, with an overall thermal retention of 80%. For photocatalytic treatment, the rated lamp power and the total reaction time were used to calculate the power input to the system. The data showed that the acoustic cavitation efficiencies (i.e., G efficiencies) obtained by Thoma *et al.* were lower than the ones obtained by other methods. However, no effort was made to optimize the energy efficiency in the acoustic cavitation method used by Thoma *et al.* The calorimetric efficiency of the reaction system studied by Thoma *et al.* was determined to be on the order of 10%, based on the nominal power supplied and the observed temperature increase in the system operated in the batch mode. The data of Thoma *et al.* (personal communication) suggested that the economics of acoustic conversion require an efficient conversion of electrical to sonic energy.

Apart from using an acoustic system that delivers an efficient conversion of electrical energy, other options to improve energy efficiency include a combination of ultrasound with other advanced oxidation processes, such as hydrogen peroxide treatment, ozonation, or UV photolysis. Thoma *et al.* also suggested the use of electrolysis in the reactor chamber to provide oxygen bubbles as nucleation sites. This may reduce the power required for the cavitation threshold and more energy may be used for the growth and collapse of cavities and the generation of free radicals rather than the creation of cavity nuclei. In summary, it is clear that if cavitation reaction engineering is to become a commercially viable technology, more attention needs to be given to efficient methods for the generation and collapse of transient cavities.

8.2f. Case Studies

The energy efficiency of hydrodynamic and acoustic cavitation was examined by Joshi and Pandit (1993), Moholkar and Pandit (1997), and Pandit and Moholkar (1996) for three case studies: typical depolymerization and repolymerization, biological cell rupture, and hydrolysis of fatty oils. Their results are briefly described below.

Depolymerization and Repolymerization. The energy input requirement for an equal decrease in the viscosity of a PEO solution was calculated for both acoustic and hydrodynamic cavitation. The values of energy required per milliliter of solution were found to be as high as 14337 J/ml for sonic irradiation, while in the case of hydrodynamic cavitation they were found to be negligibly small, 76 J/ml. This difference is, however, for a limited range of depolymerization. Acoustic cavitation was in general capable of depolymerization at a greater extent than hydrodynamic cavitation. For hydrodynamic cavitation, the increase in the viscos-

ity observed in the case of PEO solutions on continued irradiation was not observed for CMC solutions, indicating that CMC polymerization (cellulose is a naturally occurring polymer) cannot be initiated within the range of intensity obtained in hydrodynamic cavitation. Acoustic cavitation, while less energy efficient, was capable of a larger degree of repolymerization of CMC.

Biological Cell Rupture. A comparison of the energy input levels of conventional cell rupture devices and a hydrodynamic cavitation setup presented an interesting set of results. The typical energy input levels for a cell to rupture to a similar extent under similar conditions are

Mixer blender	1200 J/ml
Ultrasonic horn	600 J/ml
Hydrodynamic cavitation setup	4.5 J/ml

These results reveal that the energy efficiency of hydrodynamic cavitation is higher than conventional methods by an order of magnitude. Thus hydrodynamic cavitation reactors open up opportunities for treating in a continuous manner the large amounts of broth required industrially. The range of the achievable extent of rupture for the first two methods, however, may be higher than that possible for hydrodynamic cavitation.

Hydrolysis of Fatty Oils. For hydrolysis of fatty oils after an initial period of 100 to 200 min of ultrasonic irradiation, both the acid value and its rate of increase showed a significant increase. The rate of increase of the acid value after this initial period was found to be independent of the type of oil. While similar trends were observed for a loop system using hydrodynamic cavitation, the time of initiation in this case was quite high. The actual electrical power inputs were considered in calculating energy efficiency. Motor pump or ultrasonic horn efficiencies were neglected. Here the energy input rates were found to be 1384 J/ml for sonic cavitation and 1080 J/ml for hydrodynamic cavitation. Therefore it can be concluded that conditions similar to those of an ultrasonic generator can be created downstream of the throttled cavitating valve.

Conclusions. These three studies indicate that there is a tradeoff between energy consumption and the intensity of the reaction conditions. In general, hydrodynamic cavitation is less energy intensive but offers less severe reaction conditions than acoustic cavitation. Both hydrodynamic and acoustic cavitation compare favorably with conventional conversion processes in energy efficiency.

8.3. ECONOMICS OF CAVITATION CONVERSION PROCESSES

One of the major applications of the cavitation reactor is the treatment of aqueous waste. The conventional processes that have often been used for either the destruction or the transformation of wastes are high-temperature incineration, amended activated sludge digestion, anaerobic digestion, adsorption, and wet air oxidation. Among these processes, the common literature has shown that the biological sludge process (activated or modified activated sludge process) is the most versatile for widely differing quantities and qualities of wastewater and even for water containing inorganic impurities. Wet-air oxidation and combustion processes are attractive for high organic loading (COD), i.e., when the exothermic heat of oxidation can self-sustain the process.

Based on the published reports (Joshi *et al.*, 1985; Goodwin, 1991), it appears appropriate to compare ultrasonic conversion with the activated biological sludge process for an economic evaluation. Goodwin (1991) has shown that for hydrolysis of methyl benzoate, the cost of ultrasonic processing could be in the range of 0.15 to 15 cents/kg, depending on the ultrasonic energy required for the reaction. The costs estimated by the U.S. Department of Energy for a waste-dump cleanup operation run in the range of 0.4 to 800 cents/kg of liquid waste, with typical costs of 15 cents/kg as an average. As seen from these figures, the costs associated with sonication and activated sludge processes are comparable and hence a detailed analysis should be performed based on the actual destruction and transformation rates observed for a specific effluent when treated under well-characterized cavitation conditions. Such a detailed analysis is given for two separate case studies in the next section.

8.3a. Case Study 1

The costs of construction and the costs of operating an activated sludge process that treats effluent from the chemical industry have been reported in the literature in the form of the following empirical correlation:

$$C = 485\, Q^{0.58}(L_o/L_e)^{0.12} \tag{8.21}$$

where C is the construction cost in dollars ($\times 10^{-3}$), Q is the effluent processing rate (million gallons per day), and L_o and L_e are the inlet and outlet COD levels.

If we take a typical case of the treatment of the effluent at a rate of 250 m^3/day (0.066 mgd) having a COD reading of 2000 ppm to be brought down to 100 ppm, the process for which the reported correlation is valid is an activated sludge process which includes the cost of sludge disposal.

Thus the total construction cost is

$$C = 485 \times (0.066)^{0.58}(2000/100)^{0.12} \times 1.74^{*} \tag{8.22}$$

$$= 250{,}000 \text{ dollars} \tag{8.23}$$

*To correct for 1990 costs, the correlation has been developed in 1966 costs.

If a 3-year depreciation period is considered, then the fixed cost is 0.11 cent/kg of effluent treated (300 working days, 24-h operation)

The typical operating costs of a similar plant have also been reported in the literature as $1588 per million gallons per day (1966 basis). Thus, to treat 250 m^3/day of effluent in 1990 (using the same correction factor), the operating costs are 0.07 cent/kg.

The total treatment cost then is 0.11 + 0.07 = 0.18 cent/kg of effluent. As seen from the above analysis, this is still two orders of magnitude lower than the average cost estimates provided in the literature. It should, however, be noted that there is a difference in the cost of treating standard chemical wastes and those for treating hazardous wastes, including halogenated hydrocarbons. The literature also indicates that the operating cost estimates could vary significantly (one or two orders of magnitude), depending on the nature of the effluent.

In comparison, if sonic treatment is chosen for the same effluent quantity and quality (250 m^3/day and a COD of 2000 to 100), the work by Sweet and Casdonte (personal communication) can be used to estimate the rates of degradation of organic effluents treated with sonication. Though the details of their equipment are not available, it can be assumed that they were working with typical power densities of 10 W/cm^2. The reported rate constants for first-order degradation kinetics are in the range of 2×10^{-4} s^{-1} to 1×10^{-3} s^{-1} for the range of organic effluents typically digested in an activated sludge process.

Let us consider an average value of $k = 5 \times 10^{-4}$ s^{-1} for our case. To treat 250 m^3 effluent/day with a COD reduction from 2000 to 100, the average rate of degradation desired is

$$\text{rate of degradation} = 250 \text{ m}^3/\text{day} \times (2000 - 100)\text{g}/\text{m}^3 \tag{8.24}$$

$$= 475{,}000 \text{ g/day} \tag{8.25}$$

Thus assuming again a batch process, the average concentration of the contaminants that will provide the overall rate of degradation can be taken as (C_{avg} = (2000 + 100)/2 = 1050 g/m^3).

This gives the size of the sonic reactor required as

$$\text{desired rate of degradation} = k_1 \times C_{avg} \times V \tag{8.26}$$

$$475{,}000 = 5 \times 10^{-4} \times 3600 \times 24 \times 1050 \times V \tag{8.27}$$

Therefore

$$V = 10.5 \text{ m}^3\text{, let us say } 10.0 \text{ m}^3 \tag{8.28}$$

Let us now estimate the cost of a 10.0-m^3 sonic reactor having an average power density of 10 W/cm^3 at the transducer surface.

Goodwin (1991) reports the cost of a 5 m^3 cleaning-type sonoreactor as approximately \$75,000 to \$100,000, with 30 kWh as operating power costs. Following a similar argument and an identical procedure, a 10-m^3 sonic reactor would cost about \$375,000 and would consume about 250 kWh.

Thus the contribution of the fixed costs of treatment for the same quantity and quality effluent (250 m^3/day, COD reduction from 2000 to 100) is 0.166 cent/kg of effluent (3-year depreciation, 300 working days and 24-h operation). The operating costs can be estimated on the basis of 250 kWh of electricity consumption at a rate of 5 cents/kWh as 0.12 cent/kg of effluent. The total processing cost thus is (0.166 + 0.12 = 0.29) cent/kg of effluent.

As can be seen from the calculations, sonochemical degradation is about 35% more expensive than the conventional activated sludge process, but it is still on the lowest possible scale of the hazardous waste treatment cost reported as 0.4 cent/kg. Goodwin (1991) also discusses the fact that the cleaning bath type of reactor considered in this analysis is probably an expensive one, and immersible transducer types or flow types would enhance the ultrasonic energy deliveries by as much as 15-fold with an appropriate design (Arakeri and Chakraborty, 1990; personal communication with Arakeri). It has also been pointed out that each degradation or conversion process must be optimized with respect to the cavitation intensity desired for the required physical and chemical change. Thus, other means of generating cavitation conditions (choice of the reactor or means of generating cavitation) can also offer substantial reductions in the processing costs. The problems of microbial sensitivity to sudden and unexpected toxic loads are well known for an activated sludge process, whereas sonication or cavitation-assisted degradation or conversion does not have a similar problem.

Thus, from a process economics point of view, an optimum chemical route to the final product that might be economically most attractive requires knowledge of optimum cavitation conditions at the least possible cost. The preliminary economic analysis indeed suggests the utility of such an exercise, as can be seen from the detailed calculations.

The scaleup effects, as discussed by Goodwin (1991), can be elaborated along the lines of chemical engineering principles, as was done in Chapter 7 for the cavitation reactor. The analysis provided here should encourage the possible users

of ultrasound to look into this mode of effluent treatment as an industrially feasible alternative.

8.3b. Case Study 2

In the absence of ultrasound, the conversion of benzoic acid (esterification) requires 90 min under reflux conditions to obtain 100% conversion. Ultrasound dramatically increases the rate of reaction so that under irradiation it is complete within 20 min at room temperature. The change in rate with the use of ultrasonic intensity (represented as amplitude of vibration of the transducer) is shown in Figure 8.12. It can be seen that the rate increases when the amplitude is increased between 1 and 5 μm, but there is no further increase in rate when the amplitude is increased between 5 and 10 μm. This can be attributed to the ultrasound causing a reduction in the ester droplet size within the aqueous phase between 1 and 5 μm. This decrease in size increases the interfacial contact area between reagents and so increases the rate of reaction. There is no further decrease in droplet size between 5 and 10 μm and so there is no further increase in the rate of reaction.

The condition for optimum energy efficiency is shown in Figure 8.13; here the total ultrasonic energy delivered to the reaction mixture during the course of the reaction is plotted against the operational amplitude of the transducer. The mini-

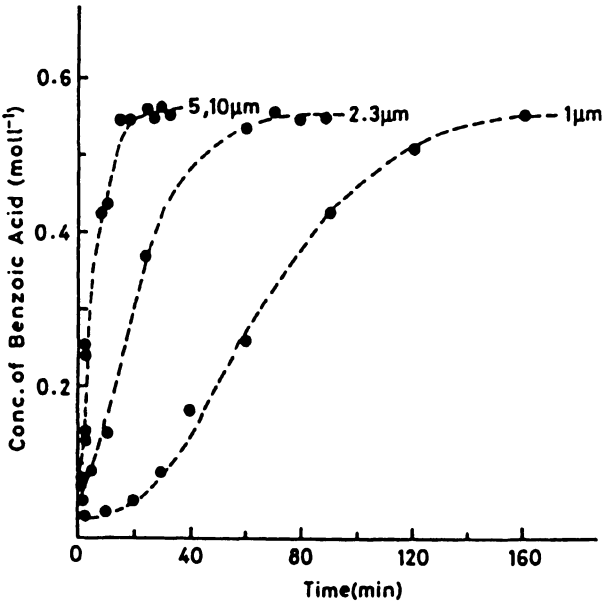

Figure 8.12. Concentration of benzoic acid versus time. (From Perkins, 1990, with permission.)

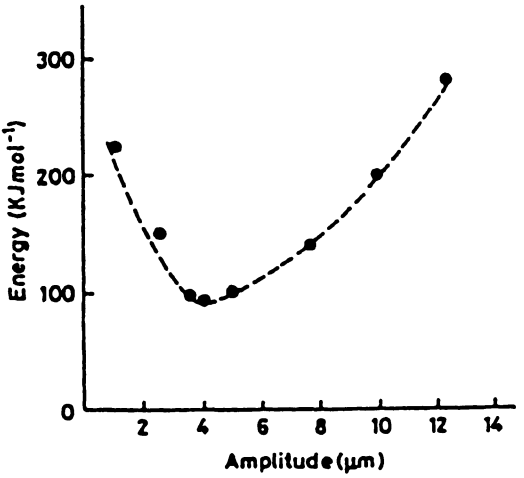

Figure 8.13. Acoustic energy delivered by sonic horn versus amplitude of vibration of horn. (From Perkins, 1990, with permission.)

mum energy required is at 4 μm; below this value, the reaction is proceeding too slowly; above this value, the reaction is being overirradiated and so ultrasonic energy is being wasted. The amount of ultrasonic energy (~100 kJ mol^{-1}) is significantly less than the amount of thermal energy (>500 kJ mol^{-1}) required to drive the reaction to completion. The amount of ultrasonic energy has been found to be dependent on the geometry of the reaction vessel; under the correct conditions it can be reduced by a factor of 15. Using this information, and other information on the capital and operating costs of ultrasonic equipment, it is possible to produce an estimate of the cost of using ultrasound to enhance a chemical reaction. Assuming the cost of processing is based on an electrical cost of approximately 1.5 cents per kWh and a capital cost of 300 p W^{-1} depreciated over 3 years, the cost of ultrasonic processing can be estimated to be on the order of 0.1–10 p kg^{-1}, depending on the amount of ultrasonic energy required for the reaction. This cost is not prohibitive and indicates that once the appropriate equipment has been developed, large-scale sonochemical processing should be economically favorable.

8.3c. Sonochemistry vs. Photochemistry

It is interesting to compare the cost and energy of a typical photochemical reactor with a typical sonochemical reactor. Such a comparison is given in Table 8.8. As shown, a typical gas–liquid sonochemical reactor is comparable in both cost and energy efficiency to a photochemical reactor. The typical gas–liquid–solid reactor is much cheaper and far better in energy efficiency than a photochemical reactor.

TABLE 8.8. Comparison of Economics Between Sonochemistry and Photochemistry[a]

	Photochemistry	Gas–liquid sonochemistry	Gas–liquid–solid sonochemistry
Source:	250-W quartz halogen lamp	200-W cell disrupter (60% power)	150-W cleaning bath
Approximate cost ($):	1800	1900	700
Typical rates:	7 mol/min	10 mol/min	500 mol/min
Electrical efficiency:	2 mmol/kWh	5 mmol/kWh	200 mmol/kWh

[a]From K. Suslick, in *Advances in Organometallic Chemistry*, vol. 25, pp. 73–113, 1986, with permission of Academic Press.

Earlier discussions also indicate that the energy dissipation level in the form of the cavitational activity can be increased manyfold by matching the driving frequency of the ultrasonic transducer with the natural frequency of the reactor. The comparative results shown in Table 8.8 may very much depend on the nature of the reaction and the reactor, and the size of the operation.

8.4. CONCLUDING REMARKS

While much remains to be done on accurate assessments of the energy efficiency and the economics of cavitation conversion processes, this chapter indicates that both hydrodynamic and acoustic cavitations are reasonably energy efficient. The degree of efficiency, however, depends on the cavitation conditions, such as frequency, power input, and presence of a gas. Much needs to be done on the effects of bubble–bubble interaction and cluster formation on energy efficiency. While the cavitation process can compare well with other conventional processes on economics grounds, successful commercial operations will greatly depend on the ability to uniformly cavitate a large-scale cavitating medium. A full understanding of the appropriate scaleup processes will be needed.

9

CAV-OX PROCESS

9.1. INTRODUCTION

In this chapter we outline the commercial viability of a patented cavitation oxidation process developed by Magnum Water Technology of El Segundo, California—CAV-OX. This process was partially developed under the Environmental Protection Agency's (EPA) Site program. A detailed description of much of the material presented in this chapter is given in the literature published by EPA and Magnum Water Technology (1994). The CAV-OX process uses hydrodynamic cavitation. To our knowledge, a similar process using acoustic cavitation has not been publicized. In principle, the concept of the CAV-OX process can be used with acoustic cavitation.

As indicated in the CAV-OX process, the commercial viability of the cavitation chemical conversion may be best achieved through a hybrid process involving cavitation (hydrodynamic or acoustic) along with other advanced oxidation processes. The value added by the cavitation in many advanced oxidation processes will provide the best commercial potential. The advantages and disadvantages of various available technologies for treating VOCs in water, including the CAV-OX process, are listed in Table 9.1.

9.2. DESCRIPTION OF PROCESS

The CAV-OX process is designed to destroy dissolved organic contaminants in water. It uses hydrodynamic cavitation, ultraviolet radiation, and hydrogen peroxide to oxidize organic compounds in water. This process produces no air emissions and generates no sludge or spent media that require further processing, handling, or disposal. Ideally, end products are water, carbon dioxide, halides (for example, chloride), and in some cases, organic acids. A schematic of the process is shown in Figure 9.1. In the process, a cavitation chamber induces hydrodynamic cavitation,

TABLE 9.1. Comparison of Technologies for Treating VOCs in Water[a]

Technology	Advantages	Disadvantages
Air stripping	Effective at all concentrations; mechanically simple; relatively inexpensive	Inefficient at low concentrations; VOCs discharged to air
Steam stripping	Effective at all concentrations; removes a wide variety of VOCs	VOCs discharged to air; high energy consumption
Air stripping with carbon adsorption of vapors	Effective at all concentrations	Inefficient at low concentrations; generates large volumes of spent carbon requiring disposal or regeneration
Air stripping with carbon adsorption of vapors combined with spent carbon regeneration	Effective at all concentrations; no carbon disposal costs; can reclaim the product	Inefficient at low and high concentrations; high energy consumption
Carbon adsorption (liquid phase)	Effective at all concentrations; low air emissions; relatively inexpensive	Inefficient at low concentrations; requires disposal or regeneration of spent carbon
Biological treatment	Low air emissions; relatively inexpensive; low energy requirements; VOCs destroyed	Inefficient at high concentrations; generally not effective for chlorinated aliphatic compounds; slow rates of removal; sludge treatment and disposal required
Other enhanced oxidation processes	Effective at hw concentrations; no air emissions; no secondary waste; VOCs destroyed	High energy consumption; not cost effective at high concentrations
CAV-OX® process	Effective at low concentrations; no air emissions; no secondary waste VOCs destroyed	High energy consumption; not cost effective at high concentrations; process mechanisms not well documented

[a]From CAV-OX, a publication of Magnum Water Technology, El Segundo, CA, and "CAV-OX Cavitation Oxidation Process," Application analysis report, EPA/540/AR-93/520, Magnum Water Technology, Inc., Risk Reduction Engineering Laboratory, Cincinnati, Ohio, 1994.

which occurs when a liquid undergoes a dynamic pressure reduction while under constant temperature. The pressure reduction causes the formation of cavities that subsequently grow and collapse. The energy released from the cavity implosion decomposes water into extremely reactive hydrogen atoms and hydroxyl radicals, which may recombine to form hydrogen peroxide and molecular hydrogen. The cavitated liquid is processed through low-energy or high-energy advanced oxidation steps that include hydrogen peroxide and UV radiation generated by mercury vapor lamps. In these steps, further oxidation occurs via hydroxyl and hydroperoxyl radicals, which are generated by the direct photolysis of hydrogen peroxide at UV wavelengths.

The skid-mounted CAV-OX setup consists of the cavitation chamber, UV reactor, and control panel unit (see Figure 9.1). Contaminated water is pumped through the cavitation chamber, where hydroxyl and hydroperoxyl radicals are produced. The water then either enters the UV reactor or is recycled through the cavitation chamber; the rate of recycle determines the hydraulic retention time. Magnum recycled water through the cavitation chamber to continue the generation of hydroxyl and hydroperoxyl radicals. Hydrogen peroxide is usually injected into the process, in line between the cavitation chamber and the UV reactor. In the UV reactor, the water flows through the space between the reactor wall and a UV transmissive quartz tube in which a UV lamp is mounted. The treated water exits the UV reactor through an effluent line.

The CAV-OX process can treat a number of contaminants, such as atrazine, chlorinated organics, halogenated organics, petroleum hydrocarbons, pesticides and herbicides, polychlorinated biphenyls (PCBs), polynuclear aromatic hydrocarbons (PAHs), benzene, toluene, ethylbenzene and xylene (BTEX), cyanides, phenol, bacteria, and viruses. A number of specific chemical species from industrial wastewater and groundwater that can be treated by the CAV-OX process are listed in Table 9.2. The cavitation process alone reduces contaminant concentrations by about 20 to 50%. The synergistic combination of cavitation and UV radiation can reduce contaminant concentrations by 95 to 99.99%. The CAV-OX process does not treat metals. It, however, does oxidize metallic ions or reduce metallic salts in the process of destroying organic contaminants. The process can be operated in one of the following modes:

- cavitation chamber only
- cavitation chamber with low-energy UV radiation and hydrogen peroxide
- cavitation chamber with high-energy UV radiation and hydrogen peroxide

Theoretically, a CAV-OX process of any size can be constructed and operated. The design is modular. For example, groups of 250-gpm units can be operated in parallel. Currently several units of 50-gpm capacity are in operation. The influent to the CAV-OX process may need to be monitored. A desirable influent characteristic is listed in Table 9.3. Excessive solids may be harmful to the UV process even though they are not particularly disruptive to the hydrodynamic cavitation process. The CAV-OX I low-energy process requires a 230-V, 3-phase, 30-A power supply. An internal transformer supplies 120-V, single-phase, 10-A power for the chemical feed pump and control panel. The CAV-OX II high-energy process requires a 480-V, single-phase, 30-A power supply, and a separate 120-V, single-phase, 10 A power supply for the chemical feed pump and control panel. The process is free from scaling of the UV tubes.

In a limited number of situations, a CAV-OX cavitation chamber and ancillary equipment can be used as a standalone process to reduce contaminant concentra-

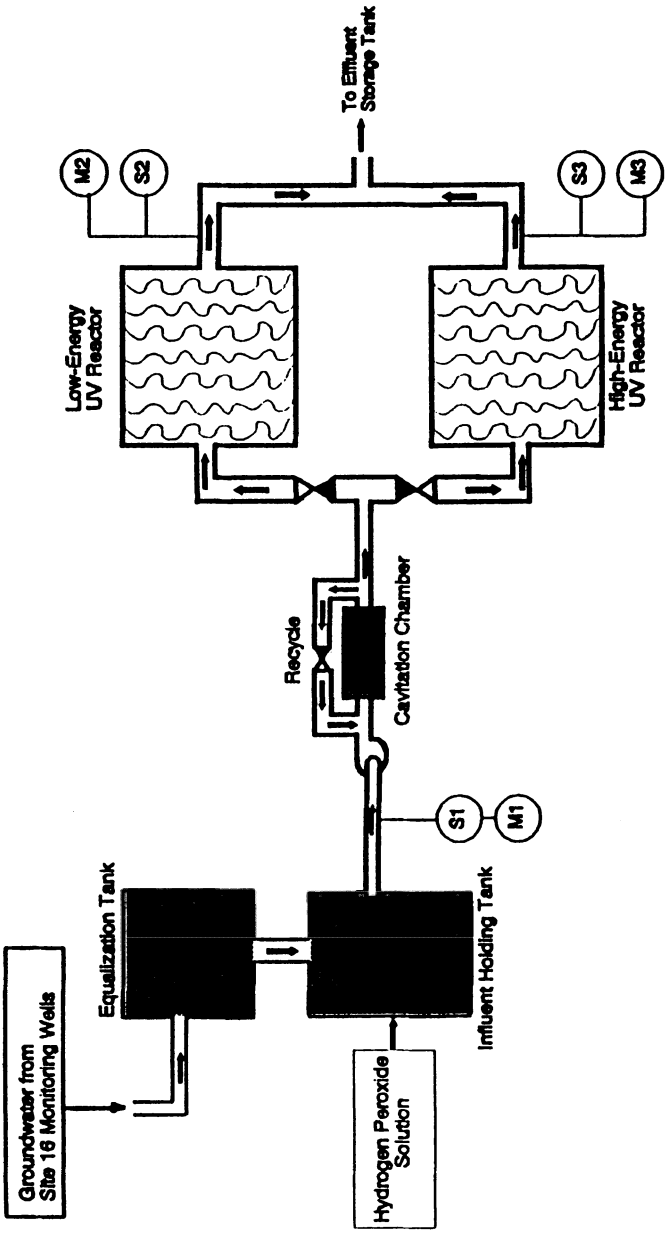
To Effluent Storage Tank
M2
S2
S3
M3
Low-Energy UV Reactor
High-Energy UV Reactor
Recycle
Cavitation Chamber
S1
M1
Equalization Tank
Influent Holding Tank
Groundwater from Site 16 Monitoring Wells
Hydrogen Peroxide Solution

SAMPLE COLLECTION (S) OR MEASUREMENT (M) LOCATION	LOCATION IDENTIFIER	PARAMETERS	
		SAMPLE	MEASUREMENT
MAIN FEED LINE FROM INFLUENT HOLDING TANK	S1 M1	TCE, BTEX, HYDROGEN PEROXIDE, TOC, TC, POC, METALS, ALKALINITY, HARDNESS, TRPH, VOCS (GC/MS), SVOC, TURBIDITY, BIOASSAY	pH, TEMPERATURE, FLOW RATE, SPECIFIC CONDUCTANCE
EFFLUENT LINE FROM CAV-OX • I UV REACTOR	S2 M2		
EFFLUENT LINE FROM CAV-OX • II UV REACTOR	S3 M3		

(S) = Sample Location

(M) = Measurement Location

Figure 9.1. CAV-OX process sample and measurement locations. (From CAV-OX, a publication of Magnum Water Technology, El Segundo, CA, and "CAV-OX Cavitation Oxidation Process," Application analysis report, EPA/540/AR-93/520, Magnum Water Technology, Inc., Risk Reduction Engineering Laboratory, Cincinnati, Ohio, 1994.)

TABLE 9.2. Contaminants Treated by CAV-OX Process[a]

Industrial wastewater	Groundwater
Amines	bis(2-chloroethyl)ether
Aniline	Creosote
Chlorinated solvents	1,2-Dichloroethane
Chlorobenzene	Dioxins
Complex cyanides	Freon 113
Creosote	MEK
Hydrazine compounds	MIBK
Isopropanol	Methylene chloride
Methyl ethyl ketone (MEK)	PCBs
Methyl isobutyl ketone (MIBK)	PCP
Methylene chloride	Pesticides
PCBs	PAHs
PCP	Tetrachloroethene
Pesticides	1,1,1-Trichloroethane
Polynitrophenols	Trichloroethene
Cyclonite	Tetrahydrofuran
2,4,6-Trinitrotoluene	Vinyl chloride
Toluene	Triglycol dichloride ether
Xylene	

[a]From CAV-OX, a publication of Magnum Water Technology, El Segundo, CA, and "CAV-OX Cavitation Oxidation Process," Application analysis report, EPA/540/AR-93/520, Magnum Water Technology, Inc., Risk Reduction Engineering Laboratory, Cincinnati, Ohio, 1994.

tions by 50 to 80%. Some typical examples for such conversions are given in Table 9.4. Although this operating mode is the least expensive, it normally is not effective for contaminants requiring high percentage reductions. Case study 1 provides an example of using the CAV-OX cavitation chamber only. In this case study, a

TABLE 9.3. Desirable Influent Characteristics[a]

Characteristic	Value
Turbidity	< 25 NTU
Iron salts	< 5 mg/liter
Color	< 25 TCU
Suspended matter	< 10 μm
Free product	< 25 mg/liter

[a]From CAV-OX, a publication of Magnum Water Technology, El Segundo, CA, and "CAV-OX Cavitation Oxidation Process," Application analysis report, EPA/540/AR-93/520, Magnum Water Technology, Inc., Risk Reduction Engineering Laboratory, Cincinnati, Ohio, 1994.

TABLE 9.4. Typical Hydrocarbon Conversion Results CAV-OX Chamber Only Tests (No UV, No H_2O_2)[a]

Percent Reduction					TCE RAW (ppb)
Benzene	Ethyl benzene	Toluene	Xylene	TCE	
		Protocol A			
67	11	37	—	65	1850
54	39.6	53	51	60	1680
41	71	49	59	45	1860
32	20	43	ND	41	1680
		Protocol B			
37	44	38	38	38	1620
37	43	37	37	37	1620
40	ND	55	ND	33	993
		Protocol C			
23	54	31	38	24	1860
17	60	26	42	22	1860
19	53	26	35	19	1860
16	24	20	23	18	1680

[a]From CAV-OX, a publication of Magnum Water Technology, El Segundo, CA, and "CAV-OX Cavitation Oxidation Process," Application analysis report, EPA/540/AR-93/520, Magnum Water Technology, Inc., Risk Reduction Engineering Laboratory, Cincinnati, Ohio, 1994.

Notes: Variations in percent reductions were the result of changing operating protocols. Neither ultraviolet radiation nor hydrogen peroxide was employed in this series of tests.

ND = not detected.

CAV-OX process capable of processing 3900 gph was designed for Southern California Edison Co. to treat 3 million gallons of contaminated seawater with a high biochemical oxygen demand using the cavitation chamber only.

9.3. PROCESS ECONOMICS

Typical operating costs for the CAV-OX process are as follows:

CAV-OX cavitation chamber only: about $0.5 per 1000 gal of treated water
CAV-OX I low-energy process: about $2 per 1000 gal of treated water
CAV-OX II high-energy process: about $4 per 1000 gal of treated water

Table 9.5 presents cost data for three groundwater treatment methods: a filter carbon process, an air carbon process, and UV radiation plus hydrogen peroxide. The contaminant was benzene and the treatment goal was to reduce its concentra-

TABLE 9.5. Economic Comparisons for Groundwater Treatment Systems for Reduction of Benzene Concentrations from 50 ppm to 50 ppb using CAV-OX I[a]

Item	Filter carbon	Air carbon	UV/hydrogen peroxide	CAV-OX® I low-energy process
	Capital cost			
Equipment	150,000	195,000	115,000	58,000
Installation	20,000	30,000	20,000	3,000
Total	170,000	225,000	135,000	61,000
	Annual operating costs			
Power ($0.08/kWh)	0	11,700	62,200	3,592
Carbon	108,000	108,000	0	0
Chemicals	0	0	12,100	1,741
Maintenance	7,500	11,250	6,750	5,114
Amortization (20% per year)	30,000	45,000	27,000	11,600
Labor (air monitoring)	0	9,000	0	0
Total	145,500	184,950	108,050	22,047
Cost per 1000 gallons	11.07	14.07	8.22	1.67

[a]From CAV-OX, a publication of Magnum Water Technology, El Segundo, CA, and "CAV-OX Cavitation Oxidation Process," Application analysis report, EPA/540/AR-93/520, Magnum Water Technology, Inc., Risk Reduction Engineering Laboratory, Cincinnati, Ohio, 1994.

Notes: All treatment processes had a flow rate of 25 gpm and were used to treat 50 mg/liter benzene in groundwater to 50 μg/liter. Cost data provided by Magnum.

tion from 50,000 μg/liter to 50 μg/liter. The results of the comparison, as shown in the last row, indicate that the CAV-OX process is considerably cheaper than the other alternatives. Table 9.6 presents the cost data for a 10-gpm CAV-OX I low-energy process and a conventional carbon adsorption process in treating two sites contaminated with BTEX, TCE, PCE, and chloroform. Once again, the CAV-OX process is shown to be a considerably cheaper alternative.

In summary, technical feasibility and an economic assessment of the CAV-OX process indicate that the main advantages of this process are:

- low capital cost
- low operating cost
- destroys organics on site, no transportation or residual liability problems
- can be operated in a batch mode, intermittently, or continuously
- fast time response from influent entry to exit of processed contaminant
- flexibility of improving contaminant reduction through recycle mode
- flexibility of adding additional modular components for changes in flow rate or degree of contaminant removal

TABLE 9.6. System Cost: Carbon System vs. CAV-OX I for Typical Groundwater Remediation Project[a]

	Flow rate 10 gpm Contaminant concentration (ppb)						
	Benzene	Toulene	Benzene	Zylenes	TCE	PCE	Chloroform
Site 1	350	340	34	270	33	33	10
Site 2	2	2	40	82	33	10	5

Carbon System Costs

The following calculations are based on primary contaminants and given flow rate. Prices were given by a local carbon vendor, calculated as S/1000 gal and as a yearly cost. Basic equipment costs not included for carbon system.

Site 1	42.5 lb carbon/day @ $1.46/lb or $4.30 per 1000 gal	$22,648/year
Site 2	26.0 lb carbon/day @ $1.46/lb or $2.46 per 1000 gal	$13,855/year

CAV-OX I System Costs

Cost of CAV-OX system amortized over a 5-year period includes all opening costs.

Site 1	Capital cost $35,000 or $2.08 per 1000 gal	$10,964/year
Site 2	Capital cost $25,000 or $1.46 per 1000 gal	$7468/year

[a]From CAV-OX, a publication of Magnum Water Technology, El Segundo, CA, and "CAV-OX Cavitation Oxidation Process," Application analysis report, EPA/540/AR-93/520, Magnum Water Technology, Inc., Risk Reduction Engineering Laboratory, Cincinnati, Ohio, 1994.

Note: Prices for both carbon and CAV-OX I systems are appropximate only and will vary according to additional contaminants encountered.

- low hydrogen peroxide consumption
- if required, minimal use of carbon for "polishing"
- can be fully automatic, needs little or no monitoring
- compact, low profile
- minimal operator training time
- safe
- clean and quiet

9.4. CASE STUDIES

In this section we briefly outline the effective applications of the CAV-OX process to nine different case studies as listed in Table 9.7. The tenth case study was carried out at the University of Natal (SA). Each case study is briefly described.

TABLE 9.7. Summary of Case Studies[a]

Case study	Facility	Contaminants	Results
1	Wood-treatment Superfund site, Pensacola, Florida	Pentachlorophenol (PCP), polynuclear aromatic hydrocarbons (PAH)	PCP reduced by 96%
2	Chevron service station, Long Beach, California	Total petroleum hydrocarbons (TPH); benzene, toluene, ethylbenzene, and xylenes (BTEX)	TPH reduced by 99.94%
3	Presidio Army Base, San Francisco, California	TPH, BTEX	Ethylbenzene and TPH reduced to nondetectable levels
4	Chemical plant, East Coast United States	Biochemical oxygen demand (BOD)	BOD reduced by 94.1%
5	Mannesmann Anlagenbau, Salzburg, Austria	Atrazine	Atrazine reduced from 1000 μg/liter to 200 μg/liter
6	Steel mill, South Korea	Cyanide, phenol	Cyanide reduced by 55% using cavitation only and more than 99.9% using cavitation and UV radiation
7	Chicken farm, Bridgewater, Virginia	*Salmonella*	*Samonella* reduced from 2,000,000 CFU/ml to 0.8 CFU/ml without hydrogen peroxide addidon; reduced to 0.01 CFU/ml after hydrogen peroxide addition
8	Southern California Edison, Los Angeles, California	BOD	reduced by 83.3 to 88.4% using cavitation only
9	Corporacion Mexicana de Investigacion en Materials, S.A. de C.V. (CMIMSA)	Phenol, pharmaceuticals	At high flow rates phenol was reduced to nondetectable levels

[a]From CAV-OX, a publication of Magnum Water Technology, El Segundo, CA, and "CAV-OX Cavitation Oxidation Process," Application analysis report, EPA/540/AR-93/520, Magnum Water Technology, Inc., Risk Reduction Engineering Laboratory, Cincinnati, Ohio, 1994.

Case 1. Superfund Site for Wood-Treatment, Pensacola, Florida

In mid-1992, Magnum used the CAV-OX process to reduce PCP in a leachate discharged from the soil-washing process of a wood-treatment Superfund site at Pensacola, Florida. The tests were carried out using a CAV-OX II high-energy unit. In the process, a 500-gal polyethylene holding tank was used to collect leachate from the soil-washing process (without pretreatment) and served as a recycle vessel for the batch process test. The initial runs showed that little UV was being transmitted and that most PCP destruction was taking place in the cavitation

chamber, aided by the addition of hydrogen peroxide. PCP was generally reduced by 22 to 50%.

The best results were obtained when the pH of the process stream was adjusted from 9 to 5.5, causing flocculation and sedimentation in the holding tank and resulting in a clearer influent to the CAV-OX process. With this clear influent, a 96% reduction in PCP levels was achieved. The PCP and PAH levels in the influent varied from 900 to 15,000 μg/liter and 16,000 to 128,000 μg/liter. Some typical effluent analyses after the CAV-OX process are given in Table 9.8.

Case 2. Chevron Service Station, Long Beach, California

In late 1990, a CAV-OX I low-energy process was installed at a former Chevron service station to remediate groundwater at the site. Gasoline storage tanks at the site had leaked for several years, resulting in a groundwater contaminant plume that was migrating toward adjoining commercial property. Since the plume had spread over a large area, 12 wells were drilled at its periphery to feed the overall treatment process and prevent the plume from spreading further. The CAV-OX I process operated at a 10 gpm level in order to reduce TPH from 200 mg/liter to a level that met local regulations. The process was operational 99.9% of the time over the 2-year period. Because of potential variations in influent quality, 400 lb. of activated carbon were included in the process to handle any free product that might pass through the CAV-OX I low-energy process. The carbon was replaced once during the 2-year period. The UV lamps were replaced twice during the 2-year period. In early 1992, the 20 mg/liter hydrogen peroxide injection before the centrifugal pump inlet was discontinued because tests indicated that it was unnecessary.

As of late 1992, when the CAV-OX I low-energy process was shut down, the influent TPH level had been reduced from 190,000 μg/liter to 120 μg/liter, a reduction of 99.94%. The overall cost was $1.62 for every 1000 gal of groundwater treated. Some typical data on the effectiveness of the CAV-OX process for removing gasoline from groundwater are shown in Table 9.9.

Case 3. Presidio Army Base, San Francisco, California

A 20-gpm CAV-OX I low-energy process was used to remove VOCs from groundwater at a service station on the Presidio army base in San Francisco, California. The CAV-OX I low-energy process was combined with other equipment, including a vacuum extraction process for soil remediation, groundwater pumps and manifold, an influent holding tank with level controls, and the necessary electrical process and interlocks.

Tests performed in 1993 indicate that contaminants in groundwater at the site were reduced dramatically with the application of this process. Some typical results are described in Table 9.10. Some additional results obtained with a 10-gpm system

TABLE 9.8. Case Study: Wood Treatment Superfund Site Effluent Analyses after CAV-OX[a]

Test Run	Time	(kWb)/gal	Concentration PCP (ppb)
Test 3	0	0	15,000
	30	25	2000
	60	50	1600
	90	75	650
Test 4	0	0	8700
	30	25	1900
	60	50	980
	90	75	200
	120	100	150
Test 5	0	0	1500
	30	25	1100
	60	50	540
	90	75	120
	120	100	100
Test 6	0	0	4000
	30	25	2700
	60	50	1700
	90	75	580
Test 7	0	0	0
	20	16	2000
Test 8	0	0	4500
	30	25	990
	60	50	120
	90	75	100

	Time Intervals(min)	
Compound Name[b]	0	20
Noncarcinogens		
Naphthalene	6100	450 J
2-Methylnaphthalene	4000	640
1-Methylnaphthalene	2300 J	250 J
Biphenyl	1400 J	280 J
2,6-Dimethylnaphthalene	950 J	340 J
Acanaphthylene	ND	ND
Acanaphthene	4400	460 J
Dibenzofuran	3400	520 J
Fluorene	4600	740
Phenanthrene	12000	4000
Anthracene	1200 J	170 J
Carbazole	370 J	ND

TABLE 9.8. (*cont.*)

Compound Name[b]	Time Intervals(min) 0	20
Fluoranthene	5500	3500
Noncarcinogen Subtotal	46,220	11,360
Carcinogens		
Pyrene	3800	1500
Benzo(a)anthracane	700 J	620
Chrysene	720 J	630
Benzo(b)fluoranthene	ND	360 J
Benzo(k)fluoranthene	ND	250 J
Benzo(e)pyrene	ND	ND
Benzo(a)pyrene	ND	ND
Indeno(1,2,3-cd)pyrene	ND	ND
Dibenzo(a,h)anthracene	ND	ND
Benzo(g,h,i)perylene	ND	ND
Carcinogen Subtotal	5220	3360
TOTAL	51,440	14,720
Pentachlorophenol	3200 J	ND

[a]From CAV-OX, a publication of Magnum Water Technology, El Segundo, CA, and "CAV-OX Cavitation Oxidation Process," Application analysis report, EPA/540/AR-93/520, Magnum Water Technology, Inc., Risk Reduction Engineering Laboratory, Cincinnati, Ohio, 1994.

[b]All concentrations are shown in parts per billion.

[c]J Denotes that the value is lower than the lowest linear .

Note: ND = not detected.

TABLE 9.9. Gasoline Removal from Groundwater, CAV-OX I System, Laboratory Unit[a]

Retention Time (min)	Influent (ppm)	Effluent (ppm)	Reduction (%)
1.8	13.6	1.1	91.9
1.8	12.0	0.5	96.0
0.68	17.5	1.5	91.4
5.4	14.4	1.2	91.6
5.4	14.3	0.2	98.6
1.08	12.5	1.3	89.6
10.8	17.0	0.5	97.0
0.054	20.0	3.0	85.0

[a]From CAV-OX, a publication of Magnum Water Technology, El Segundo, CA, and "CAV-OX Cavitation Oxidation Process," Application analysis report, EPA/540/AR-93/520, Magnum Water Technology, Inc., Risk Reduction Engineering Laboratory, Cincinnati, Ohio, 1994.

Notes: Average data points. No hydrogen peroxide used.

TABLE 9.10. Groundwater Sampling Results, August 20,1998 (μg/liter)[a]

Sample point	Benzene	Toluene	Xylenes	Ethylbenzene	TPH
Influent	450	44	100	25	80
Effluent	6	1.9	1.5	ND	ND

[a]From CAV-OX, a publication of Magnum Water Technology, El Segundo, CA, and "CAV-OX Cavitation Oxidation Process," Application analysis report, EPA/540/AR-93/520, Magnum Water Technology, Inc., Risk Reduction Engineering Laboratory, Cincinnati, Ohio, 1994.

Note: ND = not detected.

are given in Table 9.11. It was determined that the contaminant levels in soil required further remediation using the vacuum extraction process in conjunction with the CAV-OX I low-energy process. The overall cost was $1.75 for every 1000 gal of groundwater treated.

Case 4. Chemical Plant, East Coast, United States

A CAV-OX II high-energy pilot unit was used to remediate the effluent of a resin manufacturer. The waste stream was common to several of the manufacturer's facilities on the East Coast of the United States. Plant procedures required that the effluent be shipped offsite for treatment, resulting in high costs and potential liabilities. The high-energy process was chosen because of the types and concentrations of contaminants in the effluent. The unit consisted of a double reactor with a total UV output of 10 kW. Because the pilot unit consists of full-scale modules operating at 3 gpm, the results from this study can be directly extrapolated to full-scale 10-gpm or 25-gpm industrial processes.

TABLE 9.11. Some Additional Data for Removal of VOCs from Groundwater[a]

Analyte	Influent	Effluent
Acetone	7800	34.1
2-Butanone	9100	18.0
Ethylbenzene	420	ND
Methylene chloride	13,000	8.9
Toluene	2700	110.0
Total xylenes	1100	ND

[a]From CAV-OX, a publication of Magnum Water Technology, El Segundo, CA, and "CAV-OX Cavitation Oxidation Process," Application analysis report, EPA/540/AR-93/520, Magnum Water Technology, Inc., Risk Reduction Engineering Laboratory, Cincinnati, Ohio, 1994.

Note: ND = not detected.

During the process, 250 gal of effluent were first placed in a holding tank. The effluent was clear, somewhat viscous, and irritating to mucous membranes, with a strong odor. Hydrogen peroxide was then added to the holding tank to achieve a concentration of 100 mg/liter, resulting in an opaque, beige-colored solution. Because this would decrease transmission of the UV radiation, most of the contaminant destruction occurred in the cavitation chamber. The test procedure was altered to allow maximum flow through the cavitation chamber; the flow was then directed through the UV reactors at 0.75 gpm.

The CAV-OX II high-energy process, in this case, treated all constituents in the influent. Although nontargeted contaminants absorbed a significant amount of energy from the cavitation chamber and UV lamps, the BOD in the treated effluent was reduced by 94.1%.

Case 5. Mannesmann Anlagenbau, Salzburg, Austria

A CAV-OX I low-energy process with a 3-gpm flow was used to treat groundwater from Mannesmann Anlagenbau of Salzburg, Austria, which was contaminated with the herbicide atrazine. Atrazine is manufactured and sold worldwide by Ciba-Geigy Corporation. The setup consisted of nine 45-W lamps contained in three stainless steel reactors, a hydrogen peroxide injection unit, a centrifugal pump, and the cavitation chamber. The atrazine solution at a concentration of 1 mg/liter was fed to the CAV-OX I low-energy process from a 150-gal holding tank. The solution was processed using various protocols. In initial experiments, the altrazine concentration was reduced to 200 μg/liter (a reduction of 80%). With proper optimization of the process conditions, the effluent concentration of altrazine could have been reduced to nondetectable levels.

Case 6. Steel Mill, South Korea

Wastewater contaminated with phenol and cyanide from a major steel mill in South Korea was treated by the CAV-OX process with three different setups:

- a CAV-OX I low-energy laboratory scale unit
- a CAV-OX I low-energy pilot-scale unit
- a CAV-OX II high-energy unit

The laboratory-scale unit consisted of a 55-gal, stainless steel holding tank, a 1.5-hp centrifugal pump, and plumbing and bypass lines into three UV reactors. Each reactor was 3 ft long with three 45-W lamps, for a total UV output of 405 W. The reactors were plumbed in series. Effluent from the reactors flowed through the discharge lines.

The pilot unit, with a rated capacity of 3 gpm, had the same holding tank, a 2-hp centrifugal pump and one 6-ft low-pressure UV reactor with 60-W lamps for a total UV output of 360 W. The unit also included a control panel. Effluent from the reactors was either directed to the discharge lines or to the CAV-OX II high-energy unit.

The CAV-OX II high-energy unit was operated either in series with the output from the CAV-OX I units or independently. In the latter case, it consisted of a cavitation chamber, centrifugal pump, and control panel. It also had an independent power supply for operating the high-energy lamps. Its UV reactor held one UV lamp rated at 2.5 or 5 kW.

In all tests, cyanide concentrations tested were 0.65 mg/liter, 1 mg/liter, and 50 mg/liter. Phenol concentrations tested were 11 mg/liter, 20 mg/liter, and 200 mg/liter. The CAV-OX II high-energy process consistently oxidized KCN to nondetectable levels with retention times of less than 4 min and hydrogen peroxide levels as low as 20 mg/liter. Using only cavitation and UV radiation, without hydrogen peroxide, KCN levels were reduced by 46%. The effluent met discharge standards.

The CAV-OX I low-energy pilot-scale unit oxidized 1 mg/liter of KCN to nondetectable levels under the following conditions: 40 mg/liter of hydrogen peroxide, 0.75 gpm flow rate, and 13 min retention time. Using 50 mg/liter of hydrogen peroxide, a flow rate of 1 gpm, and a retention time of 10 min, 1 mg/liter of cyanide was reduced by 70%. Table 9.12 describes representative results for the CAV-OX II high-energy and CAV-OX I low-energy units. The CAV-OX I low-energy laboratory unit showed similar results. The total UV output of the laboratory unit was 360 W instead of 405 W. Similar results were obtained with sodium cyanide as the contaminant.

Typical results for phenol are described in Table 9.13. The representative results of the combined cyanide and phenol tests are given in Table 9.14. Both of these tables once again show the effectiveness of the CAV-OX process. The operating costs for the CAV-OX I low-energy pilot-scale unit are estimated at $1.93 per 1000 gal.

Case 7. Perdue Farms, Bridgewater, Virginia

Chickens contaminated with the bacterium *Salmonella* are a serious problem at U.S. chicken farms. In cooperation with Silliker Laboratories, the CAV-OX process was used to eliminate pathogens associated with chicken farming. The tests were conducted using a CAV-OX I low-energy pilot-scale unit in parallel with a CAV-OX II high-energy pilot scale unit. The CAV-OX I low-energy unit consisted of a 2-hp centrifugal pump, a cavitation chamber, a recycle loop, a low-energy UV reactor with 60-W lamps, and a control panel. The high-energy system included the same

TABLE 9.12. Cyanide Removals[a]

Test	Flow (gpm)	UV (watts)	Hydrogen peroxide (mg/liter)	Cyanide in influent (mg/liter)	Cyanide in effluent (mg/liter)	Percent reduction
CAV-OX II High-Energy Process						
1	2.5	2860	0	0 .65	0.35	46
2	0.75	2860	20	0.65	ND	> 99.9
3	1	5360	60	50	0.5	99
4	2.5	5360	60	50	0.5	99
5	2	5360	60	2	ND	> 99.9
CAV-OX Low-Energy Pilot-Scale Unit						
1	2.5	360	0	0 .65	0.5	23
2	1	360	60	50	15	70
3	2.5	360	60	11	4.95	55
4	0.75	360	40	1	ND	> 99.9
5	0.75	0	40	1	0.45	55
6	1	360	60	11	0.6	95

[a]From CAV-OX, a publication of Magnum Water Technology, El Segundo, CA, and "CAV-OX Cavitation Oxidation Process," Application analysis report, EPA/540/AR-93/520, Magnum Water Technology, Inc., Risk Reduction Engineering Laboratory, Cincinnati, Ohio, 1994.

Note: ND = not detected.

elements, an independent power supply, and a 5-ft UV reactor with a 2.5- or 5-kW lamp.

In experiments, the influent containing *Salmonella* was injected with 220 ml of 10% sodium thiosulfate. A flow rate of 1 gpm was used. The inoculated water was injected with 80 mg/liter of hydrogen peroxide and processed through the CAV-OX

TABLE 9.13. Phenol Removals[a]

Phenol (mg/liter)	Hydrogen peroxide (mg/liter)	UV output	Percent reduction
11	0	0 .36 kW	18.2
11	0	5 kW	32
11	60	5 kW (no cavitation)	77
11	60	5 kW	95.5
11	60	Cavitation only	9
12	60	0.36 kW	87

[a]From CAV-OX, a publication of Magnum Water Technology, El Segundo, CA, and "CAV-OX Cavitation Oxidation Process," Application analysis report, EPA/540/AR-93/520, Magnum Water Technology, Inc., Risk Reduction Engineering Laboratory, Cincinnati, Ohio, 1994.

TABLE 9.14. Combined Cyanide/Phenol Removals[a]

Cyanide (mg/liter)	Phenol (mg/liter)	Hydrogen peroxide (mg/liter)	UV Output	Percent reduction
10	12	0	0 .36 kW	50
10	10	60	0.36 kW + 5 kW	ND
13.5	12	60	0.36 kW	70
20	20	0	25 kW	97

[a]From CAV-OX, a publication of Magnum Water Technology, El Segundo, CA, and "CAV-OX Cavitation Oxidation Process," Application analysis report, EPA/540/AR-93/520, Magnum Water Technology, Inc., Risk Reduction Engineering Laboratory, Cincinnati, Ohio, 1994.

Notes: ND = not detected.

units. Seven samples were collected and their analyses are shown in Table 9.15. As shown, the CAV-OX process cumulatively reduced the *Salmonella* concentration a total of eight orders of magnitude.

Case 8. Southern California Edison, Los Angeles, California

The CAV-OX process was used to treat 3 million gal of seawater contaminated with fluorescent dyes, lubricating oil, and detergent emulsions. The project was supported by Southern California Edison, a major U.S. utility company. The water consisted of reverse osmosis reject water and hydrotest discharge water that was

TABLE 9.15. *Salmonella* Study Results[a]

Sample No.	Location	Concentration (CFU/mliter)
1	Untreated water from the 55-gal drum	2,000,000
2	Water exiting the cavitation chamber at 1 gpm	1,600,000
3	Water exiting the high-energy, 5-kW reactor	0.8
4	Hydrogen peroxide-treated water from the 55-gal drum	3,000,000
5	Hydrogen peroxide-treated water exiting the cavitation chamber	1,900,000
6	Hydrogen peroxide-treated water exiting the CAV-OX II UV reactor	500
7	Hydrogen peroxide-treated water exiting the CAV-OX II UV reactor	0.01

[a]From CAV-OX, a publication of Magnum Water Technology, El Segundo, CA, and "CAV-OX Cavitation Oxidation Process," Application analysis report, EPA/540/AR-93/520, Magnum Water Technology, Inc., Risk Reduction Engineering Laboratory, Cincinnati, Ohio, 1994.

methylene blue reactive, indicating the presence of detergent compounds. The water also contained oxidized iron, which caused scaling at the liquid surface.

Both UV radiation and hydrogen peroxide addition were not part of this treatment. The seawater was fed into a high-volume cavitation chamber using a 2-hp centrifugal pump. This pump transferred the process seawater into the cavitation chamber at 65 psi. The cavitation chamber vacuum was maintained at 27 in. mercury and effluent line pressure at 6 psi. The flow rate varied between 2 and 4 gpm. A 15:1 ratio was recycled to the cavitation chamber for further treatment. Discharge from the cavitation chamber flowed to a holding tank. Treatment in the cavitation chamber reduced BOD in effluent samples by 83.3 to 88.4%. The average cost to treat 1000 gallons of seawater was $0.13.

Case 9. Corporacion Mexicana de Investigacion en Materials, S.A. de C.V. (CMIMSA)

In the spring of 1993, CMIMSA used a modified CAV-OX process to treat effluent from a pharmaceutical plant. Phenol was considered the dominant contaminant from this effluent. For this treatment, the CAV-OX II process was modified as follows:

- UV window parts allowed UV output to be monitored with an optical monitor 31 in. from the top of the reactor.
- Engineering modifications substantially improved the UV lamp efficiency.

With these modifications, the results were obtained with an influent concentration of phenol at 20 g/liter and with the addition of 60 mg/liter of hydrogen peroxide. The results obtained are compared in Table 9.16 with those obtained in Case 6. These results indicate that the CAV-OX IIA modifications increased the reduction efficiency two to four times and allowed the measurement and comparison of UV flux over different operating protocols.

Case 10. University of Natal, Durban, South Africa

The University of Natal had undertaken a study to determine the effectiveness of hydrodynamic cavitation in the CAV-OX process for the disinfection of potable water. They evaluated the effectiveness of hydrodynamic cavitation *alone* for bactericidal efficiency using heterotrophic plate count (HPC) analysis. The project was designed to determine whether hydrodynamic cavitation could be used to disinfect raw water. Raw water was used as the inoculum because it was considered most representative of a water treatment project. The absolute numbers of colony-forming units (CFUs) was of secondary importance compared with the change in the CFUs/ml, which is used to determine the efficiency of the process.

TABLE 9.16. Phenol Removal Comparison[a]

Test No.	Flow (gpm)	Percent reduction	Method
	CAV-OX II (Case Study 6)		
1	1	95	Protocol A
2	2	55	Protocol B
3	4	45	Protocol C
4	6	39	Protocol D
	CAV OX II A (Modified CAV-OX Process, Case Study 9)		
1	2	100	Protocol B
2	4	99	Protocol C
3	6	96	Protocol D

[a]From CAV-OX, a publication of Magnum Water Technology, El Segundo, CA, and "CAV-OX Cavitation Oxidation Process," Application analysis report, EPA/540/AR-93/520, Magnum Water Technology, Inc., Risk Reduction Engineering Laboratory, Cincinnati, Ohio, 1994.

The results indicated that hydrodynamic cavitation alone can rupture cells, but is not successful in the inactivation of naturally occurring raw water bacteria. Some results were also obtained with acoustic cavitation and these indicated successful inactivation of bacteria. Hydrodynamic cavitation did not produce sufficient hydrogen peroxide for oxidation and therefore cannot be described as a major contributor to free radical production. This study indicated that while cavitation alone can be used as a technology for the disinfection of water, acoustic cavitation is more intense and produces stronger free radical concentrations than hydrodynamic cavitation. Wherever strong oxidation potential is required, hydrodynamic cavitation alone may not be effective.

NOMENCLATURE

Symbol	*Definition*
a	cross-sectional area of orifice, m^2
a	characteristic constant for gas concentration
a'	small variation in radius
A	cross-sectional area of pipe, m^2
A	Arrhenius frequency factor in Eq. (4.3)
b	damping coefficient
b_r	radiation damping constant
b_v	viscosity damping constant
B	constant for the mixture of the bubble content
B_g	constant for gas in the bubble content
$\overline{C}_0, \overline{C}_1$	constants in Eq. (4.3)
c, C	sonic velocity in cavitating medium, m s^{-1}
C_d	discharge coefficient (Eq. 1.2)
C_i	concentration of species i, g mol/cc
C_p	specific heat at constant pressure
C_s	velocity of sound in water
C_∞	concentration of gas in the liquid at infinity
C_0	saturation concentration of gas in the bubble
C_v	specific heat at constant volume
d	diameter of the conduit through which an eddy flows, m
d_0	diameter of orifice, m
d_p	diameter of pipe, m
D	diffusivity of dissolved gas
E_a	activation energy
f'	friction factor
f_r	resonance frequency of bubble
f_T, f	frequency of the acoustic wave, Hz
G	$[a'/P_0]$ ratio

Symbol	*Definition*
H	difference in liquid enthalpy at bubble wall
I	scale of turbulence, m
I, I_0	acoustic intensity
k_s	angular wave number
k, k_1, k_2, k_{obs} etc.	kinetic constants; unit depends on the order of the reaction
K	thermal conductivity
l	length of pressure recovery
L	latent heat
L	intensity of the acoustic wave, W cm^{-2}
L_g	thermal diffusion length in the gas
L/V	time for pressure recovery in hydrodynamic cavitation
m	mass diffusion inside the bubble
m'	mass diffusion outside the bubble
M_{eff}	effective mass felt by the bubble, kg
M_v	a parameter defined by Eq. (2.123)
M_v	mass of vapor inside the bubble
n_w	number of moles in the bubble
P	pressure $P(r, t)$ = local pressure in liquid at radius distance r and time t
P_A	acoustic pressure amplitude
$P_A(t)$	pressure threshold for rectified diffusion
P_{ac}	acoustic power
P_B	Blake threshold pressure
P_f	final recovery pressure, N/m^2
P_g	initial gas pressure in the bubble, atm
$P_{g'}$	mean pressure inside the bubble, atm
P_∞	pressure in the liquid at infinity; also equilibrium value of downstream pressure, atm
P_2	recovered discharge pressure, atm
P_i	internal pressure in the bubble (Section 2.3)
P_L	pressure in the liquid just outside the bubble wall
P_m	liquid pressure at transient collapse
P_M	power input to the system per unit mass, W/kg
P_{max}	maximum pressure that may be reached during bubble collapse
P_0	ambient pressure in the liquid
P_s	saturation pressure of gas in bulk
P_T	total pressure of gas and vapor in the cavity
P_t	pressure downstream of the orifice at any time t, atm
P_v	vapor pressure of liquid
ΔP	pressure drop
q	heat flux (energy flow per unit mass per unit volume)

Symbol	*Definition*
Q	discharge from the pump or liquid flow rate, $m^3\ s^{-1}$
Q	internal pressure of gas in the bubble
r	radial distance from center
r_b	radial displacement of bubble
R	radius at any time
R	time variation of radius of bubble, m/s
$\overline{R}$	hydrophobicity ratio in Figure 4.19
R^*	critical radius
R_B	threshold radius for Blake nucleation
R_C	critical radius for stable oscillations
R_g	gas constant
R_{max}	maximum radius of bubble for transient collapse
R_{min}	minimum radius of bubble for transient collapse
R_0	initial cavity or bubble cluster radius
R_r	resonance size of the bubble
S	stiffness
$\overline{S}$	area of bubble surface
S_v	specific heat capacity of liquid at constant volume
t	time
T	temperature
T'	mean temperature of bubble
T^∞	temperature of liquid far from bubble
T_L	temperature of liquid
T_{max}	maximum temperature reached during bubble collapse
T_v	temperature of vapor
T_v	temperature parameter defined by Eq. (2.119) and (2.122)
u	velocity at radius r; velocity of liquid in the pipe
U, V	liquid velocity, ms^{-1}
v'	isotropic turbulent fluctuation velocity, ms^{-1}
v_g	velocity of gas
v_v	velocity of vapor
v_x, v_y, v_z	instantaneous velocity of flow in x, y, and z directions, ms^{-1}
$\overline{v}_x', \overline{v}_y', \overline{v}_z'$ or v_x', v_y', v_z'	instantaneous fluctuation velocity in x, y, and z directions, ms^{-1}
$\overline{v}_x, \overline{v}_y, \overline{v}_z$	time average velocity of flow in x, y, and z directions, ms^{-1}
V	volume of the gas
V_0	mean velocity near the orifice, ms^{-1}
V_p	mean velocity in the pipe, ms^{-1}
V_{sh}	velocity at cluster boundary, ms^{-1}
V_t	velocity downstream of the orifice at any time t, ms^{-1}
Z	compression ratio of the bubble

Greek Letters

Symbol	*Definition*
α	orifice-to-pipe diameter ratio, dimensionless
α	a parameter in Eq. (7.3)
α	ratio of initial bubble radius to the diffusion length; thermal diffusivity of the bubble; also R/L_{gi}
α	absorption coefficient in Eq. (1.11)
α_L	thermal diffusivity of liquid
β'	bubble fraction in the cluster, dimensionless
β	ratio of radii, $\overline{R/R_0}$
β	ratio of orifice to pipe diameter
β_I	various stoichiometric coefficients
γ	ratio of specific heats at constant pressure to constant volume; also a parameter in Eq. (7.10)
γ'	fraction of the collapse energy conserved in the cluster, dimensionless
Γ	$P_{v0}/L\rho_v$ ratio
δ_b	bubble damping factor
δ'	dimensionless excess temperature
δ_r	radiation damping factor
δ_t	thermal damping factor
δ_v	viscous damping factor
Δ	phase shift given as $\tan^{-1}[\psi\omega/(S + 8\pi\sigma)]$
ε	a parameter defined by Eq. (2.92)
η	polytropic index
θ'	small variation in temperature
μ	viscosity
μ'	small variation in mass
ν	frequency
ξ	radial displacement of the cavitating bubble, m
ξ	$\gamma(T_v P_{v0}/\rho_v L T_0)^2/(\gamma^{-1})$ where P_{v0} = equilibrium pressure inside the bubble and T_v = temperature of vapor inside the bubble
ξ	transducer amplitude in Eq. (6.1)
ξ_b	dimensionless bubble radius
ρ	density
ρ_v	density of vapor inside the bubble
ρ_g'	mean density of gas inside the bubble
σ	surface tension
σ_c, σ_c', σ_T	cavitation numbers
τ	time constant for hydrodynamic or acoustic cavitation(s) or time for the pressure recovery downstream of orifice, s

Symbol	*Definition*
τ_I	stress tensor
Φ	velocity potential, entropy of bubble contents
Φ'	parameter expressing ratio of bubble radius to diffusion thickness
χ	a parameter defined by Eq. (2.113)
ψ'	small variation in vapor pressure
ω	angular frequency of the bubble
ω_r	resonance angular frequency of the bubble
Ω_c	volume of the bubble cluster, m^3
Ω_1	volume of the liquid surrounding the bubble cluster, m^3

REFERENCES

Anbar, M., and Pecht, I. 1964a. *J. Phys. Chem.* **68**, 352–355.

Anbar, M., and Pecht, I. 1964b. *J. Chem. Phys.* **40**, 608.

Anbar, M., and Pecht, I. 1964c. *J. Phys. Chem.* **68**, 1460–1465.

Anbar, M., and Pecht, I. 1967. *J. Phys. Chem.* **71**, 1264–1269.

Apfel, R. 1981. "Methods of experimental physics," in *Ultrasonics*, vol. 19, p. 373, Academic Press, Orlando, FL.

Arakeri, V. H., and Chakraborty, S. 1990. *Curr. Sci.* **59** (24), 1326–1333.

Barbier, P. 1899. *C. R. Acad. Sci. Paris* **128**, 110–112.

Bebchuk, A. S. 1957. *Sov. Phys. Acoust.* **3**, 95, 395.

Bebchuk, A. S., and Rozenburg, L. D. 1951. *Sov. Phys. Acoust.* **6**, 496.

Benson, T. 1995. *Infinite Energy* **1** (1), 33–37 (March-April).

Besant, W. 1889. *Hydrostatics and Hydrodynamics*, p. 170. Deighton Bell, Cambridge.

Bhatnagar, A., and Cheung, H. M. 1994. *Env. Sci. Tech.* **28**, 1481–1486.

Blake, F. 1949. "Technical Memorandum Nos. 9 and 12", Acoustics Research Laboratory, Harvard University, Cambridge, MA.

Blomberg, C., and Hartog, F.A. 1977. *Synthesis*, 18–30.

Boerner, J., and Orloff, D. 1996. "Acoustic enhancement of dry HCl gas scribbing with CaO," paper 47f, AIChE meeting.

Bogachev, I. N., and Korobeinikov, V. P. 1972. *Sov. Phys. Acoust.* **17**, 4, 454.

Botha, C. J., and Buckley, C. A. 1995. *Water Supply* **13** (2), 219–229.

Boudjouk, P. J. 1986. *Chem. Ed.* **63**, 427–429.

Boudjouk, P. 1987. "Acceleration of synthetically useful heterogeneous reactions using ultrasonic waves," in ACS Symposium Series, vol. 333, pp. 209–222, American Chemical Society, Washington, DC.

Boudjouk, P., and Han, B. H. J. 1983. *Catalysis* **79**, 489–492.

Bronskaya, L. M., Vigdernan, V. S., Sokol'skaya, A. V., and El'Piner, I. E. 1968. *Sov. Phys. Acoust.* **13** (3), 374.

Ceschia, M., and Iernetti, G. 1973. *Acustica* **29**, 3, 127.

Chambers, L. A., and Flosdorf, E. W. 1936. *J. Biol. Chem.* **114**, 75–83.

Chen, J. W., Hui, C., and Smith, G. V. 1973. "Oxidation of wastewaters with ozone/catalyst and air/catalyst/ultrasound systems," in *Proc. First International Symposium on Ozone for Water and Wastewater Treatment*, R. G. Rice and M. E. Browning, eds., pp. 120–131B, International Ozone Institute.

Chendke, P. K., and Fogler, H. S. 1974. *Chem. Eng. J.* **8**, 165–178.

Chendke, P. K., and Fogler, H. S. 1983a. *J. Phys. Chem.* **87**, 1362.
Chendke, P. K., and Fogler, H. S. 1983b. *J. Phys. Chem.* **87**, 1644.
Chervinskii, K. A., and Mal'tsev, V. N. 1966, *Ukr. Khim. Zh.* **32**, 69–71.
Cheung, H. M., Wong, J. J., Kurup, S., Jinandra, S., Chitta, C., Gaddam, K., and Jensen, C. 1993. "Sonochemical destruction of aqueous citric acid: Effects of peroxide addition," paper 160e, AIChE meeting.
Chivate, M. M., and Pandit, A. B. 1993. *Ind. Chem. Eng.* **35**, (1 and 2), 52.
Cost, M., Mills, J., Glisson, P., and Larkin, J. 1993. "Sonochemical degradation of p-nitrophenol in presence of chemical components of natural water." *Chemosphere* **27**, 1737–1743.
Crum, L. 1980. *J. Acoust. Soc. Am.* **68**, 203.
Crum, L., and Hansen, G. 1982. *J. Acoust. Soc. Am.* **72**, 1586.
Davidson, B. 1971. *J. Sound Vib.* **17**, 261.
Devin, C. 1954. *J. Acoust. Soc. Am.* **31**, 1654.
Ebeling, K. J. 1978. *Acustica* **40**, 229.
Ebeling. K. J. 1980. "Application of high speed holocinematographical methods in cavitation research," in *Cavitation and Inhomogeneities in Underwater Acoustics*, by W. Lauterborn, ed., p. 35, Springer-Verlag, New York.
Edebo, L. 1960. *J. Biochem. Microbiol. Technol. Eng.* **2**, 453.
Edmonds, P.D. 1990. "Sonochemistry - the general principles", Ch. 2 in Sonochemistry - The uses of ultrasound in chemistry," ed. by Mason, T.J., Royal Society of Chemistry, Cambridge.
Eller, A. 1972. *J. Acoust. Soc. Am.* **52**, 447.
Eller, A. 1975. *J. Acoust. Soc. Am.* **57**, 1374.
Eller, A., and Flynn, H. 1965. *J. Acoust. Soc. Am.* **37**, 493.
El'piner, I. E. 1964. *Ultrasound: Physical, Chemical and Biological Effects*, pp. 53–78, Consultants Bureau, New York.
El'piner, I. E., 1968. *Abiogenaz Nachal'nye Stadii Eval. Zhizni*, 49–51 (*Chem. Abstr.* **71**, 7443).
El'piner, I. E., and Kolesnikova, M. F. 1950. *Dokl. Akad. Nauk S.S.S.R.* **75**, 837–839.
El'piner, I. E., and Sokol'skaya, A. V. 1957. *Biofizika* **2**, 225–232.
El'piner, I. E., and Sokol'skaya, A. V. 1958. *Biofizika* **3**, 190–196.
El'piner, I. E., and Sokol'skaya, A. V. 1971a. *Zh. Fiz. Khim.* **45**, 301–3072.
El'piner, I. E., and Sokol'skaya, A. V. 1971b. *Zh. Fix. Khim.* **45**, 3073–3075.
El'piner, I. E., and Stekol'nikov, L. I. 1961. *Dokl. Akad. Nauk S.S.S.R.* **141**, 219–222.
El'piner, I. E., and Surovova, M. D. 1953. *Dokl. Akad. Nauk S.S.S.R.* **90**, 083–1086.
El'piner, I. E., Zbarskii, I. B., and Kharlamova, V. N. 1951. *Dokl. Akad. Nauk S.S.S.R.* **79**, 495–497.
El'piner, I. E., Sokol'skaya, A. V., and Margulis, M. A. 1965. *Nature (Lond.)*, **208**, 945–946.
El'piner, I. E., Sokol'skaya, A.V., and Kolocheva, A. V. 1968. *Dokl. Akad. Nauk S.S.S.R.* **181**, 737–740.
Eriksson, G. 1975. *Chem. Scr.* **8**, 100–103.
Finch, R. D. 1965. *Brit. J. Appl. Phys.* **16**, 1543.
Finch, R., and Neppiras, E. 1973. *Ultrasonics International Proceedings*, p. 73.
Fitzgerald, M. E., Griffing, V., and Sullivan, J. 1956. *J. Chem. Phys.* **25**, 926–933.
Flosdorf, E. W., and Chambers, L. A. 1933. *J. Am. Chem. Soc.* **55**, 3051–3052.
Flynn, H. G. 1964 "Physics of acoustic cavitation in liquids," in *Physical Acoustics*, W. P. Mason, ed., pp. 57–172, Academic Press, New York.
Fogler, H. S. 1971. *Proc. 7th Intl. Cong. Acoustics*, paper 25U14, p. 605.
Gandhi, K. S. 1997. *Indian Chem. Eng.* Section B, **39** (3), 239.
Gilmore, F. 1952. *Hydrodynamic Laboratory Report*, California Institute of Technology.
Goodwin, A. H. 1991. "Scale-up considerations in sonochemistry," Ch. 11 in "Practical Sonochemistry" T. J. Mason, ed., Ellis Harwood, New York.
Gould, R., 1974. *J. Acoust. Soc. Am.* **56**, 1740.
Gunther, P., Heim, E., and Borgstedt, H. 1959. *Z. Electrochem.* **63**, 43–47.

Hagenson, L. C., and Doraiswamy, L. K. 1998. *Chem. Eng. Sci.* **53** (1), 131–148.

Hagenson, L. C., Naik, S. D., and Doraiswamy, L. K. 1994. "Rate enhancements in a solid-liquid reaction using PTC, microphase, ultrasound and combinations thereof," *Chem. Eng. Sci.* **49**, 4787.

Hart, E. J., and Henglein, A. 1985. *J. Phys. Chem.* **89**, 4342–4347.

Harvey, E. 1939. *J. Acoust. Soc. Am.* **61**, 2392.

Harvey, E. N. 1960. *J. Acoust. Soc. Am.* **32**, 1459.

Harvey, E., Barnes, N., McElroy, W. D., Whiteley, A. H., Pease, D. C., and Cooper, K. W. 1944. *J. Cell. Comp. Physiol.* **24**, 1–22.

Henglein, A. 1987. *Ultrasonics*, **25**, 6.

Henglein, A. 1993. "Contribution to various aspects of cavitation chemistry," in *Advances in Sonochemistry*, vol. 3, pp. 17–83, JAI Press, Greenwich, CT.

Hentschel, W., and Lauterborn, W. 1980. "Holographic generation of multibubble systems," in *Cavitation and Inhomogeneities in Underwater Acoustics,"* W. Lauterborn, ed., pp. 47–53, Springer-Verlag, New York.

Hetherington, P., Follows, M., Dunnill, P., and Lilly, M. D. 1971. *Trans. Inst. Chem. Engrs.* **49**, 142–148.

Herring, C. 1941. *Office of Science Research and Development Report 236* (NDRC Report c-4-sr 10-010), Columbia University, New York.

Hickling, R., and Plesset, M. 1964. *Phys. Fluids* **7**, 7.

Hodnett, M., and Zequiri, B. 1997. *Ultrasonic Sonochemistry* **4**, 273–288.

Hsieh, D., and Plesset, M. 1960. *Phys. Fluids* **30**, 882.

Hsieh, D., and Plesset, M. 1961. *J. Acoust. Soc. Am.* **33**, 206.

Hua, I., Hochemer, R. H., and Hoffmann, M. R. 1995. *J. Phys. Chem.* **99** (8), 2335–2342.

Hughes, D. E., Wimpeny, J. W. T., and Loyd, D. 1971. "The disintegration of micro-organisms" in *Methods in Microbiology*, J. R. Norris and D. W. Ribbons, eds., vol. 5B, pp. 1–54, Academic Press, London.

Ibishi, M., and Brown, B. 1967. *J. Acoust. Soc. Am.* **41** (3) 569.

Igar, K., Gonzalez, A., and Olson, T. M. 1995. "Sonochemical oxidation of lindane in aqueous solution," in *Proceedings of Fifth International Symposium on Chemical Oxidation Technology for the Nineties*, W. W. Eckenfelder, A. R. Bowers, and J. A. Roth, eds., vol. 5, pp. 268–271, Technomic Publ. Co. Inc., Lancaster, PA.

Ingale, M. N., and Mahajani, V. V. 1995. *J. Chem. Tech. Biotechnology* **64**, 80.

Jensen, J. N. 1996. *Hazardous Industrial Waste* **28**, 265–274.

Johnson, H. S. 1966. *Gas Phase Reaction Rate Theory*, Ronald Press, New York.

Johnston, A. J., and Hocking, P. 1993. "Ultrasonically accelerated photocatalytic waste treatment," in *Emerging Technologies in Hazardous Waste Management III*, ACS Symposium Series 468, D. W. Tedder and F. G. Pohland, eds., Ch. 6, pp. 106–118, American Chemical Society, Washington, DC.

Josefowicz, Z., and Witekowa, S. 1995. *Soc.Sci. Lodz Acta Chim.* **40**, 105.

Joshi, J. B., and Pandit, A. B. 1993. *Chem. Eng. Sci.* **48** (19), 3, 440.

Joshi, J. B., Shah, Y. T., and Parulekar, S. J. 1985. "Engineering aspects of the treatment of aqueous waste streams," Indian Chemical Engineer **27** (2), 3–37.

Kapustina, O., and Statnikov, Y. 1970. *Sov. Phys. Acoust.* **13**, 327.

Keller, J., and Miksis, M. 1980. *J. Acoust. Soc. Am.* **68**, 628.

Kirkwood, J., and Bethe, H. 1942. *Office of Scientific Research and Development Report*, p. 588, Washington, DC.

Knapp, R. T., Daily, J. W., and Hammitt, F. G. 1970. *Cavitation*, McGraw-Hill, New York.

Kolmogoroff, A. N. 1941a. *Compt. Rend Acad. Sci. URSS* **32**, 16.

Kolmogoroff, A. N. 1941b, *Compt. Rend Acad. Sci. URSS* **30**, 101.

Kolmogoroff, A. N. 1941c. *Compt. Rend Acad. Sci. URSS* **30**, 301.

Kotronarou, A., Mills, G., and Hoffmann, M. R. 1991. *J. Phys. Chem.* **95** (9), 3630–3638.

Kotronarou, A., Mills, G., and Hoffmann, M. R. 1992a. *Environ. Sci. Technol.* **26** (7), 1460–1462.
Kotronarou, A., Mills, G., and Hoffmann, M. R. 1992b. *Environ. Sci. Technol.* **26** (12), 2420–2428.
Lamb, H. 1975. *Hydrodynamics*, Cambridge University Press, Cambridge.
Lastman, G., and Wentzell, R. 1981. *J. Acoust. Soc. Am.* **69**, 638.
Lauterborn, W. 1972. *Appl. Phys. Lett.* **21**, 27.
Lauterborn, W. 1973. "Non-steady flow of water at high speed," in *Proc. IUTAM-Symposium*, L. I. Sedov and G. Yu. Stepanov, eds., pp. 267–275, Nauka, Moscow.
Lauterborn, W. 1974. *Acustica* **31**, 51.
Lauterborn, W. 1976. *Physika* **B1**, **32**, 553.
Lauterborn, W. 1977. *Laser + electro-optik* **9**, 26.
Lauterborn, W. 1980. "Cavitation and coherent optics" in *Cavitation and Inhomogeneities in Underwater Acoustics,* W. Lauterborn, ed., pp. 3–12, Springer-Verlag, New York.
Lauterborn, W., and Bolle, H. 1975. *J. Fluid Mech.* **72**, 391.
Lauterborn, W., and Bolle, H. 1977. Film E 2353, available from Institut fur den Wissenschaftlichen Film, Nonnenstieg 72, D-3400 Gottingen, Germany.
Limon-Lason, J., Hoare, M., Orsborn, C. B., Doyle, D. J., and Dunnill, P. 1979. *Biotechnol. Bioeng.* **XXI**, 745–774.
Lindley, J. 1992. "Ultrasound in catalytic and solid supported reagent reactions," in *Current Trends in Sonochemistry*, G. J. Price, ed., Royal Society of Chemistry, Cambridge.
Lindley, J., and Mason, T. J. 1987. *Chem. Soc. Rev.* **16**, 275–311.
Luche, J. L. 1987. *Inf. Chim.* **281**, 153–156.
Luche, J. 1991. "Sonochemistry: experiment and theory," in *Advances in Sonochemistry*, vol. 2, p. 98, JAI Press, Greenwich, CT.
Luche, J. L. 1992a. *Ultrasonics* **30** (3), 156–157.
Luche, J. 1992b. "New orientation in sonochemistry," in *Current Trends in Sonochemistry*, G. J. Price, ed., vol. 4, p. 34, Royal Society of Chemistry, Cambridge, UK.
Luche, J. 1998. "New free radical reactions under sonochemical conditions," in *Sonochemistry—The Theory, Applications and Uses of Ultrasound in Chemistry*, T. Mason and J. Lorimer, eds., Ch. 7, pp. 86–101, Ellis Hardwood, Chichester.
Luche, J. L., Petrier, C., Lansard, J. P., and Greene, E. A. 1983. *J. Org. Chem.* **48**, 3837–3839.
Luche, J. L., Petrier, C., and Dupuy, C. 1984. *Tetrahedron Lett.* **25**, 3463–3466.
Einhorn, C., Einhorn, J., and Luche, J. L. 1989. *Synthesis (J. Syn. Appl. Chem.)* **11**, 787–813.
Lush, P. A. 1987. *CME, Inst. Mech. Engrs.*
Magnum Water Technology, Inc. 1994. "CAV-OX Cavitation Oxidation Process," application analysis report, EPA/540/AR-93/520, Risk Reduction Engineering Laboratory, Cincinnati, Ohio.
Mallock, A. 1910. *Proc. Royal Soc.* **A84**, 391.
Mal'tsev, A. N. 1976. *Z. Fiz. Khim.* **50**, 1641–1652.
Mal'tsev, A. N., and Margulis, M. A. 1968. *Akust. Zh.* **14**, 295–297.
Mal'tsev, A. N., and Solv'eva, I. V. 1970. *Zh. Fiz. Khim.* **44**, 1092–1095.
Margulis, M. A. 1969. *Russ. J. Acoust.* **15**, 153–173.
Margulis, M. A. 1974. *Zh. Fiz. Khim.* **48**, 2812–2818.
Margulis, M. A. 1975a. *Russ. J. Acoust.* **21**, 576–582.
Margulis, M. A. 1975b. *Russ. J. Acoust.* **21**, 760–770.
Margulis, M. A. 1976a. *Russ. J. Phys. Chem.* **50**, 897–903.
Margulis, M. A. 1976b. *Zh. Fiz. Khim.* **50**, 2267–2270.
Margulis, M. A. 1976c. *Zh. Fiz. Khim.* **50**, 2271–2274.
Margulis, M. A. 1976d. *Zh. Fiz. Khim.* **50**, 1–18, 2531–2535.
Margulis, M. A. 1980. *Russ. J. Phys. Chem.* **54**, 1509–1513.
Margulis, M. A. 1981. *Russ. J. Phys. Chem.* **55**, 154–158.
Margulis, M. A. 1985a. *Russ. J. Phys. Chem.* **59**, 1497–1503.

Margulis, M. A. 1985b. *Principles of Sonochemistry*, Visshaya Schcola, Moscow (in Russian).

Margulis, M. A. 1985c. *Ultrasonics* **23**, 157–169.

Margulis, M. A. 1986. *Sonochemical Reactions and Sonoluminescence*. Chimia, Moscow (in Russian).

Margulis, M. A. 1990. "The nature of sonochemical reactions and sonoluminescence," in *Advances in Sonochemistry*, T. Mason, ed., vol. 1, p. 39, JAI Press, Greenwich, CT.

Margulis, M. A., and Grundel, L. M. 1982. *Zh. Fiz. Khim.* **56**, 2987–2990.

Margulis, M. A., and Grundel, L. M. 1983. *Dokl. Phys. Chem. Proc. Acad. Sci. USSR* **269**, 160.

Margulis, M. A., and Mal'tsev, A. N. 1968a. *Russian J. Physical Chemistry* **42**, 751.

Margulis, M. A., and Mal'tsev, A. N. 1968b. *Zh. Fiz. Khim.* **42**, 1441–1451.

Margulis, M. A., and Mal'tsev, A. N. 1968c. *Zh. Fiz. Khim.* **42**, 2660–2663.

Martin, P. D. 1992. "Sonochemistry: A chemical engineer's view," in *Current Trends in Sonochemistry*, G. Price, ed., pp. 158–167, Royal Society of Chemistry, Cambridge, U.K.

Martin, P. D. 1993. "Sonochemistry in industry, progress and prospects," *IEE*, **48**, 3/1-8, London, England; Also IEE Colloquim on "Ultrasound in the process industry," No. 1993/159, London, England.

Martin, P., and Ward, L. 1992. *Trans. Inst. Chem. Engrs.* **70**, Part A, 296–303.

Mason, W. P. 1966. *Crystal Physics of Interaction Processes*, Academic Press, New York.

Mason, T. J. 1986. *Ultrasonics* **24**, 245–253.

Mason, T. J. 1987. *Educ. Chem.* **24** 102–105.

Mason, T. J. 1990a. "A general introduction to sonochemistry," in *Sonochemistry—Uses of Ultrasound in Chemistry*, T.J. Mason,, eds., Chapter 1, Royal Society of Chemistry, Cambridge.

Mason, T. J., ed. 1990b. *Sonochemistry—Uses of Ultrasound in Chemistry*, Royal Society of Chemistry, Cambridge.

Mason, T. J. 1990b. "A survey of commercially available sources of ultrasound suitable for sonochemistry," in *Sonochemistry: The uses of ultrasound in chemistry*, T. J. Mason, ed., Ch. 5, Royal Society of Chemistry, Cambridge, U.K.

Mason, T. J. 1991. *Practical Sonochemistry; User's Guide to Applications in Chemistry and Chemical Engineering*, Ellis Horwood, Chichester, UK.

Mason, T. J. 1992. "Sonochemistry: Current trends and future prospects," in *Current Trends in Sonochemistry*, G. J. Price, ed., pp. 168–178, Royal Society of Chemistry, Cambridge.

Mason, T. J., and Berlan, J. 1992. "Ultrasound in industrial processes: The problems of scale-up," in *Current Trends in Sonochemistry*, G. J. Price, ed., pp. 148–157, Royal Society of Chemistry, Cambridge.

Mason, T., and Lorimer, J. 1988. *Sonochemistry: Theory, Application and Uses of Ultrasound in Chemistry*, Ellis Horwood, Chichester, UK.

Mason, T. J., Lorimer, J. P., and Mistry, B. P. 1983. *Tetrahedron Lett.* **24**, 4371–4372.

Mason, T. J., Lorimer, J. P., Turner, A. T., and Harris, A. R. 1988. "Ultrasonically assisted O-Alkylation reactions of 5-hydroxychromones," *J. Chem. Res. (5)*, 80–81.

Melville, H. W. 1955. *Trans. Plast. Inst. (London)* **26**, 146–163.

Melville, H. W., and Murray, A. J. 1950. *Trans. Faraday Soc.* **46**, 996.

Moholkar, V. S. 1996. "Studies in cavitation phenomena, design and scale-up of sonic and hydrodynamic cavitation reactors," M. Sc. thesis, Department of Chemical Technology, University of Mumbai, Mumbai, India.

Moholkar, V.S., and Pandit, A. B. 1997. "Bubble behavior in hydrodynamic cavitation: effect of turbulence," *AIChE J.* **43** (6), 1641–1648.

Moholkar, V. S., Senthilkumar, P., and Pandit, A. B. 1999. "Hydrodynamic Cavitation for Sonochemical Effects" Ultrasonics Sonochemistry **6**, pp. 53–65.

Mokry, E. M., and Starchevsky, V. L. 1987. *Ultrasound in Processes of Oxidation of Organic Substances*, Visshaya Schcola, Lviv. (in Russian).

Mokry, E. M., and Starchevsky, V. L. 1993. "Initiation and catalysis of oxidation processes of organic compounds in an acoustic field," in *Advances in Sonochemistry*, T. Mason, ed., vol. 3, pp. 257–292, JAI Press, Greenwich, CT.

Mokry, E. M., Starchevsky, V. L., and Suprun, V. J. 1987. *Neftechimiya* **27**, 669.

Moriguchi, N. 1933a. *J. Chem. Soc. Jpn.* **54**, 949–957.

Moriguchi, N. 1933b. *J. Chem. Soc. Jpn.* **54**, 1047–1053.

Moriguchi, N. 1934. *J. Chem. Soc. Jpn.* **55**, 749–750.

Mostafa, M. A. K. 1958a. *J. Polym. Sci.* **33**, 295–335.

Mostafa, M. A. K. 1958b. *J. Polym. Sci.* **33**, 499–518.

Negishi, K. 1961. *J. Phys. Soc. Jpn.* **16** (7), 1450–1465.

Neppiras, E. A. 1980. *Phys. Rep., Rev. Sect. Phys. Lett.* **61**, 160–248.

Neppiras, E., and Noltingk, B. 1952. *Proc. Phys. Soc. (Lond.)*, **64B**, 1032–1038.

Noltingk, B., and Neppiras, E. 1950. *Proc. Phys. Soc. B. (Lond.)*, **63B**, 674–685.

Numachi, F., Yamabe, M., and Oba, R. 1960. *Trans. ASME J. Basic Eng.* **8**, 1–11.

Olson, T. M., and Barbier, P. F. 1994. *Water Res.* **28** (6), 1383–1391.

Pandit, A. B., and Joshi, J. B. 1993. *Chem. Eng. Sci.* **48** (19), 3440–3442.

Pandit, A. B., and Moholkar, V. S. 1996. *Chem. Eng. Prog.* (July) 57–69.

Parke, A. V., and Taylor, D. J. 1956. *Chem. Soc.* 4442–4450.

Patel, G., Nicholas, R., and Finch, R. 1985. *J. Acoust. Soc. Am.* **28**, 2122.

Perkins, J. P. 1990. "Power Ultrasound" Ch. 4 in "Sonochemistry—The Uses of Ultrasound in Chemistry," T.J. Mason, ed., Royal Society of Chemistry, Cambridge.

Peters, D. 1996. *J. Mat. Chem.* **6** (10), 1605–1618.

Peters, R., and Wu, J. 1996a. "Sonication for dissolution of $BaSO_4$ scale," paper 910, AIChE meeting.

Peters, R., and Wu, J. 1996b. "Sonication enhanced for organic destruction and scale control," paper 47g, AIChE meeting.

Petrier, C., and Luche, J. L. 1987. *Tetrahed. Lett.* **28**, 2347–2352.

Petrier, C., Gemal, A. L., and Luche, J. L. 1982. *Tetrahed. Lett.* **23**, 3361–3364.

Petrier, C., Luche, J. L., and Dupuy, C. 1984. *Tetrahed Lett.* **25**, 3463–3466.

Petrier, C., Einhorn, J., and Luche, J. L. 1985. *Tetrahed. Lett.* **26**, 1449–1452.

Petrier, C., Jeanet, A., Luche, J., and Reverdy, G. 1992. *J. Am. Chem. Soc.* **114**, 3148–3150.

Petrier, C., Micolle, M., Merlin, G., Luche, J. L., and Reverdy, G. 1992b. *Environ. Sci. Technol.* **26** (8), 1639–1642.

Plesset, M. S. 1949. *J. Appl. Mech.* **71**, 277–282.

Pode, J. 1953. David Taylor Model Basin, No. 854, U.S. Naval Ship Research and Development Center, Cabin John, MD.

Poritsky, H. 1952. "Effect of liquid viscosity on cavitation bubble dynamics," in *Proc. First US National Congress in Applied Mathematics*, p. 873, American Society of Mechanical Engineers, New York.

Porter, C. W., and Young, L. F. 1938. *J. Am. Chem. Soc.* **60**, 1497.

Porter, C. W., and Young, L. F. 1941. *J. Am. Chem. Soc.* **63**, 3434.

Prasad-Naidu, D. V., Rajan, R., Kumar, R., Gandhi, K. S., Arakeri, V. H., and Chandrasekharan, S. 1994. *Chem. Eng. Sci.* **49**, 877–888.

Price, G. J., ed. 1992. *Current Trends in Sonochemistry*, Royal Society of Chemistry, Cambridge.

Prosperetti, A. 1977. *Meccanica* **12**, 214.

Prosperetti, A. 1982. *Phys. Fluids* **25**, 409.

Prosperetti, A., and Lezzi, A. 1986. *J. Fluid Mech.* **168**, 457.

Prosperetti, A., and Lezzi, A. 1987. *J. Fluid Mech.* **185**, 289.

Prudhomme, R. O. 1950. *J. Chim. Phys.* **47**, 795–797.

Prudhomme, R. O. 1957. *Bull. Soc. Chim. Biol.* **39**, 425–430.

Prudhomme, R. O., and Grabar, P. 1949a. *J. Chim. Phys.* **46**, 323–331.

Prudhomme, R. O., and Grabar, P. 1949b. *J. Chim. Phys.* **46**, 667–670.

Prudhomme, R. O., and Grabar, P. 1958. *Bull. Soc. Chim. Biol.* **29**, 122–130.

Prudhomme, R. O., and Guilmart, T. 1957. *J. Chem. Phys.* **56**, 336.

Pugin, B., and Turner, A. T. 1990. "Influence of ultrasound on reactions with metals," in *Advances in Sonochemistry*, T. Mason, ed., vol. 1, p. 81, JAI Press, Greenwich, CT.

Quiros, M. ,and Williford, C. 1995. "Ultrasonic enhancement of oxidation of organic pollutants," paper 196e, AIChE annual meeting Nov. 12–17, Miami Beach, Florida.

Ranganathan, R., Bakhshi, N. N., and Mathews, J. F. 1971. *J. Catal.* **4**, 186–190.

Rajan, R. 1997. Ph.D. thesis "Modelling of a batch sonochemical reactor," Department of Chemical Engineering, Indian Institute of Science, Banglore, India.

Rajan, R., Kumar, R., and Gandhi, K. S. 1998. *Chem. Eng. Sci.* **53** (2), 255–271.

Ratoarinoro, F., Contamine, F., Wilhelm, A. M., Berlan, J., and Delmas, H. 1995. *Ultrasonics Sonochemistry* **2** (1), 543–547.

Rayleigh, L. 1917. *Phil. Mag.* **34**, 94.

Reifsneider, S. B., and Spurlock, L. A. 1973. *J. Am. Chem. Soc.* **95**, 299–305.

Richards, W. T., and Loomis, A. L. 1927. *J. Am. Chem. Soc.* **49**, 3086–3100.

Riesz, P. 1991. "Free radical generation by ultrasound in aqueous solutions of volatile and non-volatile solutes," in *Advances in Sonochemistry*, T. Mason, ed., vol. 2, pp. 23–64, JAI Press, Greenwich, CT.

Riesz, P., Kondo, T., and Krishna, C. 1990. *Ultrasonics* **28**, 295–303.

Romdhane, M., Gadri, A., Contamine, F., Gourdon, C., and Casamatta, G. 1997. *Ultrasounics Sonochemistry* **4**, 235–243.

Rosenberg, M. 1953. Technical Memorandum No. 26, Acoust. Research Laboratory, Harvard University, Cambridge, MA.

Sakai, Y., Sadaoka, Y., and Takamaru, Y. 1977. *J. Phys. Chem.* **81**, 509.

Saksera, T. K., and Nyborg, W. L. 1970. *J. Chem. Phys.* **53**, 1722–1734.

Sarkari, M., Gopalkrishna, J., Pandit, A. B., and Harrison, S. T. L. 1999. "Techniques for cell-disruption—comparative study," Biotech progress, Submitted for publication.

Sata, N., and Harisaka, Y. 1951. *Kolloid Z.* **124**, 36–40.

Sata, N., Okuyama, H., and Chujo, K. 1951. *Kolloid Z.* **121**, 46–49.

Save, S. S., Pandit, A. B., and Joshi, J. B. 1994. *Chem. Eng. J.* **55**, B67–B72.

Save, S. S., Pandit, A. B., and Joshi, J. B. 1997. *Chem. Eng. Res. Des.* (in press), 75 (Part C), 41–49.

Schmid, G. 1939. *Z. Phys. Chem.* **186A**, 113–128.

Schmid, G. 1940a. *Chem. Ztg.* **64**, 423–430.

Schmid, G. 1940b. *Z. Phys. Chem.* **186**, 113.

Schmid, G. 1960. *Z. Phys. Chem.* **186A**, 3, 113.

Schmid, G., and Rommel, O. 1939a. *Z. Elektrochem.* **45**, 659.

Schmid, G., and Rommel, O. 1939b. *Z. Phys. Chem.* **185A**, 97–139.

Schmid, G., Paret, P., and Pfleiderer, H. 1951. *Kolloid Z.* **124**, 150–159.

Schneider, A. 1949. Ph.D. thesis, "Some compressibility effects in cavitation bubble dynamics," California Institute of Technology, Pasadena, CA.

Schultes, H., and Gohr, H. 1936. *Angew. Chem.* **49**, 420–423.

Sehgal, C. M., and Verrall, R. E. 1982. *Ultrasonics* **20**, 37.

Sehgal, C., Steer, R. P., Sutherland, R. G., and Verrall, R. E. F. 1977a. *Chem. Phys.* **70**, 2242.

Sehgal, C. M., Steer, R. P., Sutherland, R. G., and Verrall, R. E. 1977b. *J. Phys. Chem.* **81**, 2618.

Seymour, J., and Gupta, R. 1996, "Oxidation of aqueous pollutants using ultrasound. New data and their correlation on the effect of bulk conditions," paper 91a, AIChE meeting.

Seymour, J. D., and Gupta, R. B. 1997. *Ind. Eng. Chem. Res.* **36** (9), 3453–3457.

Seymour, J. D., Wallace, H. C., and Gupta, R. B. 1997. *Ultrasonics Sonochem.* **4**, 289–293.

Shankar, C. 1988. "Intensification of heterogeneous reactions," Ph.D thesis, University of Bombay, Bombay, India.

Shirgaonkar, I. Z., and Pandit, A. B. 1996. "Sonochemistry in supplementary role," *Ultrasonics Sonochemistry* **3**, S135–139.

Shirgaonkar, I. Z., and Pandit, A. B. 1997. "Degradation of aqueous solution of potassium iodide and sodium cyanide in presence of carbon tetrachloride," *Ultrasonics Sonochemistry* **4** (1), 245–253.

Shirgaonkar, I. Z., and Pandit, A. B. 1998. "Sonophotochemical destruction of aqueous solutions of 2, 4, 6 trichlorophenol," *Ultrasonics Sonochemistry* **5**, 53–61.

Shojaie, R., Markussen, J. M., and Penndine, H. W. 1992. "A novel approach for SO_2/NO_x control using ultrasound," paper presented at AIChE spring national meeting.

Sierka, R. A., and Amy, G. L. 1985. *Ozone Sci. Eng.* **1**, 47–62.

Sierka, R. A., and Skaggs, R. L. 1979. "Ozone-ultrasound treatment of a hospital wastewater for reuse," in *Proc. Water Reuse Symposium*, vol. 2, pp. 1596–1613, Air and Water Waste Association Res. Foundation.

Siryotuk, M. G. 1966. *Sov. Phys. Acoust.* **12** (2), 199.

Siryotuk, M. G. 1971. "Experimental investigations of ultrasonic cavitation," in *High-Intensity Ultrasonic Fields*, L. D. Rozenburg, ed., p. 268, Plenum Press, New York.

Skinner, L. 1970. *J. Acoust. Soc. Am.* **47**, 327.

Skinner, L. 1972. *J. Acoust. Soc. Am.* **51**, 378.

Sochard, S., Wilhelm, A. M., and Delmas, H. 1997. *Ultrason. Chem.* **4**, 77–84.

Sochard S., Wilhelm, A. M., and Delmas, H. 1998. *Chem. Eng. Sci.* **53** (2), 239–254.

Sokol'skaya, A. V., and El'piner, I. E. 1957. *Akust. Zhur.* **3**, 293–294.

Sokol'skaya, A. V., and El'piner, I. E. 1958a. *Akust. Zhur.* **4**, 288–289.

Sokol'skaya, A. V., and El'piner, I. E. 1958b. *Dokl. Akad. Nauk S.S.S.R.* **119**, 1180.

Sokol'skaya, A. V., and El'piner, I. E. 1960. *Akust. Zhur.* **6**, 263–264.

Sokol'skaya, A. V., and El'Piner, I. E. 1973. *Sov. Phys. Acoust.* **18** (3), 411.

Spurlock, L. A., and Reifsneider, S. B. 1970. *J. Am. Chem. Soc.* **92**, 6112–6117.

Srinivasan, D. 1955. doctoral dissertation, "The Sonoluminescence of water," Univ. of Missouri, Columbia, MO.

Srinivasan, D., and Holroyd, L. V. 1955. *Phys. Rev.* **99**, 633.

Srinivasan, D., and Holroyd, L. V. 1961. *J. Appl. Phys.* **32**, 446.

Starks, M. C., and Liotta, C. 1978. *Phase Transfer Catalysis—Principles and Techniques*, Academic Press, New York.

Strasberg, M. 1976. *J. Acoust. Soc. Am.* **31**, 163.

Suslick, K. 1986a. "Organometallic sonochemistry," in *Advances in Organometallic Chemistry*, vol. 25, pp. 73–113, Academic Press, Orlando, FL.

Suslick, K. S. 1986b. "Ultrasound in synthesis," in *Modern Synthetic Methods*, R. Scheffold, ed., vol. 4, pp. 1–60, Springer-Verlag, Berlin.

Suslick, K. S. 1987. "Sonochemistry of organometallic compounds," in ACS Symposium Series, vol. 333, pp. 191–208, American Chemical Society, Washington, DC.

Suslick, K. S. 1988. "Homogeneous Sonochemistry," Ch. 4 in *Ultrasound: Chemical, Physical and Biological Effects*, K. S. Suslick, ed., VCH Publishers, New York.

Suslick, K. S. Feb., 1989. "The Chemical Effects of Ultrasound," *Scientific American*, 80.

Suslick, K. S. 1990. "Sonochemistry," *Science* **247**, 1439.

Suslick, K. S. 1995. work quoted by R. F. Service in *Science* **267**, 327–329.

Suslick, K. 1998. "Sonochemistry," in *Kirk Othmer Encyclopedia of Chemical Technology*, 4th ed., vol. 26, pp. 516–541, Wiley, New York.

Suslick, K. S., Schubert, P. F., and Goodale, J. W. 1981. *J. Am. Chem. Soc.* **103**, 7324–7324.

Suslick, K. S., Goodale, J. W., and Schubert, P. F. 1983. *J. Am. Chem. Soc.* **105**, 5781–5785.

Suslick, K. S., Gawienowski, J. J., Schubert, P. F., and Wang, H. H. 1987. *J. Phys. Chem.* **87**, 2299–2301.

Szalay, A. 1933a. *J. Phys. Chem.* **164A**, 231.

Szalay, A. 1933b. *J. Phys. Chem.* **164A**, 234.

Szalay, A. 1933c. *Phys. Z.* **35**, 293.

Taylor, K. J., and Jarman, P. D. 1970. *Aust. J. Phys.* **23**, 319–334.

Teslenko, V. S. 1980. "Experimental investigation of bubble collapse at laser induced breakdown in liquids," in *Cavitation and Inhomogeneities in Underwater Acoustics*, W. Lauterborn, ed., p. 30, Springer-Verlag, New York.

Thoma, G., Stanfield, B., and Popov, V. 1995. "Ultrasonic degradation of organochlorine contaminated wood treatment plant wastewater," paper 196f at AIChE meeting.

Thoma, G., Popov, V., Som, M., and Stanfield, B. 1996. "Ultrasonic degradation of chlorobenzene in aqueous solutions," paper 91m, AIChE meeting.

Thyagarajan, K., and Ghatak, A. K. 1981. *Laser Theory and Applications*, Plenum Press, New York.

Tullis, J. P., and Ball, J. W. 1974. "Critical cavitation number for various valves," Edinburgh; paper C153/74, Institute of Mechanical Engineers.

Tullis, R., and Govindrajan, J. 1973. *Hydraul. Div. ASCE*, **HY 13**, 417–430.

Verrall, R. E., and Nomura, H. 1977. *J. Solution Chem.* **6**, 1.

Walton, A., and Reynolds, G. 1984. *Adv. Phys.* **33**, 595.

Wang, T. 1974a. *Phys. Fluids* **17** (6), 1121.

Wang, T. 1974b. *J. Acoust. Soc. Am.* **56**, 1131.

Weissler, A. 1950. *J. Appl. Phys.* **21**, 171–173.

Weissler, A. 1951a. *J. Appl. Phys.* **23**, 370.

Weissler, A. 1951b. *Chem. Eng. Prog. Symp. Ser., Ultrasonics* **47**, 23.

Weissler, A. 1953. *J. Acous. Soc. Am.* **25**, 651.

Weissler, A. 1959. *J. Am. Chem. Soc.* **81**, 1077–1081.

Weissler, A. 1960. *J. Acous. Soc. Am.* **32**, 283.

Weissler, A. 1962. *IRE Int. Conv. Record* **10**, 24–30.

Weissler, A., Cooper, H. W., and Snyder, S. 1950. *J. Am. Chem. Soc.* **72**, 1769–1775.

Wu, J. M., Huang, H. S., and Livengood, C. D. 1992, *Env. Prog.* **11** (3), 195–201.

Yan, Y., and Thorpe, R. B. 1990. *Int. J. Multiphase Flow* **16** (6), 1023–1045.

Yan, Y., Thorpe, R. B., and Pandit, A. B. 1988. "Cavitation noise and its suppression by air in orifice flow," in *Proc. Int. Symp. Flow Induced Vibration and Noise*, pp. 25–40, American Society of Mechanical Engineers.

Young, F. 1989. *Cavitation*, McGraw-Hill, London.

PERSONAL COMMUNICATIONS

Casadonte, D. J., and Doktycz, S. 1995. Department of Chemical Engineering, Texas Tech University, Lubbock, Tx.

Contamine, F., Faid, F., Wilhelm, A. H., Berlan, J., and Delmas, H. 1997. Chemical reactions under ultrasound: descrimination of chemical and physical effects. Laboratoire de Genie chimique, URACNRS. 192, ENSIG, Chemin de la Loge, 31078, Toulouse, France.

Sweet, S., and Casadonte, W. 1995. Department of Chemical Engineering, Texas Tech University, Lubbock, TX.

Thoma, G., Popov, V., Som, M., and Seofford, J. 1997. "Sonochemical destruction of dichloromethane and o-dichlorobenzene in aqueous solution using a near-field acoustic processor," Department of Chemical Engineering, University of Arkansas, Fayetteville, AR 72701.

Sekhar, R. 1997. University Department of Chemical Technology, Bombay University, Matunga Road, Mumbai 400019, India.

Seymour, J. D., and Gupta, R. B. "Sonochemical oxidation of pollutants at 640 kHz with a salt induced enhancement", Department of Chemical Engineering, Auburn University, Auburn, AL 36849-5127.

INDEX